UNIVERSITY OF BIRMINGHAM

School of Pharmacy

College of Medical and Dental Sciences

UTILISING HOT MELT EXTRUSION AND FUSED DEPOSITION MODELLING BASED 3D PRINTING TECHNOLOGY FOR THE SYNTHESIS OF SOLID PHARMACEUTICAL DOSAGE FORMS AND INNOVATIVE DRUG DELIVERY DEVICES

BY

ALI ALKOLAIB

A thesis submitted to The University of Birmingham

for the degree of

DOCTOR OF PHILOSOPHY

May 2023

“Hide the good you do and make known the good done to you.”

Ali ibn Abi Talib
599-661 AD

Abstract

Fused deposition modelling (FDM) is a type of three dimensional (3D) printing technology that relies on melt extrusion of thermoplastic materials for the fabrication of objects with virtually limitless opportunities of designs or geometries. Therefore, involving FDM based 3D printing technology in the manufacturing of pharmaceutical dosage forms and medical devices will be a robust method for producing customised pharmaceutical dosage forms and medical devices.

Although there are no commercially available solid dosage forms produced by the FDM based 3D printing technology, the past decade has seen an increasing in research efforts that demonstrated the capacity of FDM based 3D printing to produce pharmaceutical dosage forms with customised release profiles, geometries, and dosage forms with multiple drugs (polypills). Therefore, using this type of technology in the pharmaceutical industry will allow for the printing of limitless product designs and overcome the drawbacks of conventional pharmaceutical manufacturing associated with the production of dosage forms based on the 'one-size-fits-all' approach.

The work conducted herein used hot melt extrusion (HME) and FDM based 3D printing technology to manufacture different solid pharmaceutical dosage forms and novel medical devices. The starting materials prepared in this thesis were prepared using HME technology to incorporate different types of pharmaceutical drugs into various polymers, which were later utilised as feed materials for two different types of FDM based 3D printers: filament-based 3D

printer and pellet based 3D printer. The assessment of the prepared drug loaded formulations regarding the mechanical properties, rheological characteristics, drug content and drug homogeneity was conducted to determine the quality of HME extrudates.

The first study examined the influence of various 3D printing processing parameters including (infill percentage, infill pattern, printing speed, and layer height) on 3D fabricated solid pharmaceutical dosage form (tablet) manufactured from commercially available drug free polymer; Poly lactic acid (PLA). The analysis assessed how these parameters influenced physical characteristics, including the weight, density, and dimensions of the resulting drug free tablets.

In the second study, the investigation and analysis focused on the influence of various 3D parameters on the *in vitro* drug release profile of 3D printed tablets. Initially, drug loaded polymers were prepared by incorporating caffeine into either the water soluble polymer polyvinyl alcohol (PVA) or the water insoluble polymer PLA utilising HME technology. These HME prepared drug loaded polymers (filaments) underwent characterisation to assess drug loading, filament diameter, extrusion capability, and thermal properties. Subsequently, FDM based 3D printer was employed to manufacture drug loaded tablets, employing different 3D parameters such as infill percentage, layer height, and infill patterns. Finally, the study analysed the impact of these parameters on the *in vitro* drug release of the fabricated tablets.

In the third study of this thesis, the feasibility of FDM based 3D printing technology to manufacture an oral solid dosage form (tablet) containing two different drugs Isoniazid (INH) and

Pyridoxine Hydrochloride (PDX) was investigated. The drug combination is commonly used as a monotherapy for the treatment of tuberculosis infection (TB). All the pharmaceutical components of the dosage form were manufactured from FDA approved ingredients. The preparation of the drug loaded polymer formulation was initially performed by the HME process in two different ways. The first method involved loading the two drugs in a single polymer matrix to synthesise single layer tablet. The second method involved loading the drugs separately into two different extrudates and joining them during the 3D printing process using a dual extrusion 3D printer to manufacture a bilayer tablet. The prepared pharmaceutical drug loaded tablets of both types were analysed and compared in terms of *in vitro* drug release and physical properties.

In the fourth study, FDM based 3D printing technology was utilised to manufacture an implantable drug delivery device which was designed and 3D printed to be utilised as a prototype device for localised treatment of brain tumours. The implant is prepared from two different layers, the first one is composed of a blend of Poly (lactic-co-glycolic acid) (PLGA) loaded with Irinotecan (IRN) as a chemotherapeutic agent designed in the form of cone shaped protrusions with a dimension of 6 mm height and 5 mm base diameter. These protrusions are attached to a square shaped base layer with an edge length of 15 mm, printed from Ethylene-vinyl acetate (EVA) with a vinyl acetate content of 18.2%. The manufactured implant was characterised in terms of drug content, crystallinity, thermal properties, and *in vitro* drug release.

In the fifth study, FDM based 3D printing technology is utilised to manufacture a novel drug delivery device aimed at providing localised drug delivery of a chemotherapeutic agent for the

post-surgical treatment of pancreatic cancer (PC). A cuboid-shaped device with dimensions of 35 mm in length, 12 mm in width, and 10 mm in height was manufactured from EVA 18.2% as a flexible polymer. The development and optimisation of computer-aided design (CAD) and FDM 3D printing of the device were analysed. Furthermore, the influence of different 3D printing parameters, including infill percentage, membrane thickness, pore size, and pore number on the *in vitro* drug release of the final optimised device was identified and analysed.

This thesis provides an overview of the feasibility of using FDM 3D printing for the synthesis of solid pharmaceutical dosage forms and contributes to the understanding of the advantages and limitations associated with this technique. Moreover, it provides insights into the promising applications of this technology in the manufacturing of medical devices that can be designed, customised, and modified to meet the specific requirements of individual conditions.

Acknowledgement

A significant amount of time, effort, and attention went into this project. However, without the help of many people, implementation would not have been possible. I would like to express my sincere gratitude to everyone for their help.

First and foremost, I would like to acknowledge and give my warmest thanks for my supervisor, Dr. Christopher McConville for his guidance and support carried me through all the years and phases of this project. His dedication and keen interest above his overwhelming attitude to help me had been solely and mainly responsible for completing this work. I could not have imagined having a better advisor for my PhD study.

Beside my advisor, I would also like to thank my co- supervisor Dr. Thomas Mills, school of chemical engineering, for his kind suggestions, 3D printing training, access to his lab, insightful comments, and the academic advice he provided for me through my PhD journey.

My deepest gratitude goes to all my family members for their support and encouragements, special thanks to my parents Marzook Sr and Saadah Alkolaib for dedicating their life for me and to my wife Rahmah and my children Marzook II, Mohammed, Sahab and Hadi for their endless love.

Last but not least, I would like to acknowledge with gratitude, to my home country, Kingdom of Saudi Arabia, Ministry of Education, Najran University for the financial fund and the scholarship they provided me to accomplish my PhD degree.

Covid-19 impact statement

Since the Covid-19 pandemic began at the beginning of my PhD's second year, the lockdown limitations and preventative measures have had some effects on my thesis.

Here is a list of the primary effects:

1- I did not get to do further investigations of chemotherapeutic implant designed for localised treatment of brain cancer (chapter 4) such as:
   - The influence of different drug loading on the release profile.
   - The influence of different 3D printing parameters e.g. (infill %, layer thickness, infill pattern etc.) on the *in vitro* drug release.
   - The influence of different vinyl acetate (VA) content of on the flexibility of the implant's base.

2- I did not get to do further investigations of chemotherapeutic pancreatic drug delivery device designed for localised treatment of pancreatic device (chapter 5) such as:
   - The mechanical properties of the 3D printed device e.g. (the breaking force) required to split the device apart.
   - The influence of different printing parameters on the quality of the final device such as printing resolution, layer-to-layer adhesion, and the dimension accuracy of the 3D printed device.
   - To do a swelling test of the device.

Table of contents

List of tables

List of figures

List of abbreviations

%	Percent
°	Degree
2θ	2-Theta
3D	Three-dimensional
ABS	Acrylonitrile Butadiene Styrene
AI	Artificial Intelligence
AM	Additive Manufacturing
API	Active Pharmaceutical Ingredient
ASTM	American Society for Testing and Materials
AUC	Area under the curve
CAD	Computer Aided Design
CAF	Caffeine
CV	Coefficient of variance
CVD	Cardiovascular disease
CR	Controlled Release
DDD	Drug Delivery Device
DoD	Drop on demand
DoP	Drop on powder
DP	Degree of polymerisation
DSC	Differential Scanning Calorimetry

- 3DP Three-Dimensional Printing
- EVA Ethylene-vinyl acetate
- FDA Food and Drug Administration
- FDC Fixed-dose combinations
- FDM Fused Deposition Modelling
- FFD Fused Filament Deposition
- GRAS Generally recognised as safe
- HGG High Grade Glioma
- HME Hot-Melt Extrusion
- HPLC High Performance Liquid Chromatography
- HPMC Hydroxypropyl methyl cellulose
- IR Immediate Release
- INH Isoniazid (Anti-tuberculosis agent)
- IRN Irinotecan (Chemotherapeutic agent)
- LOM Laminated object manufacturing
- MCS Multicompartment system
- MW Molecular Weight
- NCE New chemical entities
- µg Microgram
- PC Pancreatic cancer
- PCL Polycaprolactone
- PD Pancreatic device

- PDI Polydispersity Index
- PDX Pyridoxine HCL (Vitamin B6)
- PEG Polyethylene Glycol
- PLA Poly Lactic Acid
- PLGA Poly Lactic-co-Glycolic Acid
- PVA Poly-vinyl Alcohol
- QR Quick response
- RP Rapid Prototyping
- SD Solid Dispersion
- SLS Selective Laser Sintering
- SSHME Single screw hot melt extrusion
- Stl. file Standard Triangle Language
- STL Stereolithographic Apparatus
- T Temperature
- Tm Melting temperature
- TSHME Twin screw hot melt extrusion
- *Tg* Glass transition temperature
- UV Ultra-Violet
- XRD X-Ray Diffraction analysis

Chapter 1 : INTRODUCTION

1.1. Background:

The current pharmaceutical sector and consumer trends are driving the need for a shift in the traditional centralised batch manufacturing of pharmaceuticals (Algorri et al., 2022). The expensive research cost of pharmaceutical research and development for a new drug (estimated at $1141.7 million), time to market, and the possibility of failures in the product development at the later stages are among the limitations of the traditional pharmaceutical industrial sector (Lawrence & Kopcha, 2017; Reklaitis et al., 2010; Wouters et al., 2020).

The fourth industrial revolution of the 21st century has led to a remarkable technological advancement in the industrial sector with rapid prototyping (RP). RP is a technology that focuses specifically on the rapid production of physical models using additive manufacturing (AM) processes (Pal et al., 2022). RP appears to be an essential tool in the industrial sector to develop flexible and rapid prototypes of new products, thus improving the manufacturing productivity (Chaudhari et al., 2022). RP has the potential to enhance manufacturing productivity through the acceleration of the design iteration cycle. This streamlined approach to product development enables faster iterations and ultimately facilitates expedited product commercialisation. Through the reduction of time to market, RP has the capacity to decrease the expenses associated with product development by identifying design issues at an earlier stage in the design cycle. Additionally, it enhances the potential for creativity and innovation in product designs by enabling

swift evaluation and iteration of design concepts. Moreover, RP contributes to gaining a competitive edge by maintaining internal control over design plans and data until later phases of the product development process (Nee, 2014). Therefore, numerous RP techniques has been applied in diverse industries such as wood, plastic, metal and ceramic due to ease in utilisation and economic benefits (Chu et al., 2008).

RP technique works based on digital designing to develop freeform geometries with the deposition of material in a layer-by-layer fashion could be referred to as additive manufacturing (AM) or solid freeform fabrication (SFF) technique and more preferably 3D printing technology (Varghese et al., 2022). At Ohio's Battelle Memorial Institute, the first studies into the use of photopolymers to produce 3D objects were conducted in the 1960s. The experiment's goal was to polymerise resin by combining two laser beams with various wavelengths. In 1971, Wyn Swainson submitted a patent application for a similar twin laser beam technique known as photochemical machining (Min et al., 2018).

At Massachusetts Institute of Technology (MIT), 3D printing technology was established by Sachs et al. in 1992 (Sachs et al., 1992) and the first 3D printed pharmaceutical drug delivery device was fabricated by Wu et al. in 1996 using continuous inkjet printing technique (Wu et al., 1996). Since then, over the years various types of 3D printing technologies have been evolved (Goole & Amighi, 2016).

1.2. Definition of 3D printing technology

The 3D printing technology is defined by the American Society for Testing and Materials (ASTM) as the “fabrication of objects through the deposition of materials using a print head, nozzle, or another printing technology” (Mancilla-De-La-Cruz et al., 2020). However, 3D printing generally belongs to a group of technologies that build (3D) objects using data from a computer-generated model (Dzogbewu et al., 2022).

3D printing technology is frequently called AM because the final object is made by adding many thin layers one upon another instead of removing parts from a bulk, as in subtractive manufacturing (SM) methodologies as shown in Figure (1.1). Therefore, AM has many advantages over the SM such as minimising the waste of materials, reducing time and efforts and the opening of new opportunities in terms of individually customised products (Attaran, 2017; Chua & Leong, 2014).

Due to the increase in 3D printing in research and development, more than 1.5 million 3D printers were purchased globally in 2019 and are expected to reach 8 million by 2027 (Quanjin et al., 2020). Moreover, the global 3D printing market is estimated to be valued at approximately USD 40 billion by 2025 and USD 76.16 billion by 2030, in comparison to USD 30 billion in 2022 (Ekren et al., 2023; Y. Wang et al., 2021). It is also anticipated that the market for 3D printing in medical applications, which was valued at USD 2.8 billion in 2022, will increase to USD 11 billion by 2032, with a compound annual growth rate (CAGR) of 16.6% from 2023 to 2032 (Acumen Research and

Consulting, 2023). The additive manufacturing market share by region in 2022 is presented in Figure (1.2).

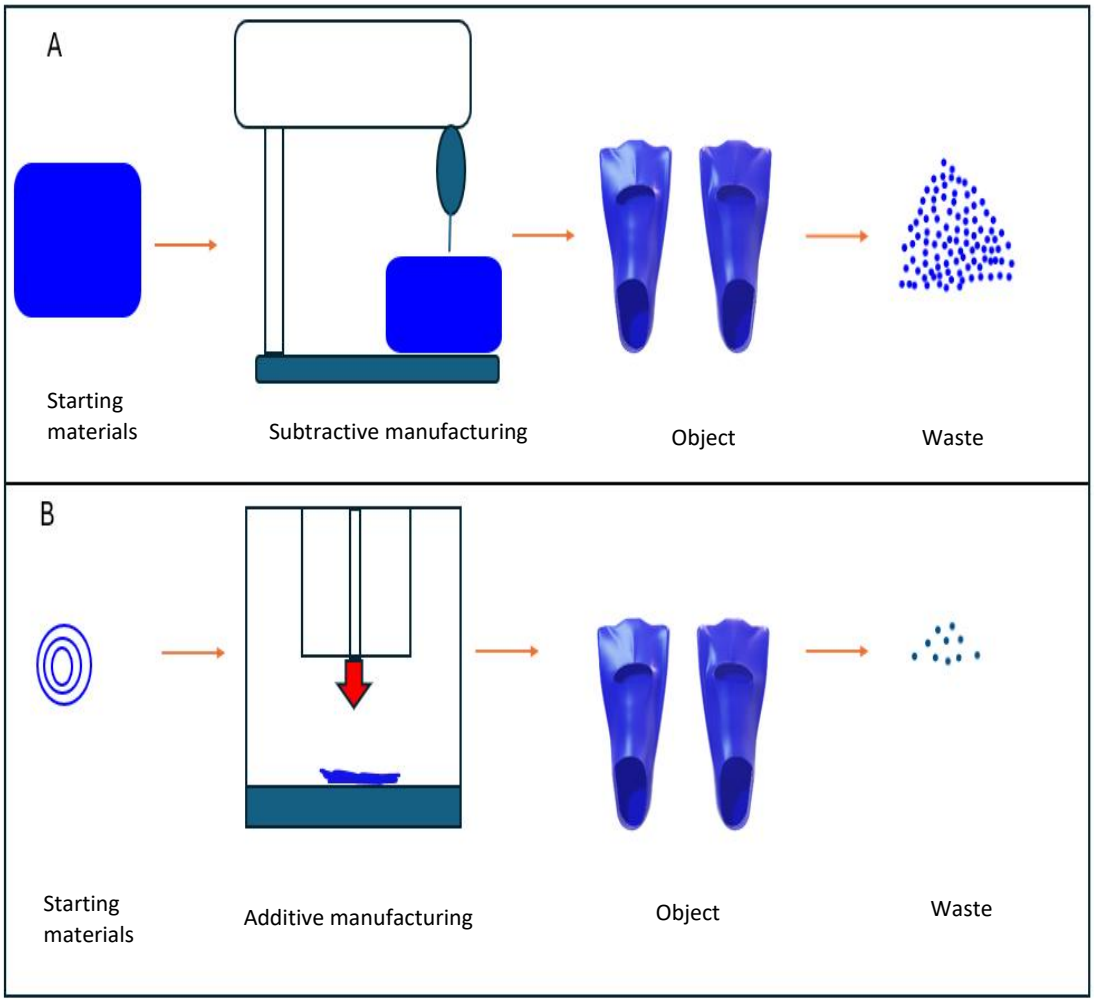

Figure 1.1: *Conceptual illustration of subtractive manufacturing (A) vs. additive manufacturing (B).*

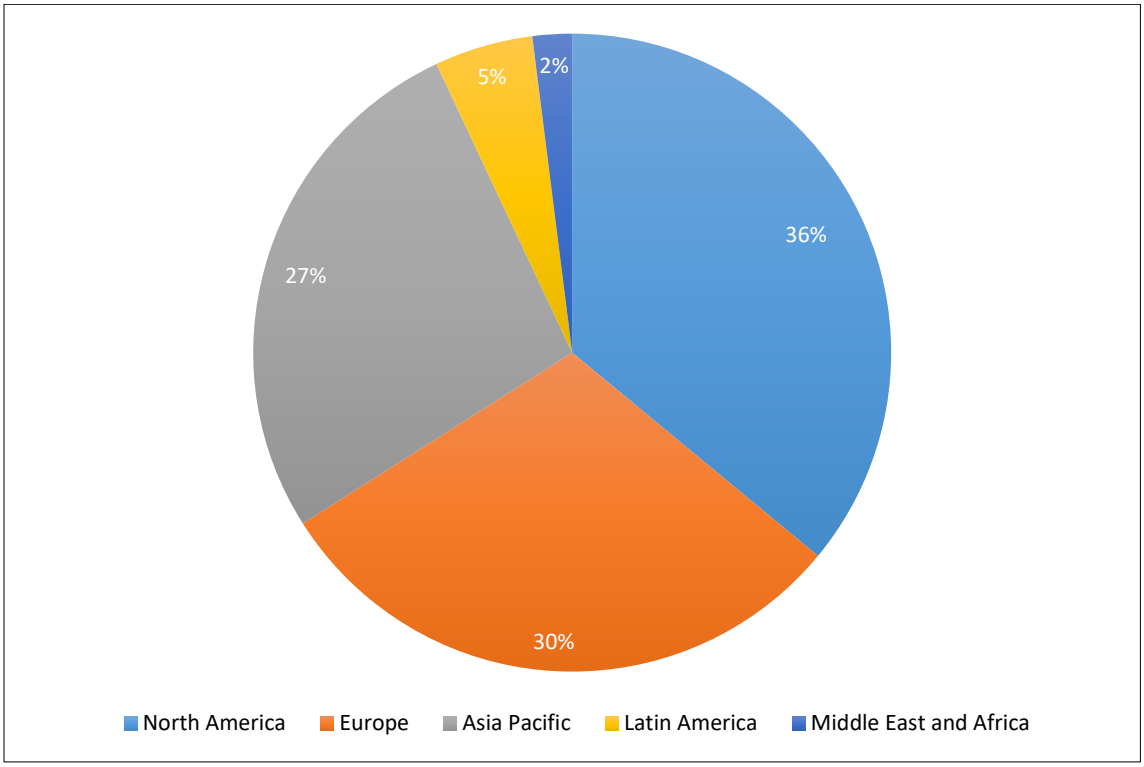

Figure 1.2: *Additive manufacturing market share by region, 2022. Adopted from (PresedenceResearch, 2023).*

1.3. Types of 3D printing techniques

The primary distinction between different varieties of 3D printing technologies is the materials employed as well as the layer by layer building mechanism of the physical objects (Alhnan et al., 2016; Norman et al., 2017). The classification of 3D printing technologies employed in pharmaceutical sector have been discussed below:

1.3.1. Stereolithography Apparatus (SLA)

SLA is also known as Vat Photopolymerisation and optical fabrication, where photosensitive liquid resin polymers are used to build up 3D objects in a layer-by-layer fashion (Jadhav & Jadhav, 2022). The acronym SLA originates from the combination of "stereo" (solid) and "lithography" (photo) suggesting the process of "writing with light." SLA employs photopolymerisable materials that solidify when exposed to light, particularly UV light. By precisely directing a laser beam, the shape and dimensions of the object are controlled. The UV light used for photopolymerisation is typically low-powered and generated from He-Cd/Nd: YVO4 laser sources (Lakkala et al., 2023).

Based on the orientation of printing, the location of the light source, and the direction of projection, The SLA 3D printing technology can be classified into two types "Top-Down" and "Bottom-Up" 3D printers (Zakeri et al., 2020). In the top-down SLA apparatus, the light source is located above the resin vat. The build platform is immersed in the liquid resin to a depth of one layer. UV irradiation from the overhead light source solidifies and cures the resin in each layer during the printing process. On the other hand, in the bottom-up SLA apparatus, the light source is situated at the base of the resin tank, emitting light in an upward direction to initiate the photopolymerisation process of the resin (Taormina et al., 2018). Both types are demonstrated in Figure (1.3).

SLA is the oldest 3D printing technology and it is commonly used to make 3D models for surgical purposes specially in dental implants (Melchels et al., 2010) as well as hydrogels formulations (Xing

et al., 2015). One of its most intriguing capabilities is the production of tiny objects like microneedles, which appears to be much more challenging when utilising other 3D printing techniques (Economidou & Douroumis, 2021). SLA 3D printers are generally capable of achieving a high level of detail and precision. The layer height, which determines the vertical resolution, can range from around 25 to 100 microns or even finer in some advanced models (Krieger et al., 2019).

The limited availability of FDA approved biocompatible and biodegradable photosensitive polymers has constrained the widespread applications of SLA technology. Nonetheless, recent advancements have resulted in the development of several biocompatible photopolymers suitable for use in SLA. Polyethylene glycol diacrylate (PEGDA) and polyethylene glycol dimethacrylate (PEGDMA) are examples of biocompatible photopolymers that have emerged in recent times as a viable option for SLA applications (Burke et al., 2020; Seo et al., 2017).

The monomers of methacrylates and acrylates are extensively utilised in pharmaceutical applications due to their rapid reaction rates, flexible mechanical properties, and stability. One drawback of these monomers is their tendency to undergo volume shrinkage during photopolymerisation, leading to the production of highly brittle 3D objects. However, this issue can be addressed by incorporating flexible oligomers. For example, the combination of (methacryloxypropyl) methylsiloxane (MAOMS) with a commercial resin forms a siloxane-methacrylate blend that exhibits improved tensile toughness, reduced glass transition temperature (*Tg*), increased tensile strength, and enhanced surface energy (Palaganas et al., 2017).

Reactive species play a vital role in initiating the photopolymerisation process of monomers/oligomers. However, since the monomers/oligomers themselves are incapable of generating the necessary reactive species, the inclusion of a photoinitiator becomes essential to fulfil this function. Various free radical photoinitiators, such as benzoin derivatives, acetophenone, hydroxyalkylphenones, and acylphosphine oxide, are commonly employed for methacrylate, acrylate, and thiol monomers (Karakurt et al., 2020; Pereira & Bártolo, 2015).

Utilisation of SLA 3D printing techniques to fabricate oral pharmaceutical dosage forms were attempted by Robles-Martinez et al. to produce polypills containing six different active pharmaceutical ingredients (APIs) (caffeine, paracetamol, aspirin, prednisolone, chloramphenicol, and naproxen) while Healey et al. used it to produce caplets hosting either aspirin or paracetamol (Healy et al., 2019; Robles-Martinez et al., 2019).

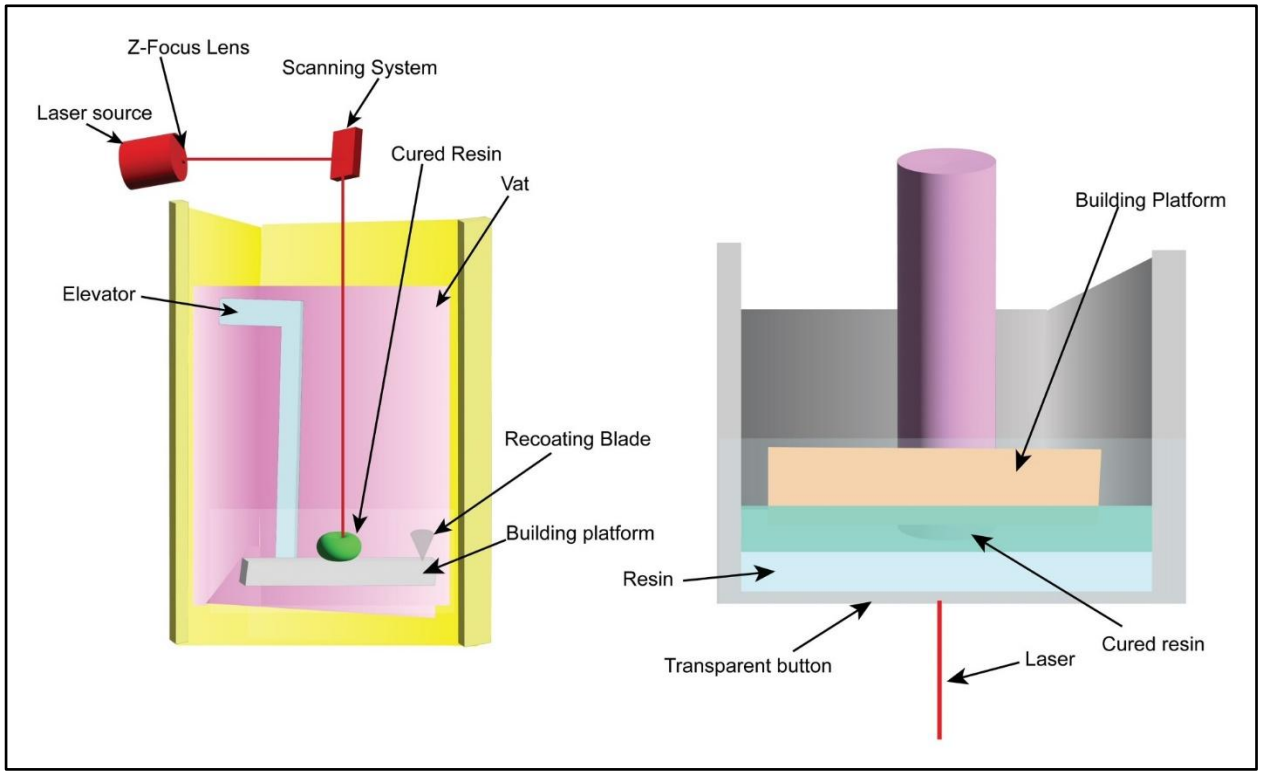

Figure 1.3: *Schematic representation of SLA (Top-Bottom Approach) left and (Bottom-Up Approach). Adopted from (Lakkala et al., 2023).*

1.3.2. Jet printing systems

A standard inkjet printer consists of a print head containing numerous tiny openings that create the desired 2D or 3D structure by placing ink droplets onto a substrate, following a layer-by-layer approach. In pharmaceutical applications, the term "ink" refers to the drug that is dissolved or dispersed within a solution of polymer, resin, solvent, or binder. The surface tension, viscosity, and volatility of the ink are crucial factors that contribute to the optimal functioning of inkjet printing technology (Chou et al., 2021).

As specified by the International Organisation for Standardisation (ISO)/ASTM standards, both binder jetting and material jetting AM technologies utilise a jet printing mechanism to create 3D objects. In binder jetting printers, a print head selectively sprays liquid agents, typically a binding agent solution, onto powder particles based on the CAD specifications. On the other hand, material jetting printers employ a print head to deposit droplets of melted material or photocurable material mixed with a medium onto a build platform. Each layer is then solidified or cured to form the final object (Alexander et al., 2021).

The jet printing system can be categorised into two types based on the technology used to control ink flow during the printing process: continuous jet (C-JT) and drop-on-demand jet (DOD-JT) printing (Prasad & Smyth, 2016) as demonstrated in Figure (1.4). In C-JT printing, high-pressure pumps are employed to consistently propel the ink through the nozzle, ensuring a continuous flow of ink during the printing process. In contrast, DOD-JT printing utilises pressure pulses to create smaller ink droplets compared to those formed in C-JT printing. This enables DOD-JT printing to achieve higher accuracy, precision, and resolution in the printed output (Jacob et al., 2020).

DOD-JT technology can be classified into two types: thermal and piezoelectric. In thermal DOD-JT, a resistor within the ink chamber rapidly heats up upon receiving electric signals, creating a vapor bubble that propels the ink out of the nozzle. The collapsing of the bubble generates negative pressure, aiding in the ink refill. This technology minimises thermal degradation risks but requires highly volatile solvents for efficient vaporisation. In contrast, piezoelectric DOD-JT utilises a ceramic piezoelectric element that undergoes mechanical movement upon electric signal

application, generating a pressure wave to eject ink droplets from the nozzle (Daly et al., 2015; Park et al., 2019).

Spritam® is a dispersible tablet with a high drug loading capacity and no complicated structures. It was created using Inkjet based 3D printing technology and was the first FDA approved 3D-printed preparation released in 2015 (Sen et al., 2021). The high drug loaded products, reaching 70%, that can be developed with this technique are due to the incorporation of the APIs either in the powder bed and or in the binder ink (Infanger et al., 2019). However, the common disadvantage of this technique may results in a highly friable pharmaceutical product due to the high porosity of the developed object (Kolakovic et al., 2013).

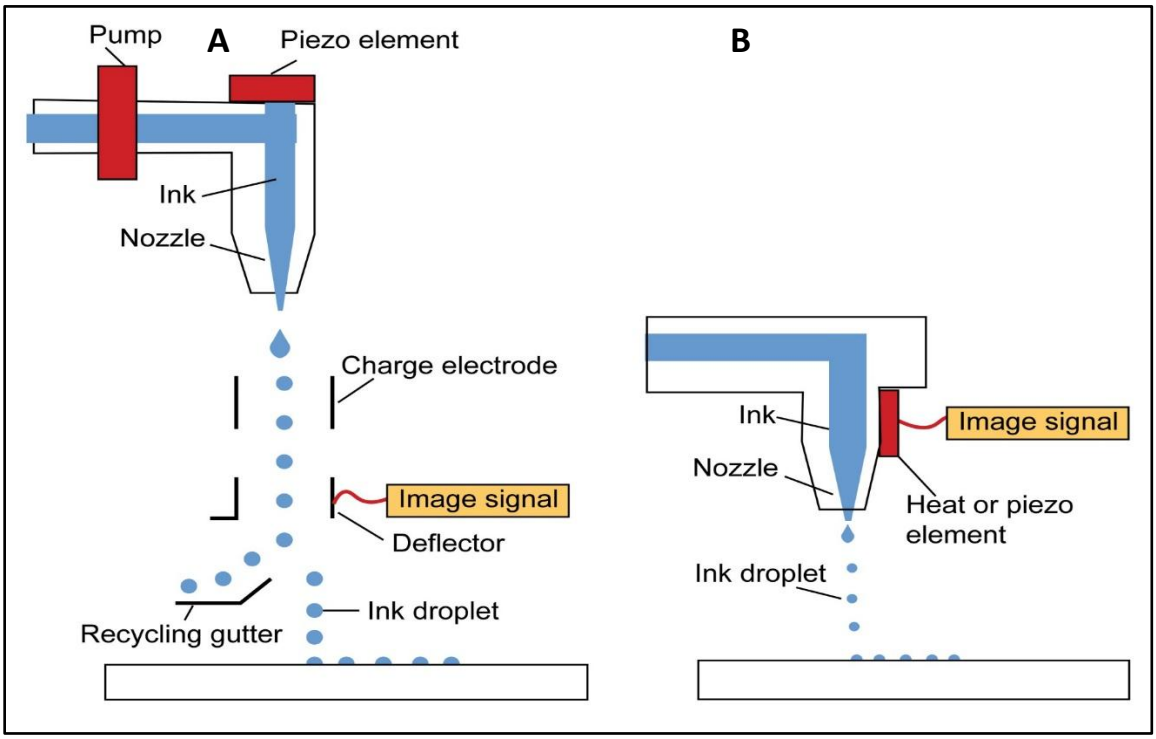

Figure 1.4: *A simplified illustration of two distinct types of jet printing mechanisms includes (A) continuous jet printing (CIJ) and (B) drop-on-demand jet printing (DOD). Adopted from (Lau & Shrestha, 2017).*

1.3.3. Selective Laser Sintering (SLS)

SLS technique was developed in mid 1980s by Carl DecKard and Joe Beaman (Gross et al., 2014). Basically, it is a powder bed fusion process that utilises a laser to fuse powder material together in a sequential layer-by-layer manner. The printed object remains surrounded by powder material throughout the printing process, eliminating the need for support materials (Evgenii et al., 2023). Carbon dioxide laser beam is used to scan a selected region of the powdered materials to create the 3D object as shown in Figure (1.5). The SLS technique is similar to drop on powder (DOP) technique in terms of utilising the powder as a building material (Jamróz et al., 2018).

SLS is a promising 3D technology that offers a single-step, solvent-free, high-resolution 30-60 µm and laser to sinter the powder instead of liquid binders. Therefore, this technique reduces the amount of time the solvent needs to evaporate. Nevertheless, one of its limitation is the use of high energy laser source which is widely recognised of destroying the drugs and other excipients (Cui et al., 2021).

In the SLS technique, the powders utilised are typically loosely packed or free flowing. They have a particle size ranging from a few microns, and several powder characteristics, including morphology, granulometry, density, and flowing capacity, are considered during their selection. The flowing capacity of the powder is a crucial property as it should be able to spread uniformly. Particle sizes can vary from 40 to 180 µm. It is also desirable for the powder to have good

sphericity. To enhance the flowing capacity and reduce the cohesion among powder particles, certain agents such as silicon dioxide (SiO2) can be used (Tabriz et al., 2023).

Several studies have explored the potential of SLS for the production of different pharmaceutical dosage forms. For example, SLS was investigated to develop floating drug delivery systems (FDDS) (Kulinowski et al., 2022), formation of solid oral dosage forms (SODF) (Gueche et al., 2021), fabrication of multi-drug miniprintelets with controlled release (Awad et al., 2019) and production of orally disintegrating tablets (ODT) (Fina et al., 2018). Overall, these investigations highlight the promising capabilities of SLS in the field of pharmaceutical manufacturing and offer insights into its potential applications for personalised medicine and advanced drug delivery systems.

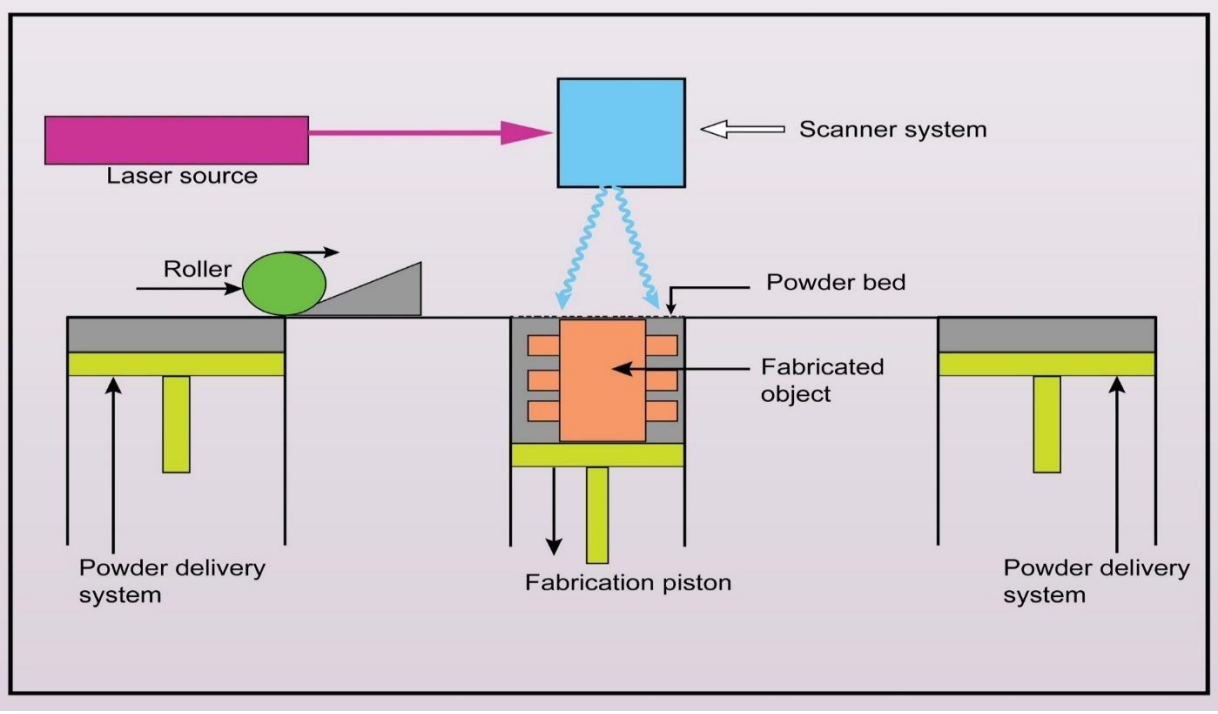

Figure 1.5: *Schematic demonstration of selective laser sintering (SLS) technique. Adopted from (Mazzoli, 2013).*

1.3.4. Laminated object manufacturing (LOM)

As demonstrated in Figure (1.6), LOM is a rapid prototyping technique involves building a part from many layers of paper (Park et al., 2000). Several types of raw materials, such paper, plastic, or metal, can be used in this procedure. A heated roller is used to laminate the material, which is then attached to the base layer. Thereafter, a laser is used to cut it (Bikas et al., 2016). LOM provides benefits such as cost-effectiveness, quicker printing speeds, and versatility in material options. Nevertheless, it may have drawbacks in terms of resolution and surface quality when compared to alternative 3D printing techniques. LOM finds frequent application in prototyping, architectural models, and functional components that do not necessitate extreme precision (Kumar & Prasad, 2021).

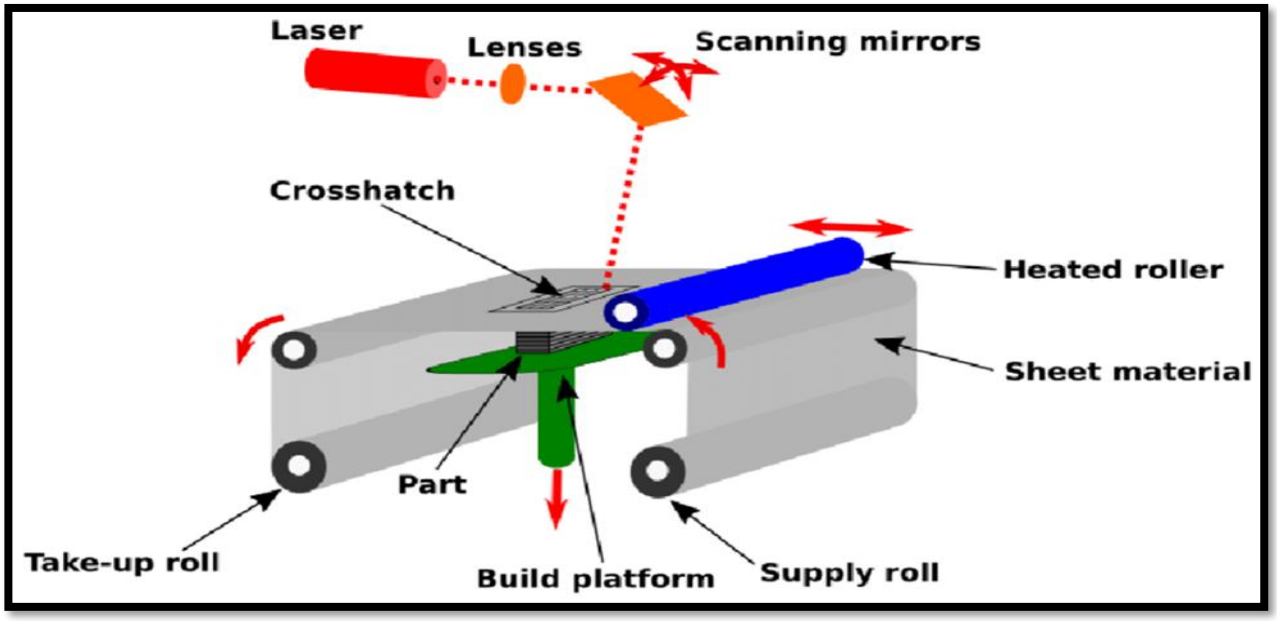

Figure 1.6: *Schematic diagram of laminated object manufacturing (LOM) adopted from (Riveiro et al., 2019).*

1.3.5. Material extrusion-based 3D printing

The basic concept of this technique is the extrusion of molten raw material through an orifice and forming it to build a new shape (Kristiawan et al., 2021). This type of technology can be further divided into two techniques; fused deposition modelling (FDM) which uses (thermoplastic materials) and the pressure-assisted microsyringes (PAM), where the starting materials are gel and paste (Awad et al., 2018; Mohammed et al., 2021). Since the FDM based 3D printing technology has been employed for work in the thesis, a detailed overview of this technique will be provided in the upcoming sections.

1.3.5.1. FDM 3D printing overview

The FDM based 3D printing is the most versatile and widely used technology among other variants of 3D printing technologies (Norman et al., 2017). It is also called fused filament fabrication (FFF). It was developed in late 1980s by Scott Crump and was commercially available by Stratasys in 1990 (Chua et al., 2020). FDM has become one of the most used 3D printing technologies in the field of pharmaceutical research due to its versatility, simplicity, affordability, capability of manufacturing objects with complex geometries and the non-use of organic solvents (Goole & Amighi, 2016; Ilyés et al., 2019).

The FDM 3D printer demonstrated in Figure (1.7) is composed of four essential elements which include extruder, hot end, printing bed and feeding material (usually thermoplastic filament). The extruder is the part responsible for thrusting filament into the hot end part by assistance of

extruder gears. Hot end is the second part receiving the thermoplastic materials (filament) from the extruder. It is composed of heat source with thermostat to regulate the required temperature to melt the filament and an extrusion tip which is a nozzle with typical diameter ranging from 0.1 to 1 mm used to deposit the molten materials. The third part is the printing bed which is the platform where 3D objects are layered during the deposition process, and it also has a thermostat and heating source to keep the printed object warm and to avoid the occurrence of any warping. The fourth part is the feedstock material which is called filament, which consists of several kinds of thermoplastic materials that have different properties such as melting temperature, elasticity, diameters and physicochemical properties(Acosta-Vélez & Wu, 2016; Mwema et al., 2020).

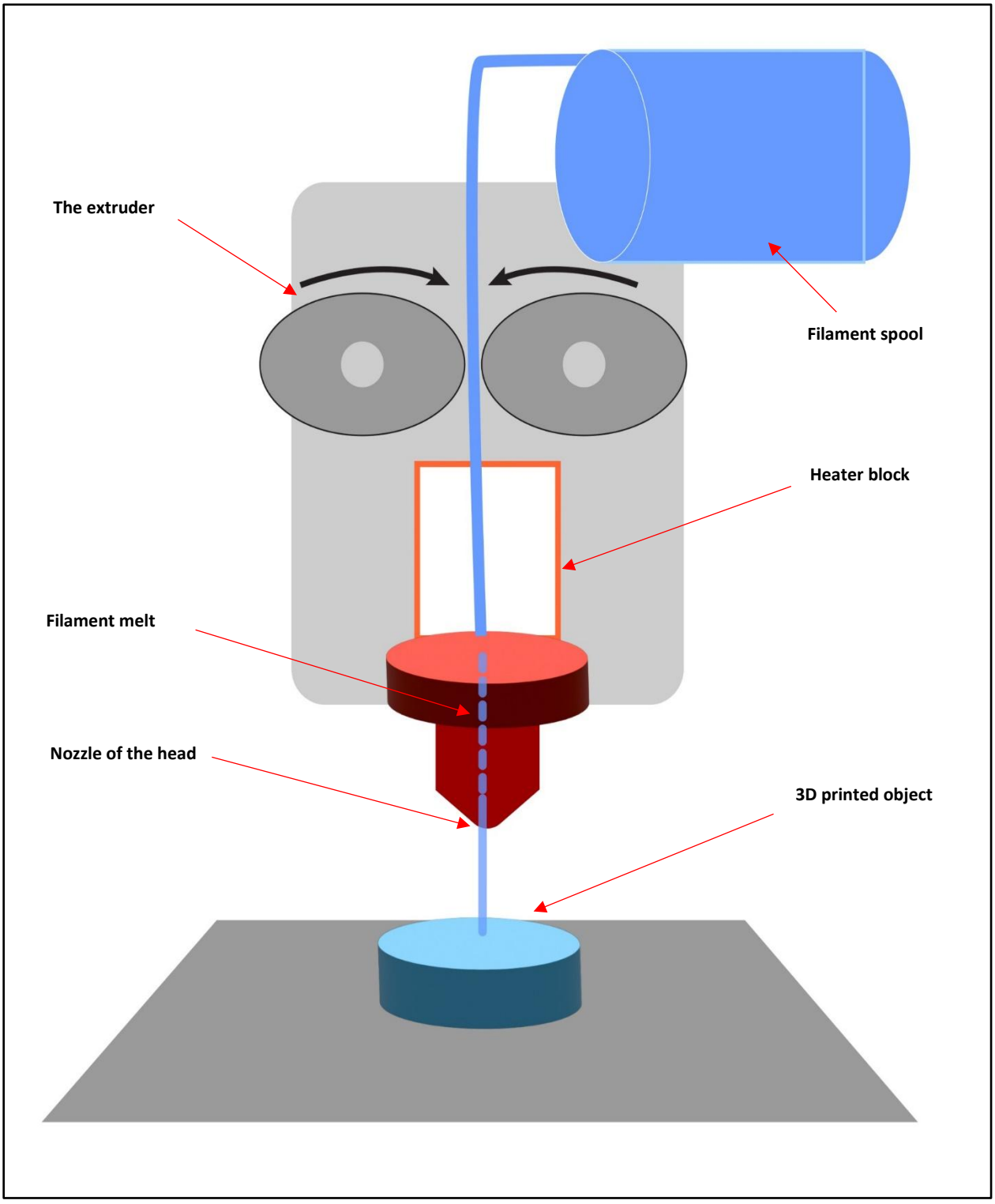

***Figure 1.7**: Schematic diagram of fused deposition modelling 3D printer. Adopted from (Acosta-Vélez & Wu, 2016).*

1.3.5.2. FDM 3D printing critical parameters

Generally, there are three main critical categories controlling the success of FDM techniques: material, operational (processing) and equipment specific parameters. Material specific parameters include mechanical characteristics of feedstocks, melt viscosity and surface morphology. Processing and equipment parameters include the temperature of printing head and build plate, infill density, printing speed, nozzle size and number of feeding heads (Bandari et al., 2021; Nasereddin et al., 2018).

The mechanical characteristics of the feedstock play a crucial role in assessing the suitability of filaments for FDM 3D printing. Filaments derived from HME need to possess sufficient mechanical strength to endure the stresses imposed during loading and printing processes. Inadequate mechanical properties of filaments can lead to breakage and subsequent nozzle blockage. Conducting a thorough filament assessment prior to printing not only ensures efficient fabrication but also prevents issues related to nozzle blockage, ultimately saving valuable time. For example, Zhang et al. conducted a study where they utilised a texture analyser to assess the mechanical properties of filaments manufactured through Hot Melt Extrusion (HME). The prepared filaments were evaluated in terms of flexibility, brittleness, and stiffness, and the results were compared to commercially available PLA filaments. The study found that the stiffness of the filaments increased when extruded at high torque and die pressure. Additionally, filaments with high viscosity due to polymer blend resulted in rough surface textures, which could potentially lead to nozzle blockage in the printer. On the other hand, soft filaments formed a molten mass that was unable to be

extruded from the printer nozzle. Filaments with larger distance at break and forces were identified as being compatible with FDM 3D printers, indicating their suitability for the printing process (Zhang et al., 2019).

The melt viscosity of the feedstock is another critical factor in determining the suitability of filaments for 3D printing. Formulations with high melt viscosity face challenges in extrusion through a 3D printer nozzle due to poor flow of the molten material. However, the addition of plasticisers can decrease viscosity and enhance the extrudability of the molten mass (Johanna Aho et al., 2019). While increasing the temperature of the 3D printer nozzle can potentially reduce viscosity, it is important to consider the potential impact on material degradation. Higher temperatures may lead to undesired chemical reactions or degradation of the material, which can affect the quality and properties of the printed object. Therefore, finding the appropriate balance between melt viscosity, plasticisers, and nozzle temperature is crucial to ensure optimal flow and extrusion of the feedstock during the 3D printing process.

In the context of processing specific parameters, FDM based 3D printing entails complex procedures influenced by multiple parameters that impact the final product's quality and material properties. These parameters encompass bed temperature, nozzle temperature, layer height, infill density, printing speed, and more. Generally, these parameters are specified during the slicing process using software before inputting design and operational parameters into the FDM machine. The interconnection among these parameters forms an intricate combination, posing challenges in understanding and optimising them. Consequently, the optimisation of these parameters plays

a vital role in ensuring the successful fabrication of 3D printed objects. (Carlier et al., 2019; Kristiawan et al., 2021; Parulski et al., 2021).

Lastly, the category pertains to machinery specific parameters, which encompass the type and number of extruders (filament-based or pellet-based), the size of the head nozzle, and the brand and model (the resolution of the 3D printer, a disposable platform used for print initialisation, and calibration methods are some of the factors that can impact the quality and accuracy of the 3D printing process) (Mora-Castaño et al., 2022). These parameters have received relatively limited attention from researchers in the pharmaceutical industry. Modifications primarily focus on enhancing the quality of the final printed object, typically involving adjustments to gear force or substituting the nozzle with one of a different diameter. (Melocchi et al., 2016; Moradi et al., 2019).

1.3.5.3. FDM 3D printing in pharmaceuticals.

The demand for personalised therapeutic interventions, the rising need for intricate drug-eluting products, medical devices, and advanced drug-device combinations, along with the increasing popularity of on demand manufacturing, are significant driving factors that strongly advocate for the utilisation of 3DP technology in the pharmaceutical and biomedical domains (Auriemma et al., 2022).

Taking advantage of the benefits offered by the combination of HME and FDM based 3D printing, numerous research groups have undertaken the development and evaluation of various dosage forms. These include traditional immediate-release tablets and capsules, controlled and modified release formulations, innovative floating systems for improved gastric retention, pulsatile release systems, transdermal and transmucosal delivery systems, as well as personalised implants and devices (Dumpa et al., 2021). Table (1.1) demonstrates examples of fabricated solid pharmaceutical dosage forms developed by the FDM based 3D printing technology.

There has been a significant rise in the quantity of scientific papers indexed in the Web of Science Core Collection that feature the term "3D printing". Specifically, the figures escalated from 513 papers in 2013 to 12071 papers in 2023. This increase highlights the growing interest and exploration of 3D printing across various fields. In the specific domain of pharmacy/pharmacology, focusing on the period from 2019 to 2023, a total of 335 scientific articles were published when considering the categories of "pharmaceutical manufacturing" and "personalised medicine". Among the various 3D printing technologies utilised in these publications, FDM accounted for 58% of the studies, followed by Jet printing at 23%, SLA at 10%, and SLS at 9% as demonstrated in Figure (1.8). These statistics demonstrate the prevalence of different types of 3D printing technologies within the pharmacy/pharmacology field during this time frame.

At the industrial level, during the period from 2020 to 2021, Triastek, a Chinese pharmaceutical and 3D printing technology firm, secured significant funding to advance the development of their first 3D printed product, T19. T19 is a chronotherapeutic drug delivery system created using melt

extrusion deposition (MED) technology and gained acceptance into the FDA's Emerging Technology Program (ETP) in April 2021. Triastek plans to submit a New Drug Application (NDA) for T19 in 2023 (Zheng et al., 2021). Additionally, in June 2023, Triastek completed the first human study for their third 3D printed drug product, T21, designed for the treatment of moderate to severe ulcerative colitis (UC). T21 utilises Triastek's 3D Microstructure for colon targeting, delivering the drug directly to the colon. This marks the first verification of the colon targeting platform in human trials (Triastek, 2023). Moreover, FabRx, a UK-based company established in 2014, is also a prominent player in the field of 3D printed drugs. They have conducted extensive research on various 3D printing (FDM, SLA, SLS) technologies and introduced the M3DIMAKER™ in 2020. This printer enables fast and flexible production of personalised drugs. FabRx is collaborating with the Centre Gustave Roussy to develop customised drugs specifically for the treatment of early-stage breast cancer (Wang et al., 2023).

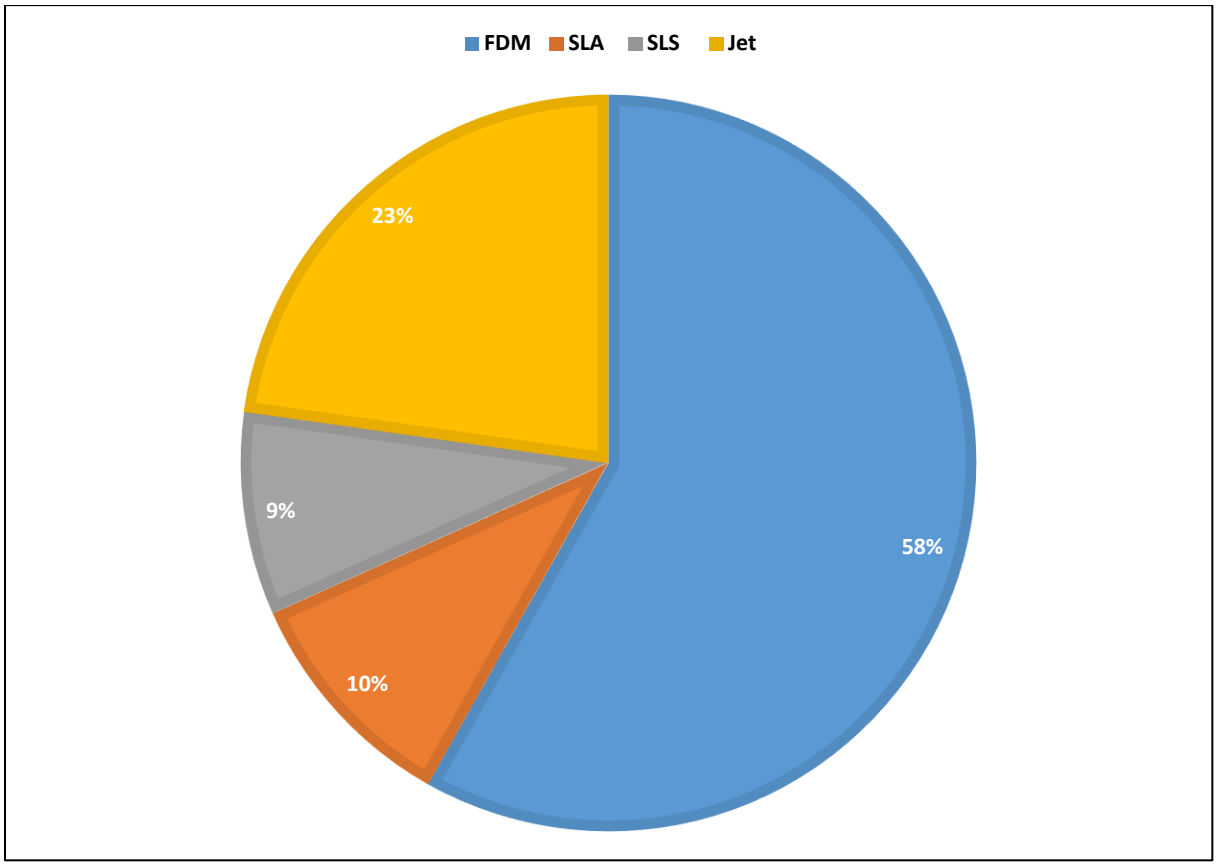

Figure 1.8: *The proportion of scientific articles (research and review) published on different types of 3D printing processes in the last five years (2019-2023, total 325 articles). (Source: Web of science database). Keywords (3D printing, pharmaceutical manufacturing, and personalised medicine).*

Table 1.1: Example of pharmaceutical dosage forms fabricated by FDM 3D printing technology.

Dosage form	API	polymer	Type of release	Ref.
Tablet	- Domperidone	HPC	Sustained release (SR)	(Chai et al., 2017)
	- Hydrochlorothiazide	Eudragit E	Immediate release (IR)	(Sadia et al., 2018)
	- Baclofen	PVA/ Sorbitol	Extended release	(Palekar et al., 2019)
Implants	- Indomethacin	PCL	Controlled release	(Holländer et al., 2016)
Transdermal microneedles	- Estradiol	PLA	Sustained release	(Khosraviboroujeni et al., 2022)
Oral film	- Paracetamol	PVA	Immediate release	(Ehtezazi et al., 2018)
	- Ibuprofen	PEO		
Intravaginal rings	Hydroxychloroquine, IgG	Hydrophilic polyurethanes	Controlled sustained drug delivery	(Chen et al., 2022)

1.4. The role of Computer Aided Design (CAD) software in 3D printing.

Although there are several types of 3D printing technologies, most of them rely on CAD software to create a digital prototype of the desired product. The CAD is the process of using computer software for the creation, manipulation, analysis, and optimisation of virtual 2D or 3D models. Based on the intended application, the CAD can be utilised to create 2D or 3D models. The 2D CAD are usually utilised in engineering and architecture, while the 3D CAD are typically used for prototyping and manufacturing applications such as the 3D printing processing (Junk & Kuen, 2016).

Examples of CAD commonly used in 3D printing designs are AutoCAD, TinkerCAD, Solidwork, SketchUp, Fusion 360 etc. The 3D CAD models are commonly saved as a standard triangle language (STL) file format which is further subjected to slicer software to convert into a 3D printer readable format (G-code). The G-codes contains the slicing information of the CAD object and will accordingly print the object in a layer-by-layer fashion (Junk & Kuen, 2016).

One of the most important future prospects of CAD is the integration of artificial intelligence (AI) application in CAD (Khosraviboroujeni et al., 2022). AI is used to define the capability of how well machines can solve complicated problems by learning and thinking like human being (Y. Xu et al., 2021). With the integrating of AI into the CAD, the lead time will be dramatically reduced and a knowledge-based design environment will be created and improved (Hunde & Woldeyohannes, 2022). In recent times, organisations have successfully implemented AI within their systems to

establish a highly efficient and effective intelligent CAD environment. For example, Dassault Systemes, the company that owns SOLIDWORKS software, stands out as one of the prominent companies that have seamlessly incorporated AI into their design product. The introduction of xDesign by the company incorporates AI as a tool for drawing and extruding in engineering design tasks. With SOLIDWORKS xDesign, users have the ability to quickly access various design solutions through cloud collaboration, generated by the AI tool. The process begins with the user creating the model and establishing the constraints. Subsequently, SOLIDWORKS xDesign utilises AI integration within its system to instantly generate the part based on the user-defined constraint (Le, 2018; Venkataramani et al., 2020).

AUTODESK has developed generative design, which is another AI-based tool used in the field of design and engineering. Generative design utilises AI algorithms to explore and generate multiple design options based on specified constraints and goals. By inputting design parameters such as material, manufacturing methods, and performance requirements, generative design can analyse countless possibilities and generate optimised design solutions. The AI algorithms consider various factors, such as weight reduction, structural integrity, and material efficiency, to create innovative and efficient designs (Gromat et al., 2023). For example, Gromate et al. introduced a new and innovative approach called Generative-Based Design (GBD) methodology, which aims to empower non-technical users to independently create functional components. The uniqueness of this methodology lies in its ability to simplify complex design tasks, making them more accessible to individuals without design expertise. The study applied this methodology to design a load-bearing part, resulting in a functional component after just two design iterations. A comparative analysis

with the traditional CAD-based process showed that the GBD methodology significantly reduced design activities by 68% and decreased the level of design difficulty by 62% in terms of required knowledge and 55% in terms of understanding (Goudswaard et al., 2023).

1.5. Hot melt extrusion (HME) technology

HME is a continuous process that involves the application of heat and pressure to thermoplastic materials, resulting in their melting and subsequent extrusion through a die or orifice. It was first established in 1930s and then became the most widely used manufacturing technology in food, plastic, and rubber processing (Patil et al., 2016). In general, the HME consists of the following main parts: motor, rotating screw, extrusion barrel, heating source and die at the end of the extruder. There has been a significant increase in the number of patents regarding the application of HME in the pharmaceutical preparations since 1980s (Repka et al., 2008).

1.6. Types of hot melt extruders

Regardless of their type, function, or process complexity, the extruders must be able to rotate the screw under controlled conditions (speed, temperature, etc) generating thermal and mechanical energy (Patil et al., 2016). However, HME utilised for pharmaceutical applications must conform to regulatory standards in order to produce dosage forms. The regulatory standards for HME are set by various organisations such as the FDA, the European Medicines Agency (EMA), and the International Conference on Harmonisation (ICH). These organisations provide guidelines on the

quality, safety, and efficacy of pharmaceutical products. For examples, cleaning and sterilisation, screw extruders in pharmaceutical applications require thorough cleaning and sterilisation procedures to prevent cross-contamination and maintain product integrity.

As demonstrated in Figure 1.8, HME can generally be classified into two main types based on the number of screws used:

1.6.1. Single screw hot melt extrusion (SSHME)

The SSHME contains one rotating screw inside the stationary barrel, which is used for feeding, mixing, and pumping of the melted polymer through the die Figure (1-9). Due to its mechanical simplicity and minimal operational principle modifications since its inception in approximately 1897, SSHME represents the predominant choice for utilisation in numerous applications (Douroumis, 2012).

There are three distinct geometrical zones of SSHME, a feed zone (with a constant channel depth), a compression zone (with a decreasing channel depth), and a metering zone (where the screw is shallower) can all be distinguished from the hopper to the die. The length of each zone as well as the maximum and minimum channel depths may vary for the same screw diameter, D, and axial length, L, leading to diverse screw profiles. This, along with the potential to alter the screw speed and set temperatures, might result in extremely different thermomechanical conditions inside the machine, as local heat conduction, heat dissipation, velocity profile, and residence duration may

change substantially (Covas & Gaspar-Cunha, 2011). Table (1.2) summarises some other features of SSHME.

1.6.2. Twin screw hot melt extruder (TSHME)

The TSHME contains two rotating screws inside the stationary barrel Figure (1.9). However, there are different types of TSHME can vary in their mechanism as well as their industrial applications. The screws in TSHME either be co-rotating (same direction) or counter-rotating (opposite direction) as demonstrated in Figure (1.10). A crucial screws design parameter is the ID/OD ratio which refers to the inner diameter (ID) and outer diameter (OD) of the screws used in HME. It determines the free volume and shaft torque that can be provided. As both free volume and torque act as boundary conditions that can potentially impact material throughput rates, it is essential to find the ideal balance between them (Martin, 2016).

The decoupling between output and screw speed is another distinguishing quality of these machines when compared to SSHME. The output of SSHME typically depends on the difference between the drag capacity, which is linearly related to the screw speed, and the sensitivity to the die resistance. This is because SSHME are often flood fed, meaning the raw material accumulates in the hopper. While in TSHME, it operates in a starve fed mode, with specific volumetric or gravimetric feeders controlling the feeding rate. Since the screws function virtually half full as a result, the severity of the thermomechanical stresses can be altered for a given feeding rate by varying the screw speed (Covas & Gaspar-Cunha, 2011). Therefore, TSHME demonstrates superior

efficiency in terms of the extrusion of multiple components, facilitating effective component mixing and ensuring seamless material flow through the extruder barrel. Table (1.2) provides a summary of the distinctive features linked to SSHME and TSHME.

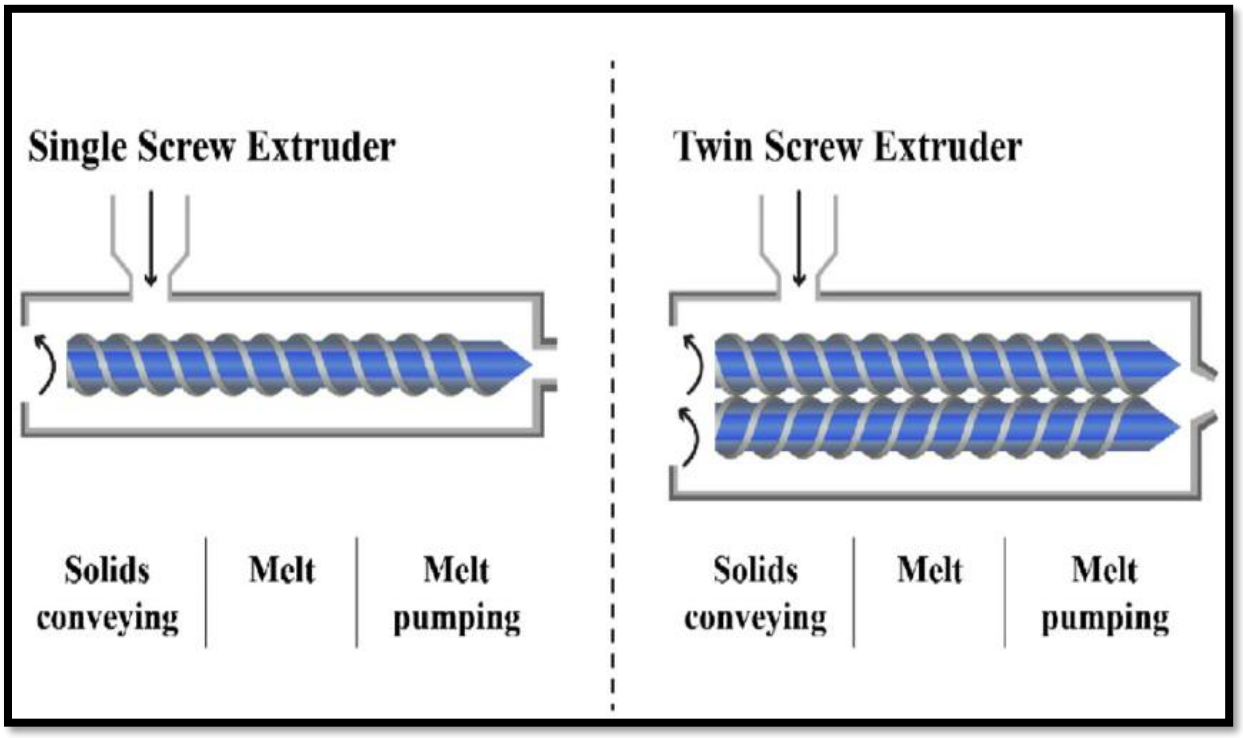

Figure 1.9: *Cross sectional of single screw vs twin screw HME. Adopted from (Patil et al., 2016).*

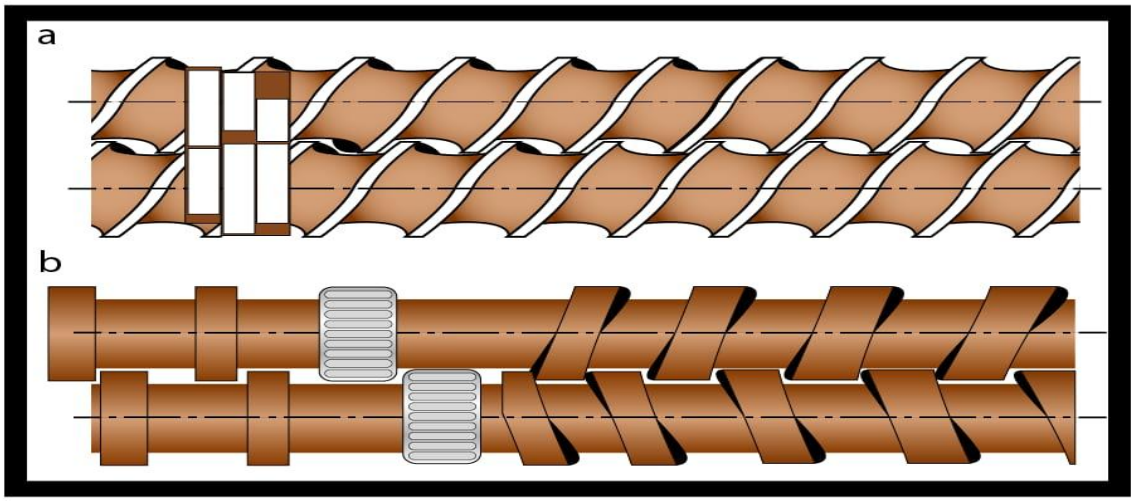

Figure 1.10: *Schematic diagram of co-rotating (a) vs counter-rotating (b) TSHME. Adopted from (Martin, 2016)*.

Table 1.2: Summarises the features of single and twin screw HME (Singhal et al., 2011).

Item	Single screw HME	Twin screw HME
Number of screws	One	Two screws (corotating or counterrotating)
Transport mechanism	Conveyed forward by friction	Positive displacement
Machine cost	Low	High
Mixing efficiency	Poor	Excellent
Shear forces	Large (up to 6000kpa)	Small (up to 4000 kpa)
Degassing	Fair	Good
Energy consumption	Low	High
Feeding	Flood feeding	Starve feeding
Cleaning	Not self-wiping	Self-wiping

1.6.3. Innovations of HME in pharmaceutical applications

There is a claim that around 80% of new chemical entities (NCE) in the drug development pipeline exhibit poor solubility, leading to potential impacts on their effectiveness and bioavailability (Narala et al., 2021). As a result, multiple approaches have been employed to enhance solubility, including methods such as HME, solvent evaporation, spray drying, freeze drying, and high-pressure homogenisation. (Savjani et al., 2012). As indicated by many publications and patents, HME has been utilised widely for the enhancement of water solubility mainly via preparation of amorphous solid dispersions by which the APIs will be molecularly dispersed into the polymer matrix under the influence of heat and shear rate of the HME process (Baghel et al., 2016; Theil et al., 2017).

Apart from previously mentioned method to improve aqueous solubility, further novel techniques have been explored to improve the solubility as well as the stability of HME formulations such as floating drug delivery, pharmaceutical co-crystallisation, reactive extrusion, and co-extrusion for fixed dose (Baghel et al., 2016; Nagy et al., 2012). In regard to the preparation of pharmaceutical co-crystals, Fernandes et al. used HME and achieved a high practical yield of carvedilol co-crystals up to 82.26% using a ratio of 1:2 carvedilol to nicotinamide (Fernandes et al., 2019). In another study, HME has showed its feasibility to develop multicomponent system (MCS) pharmaceutical forms which subsequently improve the bioavailability, solubility and the physicochemical properties of the drugs (Narala et al., 2021) .

1.6.4. Advantages and disadvantages of HME process in pharmaceutical manufacturing

HME process has a significant potential in pharmaceutical manufacturing mainly due to its "continuous processing" feature. The continuous processing is a production method by which products can be synthesised or processed continuously without interruption through a constant supplying of feeding materials (Blevins & Nixon, 2011; Tan et al., 2018).

Hot-melt extruder has a great potential in producing wide variety of pharmaceutical devices from raw materials which considered to be FDA GRAS (Generally Recognised as Safe), such as biodegradable and biocompatible polymers which can be used as drug carriers. Moreover, HME shows its potential role in dispersing the APIs into a desired drug carrier, therefore, enable the masking of unpleasant taste of the active ingredients (Pimparade et al., 2015). HME has many advantages in pharmaceutical manufacturing such as shorter production time, enhancement of the product quality, ability to enhance bioavailability of poorly soluble ingredients as well as the fabrication of modified release formulations by solid dispersion (Maniruzzaman et al., 2012; Patel et al., 2022).

Nevertheless, the utilisation of HME in pharmaceutical manufacturing encounters certain challenges that restrict its applicability. For instance, HME is limited to thermally stable (APIs) due to the requirement of heating and high energy throughout the entire HME process. Consequently, suitable polymers and plasticisers are often necessary for successful formulation in HME processes. (Singhal et al., 2011). Furthermore, the commercial application of HME is impeded by

additional barriers, including a restricted range of compatible polymers, the potential for recrystallisation of amorphous drugs, and the substantial energy input demands. These factors serve as further examples of obstacles that hamper the widespread adoption of HME in commercial settings. (Lu et al., 2014).

1.7. FDM based 3D printing joined with hot melt extrusion technology.

Since the FDM based 3D printing relies on the availability of the filament as feeding materials, HME provides the opportunity to prepare the proper filaments which are suitable to be printed by the 3D printer and at the same time meet the requirements of pharmaceutical manufacturing, such as safety for human consumption, interactions with the API or other excipients (Zhang, Yang, et al., 2017). Figure (1.11) demonstrates the integration of HME with FDM based 3D printing technology in the preparation of pharmaceutical dosage forms as illustrated in. It has many advantages over the traditional pharmaceutical manufacturing which includes simplifying the drug manufacturing process (fewer manufacturing steps) and consequently, it is a cost-effective manufacturing process, enabling the production of more complex dosage forms, improving the bioavailability of poorly water soluble API and clear the way for the development of pharmaceutical solid dispersions free from the organic solvents and with favourable properties (Tan et al., 2018).

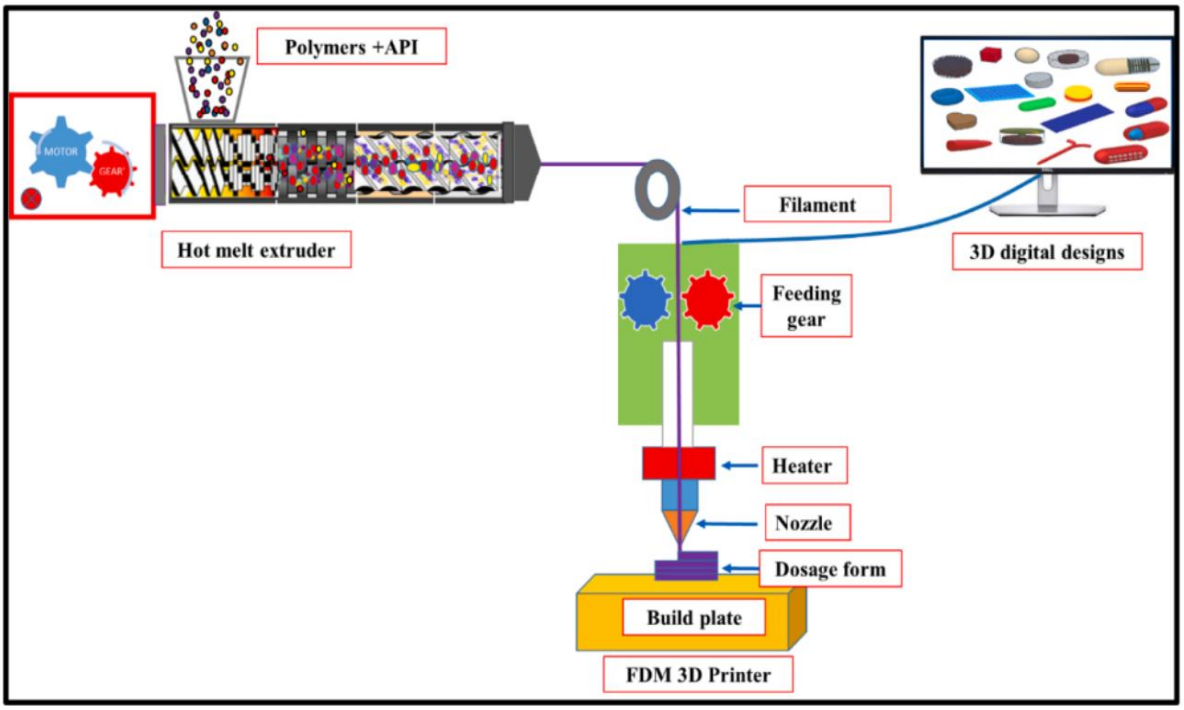

***Figure 1.11**: Graphical diagram depicting the integration of HME and FDM based 3D printing technologies for the fabrication pharmaceutical dosage forms. Adopted from (Dumpa et al., 2021).*

1.8. Examples of polymers used in HME joined with FDM based 3D printing.

Polymers are natural or synthetic substances with high molecular weight formed from many small units that can be attached together with different mechanisms. To be employed in 3D printing for medical purposes, polymers should have two important characteristics: biocompatibility and printability. Biocompatibility means the polymers can be utilised without causing harms to the host or the living organism, while the printability is the polymer's ability to maintain its original structure (Lupuleasa et al., 2018). Most stiff biomaterials such as hard polymers, ceramics and metals are widely used in medical orthopaedic applications, whereas the soft polymers can be used in biomedical engineering to produce soft tissues such as kidney and heart valves (Gasparotti

et al., 2019). The next section discusses some examples of commonly utilised polymers in both the HME and FDM based 3D printing technologies. Tables (1.3) demonstrates a summary of the thermal properties of these polymers, respectively.

1.8.1. Poly vinyl alcohol (PVA)

Polyvinyl Alcohol (PVA) has found application in drug delivery for various APIs, encompassing a range of forms such as hydrogels, films, microspheres, nanoparticles, and more (Gajra* et al., 2012). It is a water-soluble polymer, and its solubility depends on the degree of the polymerisation (DP), temperature, molecular weight and the degree of hydrolysis (Hassan et al., 2000). PVA shows its glass–to–rubber transition at 75–85°C and melts around 180–228°C. The PVA structure becomes more crystallised as the degree of vinyl acetate hydrolysis to vinyl alcohol rises, which is correlated with an increase in intermolecular pressures, melting and glass transition temperatures, and improved solubility in water (Muppalaneni & Omidian, 2013).

1.8.2. Ethylene vinyl acetate (EVA)

EVA is a biocompatible, nondegradable thermoplastic copolymer. It is composed of ethylene and vinyl acetate (VA), with a varying percentage of VA ranging from 0% to 40%. EVA is a non-toxic and water insoluble polymer. It is FDA approved for pharmaceutical applications and is commonly used for controlled release implantable dosage forms. For instance, Genina et al. fabricated indomethacin loaded EVA filament to produce intrauterine devices and subcutaneous rods. The

filaments of different grades of EVA were prepared and the medical devices were successfully 3D printed at temperature slightly above the melting point of indomethacin (Genina et al., 2016).

1.8.3. Polycaprolactone (PCL)

PCL is a semicrystalline hydrophobic polymer. Its crystallinity reduces with rising in molecular weight (Woodruff & Hutmacher, 2010). Due to its relatively low melting temperature (60°C), thermostability, biodegradability and low glass transition temperature (*Tg*) (- 60°C), it is commonly used in biomanufacturing and chemical industries (Liu et al., 2019). For example, it allows to produce scaffolds and other biological soft tissues that require lower stiffness and higher resolutions (Yeong et al., 2010; Zein et al., 2002).

1.8.4. Poly-lactic-co-glycolic acid (PLGA)

PLGA is a hydrophobic copolymer that consists of two monomers: lactic acid and glycolic acid. It is FDA approved for drug delivery (Hawker & Wooley, 2005). Molecular architecture, molar mass and the lactic to glycolic acid ratio are the main parameters controlling the physicochemical properties of PLGA (Kapoor et al., 2015). Due to its biocompatibility, effective biodegradability, ease of processing and mechanical properties, it has been widely employed to create a variety of biodegradable devices, including implants, microparticles, nanoparticles, and in situ-formed devices (Lü et al., 2009) . For application in 3D printing, Feuerbach et al., used PLGA to produce filament suitable for FDM based 3D printing. A filament with 1.75 ± 0.05 mm was produced by a

continuous HME process. However, the results indicated a direct proportion between thermal degradation and hydrophilicity (Feuerbach et al., 2019). Therefore, the degree of hydrophilicity should be considered during the HME process and more importantly in case the API has high degree of hydrophilicity as well.

1.8.5. Polyethylene glycol (PEG)

PEG is suitable for biological applications for the following reasons: soluble in water and organic solvents, low risk of toxicity and has a polydispersity index (PDI) below 1.1. The PDI is an important parameter the reflects the spread or width of the particle size distribution (Danaei et al., 2018). Compounds with PDI less than 1.1 provide a homogenous and suitable residence time in the body (Knop et al., 2010). PEG with low molecular weight (MW) up to 700 are colourless viscous liquids that can be used as a plasticiser in coating formulations, while PEG with MW of 6000 and above is used as a lubricant (D'souza & Shegokar, 2016; Shahbazova & Masimov, 2022). Additionally, PEG can be employed in solid dispersions via HME to enhance the solubility of poorly soluble drugs and to enhance the mechanical characteristics of drug loaded filaments produced. (Alhijjaj et al., 2016; Sharma & Jain, 2011).

1.8.6. Hydroxypropyl methyl cellulose (HPMC)

HPMC is a hydrophilic, thermostable polymer which is widely used to produce controlled-release pharmaceutical formulations (Yi et al., 2019). However, its applications via HME were constrained

by their high *Tg* points (184–191°C) and melt viscosity (Meena et al., 2016). Therefore, HPMC requires the addition of plasticisers or other additives to be applicable for HME (G. G. Pereira et al., 2020).

1.8.7. Polylactic Acid (PLA)

PLA is a biodegradable polymer that can degrade through the hydrolysis of its ester groups. It is also biocompatible with body fluids, making it suitable for various biomedical applications. PLA has gained popularity in these fields since it was classified as GRAS by the FDA. PLA has about 37% crystalline structure with a *Tg* of 60 to 66°C , heating resistance of 110°C and melting point at 173 – 178°C (Farah et al., 2016). In a wide range of medical applications, including tissue engineering, drug carriers, cardiovascular implants, orthopaedic treatments dental specialties, drug carriers, cancer therapy, skin and tendon mending, and medical tools and equipment, PLA has demonstrated potential as a biomaterial (DeStefano et al., 2020).

Additionally, PLA is one of the mostly utilised thermoplastic materials available for 3D printing (Tümer & Erbil, 2021) due to its good extrusion processability, low thermal expansion coefficient and high mechanical strength (Chiulan et al., 2017). As a result of the non-toxic degradation products generated by PLA, it has obtained FDA approval for its utilisation in direct contact with body fluids (DeStefano et al., 2020).

1.8.8. Polyvinyl caprolactam polyvinyl acetate-polyethylene glycol graft co-polymer (Soluplus®)

Soluplus is an amphiphilic polymer with low *Tg* of 70°C. This characteristic makes it suitable for use as both a solubilising agent and an excellent candidate for extrusion processes at relatively low temperatures. Moreover, Soluplus has advantage of low hygroscopicity which would assists to stabilise the APIs/Soluplus dispersion during the storage. However, poor dissolution and recrystallisation might occur with drug loading more than 10% (Alshahrani et al., 2015; Liu et al., 2010). As established by Hardung et al., Soluplus can boost carbamazepine solubility by up to 5 times regardless of pH, due to its non-ionic character, making it a prime choice for the creation HME solid dispersions (Hardung et al., 2010).

Table 1.3: Summary of thermal properties.

Polymer	Glass transition temperature (°C)	Melting temperature (°C)	Decomposition Temperature (°C)	Ref.
1- PVA	75-85	180-228	220–250	(Goole & Amighi, 2016; Konta et al., 2017; Reguieg et al., 2020)
2- EVA	–40	90-120	300–450	(Arsac et al., 2000; Marín et al., 1996)
3- PCL	–54	55–60	430	(Bartnikowski et al., 2019; Goyanes et al., 2016; Patlolla et al., 2010)
4- PLGA	38	170-230	-	(Lanao et al., 2013; Park, 1995)
5- PEG	–52	16 - 42	325–426	(Kou et al., 2019; Li et al., 2021)
6- HPMC	157	225-230	336	(ChemBK, 2023; Li et al., 1999; Sakellariou et al., 1985)
7- PLA	51 - 57	173–175	375	(Chen et al., 2003; Wang et al., 2018)
8- Soluplus	70	135-140	297	(Altamimi & Neau, 2018; Hardung et al., 2010)

1.9. Advantages of using 3D printing in pharmaceutical and medical sectors.

1.9.1. In pharmaceutical applications

Over the past three decades, the application of 3D printing technology has been increasingly adopted in the design and development of various pharmaceutical drug products (Mahmood et al., 2023). The following sections outline some advantages behind the utilisation of 3D printing technology in pharmaceutical manufacturing, highlighting its advantages over conventional drug manufacturing methods.

1.9.1.1. Personalised medicine

The current scenario of healthcare treatment is based on “one size fits all” approach where patients are treated with same drug, same dose, and frequencies regardless of their interindividual variabilities (Litman, 2019). This drug administration system has shown varied responses in different individuals with no therapeutic or weak therapeutic effect or adverse effects (Prodan Žitnik et al., 2018). Therefore, this needs a paradigm shift in the drug treatment system towards the personalised medicine (PM). Based on the pharmacogenomic profile of an individual patient, the drug treatment is tailored specifically to individual patient with precise dose, drug, and frequencies (Florence & Siepmann, 2016). This can lead to safer drug treatment with high efficacy and less adverse drug reactions (Mathur & Sutton, 2017).

As the technological development is progressing, 3D printing technology has limitless potential for producing patient-specific drug delivery devices (DDD) and dose forms. The ability of 3D printing to create DDD prototypes with varied levels of complexity demonstrates that drug products can be customised (Sandler & Preis, 2016). Therefore, with the advancement in genomics, the 3D printing techniques are gaining much attention for designing personalised dose medicines (Alomari et al., 2015). In the future and with the advent of personalised medicine, the fabrication of pharmaceutical dosage forms is likely to be shifted to the site of dispensing to encourage the remote and controlled provision of outpatient services (Sadia et al., 2016).

1.9.1.2. Polypills dosage forms

Polypills, also known as fixed-dose combination pills, are pharmaceutical dosage forms characterised by a single tablet or capsule composition that combines three or more drugs (Teo & Yusuf, 2018). The concept of Polypills can be customised to suit geriatric patients who are undergoing polypharmacy, offering enhanced compliance by reducing the number of pills they need to consume on a daily basis. An example of this is the work by Khaled et al., who implemented 3D printing technology to create polypills comprised of five drugs. The tablet consisted of three sustained release chambers containing pravastatin, atenolol, and ramipril, along with two immediate release compartments containing aspirin and hydrochlorothiazide. This configuration represented a cardiovascular therapy plan tailored for the specific needs of the patient (Khaled et al., 2015).

Moreover, a customised release profile of polypills capsule containing multiple drugs was achieved by utilising FDM based 3D printer combined with hot-filling syringes as shown in Figure (1.12). Two capsule skeletons with four distinct compartments were developed; one had a parallel configuration with non-dissolving capsule shells with free pass corridors and dissolution rate limiting pores used to achieve early and retarded release, and the other had a concentrical configuration with two outer compartments for early release and two inner compartments for retarded release. PLA and PVA were utilised to create the capsule's outer shell. By adjusting the size of the rate limiting orifices in the parallel configuration, Figure (1.12 A), or the thickness of the shell in the concentric configuration, Figure (1.12 B), a customised release profiles were achieved (B. C. Pereira et al., 2020).

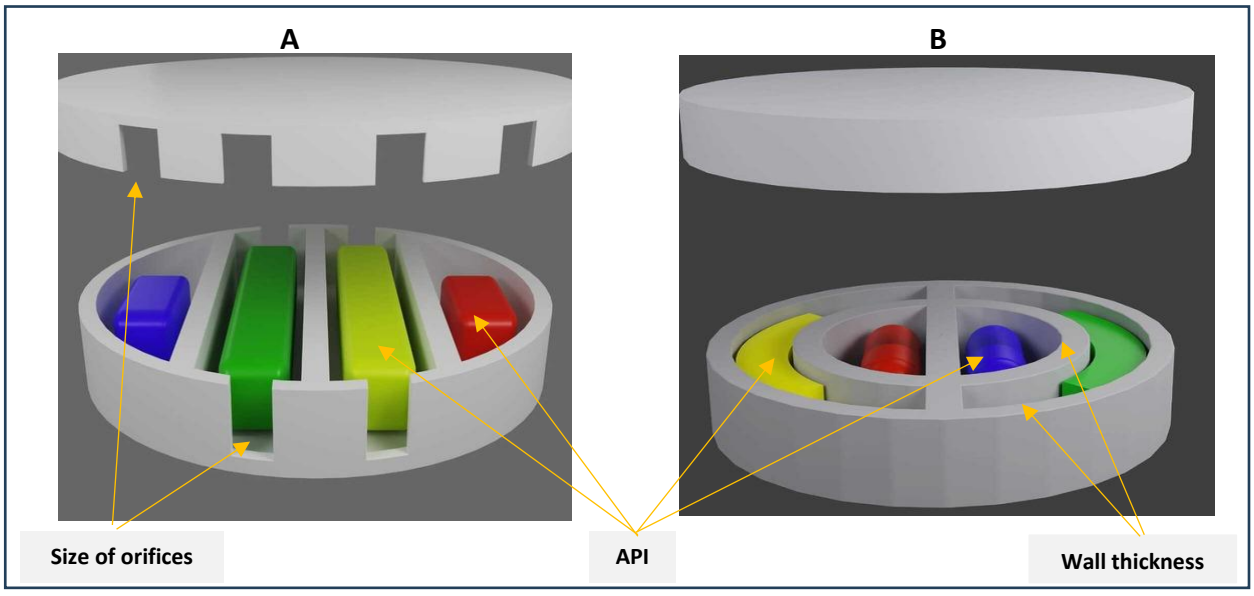

Figure 1.12: *CAD image of 3D printed polypills, (A): parallel configuration, (B): concentric configuration. Adopted from (B. C. Pereira et al., 2020).*

1.9.1.3. Paediatrics dosage forms

Even though oral administration may appear most practical, it can be challenging when dealing with children due to their personal preferences such as shape, smell, or the taste of the dosage forms. For instance, one study has concluded that children prefer minitablets of a diameter of 4 mm over other dosage forms (Trenfield et al., 2019) and another study has found that orally disintegrating strip (ODS) dosage forms are more appropriate for usage in children's medicine than oral powders in unit-dose sachets (Öblom et al., 2019).

3D printing may be useful when it comes to meeting children's specific preferences. For example, Goyanes et al. has successfully fabricated 3D printed chewable tablets with various colours (green, yellow, orange, etc) and different flavour (banana, raspberry, lemon, etc) and were found accepted by children and can be used to advance the development of PM (Goyanes et al., 2019). In a different study, chewable chocolate-based dosage forms in a variety of shapes were effectively fabricated by 3D printing (Karavasili et al., 2020).

1.9.1.4. Nanomedicine

The application of 3D printing techniques extends beyond solid polymeric drug delivery systems and includes the fabrication of lipid based nanomedicine. For instance, Johannesson et al. fabricated lipid based solid tablets of fenofibrate from emulsion gel. The tablets were printed using a semisolid extrusion printer at room temperature. The hydrogel paste for 3D printing purpose was prepared from oil in water emulsions with the incorporation of methylcellulose and

croscarmellose sodium. The printed tablet showed rapid disintegration in less than 15 minutes. The oil droplet constitution after dispersion of 3D printed tablets was similar to liquid lipid-based emulsions (Johannesson et al., 2021).

In another occasion, polymeric PCL nano-capsules containing curcumin and resveratrol were 3D printed as solid dosage form by incorporating carboxymethyl cellulose hydrogel using PAM 3D printing technique (W. Xu et al., 2021). Similarly, self-nanoemulsifying drug delivery system (SNEDDS) tablets were also fabricated from self-Nano emulsifying liquid based formulations using 3D printing technique (Algahtani et al., 2021).

1.9.2. Advantages of 3D printing in medical applications

In medicine, 3D printing has many potential applications such as developing educational and training tools as well as the fabrication of personalised organs, which would improve preoperative planning and decrease the probability of organ rejection in the case of organ grafting (Ploch et al., 2016). 3D Printing of metallic biomaterials comprising of iron, zinc, cobalt, magnesium, titanium, and stainless steel are gaining much more attention in the medical field. Iron-based alloys used in the fabrication of temporary cardiovascular stents (Francis et al., 2015). Moreover, stainless steel alloys are used in the design of artificial heart valves, needles, catheters and orthopaedic implants (Yang & Ren, 2010). Titanium is used in orthopaedic and dentistry (Jakubowicz, 2020) and similarly Zinc is used to fabricate orthopaedic devices, cardiovascular stents and wound closure devices via 3D printing technique (Liu et al., 2022).

1.10. Limitations of 3D printing technology in pharmaceutical applications

Despite the significant potential and extensive research being conducted on 3D printing technology for pharmaceutical product and medical device manufacturing (Mathew, Pitzanti et al. 2020). However, certain limitations exist that require careful attention and optimisation to maximise its application. The following are example of these limitations:

1.10.1. Technology related issues.

Nozzle clogging, poor bed adherence, stringing and printing of overhanded objects are some examples of technical issues that frequently lead to the failure of FDM based 3D printing process.

1.10.1.1. Nozzle clogging

Nozzle clogging, as demonstrated in Figure (1.13 A), occurs when the extrusion nozzle becomes partially or fully blocked due to various factors such as debris, poor quality filament, or improper temperature control. This can result in inconsistent material flow or even complete blockage, leading to gaps or interruptions in the printed object (Kim et al., 2015). Currently, the operator of the machine identifies the occurrence of clogging, halts the printing process, manually cleans the nozzle, and restarts the fabrication of the part from the beginning.

One potential solution for nozzle clogging is to create a technique for monitoring the condition of the nozzle during the process of 3D printing. Tlegenov et al. proposed a nozzle condition

monitoring technique in FFF 3D printing to monitor the nozzle clogging using an accelerometer sensor by measuring extruder's bar mount vibrations (Tlegenov et al., 2018). Additionally, Wu et al. proposed an in-situ monitoring approach for assessing the condition of a fused filament fabrication (FFF) machine using the acoustic emission technique. They utilised time-domain features extracted from acoustic emission data to identify various abnormal states of a 3D printer, including material depletion, partially blocked extruder, and completely blocked extruder, through experimental analysis (Wu et al., 2016).

1.10.1.2. Poor bed adherence

Bed adherence, as demonstrated in Figure (1.13 B), refers to the ability of the printed object to adhere securely to the printing bed during the printing process. Insufficient bed adhesion can cause the printed object to detach or warp during printing, resulting in a failed print (Carneiro et al., 2015). Therefore, it is crucial for the extruded polymer to exhibit strong adhesion to the printing bed during the printing process to ensure the stability of the printed object. However, once the printing is completed, the adhesion should be reduced to facilitate easy removal of the part from the printing bed without causing any damage to the produced object or the bed surface (Gonzalez-Gutierrez et al., 2017).

To enhance the adhesion of the first layer to the printing bed, there are several recommended approaches. Firstly, it is advised to thoroughly clean the printing surface to eliminate any grease, or residues present on the bed. Secondly, ensure the printing bed is properly levelled to ensure

close contact between the first layer and the bed. Thirdly, incorporating adhesion support such as a brim or raft can provide a larger contact area and improve adhesion. Additionally, lightly sanding the tape can increase its surface roughness. Applying water-soluble glues, hair sprays, or special coatings can also improve adhesion. Printing on a plate or film made of the same material being printed is another strategy. Lastly, increasing the temperature of the printing bed to the recommended value for the specific material being used is beneficial (Devicharan & Garg, 2019; Hsiang Loh et al., 2020; Spoerk et al., 2018).

1.10.1.3. Stringing

Stringing, as demonstrated in Figure (1.13 C), refers to the occurrence of thin strands or strings of material between different parts of the printed object where they should not be present. It occurs when the material continues to ooze or drip from the nozzle while moving between different print locations. This issue can lead to undesirable visual defects and affect the overall quality of the printed object (Nuchitprasitchai et al., 2017).

To address the stringing issue in 3D printing, several scientific solutions can be implemented. These include adjusting retraction settings to increase distance and speed, optimising print temperature to reduce filament viscosity, increasing travel speed between printed parts, enabling features like Z-hop or retraction on travel, configuring cooling fans properly, using high-quality filament, adjusting retraction prime settings, employing post-processing techniques like trimming or sanding, and conducting systematic experimentation to fine-tune settings. By implementing these

solutions, stringing can be minimised or eliminated, leading to improved print quality (MorCh, 2023; SIMPLIFY3D, 2023). Moreover, using AI to address the stringing issue in 3D printing is an innovative approach that can potentially yield positive results. For example, Paraskevoudis et al., developed a neural network for identifying 3D printing defects during the printing process through an AI-based computer vision. Specifically, an AI model, Deep Convolutional Neural Network (DCNN), was trained on images that clearly show the stringing issue in 3D printing. This AI model was then deployed in a live environment to detect and predict stringing occurrences based on a video camera feed. By utilising this AI model, real-time detections and predictions can be made during the printing process, allowing for prompt adjustments to mitigate or prevent stringing (Paraskevoudis et al., 2020).

1.10.1.4. Over-hanged objects

Over-hanged objects, as demonstrated in Figure (1.13 D), are structures or features that extend beyond the support of the underlying layers. If the angle created between the printing Z axis and overhangs is below 50°, these overhangs are generally considered to have minimal impact. However, for any steeper angle, can result in the collapse or deformation of the overhanging parts if adequate precautions are not implemented (Barile et al., 2020).

In order to tackle this challenge, one of the possible approaches is to adopt the "design for printability" technique, which involves considering specific design criteria during the object-design stage. The goal is to create a functional and supportless 3D printable object. However, it is important to note that this process can be complex and challenging, and it may not always be

feasible to achieve a completely supportless design (Ma et al., 2015; Mohammed et al., 2017). An alternative approach is to divide a complex design into multiple sub-blocks that are individually 3D printable without the need for support structures. This method can save material by avoiding the generation of supports. However, it introduces a post processing step for assembling, adhering, and polishing the individual printed parts. This additional step can be time-consuming and may potentially impact the overall quality of the printed object. Careful consideration should be given to ensure proper alignment, stability, and surface finish during the post processing stage to achieve the desired final quality of the assembled object (Wei et al., 2017).

Another effective solution entails utilising software capable of automatically generating support structures to ensure stability for floating or overhanging structures during the 3D printing process. These supports come in two primary types: non-dissolvable (standard) and dissolvable. Non-dissolvable supports are typically printed using the same material as the object itself and necessitate manual removal after printing, making them suitable for single extrusion 3D printers. On the other hand, dissolvable supports are constructed using a separate material that can be dissolved or removed through specific solutions (the object only needs to be submerged in water or acetone), eliminating the need for manual support removal. However, the implementation of dissolvable supports requires a dual-extrusion setup, resulting in higher machinery costs. It is important to note that both methods have inherent limitations, including increased printing time and material waste (Barile et al., 2020; Duran et al., 2015).

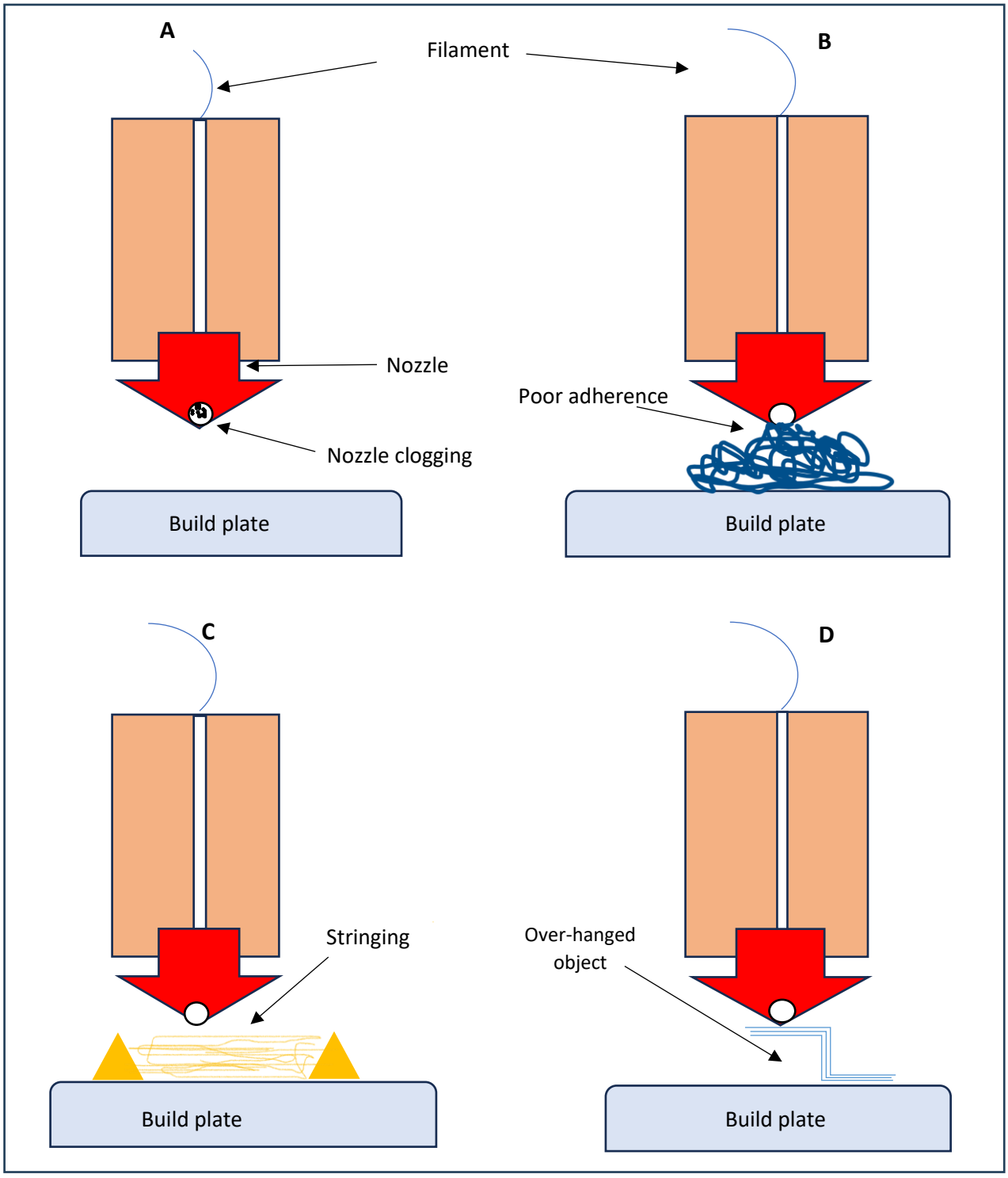

***Figure 1.13**: Diagram illustrates different types of machinery issues (A): nozzle clogging, (B): poor adherence; (C): stringing and (D): Over-hanged object.*

1.10.2. Material related issues.

The range of materials available for printing has experienced exponential growth in the past decade (Hospodiuk et al., 2017; Lee et al., 2017). However, there are still various challenges, primarily associated with filament properties and materials, that restrict the widespread adoption of 3D printing in pharmaceutical production. The mechanical properties of filaments, including parameters like elastic modulus and strain at yield, along with the viscosity of the melted state, have a profound influence on the filament extrusion process in 3D printing. Furthermore, rheological properties such as viscosity, surface tension, and relaxation dynamics have a significant impact on layer adhesion and intralayer bonding, thereby affecting the precision and resolution of printed objects. Additionally, thermal properties, including conductivity, heat capacity, coefficient of thermal expansion, and crystallinity, play a critical role in determining the process parameters. These thermal properties can contribute to challenges such as fibre shrinkage and warpage (Kjar & Huang, 2019; Tan et al., 2020).

Moreover, there is also a limited supply of regulatory approved pharmaceutical grade materials with which to manufacture filaments, as well as the influence of high temperature on thermolabile APIs. Another issue is the difficulty to prepare drug loaded filaments with suitable properties such as elasticity, homogeneity of drug distribution and the limited availability of biocompatible and biodegradable polymer blends (Jamróz et al., 2018; Lamichhane et al., 2019).

1.10.3. Safety aspects

Some materials may release toxic airborne particles during heating, extrusion, and fusing that could irritate the skin or respiratory system. As a result, conventional manufacturing guidelines and safety precautions should be acquired and appropriately implemented to reduce the likelihood of such a hazardous exposure (Gioumouxouzis et al., 2019).

By implementing proper ventilation, utilising personal protective equipment (PPE), maintaining a clean workspace, and providing adequate training, the risk of exposure to harmful substances can be effectively minimised, ensuring a safer working environment for all individuals involved in 3D printing operations.

1.10.4. Regulatory framework

The absence of a regulatory framework for the manufacturing of pharmaceuticals is a notable challenge when it comes to implementing 3D printing technology in this field. The regulatory landscape for traditional pharmaceutical manufacturing is well-established, with rigorous guidelines and standards in place to ensure the safety, efficacy, and quality of pharmaceutical products. However, these regulations do not adequately address the unique considerations and complexities associated with 3D printed pharmaceuticals (Karalia et al., 2021).

Despite this regulatory gap, there has been some progress in the approval of 3D printed pharmaceutical products. In 2015, the FDA granted approval for the first 3D printed medication,

Spritam, which is used to treat epilepsy. This milestone demonstrated the potential of 3D printing in the pharmaceutical industry and opened up new possibilities for personalised medicine and dosage customisation. However, the approval of Spritam does not indicate a comprehensive regulatory framework for 3D printed pharmaceuticals. The existing regulations primarily focus on the 3D printing of medical devices rather than pharmaceutical products . In 2017, the FDA issued guidance on technical considerations for additive manufacturing of medical devices, providing some direction for manufacturers in terms of quality control and documentation requirements. However, this guidance does not cover the specific aspects related to pharmaceutical manufacturing, such as drug formulation, release mechanisms, and dosage accuracy.

To fully harness the potential of 3D printing in pharmaceuticals, comprehensive regulations are necessary. These regulations should address critical aspects, including the materials used, the printing process, quality control measures, post-processing requirements, and the validation of 3D printed pharmaceutical products. Additionally, considerations for intellectual property, supply chain management, and distribution should also be considered. Efforts are underway to bridge this regulatory gap. Regulatory agencies, industry stakeholders, and researchers are collaborating to develop guidelines and standards for 3D printed pharmaceuticals. These efforts aim to ensure patient safety, product quality, and regulatory compliance while fostering innovation in the pharmaceutical industry (Vaz & Kumar, 2021).

1.10.5. Anti-counterfeiting

Due to the lack of regulations and easy manufacturing at low costs, the fraudulent medicines would be a challenge in implementing 3D in pharmaceutical manufacturing. Trenfield, Tan et al. has produced a novel anti-counterfeit measures which use quick response (QR) code that can be scanned by smartphone device. It contains the information such as the drug product, the prescriber, and the patient information. This innovative method would improve the transparency and tracking of 3D-printed pharmaceuticals across the supply chain, providing patients with a safer treatment options (Trenfield et al., 2019). Moreover, FabRx has introduced the M3DIMAKERTM 3D printer, specifically designed for the production of personalised medicines. They have recently announced an upgraded version called Mark II M3DIMAKER, which offers enhanced features such as multi-nozzle functionality, higher throughput, and increased automation. Importantly, to ensure the system's operation is limited to authorised users only, security measures such as fingerprint access control and a data matrix reader are implemented. These features help prevent unauthorised use of the system and enhance its overall security (Rodríguez-Pombo et al., 2022; Timothy Tracy et al., 2023).

1.11. Aim and objectives.

Considering the emergence of 3D printing technology as a significant technological revolution, the aim of this research project is to explore the feasibility of utilising FDM based 3D printing technology for the manufacturing of solid pharmaceutical dosage forms, including oral tablets, implants, and novel drug delivery devices. This will be achieved via the following objectives:

- The first objective is to employ CAD software, such as AutoCAD and TinkerCAD, to develop the virtual digital design of the desired pharmaceutical dosage forms.

- The second objective is to prepare and characterise diverse drug loaded polymer formulations that will serve as the feedstock for synthesising pharmaceutical dosage forms utilising HME technology.

- The third objective is the utilisation of FDM based 3D printer to manufacture various types of pharmaceutical dosage forms.

- The fourth objective is to investigate the influence of various 3D printing parameters and designs including infill percentage, infill pattern and layer height on the properties and *in vitro* drug release of the manufactured dosage forms.

Chapter 2 EXPLORING THE IMPACT OF VARIOUS 3D PARAMETERS ON THE PHYSICAL ATTRIBUTES OF FABRICATED DRUG FREE ORAL DOSAGE FORMS

2.1. Introduction

In the pharmaceutical field, it is widely recognised that solid oral dosage forms (SODFs) like capsules, tablets, and orally disintegrating tablets are the most convenient and favoured administration route (Hartzke et al., 2022). Noteworthy benefits of SODFs encompass self-administration, ease of handling, stability, transportability, and good patient adherence (Arshad et al., 2021). However, offering customised dosages, particularly for children and elderly individuals, poses a difficulty. Therefore, tablets often necessitate adjustment by healthcare providers and family members, such as manually dividing them, employing knives, or utilising dedicated tablet splitters (Januskaite et al., 2020).

Over the last three decades, the scope of 3D printing has witnessed substantial expansion, and its utilisation in pharmaceutical manufacturing is advancing at a rapid pace (Charoo et al., 2020). The technology has advanced considerably, enabling the production of complex structures and precise dosage forms with customised features (Derick Muhindo et al., 2023). Many 3D printing technologies have been explored for manufacturing SODFs. Within this realm, the prevalent methods utilised in the production of SODFs include extrusion based 3D printing, powder based 3D printing, vat photopolymerisation, and inkjet 3D printing.

Among various 3D printing methodologies, FDM based 3D printing technology has been extensively researched for the production of pharmaceutical dosage forms (Brambilla et al., 2021). This examination is driven by its cost effective attributes, operational simplicity, and ability to generate intricate shapes and geometries beyond the capabilities of conventional powder compaction techniques (Bandari et al., 2021). However, there is currently no FDM printer specifically engineered for pharmaceutical applications. Instead, mainstream printers like those belonging to the MakerBot® series, originally intended for plastic prototype fabrication, are commonly utilised in the creation of pharmaceutical dosage forms, as evidenced in diverse academic studies (Alhijjaj et al., 2016; Oladeji et al., 2022; Solanki et al., 2018; Zhang et al., 2024).

Therefore, the ability of FDM printer to produce pharmaceutical dosage forms with aesthetically pleasing geometries presents a challenge in its integration within the pharmaceutical industry (Mohamed et al., 2016). Multiple factors affect the quality of final 3D prints, including material properties, 3D printing parameters, design complexity, environmental conditions, and others.

The primary objective of this experimental chapter is to examine the influence of various 3D parameters such as infill percentage, layer height, printing speed, and infill pattern on the physical attributes of fabricated drug free tablets. The analysis will explore their effects on the weight, density, and dimensions of the manufactured tablet specimens.

2.2. Materials and method

2.2.1. Materials

Poly-lactic acid (PLA) commercial feedstock filaments, 1.75 mm in diameter, print temperature (200-220°C), purchased from Verbatim GmbH (Hesse, Germany).

2.2.2. Investigating the influence of 3D parameters on the physical properties of fabricated placebo dosage forms.

2.2.2.1. CAD digital design of the desired dosage forms.

CAD software TinkerCAD (Autodesk Inc., CA, USA) was used to produce the digital design of a cylindrical tablet with dimensions of 10 and 5 mm for the tablet diameter and height, respectively. The chosen dimensions of the tablet were selected to meet two objectives: first, to ensure that the 3D fabricated tablet contains a sufficient quantity of the drug for analysis purposes, and second, to be smaller than the largest dimensions of tablet recommended by the FDA which set at 22 mm (Research, 2022). The designed digital form was exported as STL file. The STL format encodes only the superficial data providing information solely regarding the shape and structure of the object's exterior surfaces. This format does not encompass or include details regarding internal features or volumetric properties of the object. To define the interior details and specific printing instructions, the STL file needs to be converted into Gcode using Cura software (version 3.0, Ultimaker, Netherland).

2.2.2.2. The different 3D printing parameters to be investigated and the reasons for their selection.

Four different 3D parameters were applied to investigate their influence on the fabricated dosage form including: infill percentage, layer height, infill pattern and printing speed. These parameters were adjusted during the slicing process of the digital design. Infill pattern refers to the internal structure that fill the empty spaces within the outer shells of a printed object. Figure (2.1) demonstrates the schematic shape of the three different infill patterns that were chosen to be investigated in this experiment.

The rationale for selecting and investigating these parameters to assess their impact on physical properties, including weight, dimensions, and density, of fabricated 3D printed dosage forms in this experiment is motivated by the following considerations:

Firstly, these types of parameters have been chosen due to their direct influence on the physical properties of the final 3D printed objects and their practical adjustability within the printing process. Secondly, in the field of pharmaceutical applications, where FDM printed objects are intended for use as oral solid dosage forms, the attainment of precise and highly reproducible dimensions and weight assumes critical importance. The meticulous control over these properties is essential to guarantee the efficacy and reliability of the dosage forms, ensuring consistent drug delivery and patient safety (Alhijjaj et al., 2019). Thirdly, the literature is largely concerned with the influence of different 3D printing parameters on the mechanical properties of 3D printed objects with little attention to the physical properties. For example, the influence of different 3D

printing parameters on the impact strength (Mishra et al., 2021), on the flexural strength (Nugroho et al., 2018), on the tensile strength and Young's modulus (Moradi et al., 2021) and on the mechanical strength (Al Rashid & Koç, 2022) etc. Therefore, this work is conducted to investigate the influence of these different 3D printing parameters on the physical properties of fabricated 3D printed tablet and to determine which one of these parameters exhibits the highest degree of influence and the extent of its impact.

2.2.2.3. Prepared formulations and 3D printing conditions.

Placebo tablets were manufactured from drug free PLA filament through using a standard FDM based 3D printer (Prusa i3, Czech Republic). The specific 3D printing conditions employed during the process are outlined in Table (2.1). All 3D printing operations were conducted at room temperature. The printing temperature and build plate temperature were adjusted according to the recommendations provided by the filament manufacturer. Nine different formulations were prepared, as illustrated in Table (2.2).

Table 2.1: 3D printing conditions of placebo tablet.

Printing conditions	Option/value
Feeding material	PLA commercial filament (drug free)
Printing temperature (nozzle)	205˚C
Build plate temperature	60˚C
Nozzle size	0.4 mm
Filament diameter	1.75 mm
Adhesion support	Brim
Resolution	Standard

Table 2.2: Different types of prepared formulations.

FORMULATION NO	INFILL (%)	LAYER HEIGHT (mm)	INFILL PATTERN	PRINTING SPEED (mm/s)
F1	25	0.2	Line	75
F2	50	0.2	Line	75
F3	100	0.2	Line	75
F4	50	0.1	Line	75
F5	50	0.3	Line	75
F6	50	0.2	Triangle	75
F7	50	0.2	Zigzag	75
F8	50	0.2	Line	50
F9	50	0.2	Line	100

2.2.2.4. Determination of the impact of different 3D parameters on the physical properties of printed placebo tablets

The weight of the fabricated placebo tablets was measured using a VWR® T electrical balance (Leicestershire, UK), while the dimensions of the tablets were assessed using a digital calliper Digimax Camlab (Cambridge, UK). The volume of the fabricated tablets was determined using Equation (2.1), while the density of the fabricated tablets was determined using Equation (2.2).

$$V = \pi r^2 h \qquad 2.1$$

Where, V= volume (mm^3), r= radius (mm), h= cylinder height (mm).

$$D = \frac{m}{v} \qquad 2.2$$

where, D= density (mg/mm^3), m= mass (mg) and v= volume (mm^3)

The data were represented as the mean (n=3) ± standard deviation (SD).

2.2.2.5. Statistical analysis

All data are expressed as mean ± standard deviation. Statistical analysis was performed using a one way analysis of variance (ANOVA) using Microsoft Excel 365 (version 2401) expanded with the statistical data analysis add-on. Differences equal or below the probability level ($p \leq 0.05$) were considered statistically significant, while differences above the probability level ($p > 0.05$) were considered not statistically significant.

2.3. Results and discussions

2.3.1. Impact of different 3D parameters on the weight of fabricated tablet.

The study was conducted to evaluate the impact of a range of 3D printing parameters on the weight of 3D fabricated solid dosage forms (placebo tablets). The results demonstrated that tablets with infill percentages of 25, 50, and 100% exhibited average weights of 253, 308, and 402 mg, respectively, highlighting a substantial correlation between infill percentages and tablet weight as shown in Figure (2.1). However, when considering the effect of different layer heights, tablets manufactured at 0.1, 0.2, and 0.3 mm displayed average weights of 305, 301, and 309 mg, respectively, as depicted in Figure (2.2). Analysis of various infill patterns revealed average weights of 298, 310, and 317 mg for tablets created with line, triangle, and zigzag patterns, respectively, as indicated in Figure (2.3). Likewise, alterations in printing speeds showed minimal impact on tablet weight, with tablets produced at speeds of 50, 75, and 100 mm/s registering average weights of 296, 304, and 308 mg, respectively, as shown in Figure (2.4).

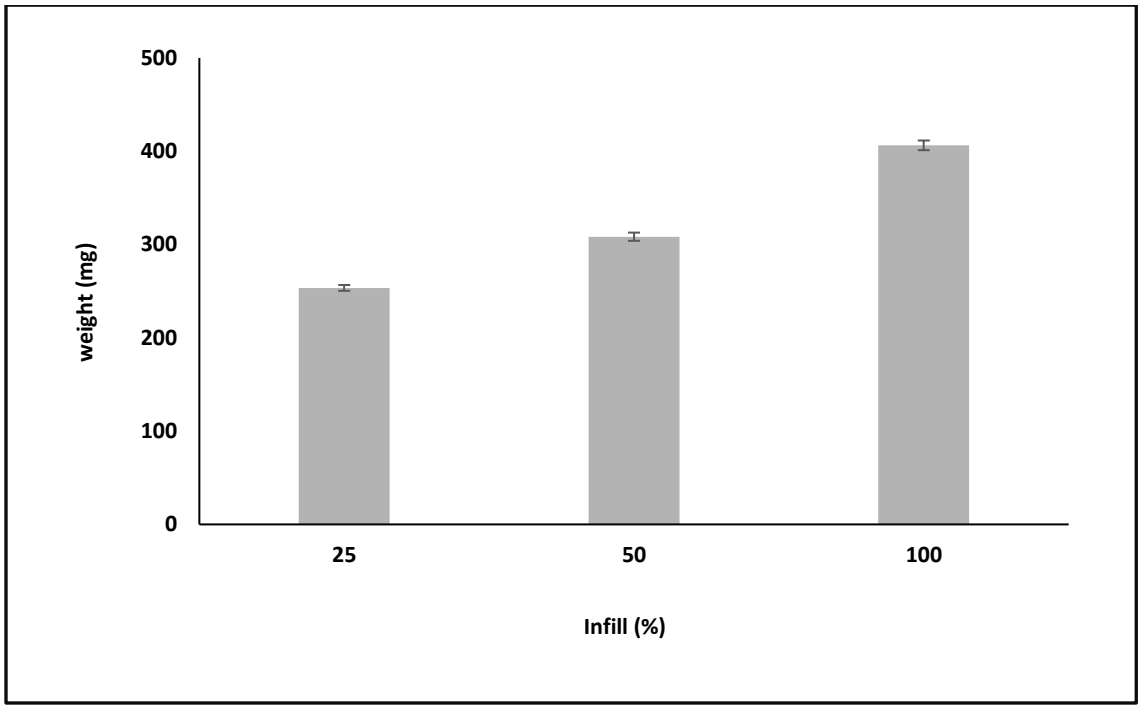

Figure 2.1: *The influence of different infill percentages on the weight. Results shown as mean (n=3) ± SD.*

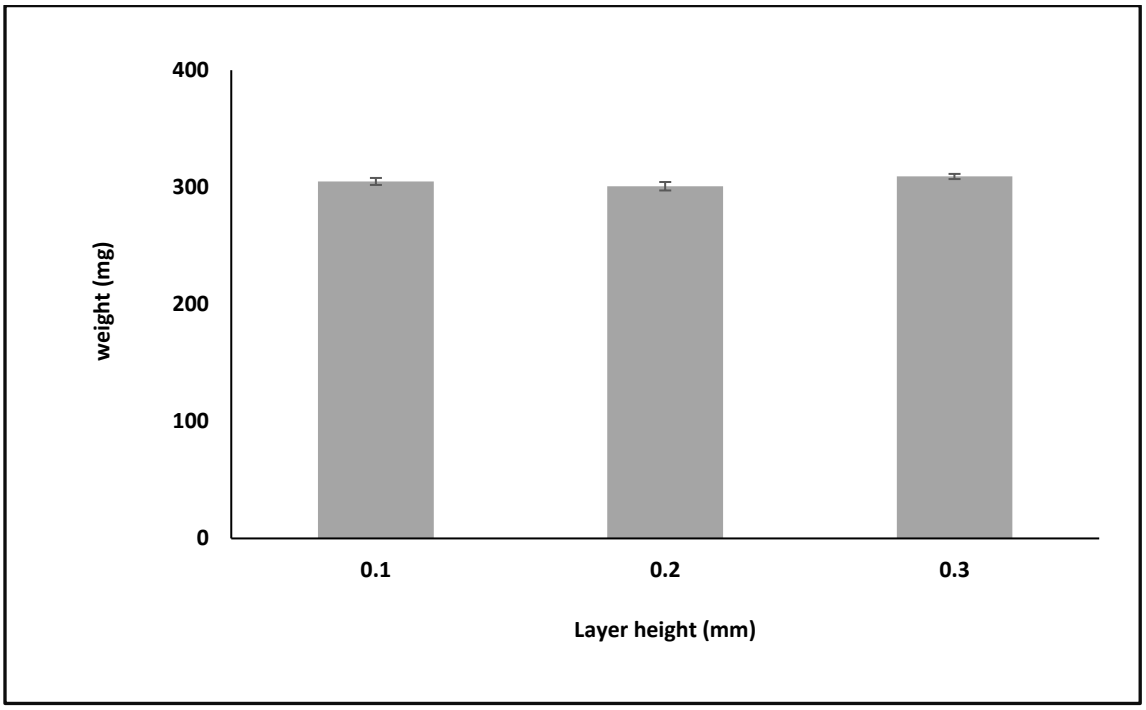

Figure 2.2*: The impact of different layer heights on the weight. Results shown as mean (n=3) ± SD.*

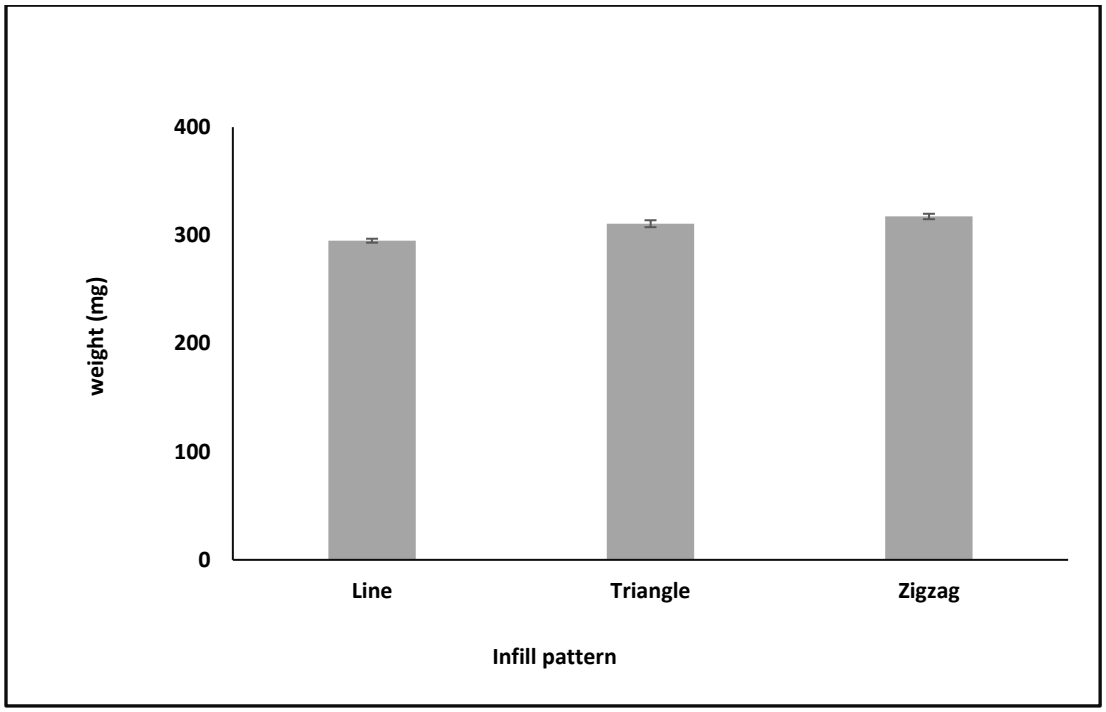

Figure 2.3: *The influence of different infill patterns on the weight. Result shown as mean (n=3) ± SD.*

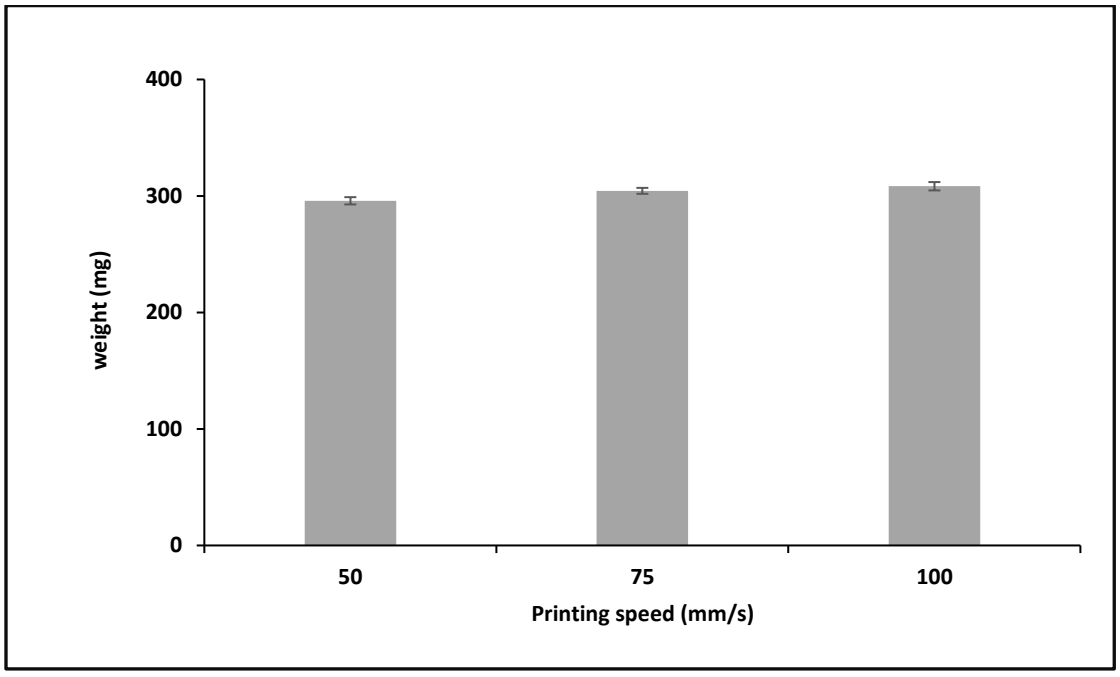

Figure 2.4*: The impact of different printing speeds on the weight. Results shown as mean (n=3) ± SD.*

2.3.2. Impact of different 3D parameters on the density of fabricated tablet.

The density variations of fabricated tablets were explored across different infill percentages, layer heights, infill pattern settings, and printing speeds. The influence of different infill percentages on the density of fabricated tablets is demonstrated in Figure (2.5). Results showed that the density of the fabricated tablets printed with infill percentages of 25, 50, and 100%, was determined to be 0.79, 0.95, and 1.09 mg/mm³, respectively. However, in the case of 3D printing with various layer heights of 0.1, 0.2 and 0.3 mm, shown in Figure (2.6), the determined density of fabricated tablets was 0.75, 0.73 and 0.77 mg/mm³, respectively. The influence of 3D printing with different infill pattern settings is demonstrated in Figure (2.7). Results showed that density of tablet manufactured with line, triangle and zigzag was measured at 0.68, 0.75 and 0.76 mg/mm³, respectively. In terms of the influence of the different printing speeds, results revealed that the density of tablets produced with printing speeds of 50, 75 and 100 mm/s was found to be 0.71, 0.69 and 0.78 mg/mm³, respectively as depicted in Figure (2.8).

Therefore, based on these findings, it is noteworthy that 3D printing with different printing speeds, infill patterns, and layer heights did not exert a statistically significant influence on the density of the 3D printed tablet. In contrast, 3D printing with various infill percentages showed a statistically significant impact ($p < 0.05$) on the density of the fabricated tablets.

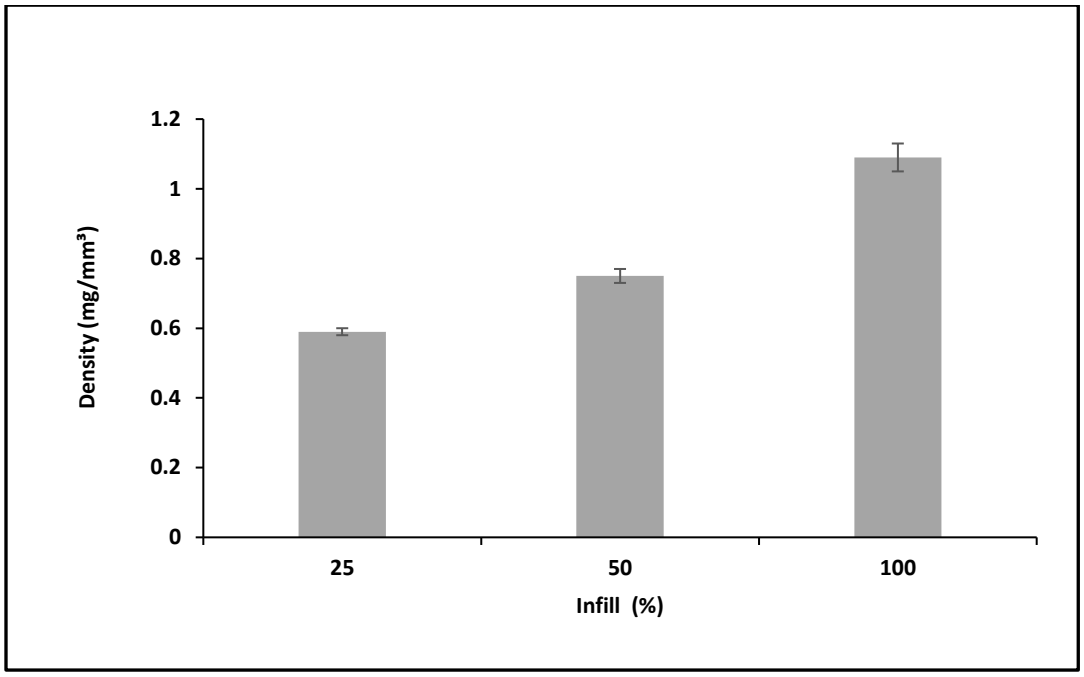

Figure 2.5: *The influence of different infill percentages on the density. Results shown as mean (n=3) ± SD.*

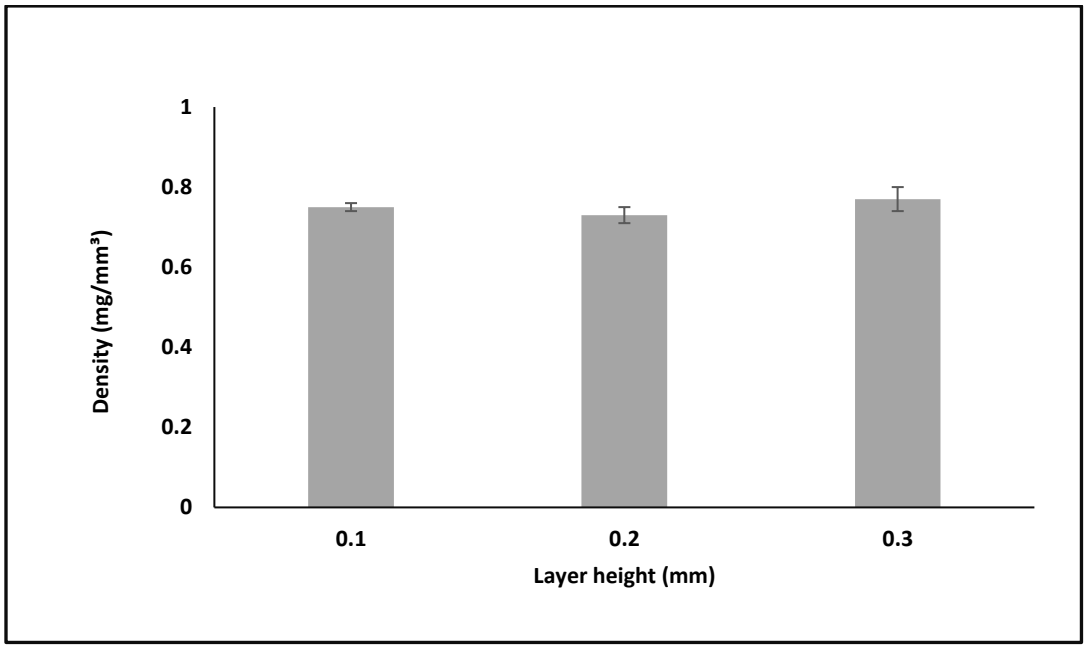

Figure 2.6: *The influence of different layer heights on the density. Results shown as mean (n=3) ± SD.*

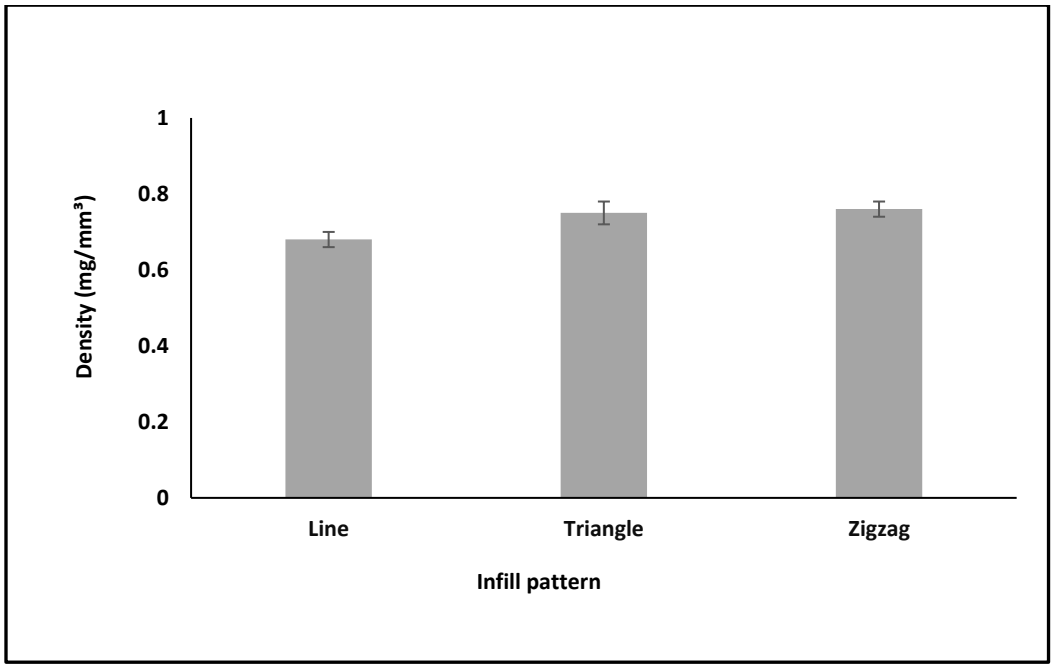

Figure 2.7: *The influence of different infill patterns on the density. Results shown as mean (n=3) ± SD.*

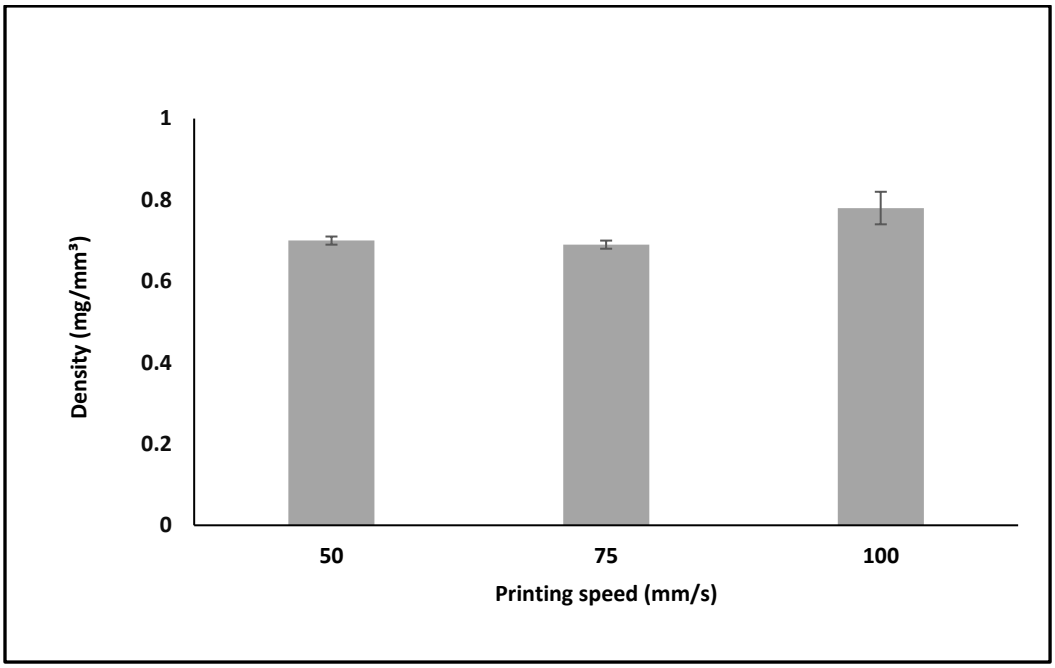

Figure 2.8: *The influence of different printing speeds on the density. Results shown as mean (n=3) ± SD.*

2.3.3. Impact of different 3D parameters on the tablet dimensions.

The study examined how various 3D printing factors, including diverse infill percentages, layer heights, infill patterns, and printing speeds, impacted the dimensions (specifically the diameter and height) of the manufactured tablet. The influence of different infill percentages on the dimensions of fabricated tablets is demonstrated in Figure (2.9). At 25% infill, tablets exhibited a diameter of 10.03 mm and a height of 5.11 mm, with subsequent increases to 10.20 mm in diameter and 5.23 mm in height at 50% infill. However, at 100% infill, the tablet diameter slightly decreased to 10.16 mm, while the height reduced to 5.17 mm.

Results of analysing the impact of varying layer heights on 3D printed tablet dimensions is demonstrated in Figure (2.10). At a layer height of 0.1 mm, tablets displayed a diameter of 9.98 mm and a height of 5.13 mm. Increasing the layer height to 0.2 mm resulted in a diameter of 10.26 mm and a height of 5.31 mm. However, at a layer height of 0.3 mm, the tablet diameter stabilised at 10.51 mm, while the height remained consistent at 5.43 mm.

The investigation of different infill patterns and their impacts on tablet dimensions is illustrated in Figure (2.11). Tablets printed with a line infill pattern exhibited a diameter of 9.96 mm and a height of 4.46 mm. Conversely, tablets utilising a triangular infill pattern featured a slightly smaller diameter of 9.90 mm but a greater height of 5.36 mm. However, tablets manufactured with a zigzag infill pattern displayed a larger diameter of 10.23 mm and a height of 5.06 mm

The evaluation of the influence of different printing speeds on the dimensions of fabricated tablets is depicted in Figure (2.12). Tablets produced at a printing speed of 50 mm/s, showcased a diameter of 9.93 mm and a height of 5.4 mm. Similarly, tablets printed at a speed of 75 mm/s, exhibited consistent diameter dimensions of 9.93 mm but a slightly reduced height of 5.36 mm. However, at a printing speed of 100 mm/s, the tablets displayed a decreased diameter of 9.86 mm alongside a height of 5.33 mm.

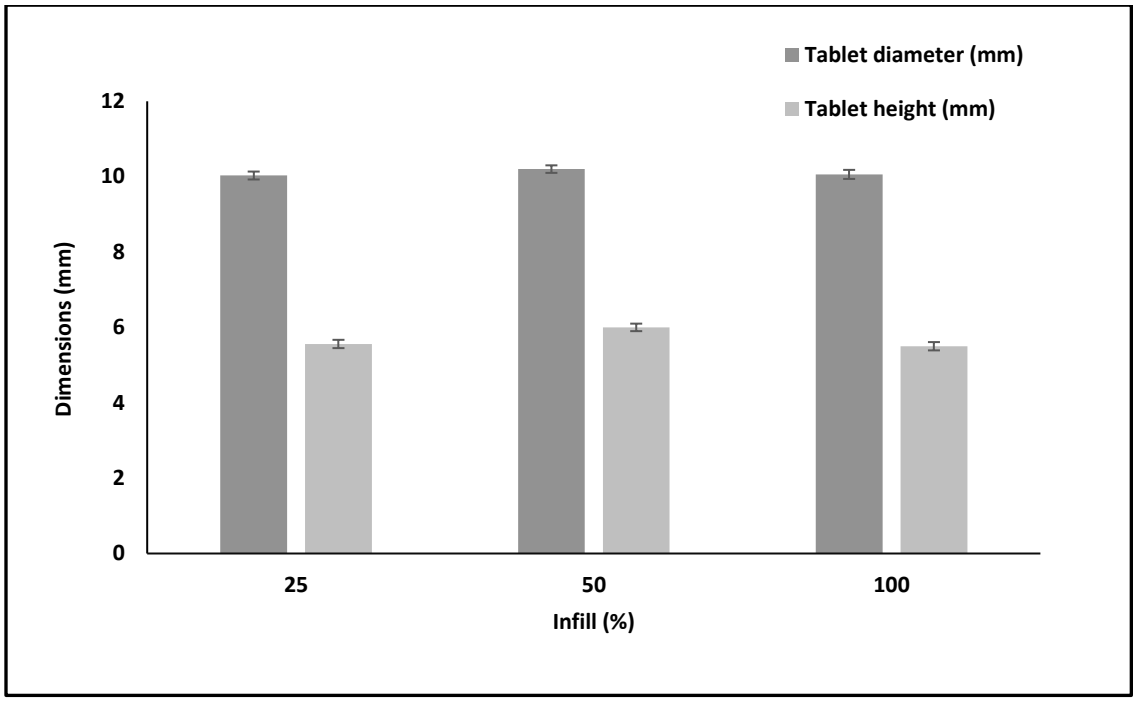

Figure 2.9: *The influence of different infill percentages on the dimensions. Results shown as mean (n=3) ± SD.*

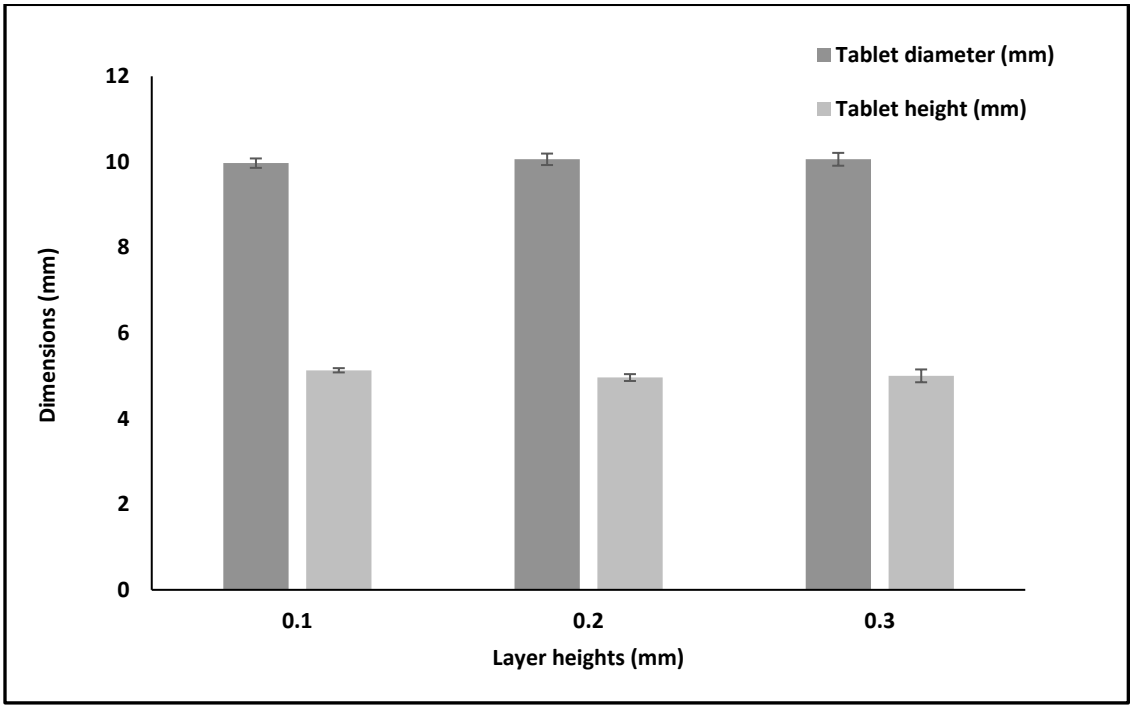

Figure 2.10*: The influence of different layer heights on the dimensions. Results shown as mean (n=3) ± SD.*

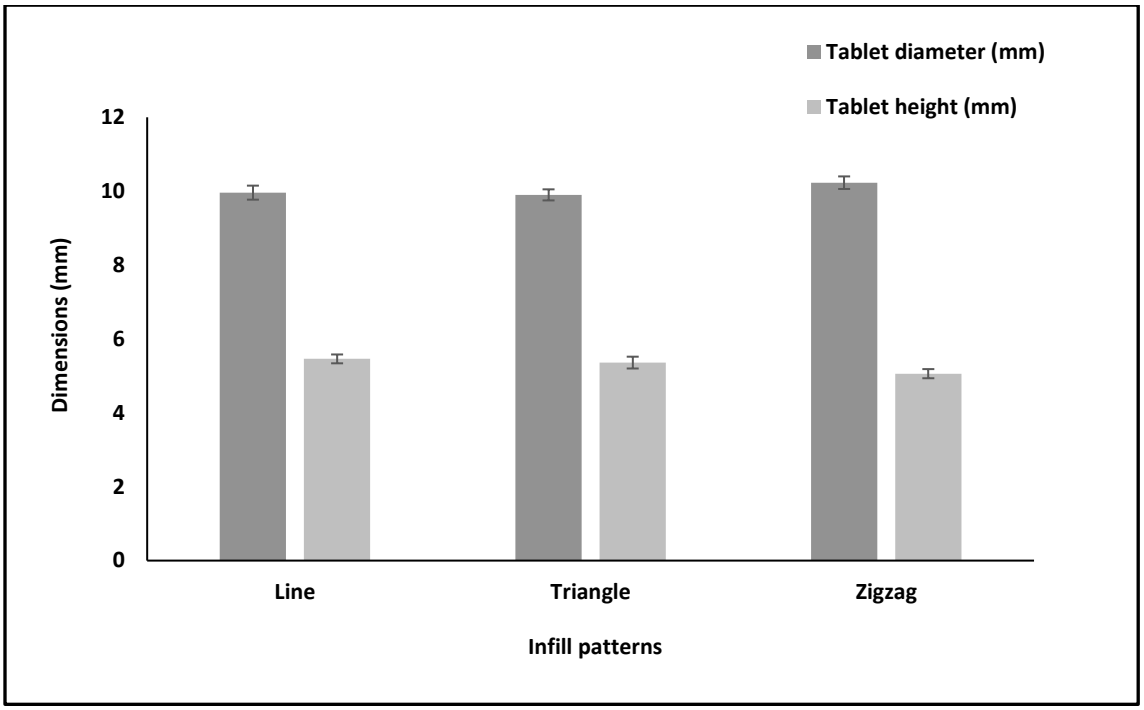

Figure 2.11: *The influence of different infill patterns on the dimensions. Results shown as mean (n=3) ± SD.*

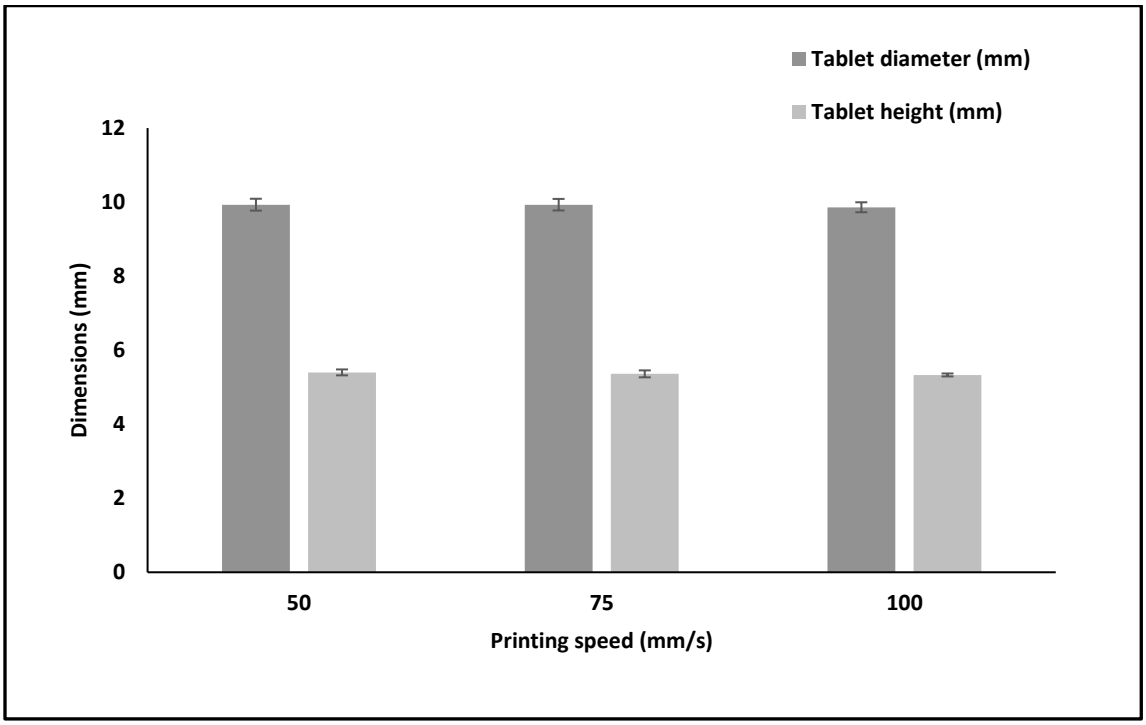

Figure 2.12: *The influence of different printing speeds on the dimensions. Results shown as mean (n=3) ± SD.*

2.4. Discussions

In the experimental section, an investigation was conducted into the effects of different 3D parameters on the physical characteristics of drug free tablets. The study focussed on examining the influence of varying infill percentages, layer heights, infill patterns, and printing speeds on the weight, density, and dimensions of 3D printed tablets. Among the different parameters examined, the infill percentage was found to have the most significant influence on the weight of the 3D fabricated drug free tablets. For example, the results indicated a proportional increase in the average weight of the fabricated tablets with higher infill percentages. This observation indicates that by solely altering the infill percentage from 25% to 100%, the tablet's weight can be increased by a factor of more than 1.5, indicating the significant of this parameter. These findings align with previous research conducted by Zhang, et al., where altering parameters such as infill, shell thickness, and layer height nearly doubled the tablet weight (Zhang et al., 2020). On the other hand, the employment of different layer heights, infill patterns and printing speeds did not show any significant influence on the weight of fabricated tablets. The influence of different infill % on the tablet weight of fabricated tablet was attributed to the fact that 3D printing with no infill will produce a hollow object, while increasing the infill % will increase the mass of internal structure of the printed object.

In terms of the influence of different 3d parameters on the density of fabricated tablet, the results showed that among the different parameters investigated, only difference in infill percentages exhibited a statistically significant influence on the density of fabricated tablets. This could be

attributed to the fact that tablets manufactured with lower infill percentages tend to possess higher air content, leading to a decrease in overall density. This observation aligns with previous research, which reported that tablets manufactured with lower infill percentages exhibited a floating ability during *in vitro* dissolution studies due to their reduced density.(Giri et al., 2020). However, density might be not affected only by weight variations but also minor variations in the dimensions of the fabricated leads to variations in the volume which consequently affect the density of the fabricated tablets as demonstrated in previously mentioned equation (eq. 2.1).

Although the intended tablet dimensions, diameter and cylinder height, were designed to be 10 mm and 5 mm, respectively, the different investigated parameters had a minor influence on the dimensions of 3D fabricated tablets. Tablets fabricated with varying infill percentages did not demonstrate statistically significant variations in dimensions, contrasting with the observed changes in weight and density. Similarly, parameters including different infill patterns, layer heights, and printing speeds did not exert a significant impact on the dimensions of the fabricated tablets. However, among the parameters investigated, it was found that a layer height of 0.1 mm, an infill percentage of 25%, an infill pattern of line and a printing speed of 50 mm/s resulted in 3D printed tablets with dimensions that closely matched the theoretical dimensions of the CAD designed tablets.

2.5. Conclusion

In this experimental chapter, diverse 3D printed formulations were prepared, employing an array of distinct 3D parameters, encompassing varying infill percentages, infill patterns, printing speeds, and layer heights. The examination focused on assessing the influence of these specific parameters on the physical characteristics of the produced drug free tablets. Results showed that the infill percentage has significant impact on both the weight and density of the placebo tablets. Conversely, with respect to tablet dimensions, the analysis revealed that alterations in infill percentages did not yield significant changes in the measured dimensions of the fabricated tablets. Moreover, the exploration of different printing speeds, layer heights, and infill patterns demonstrated no discernible impact on the physical attributes of the manufactured tablets.

Chapter 3 : INVESTIGATING THE INFLUENCE OF DIFFERENT 3D PARAMETERS ON THE DRUG RELEASE FROM FABRICATED SOLID PHARMACEUTICAL DOSAGE FORMS

3.1. Introduction

Over the last three decades, the scope of 3D printing has witnessed substantial expansion, and its utilisation in pharmaceutical manufacturing is advancing at a rapid pace (Charoo et al., 2020). The technology has advanced considerably, enabling the production of complex structures and precise dosage forms with customised features (Derick Muhindo et al., 2023). Spritam, designed by Aprecia Pharmaceuticals in 2015, is the first FDA approved product manufactured using ZipDose 3D printing technology. This technology facilitates rapid disintegration, enables high drug loading, and effectively masks the bitter taste of the product. These attributes contribute to improved patient compliance (Okafor-Muo et al., 2020).

Oral solid dosage forms, such as tablets, capsules, and caplets are the most commonly used forms of pharmaceutical products (Hartzke et al., 2022). One key advantage of oral solid dosage forms is their ease of administration. This ease of administration is especially beneficial for patients who prefer a simple and uncomplicated method of medication intake. Additionally, these dosage forms offer advantages in terms of patient adherence to prescribed medication regimens. The solid and compact nature of tablets, capsules, and caplets facilitates accurate dosing and simplifies medication management for patients (Liang et al., 2019). However, the level of consumer preference for oral solid dosage forms is influenced by various factors, including the ease of

swallowing, the gender and age of the consumer, and their perception of the therapeutic benefits (Ibrahim et al., 2012).

The traditional pharmaceutical manufacturing of oral solid dosage forms involves a series of sequential processes such as powder preparation, grinding, mixing, granulation, and compression resulting in a complex process followed by an additional step of coating. The issue of interindividual variability poses a significant global concern in the treatment of patients with diverse backgrounds, customs, metabolism, and individual requirements. Currently, dose adjustment strategies primarily rely on empirical methods, lacking precision and individualisation which consequently increases the likelihood of undesirable side effects occurring (Konta et al., 2017). The 3D printing technology provides a novel advantage of manufacturing which provides the opportunity for flexibility in pharmaceutical manufacturing with respect to dose, size, shape, and drug release characteristics according to the patient's needs (Al-Hashimi et al., 2018; Beer et al., 2021).

FDM based 3D printing technique is one the most utilised type of additive manufacturing investigated for producing solid pharmaceutical dosage forms (Norman et al., 2017). Despite some limitations such as the thermal degradation of the heat sensitive materials, shortage of suitable polymeric carriers and poor drug loading, the FDM based 3D printing techniques has many advantages including the cheap cost, simplicity, solvent free, ease of accessibility, no post processing of the printed object, product design with high mechanical strength and better

reproducibility compared to other 3D printing techniques such as Inkjet printing (Kempin et al., 2018; Tan et al., 2018).

In the literature, FDM based 3D printing has succeeded in producing several types of oral solid dosage forms containing one or more (APIs) with extended release (Chai et al., 2017; Zhang, Feng, et al., 2017) as well as an immediate release (Khaled et al., 2018; Okwuosa et al., 2016). However, there are several 3D printing parameters that have demonstrated an impact on the release profile of the 3D printed dosage forms. For example, the influence of geometry of dosage forms (Goyanes, Martinez, et al., 2015) as well as the influence of the infill pattern and the wall thickness (Obeid, Madžarević, et al., 2021a).

In a different study, a liquid filled capsule shell was fabricated using FDM based 3D printer in coordination with a liquid dispenser to fill the shell with API in a solution or suspension form. The drug release of this liquid filled capsule shell has been modified by altering the thickness of the shell without modifying the liquid formulation (Okwuosa et al., 2018). However, the influence of various 3D printing processing parameters extends beyond the drug release profile of the printed dosage form. These parameters can also significantly impact the physical properties of the 3D printed product. For example, changes in parameters such as infill percentage, layer height, infill pattern, and coating designs can affect characteristics such as structural integrity, mechanical strength, porosity, surface roughness, and overall physical stability of the printed dosage form (Durgun & Ertan, 2014; Nidagundi et al., 2015).

The primary purpose of this experimental chapter is to analyse the influence of different 3D printing parameters on the *in vitro* drug release characteristics of fabricated pharmaceutical dosage form (tablet). The first part will investigate the influence of infill percentage, infill pattern and layer height on the drug release of drug loaded tablets. While the second part of this chapter will investigate the influence of different designs of 3D printed coating shells on the *in vitro* drug release of immediate release tablets.

3.2. Materials and method

3.2.1. Materials

Poly-lactic acid (PLA) and Polyvinyl alcohol (PVA) commercial feedstock filaments, 1.75 mm in diameter, print temperature (200-220°C), purchased from Verbatim GmbH (Hesse, Germany). Caffeine pure powder (99%) was purchased from Alfa Aesar (England, UK). Polyvinyl alcohol (PVA) (MW 89000) and Talc powder was purchased from Sigma-Aldrich (Dorset, UK). Natural PLA pellets were purchased from Pollen (Paris, France). Acetonitrile, Methanol and Dichloromethane were purchased from Fisher Scientific (Leicestershire, UK). Type (I) deionised water (dH_2O) supplied by laboratory Triple Red water system (Buckinghamshire, UK).

3.2.2. Investigating the influence of different 3D parameters on the drug release of caffeine loaded tablets.

3.2.2.1. Preparation of drug loaded filaments by hot melt extrusion (HME)

A single screw hot melt extrusion (SSHME) (3devo, The Netherlands) was utilised to prepare four different formulations. Caffeine (CAF) was used as model drugs while PLA, and PVA were used as the polymer carriers. The drug polymer ratios and the hot melt extrusion processing conditions are presented in Table (3.1).

Table 3.1: HME processing parameters.

Formulation name	Drug/polymer ratio	Zone temperatures (°C)				Screw speed (RPM)	Die size (mm)
		1	2	3	4		
F1	CAF/PLA (5% w/w)	170	190	195	160	6	3
F2	CAF/PLA (10% w/w)	170	190	195	160	6	3
F3	CAF/PVA (5% w/w)	160	180	180	150	6	3
F4	CAF/PVA (10% w/w)	160	180	180	150	6	3

3.2.2.2. Drug loading efficiency analysis

Three samples, each weighing 20 mg, were collected from three different sections of each extrudate (beginning, middle and end) to assess the caffeine content exist in the filaments. Each sample, consisting of PLA filaments, was dissolved in 20 mL of Dichloromethane (DCM). The solution was covered and subjected to magnetic stirring at speed of 250 RPM while being heated to 40˚C until complete dissolution. Subsequently, the solution was stored in a fume hood for 3

hours to ensure complete evaporation of the DCM. The drug extraction process involved adding 20 mL of a mobile phase to the sample, followed by sonication for 10 minutes at a temperature of 37°C using a VWR ultrasonic bath (Leicestershire, UK). After sonication, the samples were subjected to centrifugation at a speed of 13,000 RPM for 10 minutes using Labnet Prism R centrifuge (Edison NJ, USA). The resulting supernatants were collected and analysed using HPLC. For the determination of the drug content in the PVA based filament, a similar procedure was followed with a slight modification. Instead of using DCM, the PVA filaments were dissolved in dH_2O. The remaining steps, including sonication, centrifugation, and HPLC analysis, remained the same. Loading efficiency was calculated using Equation (3.1). The results were presented as mean (n=3) ± SD.

$$Drug\ loading\ efficiency\ \% = \frac{Mass\ of\ the\ drug\ in\ extrudate}{Mass\ of\ the\ drug\ in\ feed} \times 100 \qquad 3.1$$

3.2.2.3. Filament diameter analysis

A digital calliper Digimax (Camlab, Cambridge, UK), was used to determine the diameter of prepared filament by measuring the diameter of 2 meter-length of each prepared filament formulation at specified points of 10 cm gap. The results were presented as mean (n=20) ± SD.

3.2.2.4. Filament extrusionability and feedability test

Filament extrusionability refers to the ability of a filament material to extrude through the nozzle of a 3D printer smoothly and consistently during the printing process. The prepared filaments were loaded directly to the printing head of a commercial filament based 3D printer (Flashforge creator, China). The amount of the extruded filament at specified time intervals (30 seconds) was collected and weighed using VWR® T electrical balance (Leicestershire, UK). Nozzle size and gear speed were kept constant at 0.4 mm and 35 mm/sec, respectively. Extrusion temperatures was set at 205°C and 200°C for PLA and PVA based filaments, respectively. Filaments that were able to successfully pass through the 0.4 mm nozzle tip of the printer were considered feedable, irrespective of the quality of the 3D printing process. Extrusion temperature was selected based on the recommended temperature of the manufacturer data sheet, while the extrusion speed determined to be 35 mm/s as the FDM based 3D printers have extrusion speed ranging from about 25 to 100 mm/s and this speed was found to be suitable during the preliminary trials (BARDWELL, 2023).

3.2.2.5. Diffraction scanning calorimetry (DSC) analysis

A Discovery DSC 250, (TA Instruments, USA) was utilised to determine the glass transition temperatures (Tg) and melting peaks of the raw polymer and API. Samples weighing between 4-6 mg were placed in Tzero aluminium pans and analysed. The DSC thermograms were acquired in a cooling-heating ramps from 25°C to 250°C, with a heating rate of 10°C /min. The measurements were conducted under a nitrogen atmosphere to minimise the effects of oxidation or other atmospheric factors.

3.2.2.6. Complex viscosity (η) test

A rheometer (Discovery HR-1, TA instruments, USA) was used to investigate the complex viscosity vs temperature of pure polymer as well as the drug polymer physical mixture. Dynamic oscillatory measurements were obtained using a parallel plate geometry with 20 mm diameter with gap distance of 1000 µm at temperature starting from 200°C to 100°C at cooling rate of 10°C/5 minutes ramps.

3.2.2.7. CAD design and 3D printing of different formulations of the drug loaded tablets.

The model tablets were designed using (TinkerCAD, Autodesk, USA) and converted to (Gcode) using Cura software (version 3.0, Ultimaker, Netherland). Tablets with predetermined dimensions diameter, 10 mm; height 5 mm were 3D printed using the commercial FDM based 3D printer (Flashforge creator, China). Fourteen different formulations were prepared, as illustrated in Table (3.2). The central values for infill percentage, infill pattern, layer height, were set at 50%, Line, 0.2 mm, respectively. Filaments with 10% caffeine content were chosen for the fabrication of the dosage forms due to the fact that higher drug concentrations in the filaments can lead to more pronounced drug release profiles, making it easier to detect and quantify the released drug during *in vitro* release studies. Table (3.3) outlines the 3D printing conditions. In the preceding chapter, the Prusa i3 3D printer was employed to explore solely the impact of 3D parameters on the physical attributes of a placebo tablet. In contrast, for the current chapter's experiment investigating the effects of various parameters on in vitro drug release, the Flashforge printer was utilised to manufacture tablets from drug loaded filament prepared through HME. These experiments were

conducted independently, with the focus in the previous chapter being on the influence on physical properties (such as weight, dimensions, and density) of the placebo tablet, while the current chapter centres on the *in vitro* release. Consequently, we deduce that altering the printer will not affect the findings presented in this thesis.

Table 3.2: Different types of 3D printed formulations.

FORMULATION NO	Filament base polymer	Filament drug/polymer ratio (w/w%)	INFILL (%)	LAYER HEIGHT (mm)	INFILL PATTERN
F1	PLA	10/90	25	0.2	Line
F2	PLA	10/90	50	0.2	Line
F3	PLA	10/90	100	0.2	Line
F4	PLA	10/90	50	0.1	Line
F5	PLA	10/90	50	0.3	Line
F6	PLA	10/90	50	0.2	Triangle
F7	PLA	10/90	50	0.2	Zigzag
F8	PVA	10/90	25	0.2	Line
F9	PVA	10/90	50	0.2	Line
F10	PVA	10/90	100	0.2	Line
F11	PVA	10/90	50	0.1	Line
F12	PVA	10/90	50	0.3	Line
F13	PVA	10/90	50	0.2	Triangle
F14	PVA	10/90	50	0.2	Zigzag

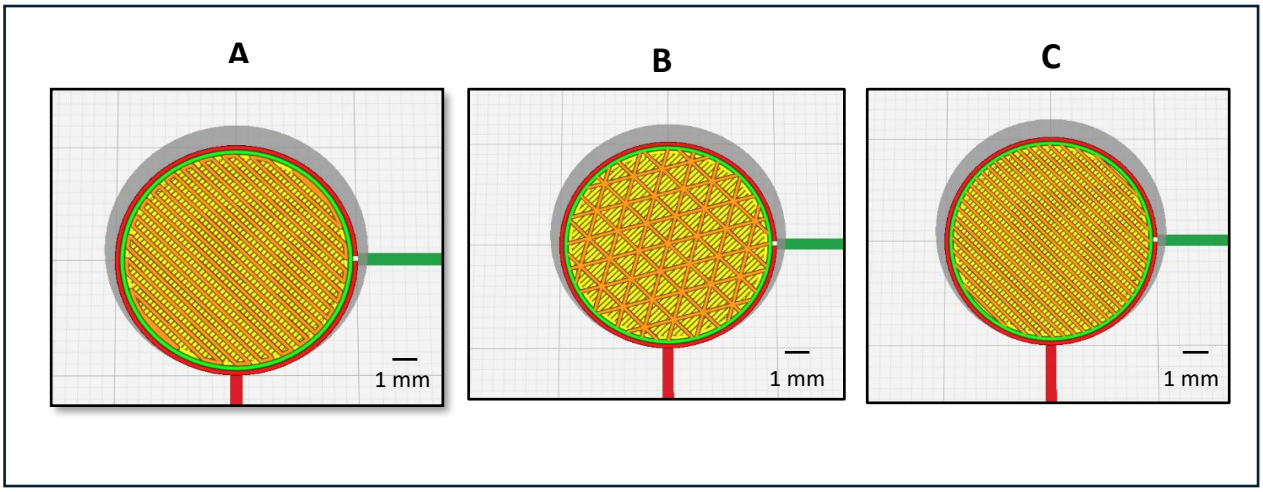

Figure 3.1: *Schematic diagram shows different types of infill patterns at a 50% infill percentage. Zigzag (A), Triangle (B) and Line (C).*

Table 3.3: 3D printing conditions of drug loaded tablet.

Printing conditions	Option/value
Feeding material	HME prepared filaments
Printing temperature (nozzle)	200°C (PVA), 205˚C (PLA)
Build plate temperature	60˚C
Nozzle size	0.4 mm
Printing speed	50 mm/sec
Travelling speed	65 mm/sec
Adhesion support	Raft

3.2.2.8. Caffeine stability and solubility

An excess amount of caffeine was dissolved in 1 mL of each of dH_2O (37˚C), dH_2O (25˚C) and PBS (37˚C). After 48 hrs, samples were centrifuged, and the supernatant diluted and analysed by HPLC. To determine the caffeine stability, 10 mg was dissolved in 30 mL of dH_2O and the prepared solution stored in an orbital shaking incubator, Unitron INFORS HT (Surrey, UK), operating at a speed of 100 RPM and a temperature of 37˚C. Samples were withdrawn after 1, 3, 5, 7, 10, 14, 20, 25, 30 and 35 days and analysed by HPLC. Results were presented as mean (n=3) ± SD.

3.2.2.9. In vitro drug release analysis of drug loaded tablets.

The PLA based 3D printed tablets were immersed in 30 mL of dH_2O release media and placed in an orbital shaking incubator, Unitron INFORS HT (Surrey, UK), set at a speed of 100 RPM and a temperature of 37˚C. At specific time intervals of 1, 2, 5, 10, 15, 20, and 30 days, 1 mL samples were collected and replenished with fresh release medium. The collected samples were subjected to centrifugation at 13000 RPM for 10 minutes using Labnet Prism R centrifuge (Edison NJ, USA). Supernatant was analysed using HPLC to calculate the drug release using the Equation (3.2). Results were reported as mean (n=3) ± standard deviation (SD). The release conditions for PVA-based 3D printed tablets were similar to those of the PLA tablets, with the only difference being the intervals for sample collection. Samples were collected and replaced with fresh release medium at 0.5, 1, 2, 3, 4, 5, 6, and 12 hours. The results were reported as the mean (n=3) ± SD.

Drug release (%) = (Released drug/ Total drug) ×100 *3.2*

3.2.3. Investigation the feasibility of different 3D printing coating systems (shell) to modify the release profile of immediate release tablets.

3.2.3.1. Preparation of the immediate release tablets (reservoir tablets)

An immediate release tablet containing caffeine was formulated through direct compression. The tablet was composed of a physical mixture of caffeine, PVA (MW 89000), and talc powder in specific weight proportions 30/50/20 w/w/w%. The mixture, weighing 300 mg, was compressed using a manual bench press (Specac, London, UK) under a consistent compressive force (20 kN/m²). The resulting tablets were stored in a vacuum desiccator, shielded from light and humidity. These tablets, with average dimensions of 10 mm in diameter and 3 mm in height. The dimensions of the tablets were determined to fit to the pre-established cavity size specified in the CAD designs of the 3D fabricated coating shells. Prepared tablets will be manually inserted into different 3D printed coated shells. The influence the different types of fabricated coating shells on the *in vitro* release profiles will be investigated.

3.2.3.2. Computer-aided design and 3D printing of the shell coating system

Two different types of tablet coating shells were designed using TinkerCAD software. The first type of coating shell was fabricated using PLA commercial filament and featured pores with varying

diameters: 1, 1.5, and 2 mm. The second type of coating shell was specifically designed to have different wall thicknesses, 1, 1.5, and 2 mm, and was 3D printed using PVA commercial filament.

The 3D printing process parameters were configured as follows: 100% infill, with a line pattern for the infill, and a layer height of 0.1 mm. The tablet shell system was printed using a single step printing process. Initially, the base and walls of the coating shell were 3D printed to form a hollow shell. The 3D printing process was then paused when it reached a specified height of 4 mm. At this point, an immediate release tablet was manually placed inside the shell. Subsequently, the top of the shell was 3D printed to complete the assembly, resulting in a single unit tablet shell that enclosed an immediate release caffeine tablet. The different prepared formulations of coating shells are outlined in Table (3.4). The printing conditions are demonstrated in Table (3.5).

Table 3.4: Different formulations of coating shells.

Formulation No.	Coating shell base polymer	Coating shell wall thickness (mm)	Number of pores	Pore size (mm)
F1	PLA	1	4	1
F2	PLA	1	4	1.5
F3	PLA	1	4	2
F4	PVA	1	0	-
F5	PVA	1.5	0	-
F6	PVA	2	0	-

Table 3.5: Printing conditions of coating shells.

Printing conditions	Option/value
Feeding material	HME prepared filaments
Printing temperature (nozzle)	200°C (PVA), 205˚C (PLA)
Build plate temperature	60˚C
Nozzle size	0.4 mm
Printing speed	50 mm/sec
Travelling speed	65 mm/sec
Adhesion support	Raft
Resolution	Standard (± 0.2 mm)

3.2.3.3. Analysis of the drug release of the coated immediate release tablets

The 3D printed coated tablets were immersed in 30 mL of dH_2O release media and placed inside an orbital shaking incubator, Unitron INFORS HT (Surrey, UK) operating at a speed of 100 RPM and maintained at a temperature of 37˚C. At specific time intervals of 0.5, 1, 2, 4, 6, 8, 10, 12, and 24 hours, 1 mL samples were collected and replaced with fresh media. These collected samples were then subjected to centrifugation at a speed of 13000 RPM for 10 min using Labnet Prism R centrifuge (Edison NJ, USA) and subsequently analysed using HPLC to determine the drug release. During the release study, a control reference tablet, which did not possess a 3D printed coating, was employed.

3.2.4. HPLC Analysis

3.2.4.1. HPLC Chromatographic conditions

Caffeine was analysed using an Agilent HPLC (infinity II, Santa Clara, California, USA). The mobile phase composed of a mixture of deionised water (dH_2O) and methanol (60:40). Chromatographic determination was performed by using a Thermo Scientific® C18 column (150 mm x 4.5 mm), particle size of 5 µm at room temperature. The UV wavelength detector was set at 272 nm with a run time of 10 min. The injection volume was 10 µL with a flow rate of 1 mL/min. The retention time was around 4.5 minutes.

3.2.4.2. Stock solution and standard calibration curve

10 mg of caffeine weighed and dissolved in 100 mL of the mobile phase deionised water: methanol (60:40 v/v). The solution was subjected for sonication for 10 minutes at a temperature of 37°C using a VWR ultrasonic bath (Leicestershire, UK) to ensure complete dissolution and the removal of any air bubbles. 10 mL of prepared solution was transferred into a 25 mL volumetric flask and filled up to mark to produce a stock solution of 40 µg/mL. Standard solutions with concentrations of 8, 12, 16, 20, 24, 28, and 32 µg/mL were prepared from the stock solution. The calibration curve was created by plotting the AUC vs concentrations.

3.2.5. Statistical analysis

Statistical analysis was performed using a one way analysis of variance (ANOVA) using Microsoft Excel 365 (version 2401) expanded with the statistical data analysis add-on. Post-hoc comparisons of the means were performed using Bonferroni significance difference test. Differences equal or below the probability level ($p \leq 0.05$) were considered statistically significant, while differences above the probability level ($p > 0.05$) were considered not statistically significant.

3.3. Results and discussions

3.3.1. The preparation of caffeine loaded filaments using hot melt extrusion.

The preparation of drug loaded filaments for use as feeding materials in FDM based 3D printing is typically accomplished through either solvent impregnation or HME techniques. Existing literature indicates that solvent impregnation is capable of achieving only low drug loadings, typically ≤ 2%. On the other hand, HME offers the advantage of allowing for high drug loadings of up to 60% to be attained. (Cantin et al., 2021; Kukkonen et al., 2022). In this study, the filaments used were prepared through the HME method, and their characteristics were examined in the subsequent sections.

3.3.1.1. Prepared caffeine (CAF) loaded filaments.

Table (3.6) presents the CAF loading percentages (% w/w) in the PLA and PVA filaments prepared via HME. For the PLA 5% formulation, the actual CAF content ranged from 4.18 ± 0.58 to 4.97 ± 0.41% (w/w), while for the PLA 10% formulation, it ranged from 8.32 ± 0.79 to 9.67 ± 0.85% (w/w). In the case of the PVA 5% formulation, the caffeine content ranged from 4.29 ± 0.67 to 4.81 ± 0.57% (w/w), and for the PVA 10% formulation, it ranged from 8.14 ± 0.71 to 9.48 ± 0.81% (w/w).

During the drug content analysis, three distinct sections of each extrudate were chosen to assess the variation in drug loading. The results indicated that the drug loading efficiency of the HME exhibited a slight improvement in the final part of the extrudate compared to the earlier produced sections. These variations in drug content among different parts of the extrudate could be attributed to two potential factors. Firstly, the relatively inadequate mixing characteristics of the single screw HME might contribute to uneven drug distribution. Secondly, the adherence of the drug to the HME barrel during the initial stages of the process could also play a role in the observed variations.

Despite the inherent differences in water solubility properties between the two polymers, it was observed that the drug loading percentages were almost similar for both PLA (hydrophobic) and PVA (hydrophilic). In this study, the average loading efficiency of PLA 5% was determined to be 91.7%, indicating that approximately 91.7% of the intended drug content was incorporated into the PLA filaments. Similarly, for PVA 5%, the average loading efficiency was found to be 91%, suggesting that around 91% of the desired drug content was loaded into the prepared PVA filaments. Moreover, the drug loading performance of the HME showed minimal variation with respect to the drug loading percentages of each polymer type (5% and 10%). This suggests that the drug loading process is not influenced by the drug loading percentage within the tested range for both hydrophobic and hydrophilic polymers.

3.3.1.2. Filament diameter

Figure (3.2) illustrates the average diameter of the prepared filaments in this study. Results showed that the average diameter for PLA filaments was 1.71 ± 0.13 mm for PLA 5% and 1.76 ± 0.1 mm for PLA 10%. In terms of PVA filaments, the average diameter was 1.58 ± 0.12 mm for PVA 5% and 1.66 ± 0.11 mm for PVA 10%. While the literature suggests that FDM based 3D printers can successfully print filaments with diameters ranging from 1.61 to 1.82 mm (Linares et al., 2021). However, another reference stated that the accepted tolerance for filament diameter variation is around 10%. This means that if the intended filament diameter is, for example, 1.75 mm, variations of ±10% (i.e., 1.58 mm to 1.93 mm) would typically be considered acceptable (Serrano et al., 2023). The findings of this study demonstrated that filaments prepared using HME with diameters ranging from 1.58 to 1.76 mm were successfully printable.

The average filament diameters in this study were found to be in close proximity to the target diameter of 1.75 mm. This can be attributed to the utilisation of a HME equipped with an optical sensor with an accuracy of 43 microns. The detector was capable of sensing diameter variations during the extrusion process and adjusting the speed of the spool winder accordingly. As a result, the filament diameter was automatically adjusted throughout the entire process, ensuring consistency, and maintaining it close to the target diameter.

3.3.1.3. Filament extrusionability and feedability

The results of filament extrusionability and feedability are presented in Table (3.7). Extrusionability was assessed for all the prepared filaments by measuring the amount of filament extruded through

the printer nozzle in milligrams per second (mg/s). For PLA filaments, the extrusionability was determined to be 8.8 ± 0.21 mg/s for PLA CAF 5% and 8.9 ± 0.24 mg/s for PLA CAF 10%. In comparison, the extrusionability of the PLA commercial filament was measured to be 9.1 ± 0.07 mg/s. Regarding to the prepared PVA filaments, the extrusionability was found to be 8.2 ± 0.32 mg/s for PVA 5% and 8.4 ± 0.43 mg/s for PVA 10%, in comparison to 9.2 ± 0.11 mg/s revealed by the commercial PVA filament.

The findings indicate that the extrusion rates of the prepared PLA and PVA filaments were slightly lower than those of the commercial filaments. Notably, the PLA filament formulations exhibited values closer to those of the commercial filament in comparison to the prepared PVA filaments. This observation could be attributed to the precise diameters of the PLA filaments. Filaments with smaller diameters tend to extrude a lesser amount of filament per unit of time, which is a factor that could contribute to the lower extrusion rates observed for the prepared PVA filaments.

The feedability of the prepared filaments was assessed based on their ability to be extruded smoothly without fracturing inside the printer head or causing nozzle blockages. All the prepared filaments, irrespective of the polymer type or drug concentrations used, were found feedable. This suggests that the formulated filaments are suitable for 3D printing purposes, as they demonstrated the capability to be extruded reliably without any significant issues during the printing process.

Table 3.6: Caffeine loading % (w/w) of the prepared filament formulations.

Formulation name	Sample	Theoretical CAF content % (w/w)	Actual CAF content % (w/w)			Loading efficiency (%)
			Filament beginning	Filament middle	Filament end	
F1	PLA 5 % CAF	5	4.2 ± 0.6	4.6 ± 0.7	4.9 ± 0.4	92
F2	PLA 10 % CAF	10	8.3 ± 0.8	8.8 ± 0.6	9.7 ± 0.8	89
F3	PVA 5% CAF	5	4.3 ± 0.7	4.5 ± 0.5	4.8 ± 0.6	91
F4	PVA 10% CAF	10	8.1 ± 0.7	8.8 ± 0.4	9.5 ± 0.8	88

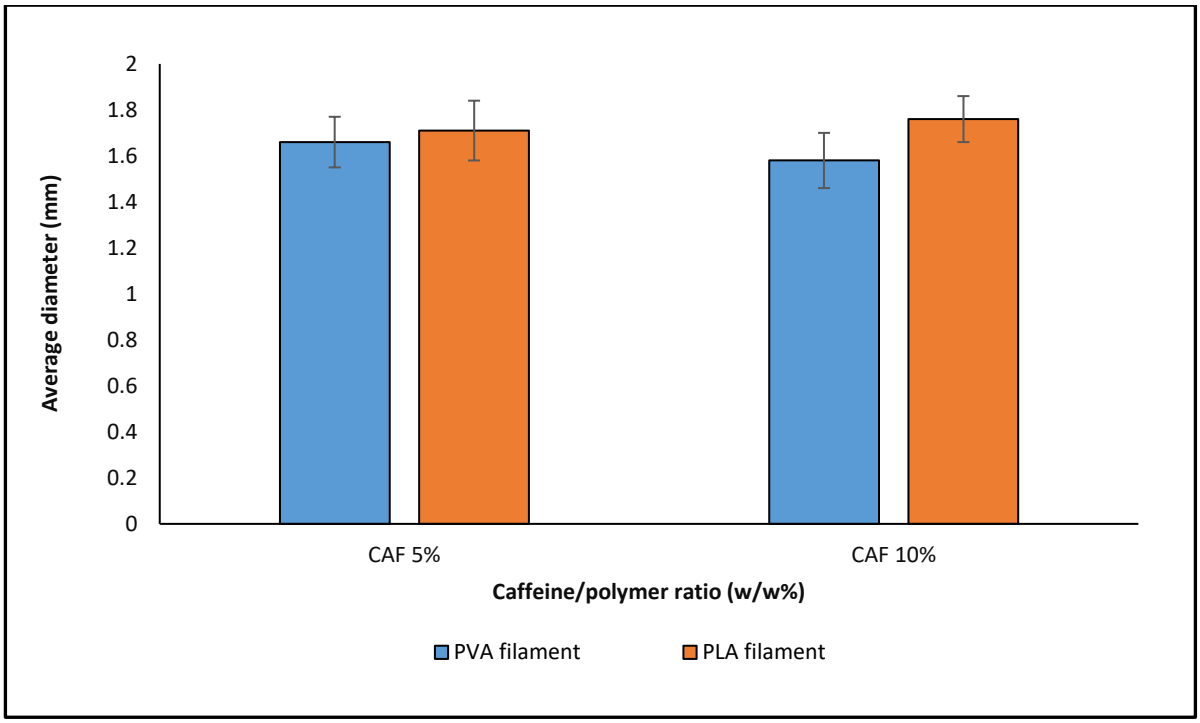

***Figure 3.2**: The average diameter of HME prepared filaments. Result shown as mean (n=3) ± SD.*

Table 3.7: The extrusionability and feedability of prepared HME filaments.

Formulation Name	Content	Extrusion duration (Sec)	Extrusionability (mg/s) (n=3) ± SD	Extruding temperature (°C)	Extruder speed (mm/s)	Feedability
F1	PLA CAF 5 % (w/w)	30	8.8 ± 0.2	205 ± 5	35	Y
F2	PLA CAF 10 % (w/w)	30	8.9 ± 0.2	205 ± 5	35	Y
F3	PVA CAF 5 % (w/w)	30	8.2 ± 0.3	200 ± 5	35	Y
F4	PVA CAF 10% (w/w)	30	8.4 ± 0.4	200 ± 5	35	Y
-	PLA commercial filament	30	9.1 ± 0.1	205 ± 5	35	Y
-	PVA commercial filament	30	9.2 ± 0.1	200 ± 5	35	Y

3.3.1.4. DSC results

Figure (3.3) displays the DSC thermograms of the raw materials used in the preparation of the filament formulation. The thermograms reveal important temperature characteristics of the materials. For PLA, the thermogram shows a glass transition temperature (*Tg*) at 60°C and the melting temperature is observed at 150°C. For PVA, the *Tg* was seen at 80°C while its melting temperature is observed at around 175°C. CAF, on the other hand, demonstrates a strong endothermic peak at approximately 233°C, corresponding to its melting temperature and its *Tg* is observed at around 155°C.

The ideal temperature range for processing is often determined by the melting point, thermal stability, and glass transition point (Alshetaili et al., 2020). For instance, DSC helps determine the temperature range within which the materials remain stable without undergoing degradation or decomposition. This information is vital for setting the upper temperature limit during extrusion. Operating within the thermal stability range ensures that the materials maintain their integrity and do not undergo unwanted chemical or physical changes. Similarly, the DSC can identify the temperatures at which the materials transition from a solid to a liquid state (melting point). Adjusting the extrusion temperature to match or slightly exceed the melting temperature ensures efficient melting and flow of the materials through the extruder.

By integrating the DSC data during the preformulation stage of HME, DSC can guide the selection of appropriate temperature profiles to facilitate efficient melting, mixing, and extrusion of the materials.

3.3.1.5. Rheology results

The rheometer results are presented in Figures (3.4) and Figure (3.5) for PLA and PVA formulations, respectively. The focus was on examining the impact of temperature on the complex viscosity of PLA and PVA, as well as their drug-polymer mixtures. The rheometer measurements provided insights into the viscosity behaviour of these materials as temperature was varied. It was observed that as the temperature increased, the viscosity of both PLA and PVA decreased. This behaviour is commonly observed in many polymers, where higher temperatures promote increased molecular mobility and reduced resistance to flow. However, the concentration of the drug, caffeine (CAF), was found to influence the viscosity profile of the molten mixture. Specifically, higher drug concentrations led to higher viscosity profiles.

For a small scale pharmaceutical extruder, it is generally desirable to maintain the viscosity within an ideal range of 1000 to 10000 Pa.s. This range ensures optimal processing conditions and product quality. (Gupta et al., 2016; Vlachopoulos & Strutt, 2003). The results showed that PLA and PVA placebo polymers had viscosity between 1000 and 10000 Pa.s at 170-200°C and 165-195°C, respectively.

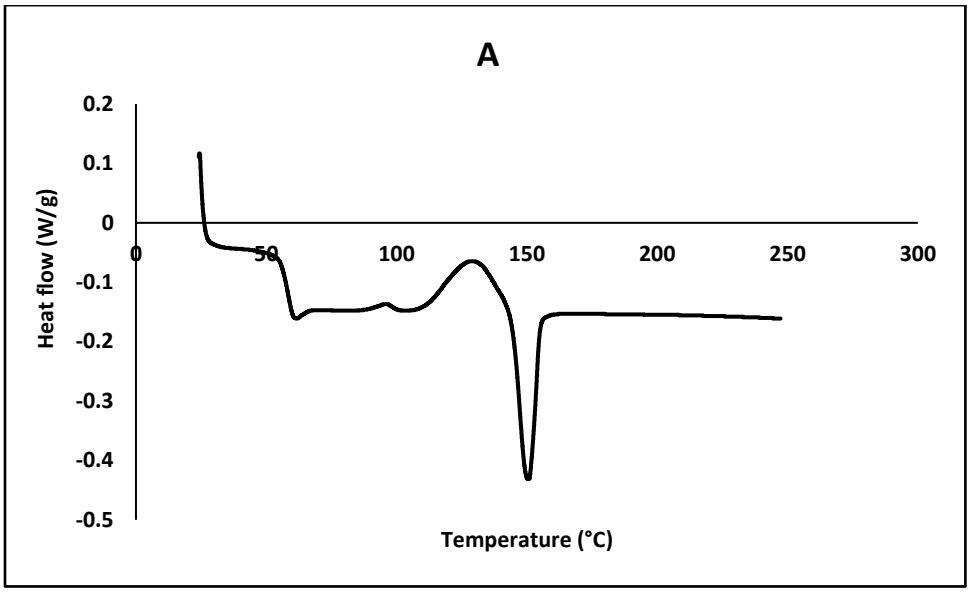
A
0.2
0.1
0
-0.1
-0.2
-0.3
-0.4
-0.5
0
50
100
150
200
250
300
Heat flow (W/g)
Temperature (°C)

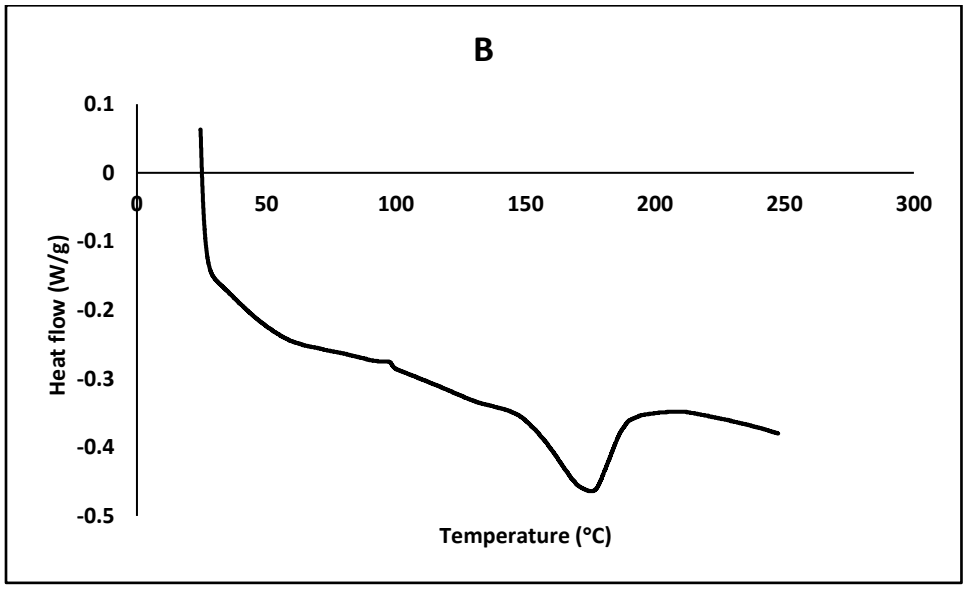
B
0.1
0
-0.1
-0.2
-0.3
-0.4
-0.5
0
50
100
150
200
250
300
Heat flow (W/g)
Temperature (°C)

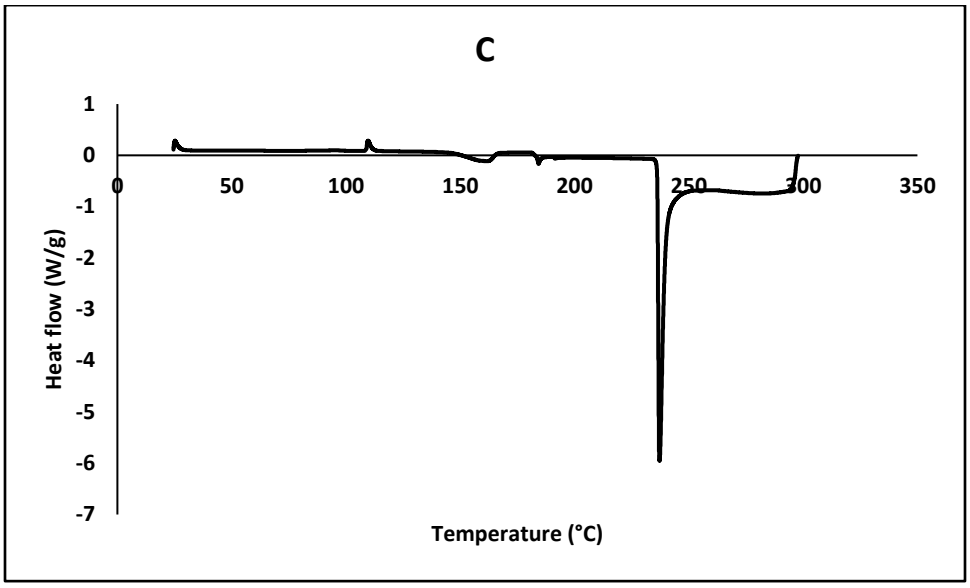

Figure 3.3: *The DSC thermogram of (A) PLA placebo polymer, (B) PVA placebo polymer, (C) caffeine powder.*

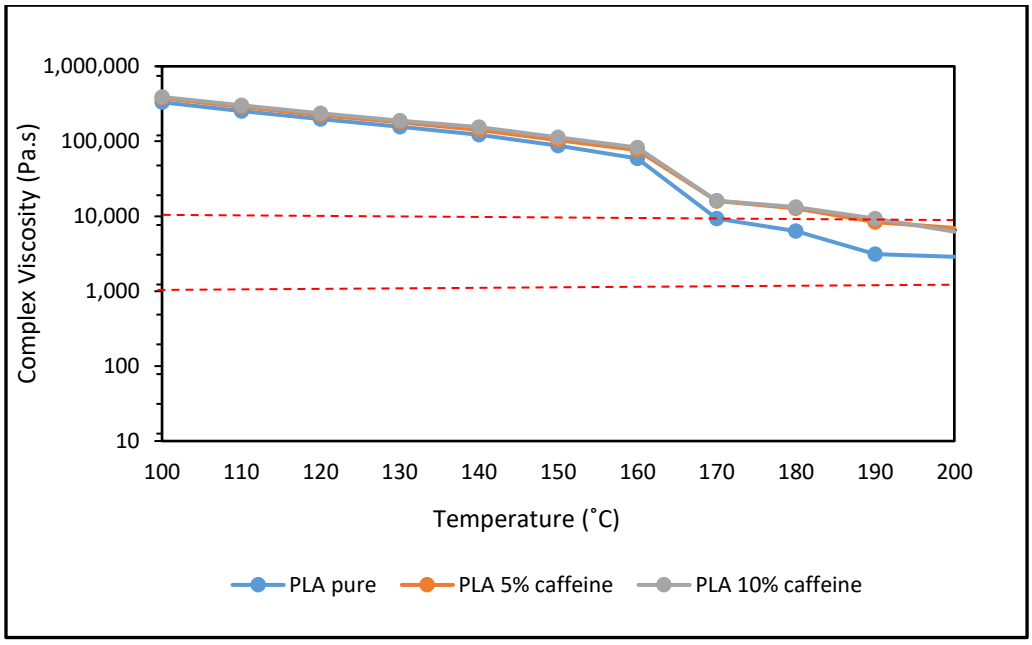

Figure 3.4: *Rheometer results of PLA complex viscosity (Pa.s) vs temperature (°C).*

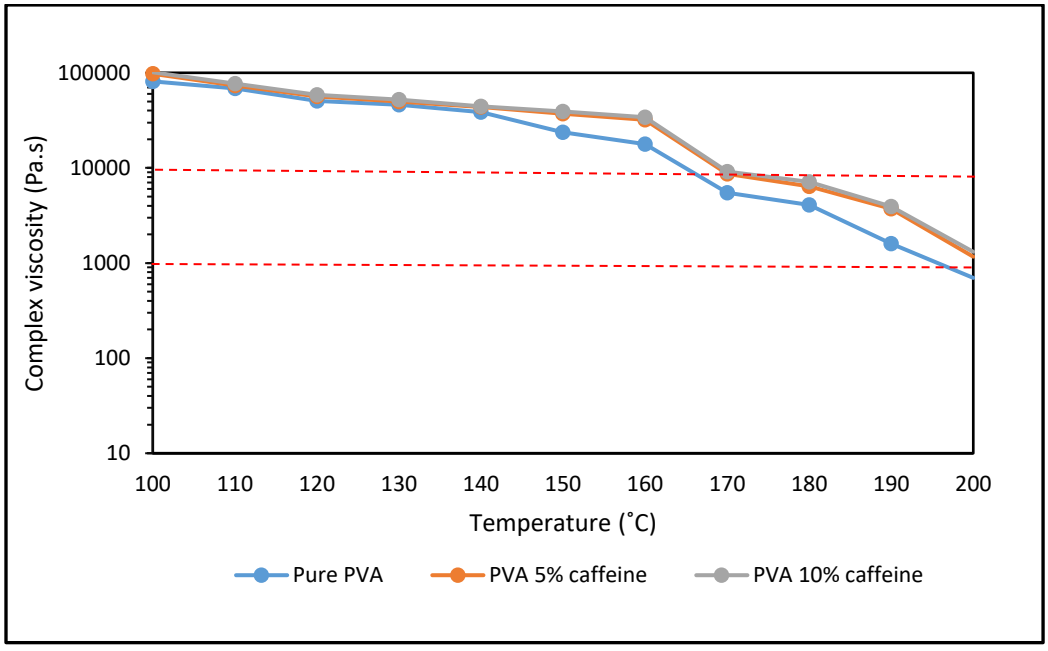

Figure 3.5: *Rheometer results of PVA complex viscosity (Pa.s) vs temperature (°C).*

3.3.2. HPLC analysis of caffeine

Figure (3.6) exhibits the caffeine standard curve, which encompasses eight distinct concentrations of caffeine measured using HPLC. The obtained linearity parameters and regression data indicated an excellent linear relationship (R^2=1) across the chosen concentration range of 8 to 32 µg/mL. The limit of detection (LOD) and limit of quantification (LOQ) were determined to be 0.77 µg/mL and 2.33 µg/mL, respectively. Table (3.8) provides a comprehensive summary of the results obtained for the HPLC assay parameters.

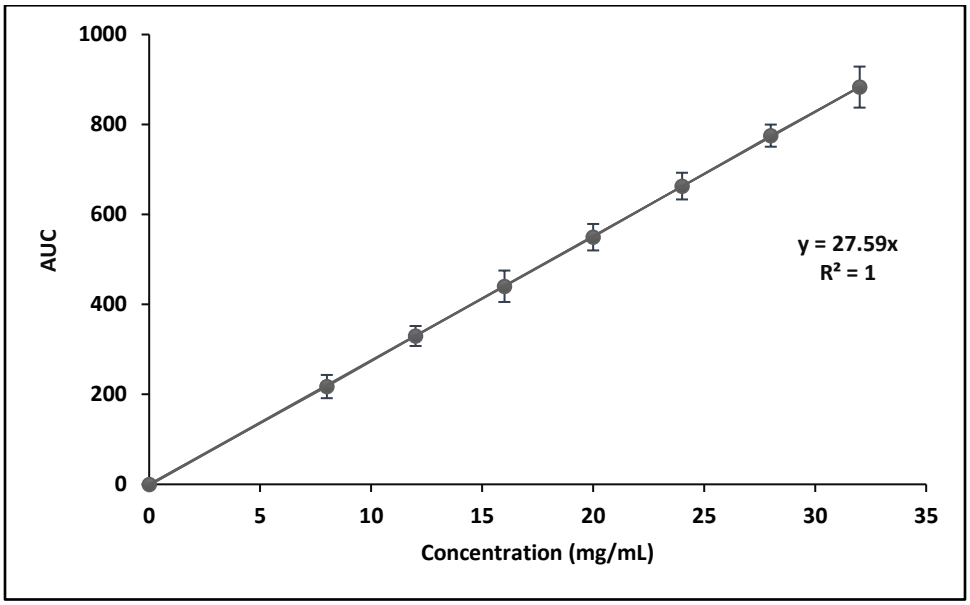

Figure 3.6: *HPLC standard calibration curve of caffeine. Results shown as mean (n=9) ± SD.*

Table 3.8: Assay parameters of caffeine HPLC method.

Assay parameters	Results
Accuracy	99.747 % ± 0.57
Slope	27.591
Intercept	0
Corelation coefficient (R^2)	1
Linearity range	8-32 µg/mL
SE of intercept	1
SD of intercept	1.42
Limit of detection (LOD)	0.77 µg/mL
Limit of quantification (LOQ)	2.35 µg/mL

3.3.3. Caffeine stability and solubility

The result of stability study indicated that caffeine could retain up to 90% of its stability over 35 days in (dH_2O) with temperature having non-remarkable effect. However, caffeine loses more than 65% of its stability in PBS within the first 2 days and remains constant over 35 days with negligible effect of temperature as demonstrated in Figure (2.10 A).

Figure (2.10 B) showed that caffeine exhibits higher solubility in dH_2O in comparison to PBS. At 37˚C, the solubility of caffeine in dH_2O was determined to be 27.82 mg/mL, whereas at 25°C, it was 18.44 mg/mL. In contrast, the solubility of caffeine in PBS is lower, with values of 5.66 mg/mL and 4.81 mg/mL in PBS at 37°C and 25°C, respectively. These findings highlight the superior solubility of caffeine in dH_2O, particularly at both temperatures. Based on these results, dH_2O was deemed to be the suitable release medium for this study.

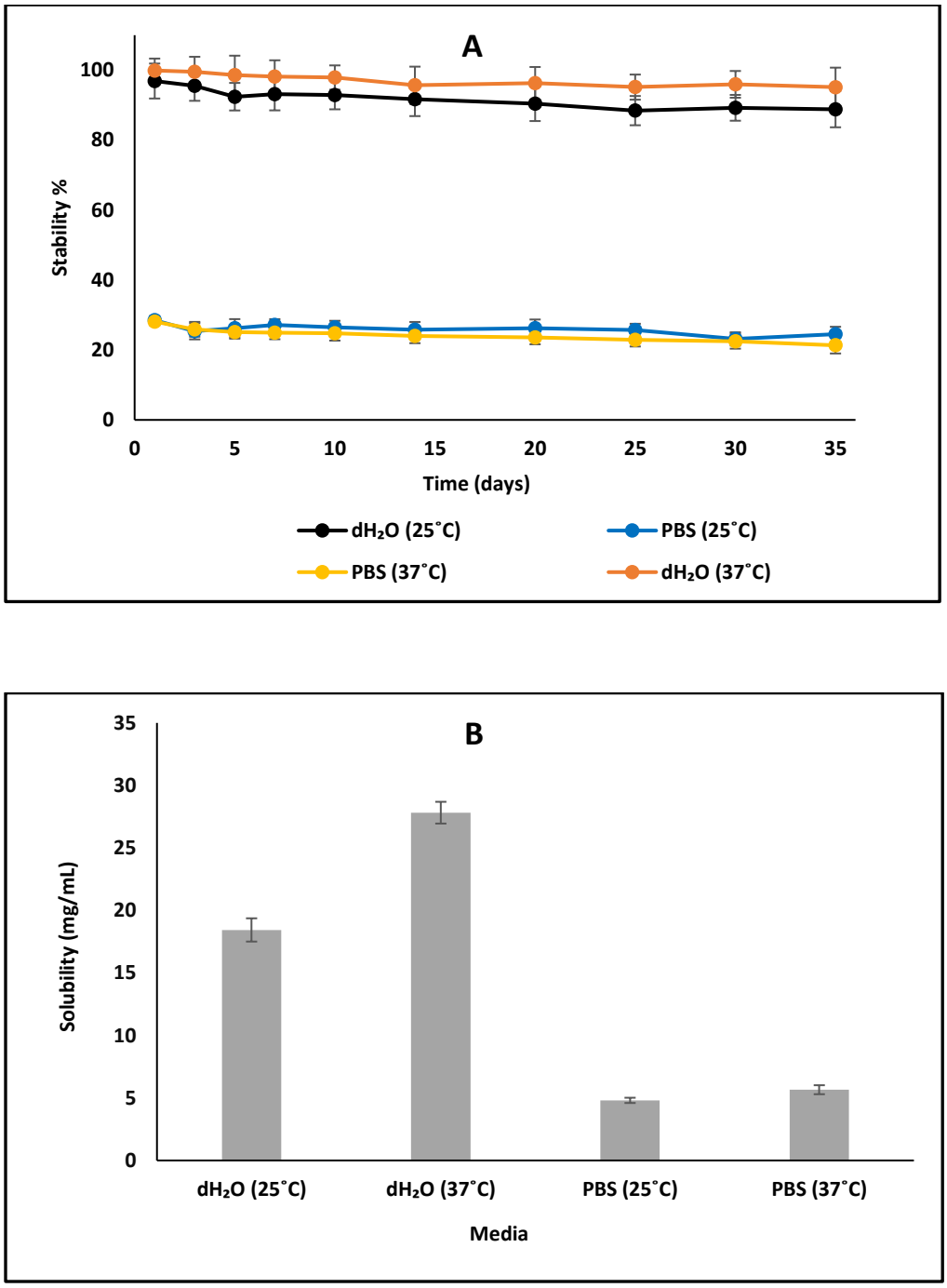

***Figure 3.7**: Caffeine stability in different media (A) and caffeine solubility in different media (B). Result presented as mean (n=3) ± SD.*

3.3.4. Impact of different 3D printing parameter on the *in vitro* drug release

The *in vitro* drug release analysis reveals distinct release profiles between tablets fabricated using PVA based filaments as depicted in Figure (3.8) and those utilising PLA based filaments as shown in Figure (3.9). Tablets composed of PLA based filaments exhibited sustained and progressively increasing drug release patterns over a 30-day duration. Conversely, tablets manufactured from PVA based filaments displayed an initial burst release, with more than 65% of the drug being released within the first six hours, irrespective of the varied 3D printing parameters explored. These results underscore the significant influence ($P < 0.05$) of the type polymer carrier on the drug release profile of the tablets, in alignment with prior literature studies (Funk et al., 2022; Kempin et al., 2017).

The drug release exhibited by PVA based 3D printed tablets is demonstrated in Figure (3.8). In terms of the influence of different layer heights, as shown in Figure (3.8 A), tablets with a layer height of 0.1 mm exhibited a drug release of 85% within the first 4 hours, whereas tablets with layer heights of 0.2 and 0.3 mm released 67.3% and 50.2% of the drug, respectively. Regarding the impact of different infill percentages, results showed that tablets prepared with 25% infill released approximately 80% of the drug within the initial 4 hours, whereas tablets with 50% and 100% infill released 66% and 47% of the drug, respectively as demonstrated in Figure (3.8 B). In terms of the influence of different infill patterns, as shown in Figure (3.8 C), results displayed that tablet manufactured with a zigzag infill pattern achieved a drug release of approximately 75% within 4

hours, whereas tablets with triangle and line patterns released 65% and 48% of the drug, respectively.

The drug release of PLA based 3D printed tablets is illustrated in Figure (3.9). Regarding the impact of various layer heights, as depicted in Figure (3.9 A), tablets with a layer height of 0.1 mm demonstrated a maximum drug release of 60.1%. In contrast, tablets with layer heights of 0.2 mm and 0.3 mm showed a maximum drug release of 46.2% and 41.3%, respectively. Regarding the influence of different infill percentages as shown in Figure (3.9 B). The results clearly indicated that tablets prepared with 25% infill achieved a maximum drug release of approximately 64.5%. In comparison, tablets with 50% and 100% infill released 56.5% and 40.1% of the drug, respectively, within the same time frame. Concerning the impact of different infill patterns, as depicted in Figure (3.9 C), tablets manufactured with a zigzag infill pattern achieved a drug release of approximately 65.7%, while tablets with triangle and line patterns released 39.1% and 47.2% of the drug, respectively. These findings highlight the significant impact of infill percentage, layer thickness, and infill pattern on the drug release behaviour of 3D printed tablets.

The release profiles differed between PLA and PVA polymer-based tablets, but the impact of various 3D printing parameters remained consistent for both types of tablets. The infill percentage, infill pattern, and layer height affected the drug release behaviour of the fabricated dosage forms. These parameters influenced both sustained release (in PLA-based tablets) and immediate release (in PVA-based tablets), underscoring their importance in controlling the release mechanism regardless of the polymer used.

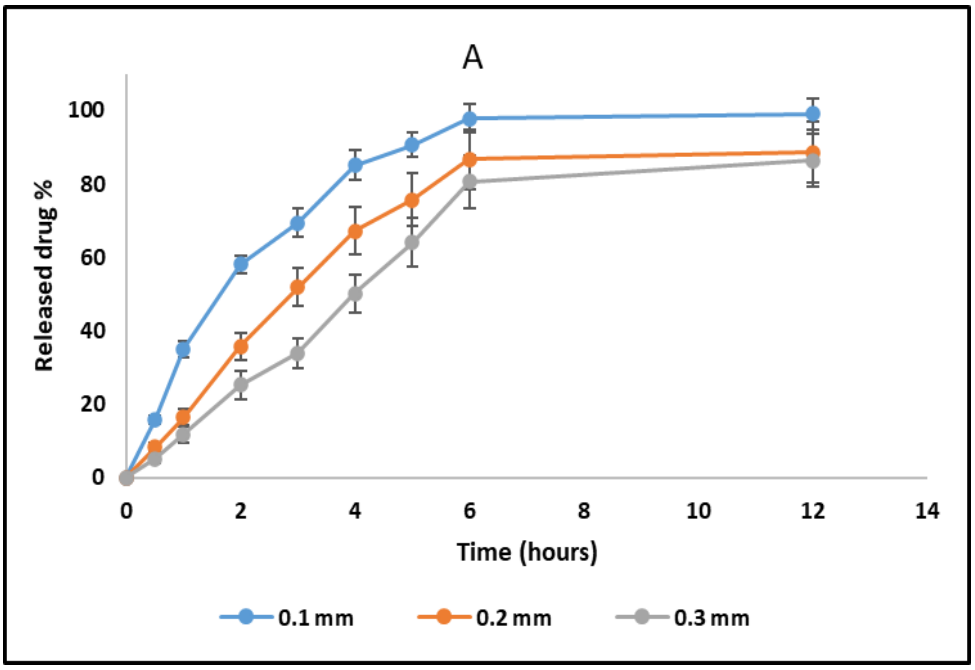
A
Released drug %
100
80
60
40
20
0
0
2
4
6
8
10
12
14
Time (hours)
0.1 mm
0.2 mm
0.3 mm

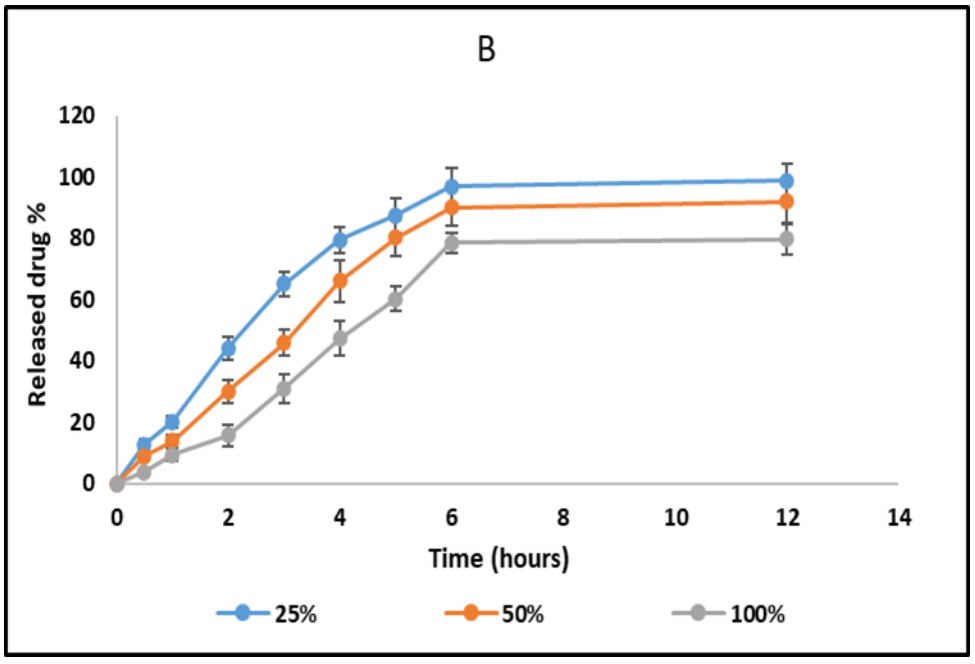
B
Released drug %
120
100
80
60
40
20
0
0
2
4
6
8
10
12
14
Time (hours)
25%
50%
100%

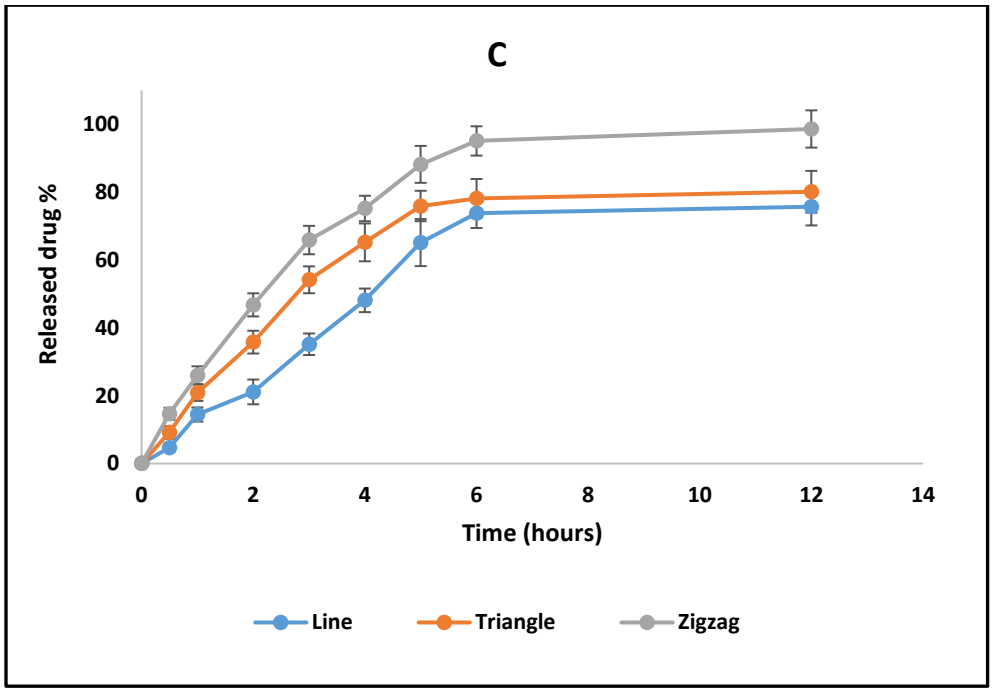

Figure 3.8: *The influence of different 3D printing parameters on the drug release of PVA based tablet loaded with caffeine. (A) different layer heights (mm), (B) different infill %, (C) different infill patterns. Results presented as mean (n=3) ± SD.*

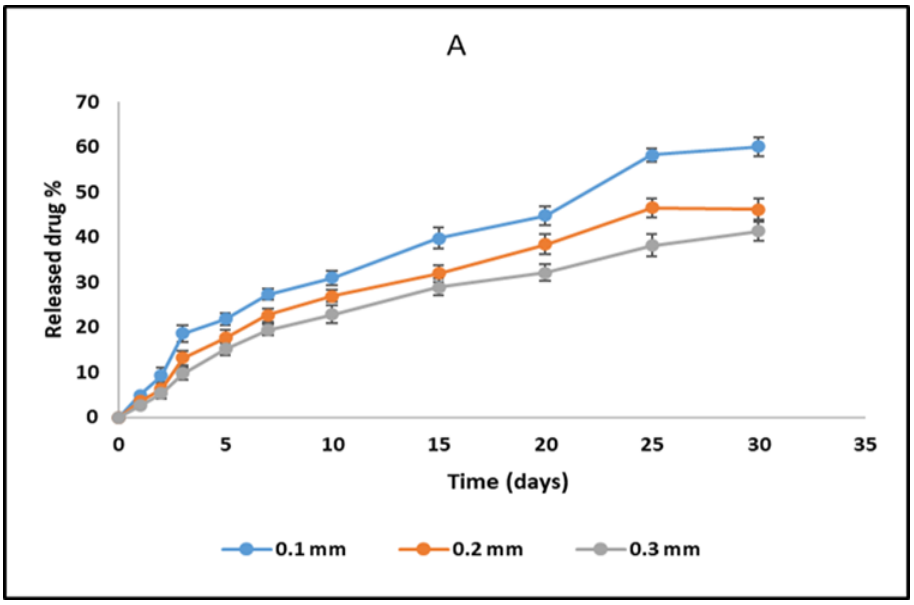
A
Released drug %
70
60
50
40
30
20
10
0
0
5
10
15
20
25
30
35
Time (days)
0.1 mm
0.2 mm
0.3 mm

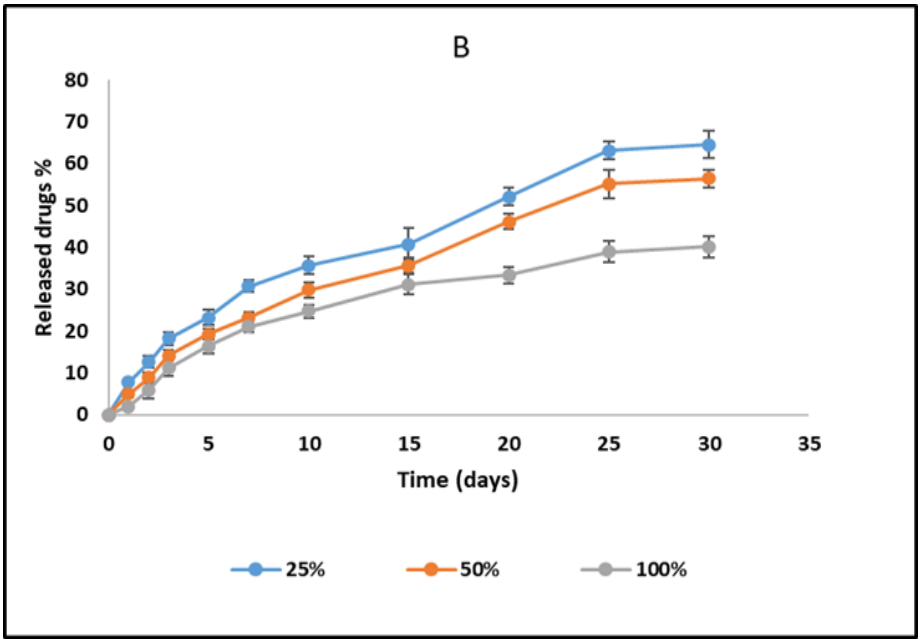
B
Released drugs %
80
70
60
50
40
30
20
10
0
0
5
10
15
20
25
30
35
Time (days)
25%
50%
100%

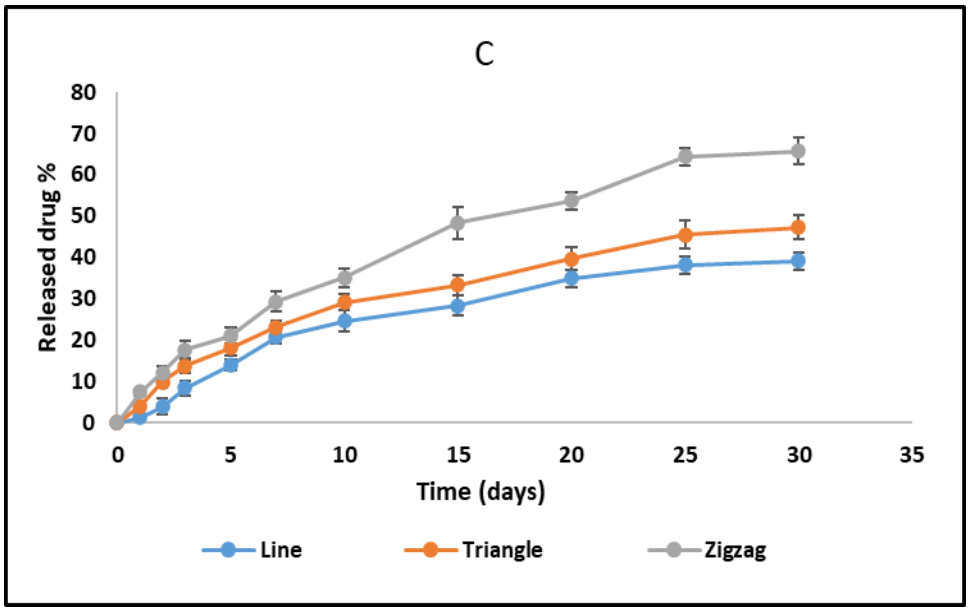

Figure 3.9: *The influence of different 3D printing parameters on the drug release of PLA based tablet loaded with caffeine. (A) different layer thickness (mm), (B) different infill %, (C) different infill patterns. Results shown as mean (n=3) ± SD.*

3.3.5. 3D printed tablets with different coating shells.

3.3.5.1. 3D printed tablets

The study involved the successful 3D printing of two types of shell coated tablets using an FDM-based 3D printer. Figure (3.10) showcases the tablets coated with PLA with varying pore sizes of 1 mm, 1.5 mm, and 2 mm. On the other hand, Figure (3.11) displays the tablet coated with PVA with different wall thicknesses of 1 mm, 1.5 mm, and 2 mm.

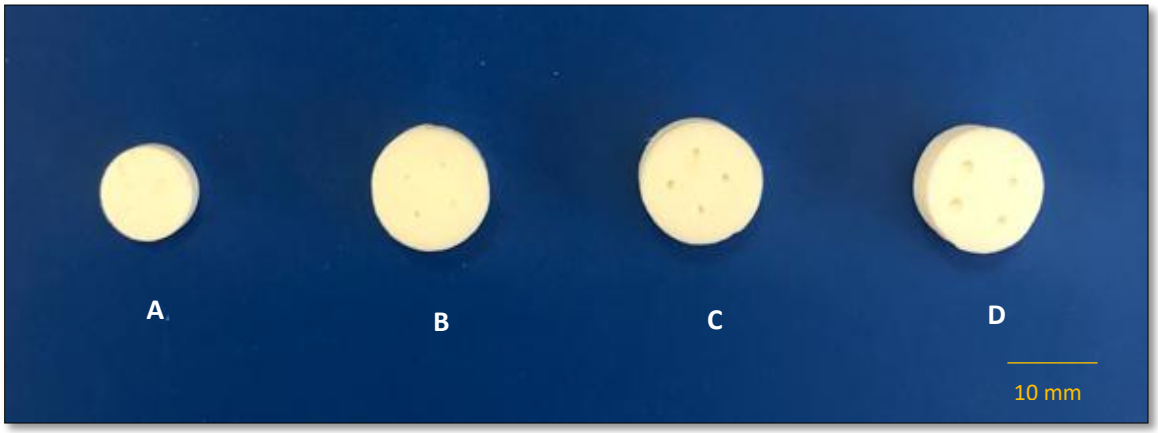

Figure 3.10: *Tablet coated with PLA of different pore sizes. Control tablet (A), 1 mm pore size (B), 1.5 mm pore size (C), 2 mm pore size (D).*

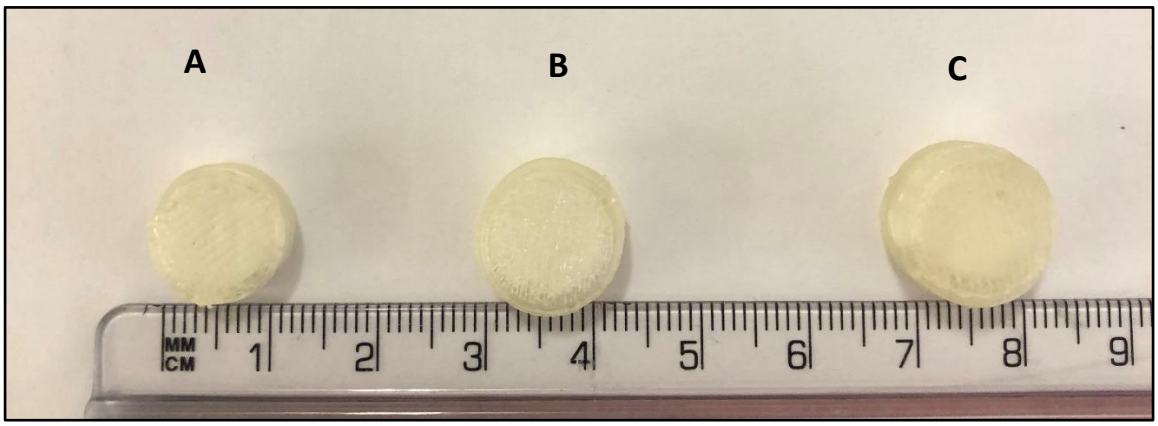

Figure 3.11: *Table coated with PVA with different wall thicknesses. (A) 1 mm wall thickness (B) 1.5 mm wall thickness, (C) 2 mm wall thickness.*

3.3.5.2. The in vitro release of PVA shell coating system of different wall thicknesses.

A PVA based shell coating system was developed to encapsulate an immediate release caffeine tablet to demonstrate the effect of shell wall thickness on the drug release profile Figure (3.11 A). The results revealed that an increase in shell wall thickness showed a decrease in the drug released from the shell tablet over the first 6 hours of release.

The immediate release caffeine tablet exhibited ≥ 90% drug release in 1 hour. However, the 3D printed shell sustained this release in correlation with shell wall thickness. The shell tablet with 1mm, 1.5mm and 2mm wall thickness exhibited a drug release of 90, 85 and 71%, respectively during the first 6 hours' time. The drug release from PVA based shell was due to erosion of the shell wall and dissolution of the PVA as PVA is water soluble, which facilitates the drug release in the dissolution media from the tablet. This phenomenon of erosion based drug release was

previously reported in the literature (Algahtani et al., 2020). The drug release from the PVA coated tablet has followed mostly the Korsmeyer-Peppas and Higuchi models as demonstrated by their coefficient values (R^2) in Table (3.10).

These findings provide compelling evidence of the impact of shell wall thickness on the drug release profile of the encapsulated tablet. The increase in shell wall thickness demonstrated a corresponding decrease in the rate of drug release during the initial 6 hours. This suggests that the shell wall thickness can be effectively manipulated to modulate the release kinetics of the enclosed drug, offering potential applications in controlled drug delivery systems.

3.3.5.3. The in vitro release of PLA shell coating system of different pore sizes.

The study specifically investigated the impact of pore size on the drug release behaviour of PLA shell tablets enclosing immediate release caffeine tablets as shown in Figure (3.11 B). The uncoated caffeine tablets demonstrated rapid drug release, with over 90% released within one hour. However, a controlled drug release profile was achieved when the immediate release tablets were enclosed within 3D printed PLA shells with varying pore sizes.

The results of the drug release studies demonstrated a significant impact of pore size on drug release within the first 8 hours ($p < 0.05$). It is noteworthy that the coated tablet with a larger pore size exhibited a higher drug release compared to the shell tablet with a smaller pore size. Specifically, within a 12 hour timeframe, the drug release percentages from the shell tablets with

pore sizes of 1 mm, 1.5 mm, and 2 mm were measured at 75.23, 92.87, and 94.91%, respectively. These findings highlight the potential of using 3D printed PLA shells with varying pore sizes to achieve controlled drug release from immediate release tablets. This approach provides a versatile and customisable method for tailoring the release profile of pharmaceutical formulations. The drug release from PLA based shell was attributed to drug diffusion through pores as suggested by the release models outlined in Table (3.9) in addition to the fact that PLA is water insoluble polymer, and the shell remained intact during the dissolution study.

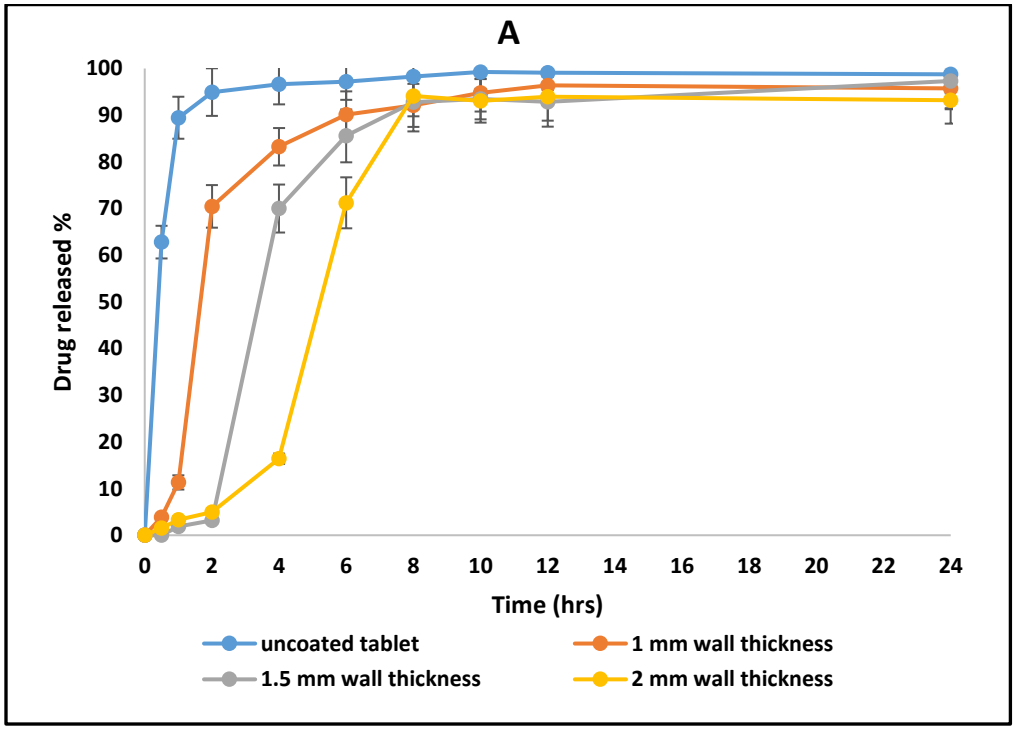

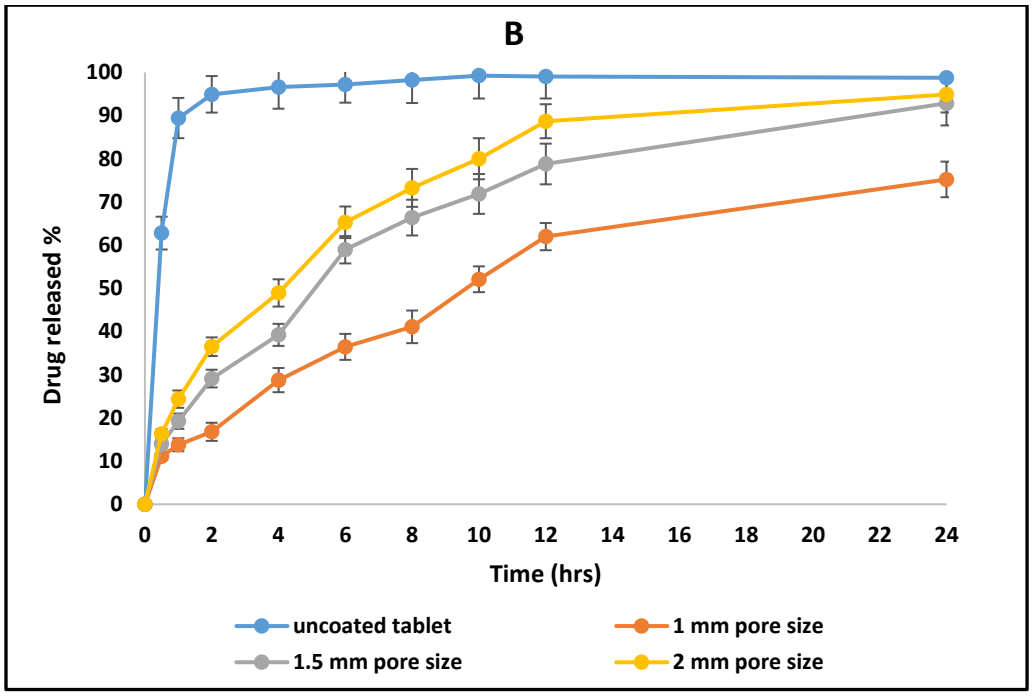

***Figure 3.12**: The drug release from shell coated tablet. (A) PVA coating shell of different wall thickness, (B) PLA coating shell of different pore sizes. Results shown as mean (n=3) ± SD.*

Table 3.9: Release constants (k) and correlation coefficient (R^2) of release models for PLA coating shell with different pore sizes.

PLA shell with different pore sizes	Zero-Order		First-Order		Higuchi		Korsmeyer–Peppas		
	R^2	k (% h^{-1})	R^2	K (h^{-1})	R^2	k (% $h^{-0.5}$)	R^2	k (%h^{-n})	n
1 mm	0.91	4.02	0.96	0.025	0.99	14.63	0.77	1.63	0.71
1.5 mm	0.86	5.33	0.98	0.04	0.97	20.82	0.75	1.77	0.76
2 mm	0.83	5.76	0.95	0.05	0.98	23.37	0.74	1.81	0.78

Table 3.10: Release constants (k) and correlation coefficient (R^2) of release models for PVA coating shells with different wall thicknesses.

PVA coating shell with different wall thicknesses	Zero-Order		First-Order		Higuchi		Korsmeyer–Peppas		
	R^2	k (% h^{-1})	R^2	K (h^{-1})	R^2	k (% $h^{-0.5}$)	R^2	k (%h^{-n})	n
1 mm	0.72	6.55	0.66	0.06	0.92	27.61	0.81	1.94	0.84
1.5 mm	0.78	6.29	0.81	0.07	0.91	25.37	0.93	1.89	0.81
2 mm	0.81	5.91	0.64	0.06	0.9	23.12	0.93	1.81	0.87

3.4. Discussions

The development of drug loaded filaments with enhanced properties is a crucial aspect in ensuring a successful 3D printing process. One approach that has been reported for the preparation of such filaments, intended for use in FDM based 3D printing, is HME technology. (Tan et al., 2018). However, adjusting the process parameters such as temperature, speed and size of dies is required to synthesise a printable filament. The prepared drug loaded filaments was characterised regarding their drug content, filament diameter, extrusionability and feedability. The results showed that the HME prepared filaments were acceptable in terms of drug polymer stability as revealed by the analysis of drug content. This stability was observed due to the fact that the processing temperature employed during HME was below the degradation temperatures of both the polymers and caffeine. Furthermore, the successful printability of the prepared filaments can be attributed to their acceptable diameters and the inherent high mechanical properties of the base polymers, PLA and PVA. These polymers possess characteristics such as a high breaking force

and high elongation at break, which enable the printed objects to endure external forces and retain their structural integrity (Decuir et al., 2016; Obeid, Madžarević, Krkobabić, et al., 2021).

The influence of different 3D parameters on the manufactured drug loaded tablets showed remarkable impact on the *in vitro* release profile. There was an inverse relation between the infill % and amount of drug released. This relation can be explained that the lower infill % dosage forms will be higher in porosity which subsequently facilitate the entry of release fluid into the core of the tablets resulting in faster drug release (Reddy Dumpa et al., 2020). While the higher infill % is reported to cause reduction of the total surface area which eventually leads to slower drug release (Chen et al., 2020). Such an impact was previously investigated in different studies. For example, Goyanes et al*.,* investigated the influence of different infill %, namely 10, 50 and 90%, on the release profile of 3D printed tablets containing 5-aminosalicylic acid and 4-aminosalicylic acid loaded into PVA. The obtained results indicated that the infill % of 10 exhibited higher drug release followed by the 50% and at the least release was demonstrated by the 90 % infill (Goyanes, Buanz, et al., 2015). Additionally, Kadry, Al-Hilal et al*.,* examined different infill % on 3D printed tablet manufactured from Hydroxypropyl-methylcellulose (HPMC) loaded with diltiazem as a model drug. The obtained results showed that the released drug was dramatically declined when the infill % was increased to 100% (Kadry et al., 2018).

3D printing technology offers a range of infill pattern options, including line, triangular, zigzag, cubic, concentric, trihexagonal, and more. When considering the impact of infill pattern on drug release, it was found that the zigzag pattern exhibited the highest drug release compared to the

other examined infill patterns. To some extent, it was correlated with the literature where zigzag infill pattern demonstrated the highest release profile compared with cubic, concentric and trihexagonal (Obeid, Madžarević, et al., 2021b). However, based on my current knowledge, there is no study available that specifically compares the influence of the zigzag, line, and triangular infill patterns on a specific parameter such as drug release. The findings indicate that various infill patterns have the potential to serve as parameters for modifying release behaviour. However, it is important to note that the observed influence of these different infill patterns was investigated under a constant infill percentage of 50%. Because at elevated infill percentages, such as 100%, the internal structure of a 3D printed object will demonstrate complete solidity irrespective of the chosen infill pattern. This implies that the entirety of the object's interior will be occupied by the printing material, resulting in the absence of any voids or empty spaces.

In relation to the influence of layer height on the drug release of fabricated tablets, the results showed a clear inverse relationship between the layer height and the amount of drug release. Specifically, higher layer heights were associated with lower levels of drug release. Although the influence of different layer heights on the mechanical properties and printing time of the 3D printed objects was previously investigated (Murugan et al., 2019), however, to our knowledge no study has yet examined their impact on the *in vitro* release profile of 3D printed dosage form. Our results will provide better understanding of the influence of layer height on the release profile of 3D fabricated dosage forms. However, it is important to consider that 3D printing with smaller layer heights is associated with longer printing durations. This is due to the increased number of

deposited layers required to create the desired object, which subsequently extends the overall printing time.

Altering the release profile of an immediate release tablet by 3D printing of coating shell was found applicable in this study. Two different types of coating shells were manufactured using 3D printing techniques, and they had a significant impact on the release behaviour of the enclosed immediate release tablet. The influence of different pore sizes of the PLA coating shell on the release behaviour was found to be directly proportional to the pore size. This means that higher pore sizes allowed the release media to move more easily inside the tablet core, resulting in faster drug release. On the other hand, the influence of the PVA coating shell with variable wall thicknesses exhibited an inverse relationship with the *in vitro* drug release. This suggests that thicker wall thicknesses in the PVA coating shell resulted in slower drug release. These results were consistent with previously reported studies (Algahtani et al., 2020; Reddy Dumpa et al., 2020). These outcomes demonstrate the feasibility of using FDM based 3D printers to manufacture coating shells that can effectively modify the *in vitro* release of pre-existing dosage forms.

3.5. Conclusion

In this study, the influence of different 3D printing parameters on the *in vitro* drug release from the 3D printed drug loaded tablets was examined. The results indicated that the type of base polymer played a crucial role in determining the amount and release behaviour of the drug. Furthermore, when considering the impact of different 3D printing parameters, it was observed that an infill percentage of 25%, Zigzag infill pattern, and a layer height of 0.1 mm resulted in higher drug release compared to other parameters, regardless of the types of base polymers used. Moreover, the 3D fabrication of a coating shell with various pore sizes and shell wall thicknesses demonstrated that the drug release of a formulation could be altered without changing its composition. These findings highlight the potential capacity of 3D printing to modify and customise the drug release of pharmaceutical products. By adjusting specific 3D printing parameters, such as infill percentage, infill pattern, layer height, and coating shell characteristics, it becomes possible to control the release profile of drugs, offering opportunities for personalised and optimised drug delivery system. Furthermore, FDM based 3D printing technology demonstrated its effectiveness in altering *in vitro* drug release through the utilisation of various designs of coating shells.

Chapter 4 : 3D PRINTING OF PHARMACEUTICAL DOSAGE FORM CONTAINING (ISONIAZID AND PYRIDOXINE HCL) AS SINGLE AND BILAYER DOSAGE FORMS FOR THE TREATMENT OF TUBERCULOSIS

4.1. Introduction

Mycobacterium tuberculosis, the causative agent of tuberculosis (TB), is estimated to infect approximately one-fourth of the global population, equivalent to around 2 billion people (Sterling et al., 2020). A significant proportion of individuals with TB are asymptomatic and are diagnosed with latent TB infection (LTBI). The World Health Organisation (WHO) defines LTBI as a condition in which the immune system remains responsive to the stimulation of Mycobacterium tuberculosis antigens, despite the absence of clinically apparent active TB symptoms. In cases of LTBI, there is either an absence of bacillary replication or the replication occurs below a certain threshold, attributed to immunological control. (Dartois & Rubin, 2022). If the LTBI left untreated, about 5% to 10% are vulnerable to develop active TB infection during their lifetime (Cohn et al., 2000). However, immunocompromised patients for a variety of reasons and children under five years with LTBI are at higher risk of developing active TB infection (Chapman & Lauzardo, 2014).

Isoniazid (INH) is a medication commonly prescribed for the treatment of tuberculosis TB. It is used as part of a combination therapy regimen for active TB or as a long-term monotherapy for the preventive treatment of LTBI. Studies have shown that administering INH as chemoprophylaxis for a duration of 12 months significantly reduces the risk of developing active TB by up to 75% in individuals with LTBI (Ai et al., 2016; Zenner et al., 2017). Therefore, a single daily dose of INH for 6 to 9 months is recommended for the management of LTBI. However, long term use of INH

therapy, competitively inhibits the metabolism of Pyridoxine Hydrochloride (PDX) which consequently causes peripheral neuropathy as a side effect. Therefore, PDX supplementation during the long term INH therapy is recommended to reduce the incidence of developing the peripheral neuropathy (Shakya et al., 2012).

Fixed-dose combinations (FDCs) are dosage forms that contains two or more medications within the same dosage form. FDCs use in the treatment of chronic diseases such as hypertension, diabetes, and HIV and can improve the patient compliance and subsequently increase the treatment safety and effectiveness (Kim & Weon, 2021). Various pharmaceutical technologies such as bilayer system, multiarticulate system (MAS), hot melt extrusion and 3D printing can be used to produce such a dosage form that might help to combine more than two drugs and improve the treatment efficacy and tolerability (Janczura et al., 2022).

The aim of this chapter is to assess the viability of FDM based 3D printing for the production of a FDC solid oral dosage form in the form of a tablet. The tablet will contain two distinct APIs namely INH and PDX to mimic the drug combinations that are usually used for the treatment of LTBI. The two drugs, INH and PDX, will be incorporated into a pharmaceutically approved polymer (Soluplus), along with other excipients that aid in the manufacturing process. Two different types of tablets will be produced. The first type of tablet will contain both drugs in a single-layer tablet. The second type of tablet will be a two-compartment (two-layer) tablet, with each layer containing only one drug separately. Both tablet types will be assessed for drug content and *in vitro* drug release.

4.2. Materials and method

4.2.1. Materials

Polyvinyl caprolactam-polyvinyl acetate-polyethylene glycol graft co-polymer (Soluplus) purchased from (BASF pharma, France). Hydroxypropyl cellulose (HPC), MW-80000 and Polyethylene glycol (PEG), MW 1000, were acquired from (Sigma-Aldrich, UK). Isonicotinic acid hydrazide (Isoniazid) powder 99% purchased from Across organics (India). Pyridoxine Hydrochloride (PDX) purchased from (Sigma-Aldrich, UK). Type (I) deionised water (dH_2O) supplied by laboratory Triple Red water system (Buckinghamshire, UK). Phosphate buffered saline (PBS) tablets was purchased from VWR (England, UK).

4.2.2. HPLC method development

4.2.2.1. Materials and reagents

HPLC grade Acetonitrile (ACN) and HPLC grade methanol 99.9% were purchased from ThermoFisher Scientific (Loughborough, UK), Potassium dihydrogen ortho-phosphate (MW 136.08 g/mol) and orthophosphoric acid (MW 98 g/mol), were purchased from Sigma-Aldrich (Dorset, Gillingham, UK).

4.2.2.2. HPLC chromatographic conditions

HPLC analysis was performed using an Agilent Technologies 1260 infinity II HPLC (California, United States), composed of a quaternary pump. The separation process was performed at 25°C using a C18 silica-based column (150 mm × 4.6 cm) with a particle size of 5 µm. The UV detection was set at 280 nm. The mobile phase was composed of a mixture of; Potassium dihydrogen ortho-phosphate solution (2.27 g dissolved in 1000 mL of deionised water): Acetonitrile: Methanol in the ratio of (90:5:5 v/v/v). Orthophosphoric acid was used to adjust the pH at 1.9. The injection volume was 5 µL with a flow rate of 1 mL/min and a run time of 10 min.

4.2.2.3. Preparation of standard stock solution and sample solutions

100 mg of INH and PDX were transferred into two separate 100 mL volumetric flasks and dissolved in 10 mL of dH_2O, sonicated for 10 min at 37°C using VWR ultrasonic bath (Leicestershire, UK). The volumes made up to 100 mL with dH_2O to prepare a final stock solution of 1000 µg/mL.

4.2.2.4. Linearity evaluation

Linearity analysis was conducted individually for INH and PDX. For each drug, seven aliquots ranging from 0.25 mL to 1.75 mL were withdrawn from the stock solution. These aliquots were then diluted with dH_2O to a final volume of 10 mL, resulting in various concentrations ranging from 25 µg/mL to 175 µg/mL. Each concentration was prepared in triplicate for both drugs. The prepared samples were subsequently analysed via HPLC. The peak areas obtained were used to

construct calibration plots of peak area versus concentration for each drug. Results were presented as mean (n=6) ± standard deviation (SD).

4.2.2.5. Specificity determination

The specificity of the analysis was examined to confirm the absence of any interference or overlapping peaks between the analytes in the chromatogram. This assessment involved injecting a 20 µL sample of the placebo (matrix) and a mixture containing both INH and PDX separately.

4.2.2.6. Accuracy determination

The accuracy of the method is a measure of how closely the results obtained using the method align with the true value. In this study, accuracy was assessed by calculating the recovery ratio and the coefficient of variance (CV). To evaluate accuracy, three different concentrations (25 µg/mL, 100 µg/mL, and 175 µg/mL) were prepared for both INH and PDX. Each concentration was prepared in triplicate, representing the lowest, middle, and highest concentrations of the calibration plot. The accuracy test was performed for both INH and PDX separately.

4.2.2.7. Precision evaluation

The precision of the method was assessed through both repeatability and reproducibility measurements. Repeatability refers to the precision achieved within a single day, while reproducibility measures the intermediate precision across different days. Samples of INH and PDX

with three different concentrations (25 µg/mL, 100 µg/mL, and 175 µg/mL) were prepared separately from the stock solution. Six replicates of each concentration of each drug were injected on two different days.

4.2.2.8. Sensitivity test

The sensitivity of the method was evaluated by calculating the limit of detection (LOD) and the limit of quantification (LOQ). The LOD represents the smallest amount of analyte that can be detected but not necessarily quantified in a sample, while the LOQ indicates the smallest amount of analyte in a sample that can be quantified with reasonable accuracy. To determine the LOD and LOQ, the linearity plot obtained from the calibration curve was utilised. The calculation of LOD and LOQ can be performed using Equation (4.1).

$$LOD = 3.3\sigma/S \; and \; LOQ = 10\sigma/S \qquad 4.1$$

where (σ) is standard deviation of the intercept and (S) is the slope of the calibration curve.

4.2.3. INH and PDX stability in different release media.

10 mg of each pure drug (INH and PDX) was separately dissolved in two different solutions. One solution contained 10 mL of dH2O with a pH of 5.4, and the other solution contained phosphate buffer solution (PBS) with a pH of 7.4. Both solutions were sonicated in a water bath for 10 minutes, using VWR ultrasonic bath (Leicestershire, UK), to ensure complete dissolution of the drugs. Once dissolved, the samples were filtered and stored at different temperature zones: 37˚C, 25˚C, and 4˚C. Samples were collected at specific time intervals of 1, 6, 24, 48, and 72 hours and subsequently analysed using HPLC. The data obtained from the analysis were presented as the mean value (n=3) ± standard deviation (SD).

4.2.4. INH and PDX solubility test

Separate over-saturated solutions were prepared for both drugs (INH and PDX) by dissolving excess amounts of each drug in 5 mL of dH_2O. Samples were kept for 48 hours in an orbital shaking incubator, Unitron HT infors (Surrey , UK), operating at temperature of 37˚C and a speed of 100 RPM. Samples then were subjected to centrifugation at a speed of 13000 RPM for 5 min using Labnet Prism R centrifuge (Edison NJ, USA). The supernatant was analysed via HPLC. Results were presented as mean (n=3) ± SD.

4.2.5. Thermal stability of INH and PDX

50 mg PDX and 35 mg of INH were weighed into 50 mL glass volumetric flasks. The samples were stored in laboratory oven, VWR DRY-line (Leicestershire, UK), at three different temperatures (130, 140 and 150˚C) for 90 min. After each exposure, the stressed samples were subsequently dissolved in 50 mL of dH_2O and analysed by HPLC to find the percentage of drug remaining using Equation (4.2).

$$The\ drug\ remaining\ \% = \frac{Amount\ of\ found\ drug}{Amount\ of\ initial\ drug} \times 100 \qquad 4.2$$

4.2.6. Preparation of drug loaded formulations by HME

A 10 mm co-rotating twin screw hot melt extruder (Kapex, USA) was employed to prepare three different formulations loaded with drugs. The APIs, INH and PDX, were loaded separately into two of the formulations. The third formulation involved a combination of both APIs. Various excipients were utilised. These included Soluplus, polyethylene glycol (PEG), and hydroxypropyl cellulose (HPC). The specific ratios of APIs and excipients in each formulation are outlined in Table (4.1). Each batch, with a mass of 100 g, was prepared separately and mixed using a Turbula mixer for a duration of 2 minutes. Subsequently, the resulting mixture was transferred to a light-protected vacuum desiccator and stored until required for the HME process. During the HME process, the physical mixture was fed into the extruder, which had three different heating zones: feeding,

mixing, and conveying. The formulations were extruded through a circular 2 mm die and subsequently hauled off using an air-cooled conveyor system.

The screw speed of the extruder was consistently set at 20 RPM for all formulations in this study while the barrel temperatures were varied within the range of 112 to 135°C. The specific screw speed and barrel temperature settings were established through preliminary experiments, considering data from analysis techniques such as DSC and rheometer (complex viscosity). These determined conditions led to the preparation of the most desirable extrudate characteristics in terms of appearance and texture as well as the miscibility between the drug and polymer components.

Following the hot melt extrusion (HME) process, the extrudates from each formulation were fed into a 3devo pelletiser (Utrecht, The Netherlands). The purpose of this step was to convert the extrudates into pellets with a size range of 4 to 6 mm. These pellets were then stored in a vacuum desiccator, protected from light exposure, until they were required for 3D printing applications. The drug content of the each extrudate was determined by HPLC.

Table 4.1: Composition of HME formulations.

Formulation No.	Formulation Code	Formulation content	Content Ratios (% w/w)
1	L1	Soluplus/**INH**/**PDX**/PEG/HPC	63.5/16/5.5/10/5
2	L2	Soluplus/**INH**/PEG/HPC	60/25/10/5
3	L3	Soluplus/**PDX**/PEG/HPC	70/15/10/5

4.2.7. Characterisation of hot melt extrudate.

4.2.7.1. Drug content analysis

100 mg samples of the extrudate were randomly collected from three distinct sections (beginning, middle, and end) of each extrudate. These samples were individually dissolved in 20 mL of deionised water (dH_2O). To expedite the dissolution process, the solutions were sonicated for 10 minutes at a temperature of 37°C using a VWR ultrasonic bath (Leicestershire, UK). Following sonication, the solutions were filtered through a 0.45 µm filter and subjected to analysis using HPLC. Results were presented as mean (n=3) ± SD.

4.2.7.2. Raman mapping for drug homogeneity

Drug distribution among the polymer matrix was investigated using Raman mapping. Raman measurements were performed on a DXR™ Raman Microscope (Thermo-Fisher scientific, UK) using 780 nm laser source, 10X objective lens and step size of 50*50 μm^2. Data were collected and analysed using OMNIC™ Series Software (Thermo-Fisher Scientific, UK). The components distributions were estimated using the classical least squares (CLS) method. In this approach, reference spectra of the pure components were obtained on the same instrument under identical experimental conditions. The CLS method utilised these reference spectra to analyse the collected data and estimate the distribution of the components within the sample. By comparing the measured spectra with the reference spectra, the CLS method provided insights into the relative concentrations and spatial distribution of the different components in the sample.

4.2.7.3. Differential scanning calorimetry (DSC) analysis

DSC measurements were performed using a Discovery DSC 250 (TA Instruments, USA). Samples were weighed as 6-8 mg and enclosed in Tzero aluminium pans. An empty sealed aluminium pan was used as reference. DSC thermograms were acquired in a cooling-heating ramps from 25°C to 250°C at a heating rate of 10°C /min performed under nitrogen atmosphere.

4.2.7.4. Rheology

A rheometer, Discovery HR-1 (TA instruments, USA), was used to investigate the rheological properties of all pure polymers as well as the polymer- API physical mixtures. Dynamic oscillatory measurements were obtained using a parallel plate geometry with 20 mm diameter with gap distance of 1000 µm at temperature starting from 200°C to 100°C at a cooling rate of 10 °C/5 min. The tests were performed under a constant frequency of 5 rad/s to ensure consistent and reliable data acquisition.

4.2.7.5. X-Ray diffractometer (XRD) analysis

Crystallinity of both drugs (INH and PDX) were evaluated by XRD measurements for INH pure powder, PDX pure powder and INH/PDX/polymer extrudate (formulation L1). The XRD patterns were recorded by Rigaku MiniFlex 600 (Rigaku, USA) using Cu-Kα radiation (1.542 Å). The applied voltage was 40 kV while the current was 15 mA. Scanning was performed up to 2ɵ of 90°.

4.2.8. Computer-aided design CAD of the pharmaceutical dosage forms

The CAD of the dosage forms were created using AutoCAD (Autodesk Inc, California, USA) version 2021, was exported in the STL format. Subsequently, it was converted to the G-code format using the slicer software Cura3.0 (Ultimaker, USA). Two different designs were developed for the tablet, each containing both APIs (INH and PDX). The first design consisted of a single tablet, where

formulation (L1) was used as the feeding material as shown in Figure (4.1 A). The second design involved a two-layer tablet, made from formulations (L2) and (L3) as the feeding materials as demonstrated in Figure (4.1 B). In the context of the study, AutoCAD was employed instead of TinkerCAD to ensure the alignment of the two layers in the tablet design. This allowed for precise positioning and alignment of the layers, ensuring the integrity and functionality of the final product. Additionally, AutoCAD facilitated the accurate determination of the percentage of each layer's height, which is crucial for controlling and maintaining the desired drug composition within the tablet.

4.2.9. Selecting the dimensions and drug content of both tablet designs.

The dimensions of the designed dosage form were established to be a cylinder tablet with a diameter of 10 mm. The cylinder height was determined to be 6 mm, and the average weight of the tablet was measured at 350 mg. Mathematical calculations were conducted to determine the height of each layer in the two-layer tablets, ensuring that they contained a similar drug strength compared to the one layer tablet. These calculations were based on the expected drug content of the HME formulations and the tablet's weight. In a single-layer tablet (illustrated in Figure 3.1 A), approximately 56 mg of INH and 19 mg of PDX were estimated to be distributed across 60 layers (each 0.1 mm thick) with a total weight of 350 mg. For a bilayer tablet (as shown in Figure 3.1 B) to achieve a similar drug strength, considering formulations L2 and L3, about 38 layers of L2 (weighing around 223.3 mg) followed by 22 layers of L3 (weighing 126.7 mg) out of the total 350 mg would provide the desired drug content. This corresponds to a cylinder height of 2.18 mm for

L3 out of 6 mm and 3.82 mm for L2 out of 6 mm. The 3D printed formulations are outlined in Table (4.2).

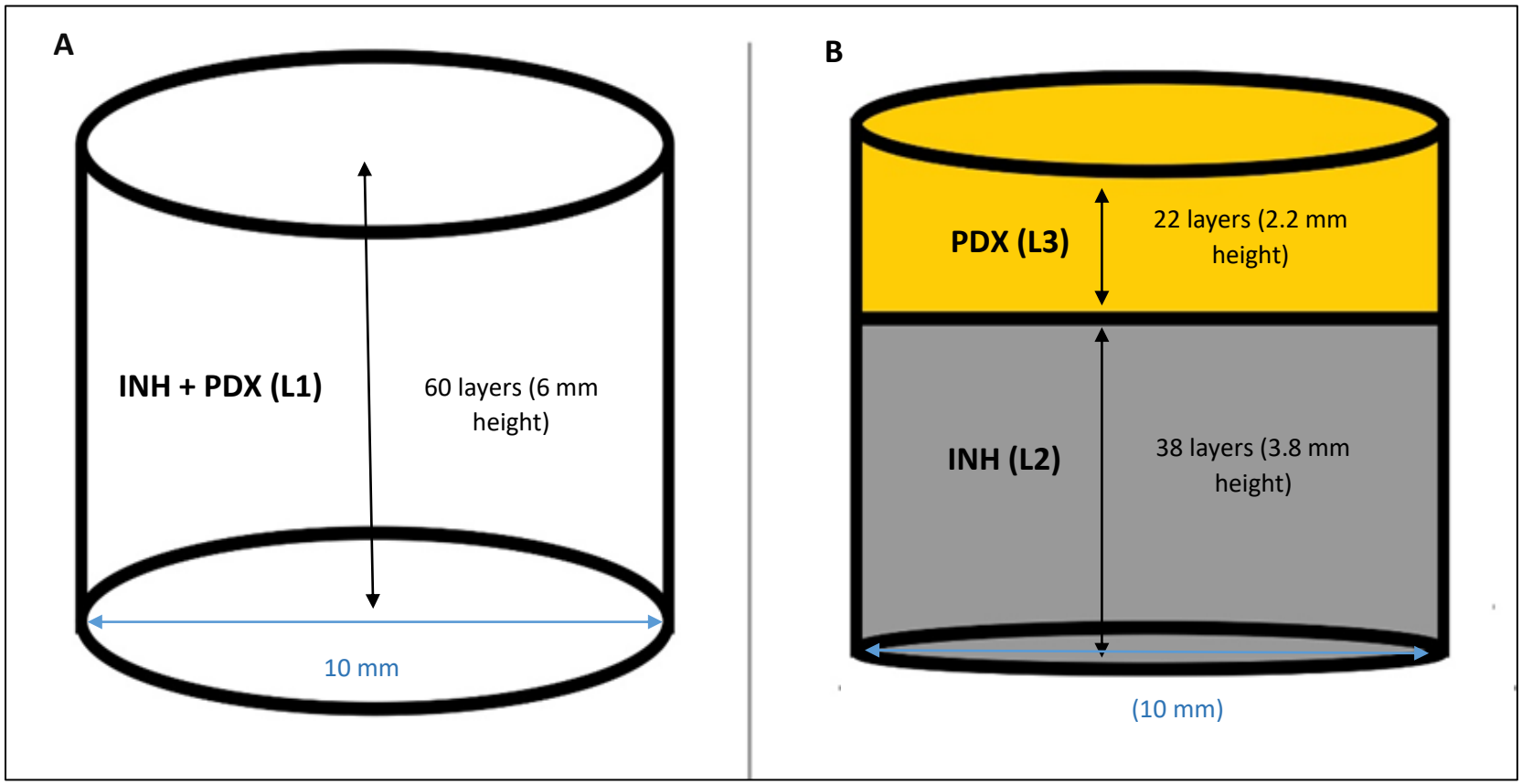

Figure 4.1: *Schematic diagram shows the CAD of single layer (A) vs two-layer tablets (B).*

Table 4.2: The 3D printed formulations.

For. No.	Filament components (HME formulation)	Drug/polymer ratio of filament (w/w%)	Total tablet height (mm)	Tablet diameter (mm)	Number of Compart-ment	Total weight of tablet (mg)	Thickness of each deposited layers (mm)	Number of deposited layers	Weight of each deposited layer (mg)	Drug content (mg)	
										INH	PDX
F1	Soluplus/INH/PDX/PEG/HPC (L1)	63.5/16/5.5/10/5	6	10	1	350	0.1	60	5.8	56	19
F2	Soluplus/INH/PEG/HPC (L2)	60/25/10/5	6	10	2	350	0.1	38	5.8	56	0
	Soluplus/PDX/PEG/HPC (L3)	70/15/10/5					0.1	22	5.8	0	19

4.2.10. Rational behind the selected drug loading in prepared tablets.

In the realm of pharmaceutical research, commercially available Isoniazid (INH) tablets are found in varying strengths of 50, 100, 300, and 400 mg, while Pyridoxine (PDX) tablets are available in strengths of 5, 10, 20, 25, 40, and 50 mg. However, up to our knowledge, there is no existing commercial tablet combines both drugs in a single formulation. Justification for 3D printing a tablet containing 56 mg of INH and 19 mg of PDX is founded on the following rationales:

1- The tablet's drug content can be tailored through two mechanisms: adjustment during hot melt extrusion (modifying drug content within the polymer) and customisation during the 3D printing process (altering tablet dimensions, infill percentage, layer ratios in the case of bilayer tablets, and other parameters).

2- Our current focus is on assessing the feasibility of the FDM based 3D printing for producing a pharmaceutical dosage form containing both INH and PDX. Our secondary objective involves exploring the impact of two distinct designs: one where both drugs are housed within a single compartment tablet, and another where they are segregated into two distinct compartments within the tablet. This investigation aims to elucidate how these design variations influence the in vitro release profiles of both drugs.

4.2.11. 3D printing conditions

3D printing of the tablet was performed using FDM based 3D printer PAM pollen (Paris, France). This specific type of FDM 3D printer utilises feeding materials in the form of pellets, which resolves the challenge of filament diameter encountered in twin screw HME formulations. The HME pellets were loaded into the hopper of the printer. The printing conditions set by the software were: printing temperature 145˚C, bed temperature fixed at 60˚C, printing speed was 20 mm/s, infill density and infill pattern were set to be of 100% and line, respectively. The percent of material flow through extruder described as ‘’flow rate’’ was set as 45%. The layer height and the top/bottom thickness were set to be 0.1 mm and 0.8 mm, respectively.

The printing conditions were determined during the initial steps of creating the materials profile. The Pollen 3D printer offers the capability to generate a new profile for any new feeding materials. The steps followed in this study can be summarised as follows:

1- Define the starting temperatures for the feeding materials based on thermal analysis (DSC) and rheological properties (complex viscosity). It is recommended to set the temperatures above the melting point but below the degradation point, with the complex viscosity ranging between 1000 and 10000 Pa.s.
2- Begin the extrusion process without the nozzle attached.
3- Adjusting the temperatures based on the consistency of the material flow.
4- Reattaching the printer nozzle and perform flow measurements. The average mass flow (mg/min) should be calculated based on 10 replicates.

5- Entering the measured flow data into the manufacturer's calculator sheet. (An Excel sheet can be provided upon request for this purpose).
6- Incorporating the output values from the calculator into the new profile within the slicer software.
7- Start using the new profile for slicing the new material and commence the printing process.

4.2.12. *In vitro* drug release analysis

The 3D printed tablets were placed in 30 mL of dH_2O release media (dH_2O) and kept in an orbital shaking incubator, Unitron HT infors (Surrey , UK), operating at temperature of 37˚C and a speed of 100 RPM. 0.5 mL samples were withdrawn and replaced with the same volume of fresh media at 0.25, 0.5, 1, 2, 4, 6, 12 and 24 hours. The collected samples were subjected for centrifugation at 13000 RPM for 5 min using Labnet Prism R centrifuge (Edison NJ, USA) and analysed by HPLC to determine the concentration of drug(s) released from the tablets. Drug release was calculated as mean (n=3) ± SD using Equation (4.3).

$$Drug\ release\ (\%) = \frac{Released\ drug}{Total\ drug} \times 100 \qquad 4.3$$

4.2.13. Statistical analysis

Independent sample T-tests were conducted using Microsoft Excel 365 (version 2401) expanded with the statistical data analysis add-on. Differences below the probability level ($p \leq 0.05$) were considered statistically significant, while differences above the probability level ($p > 0.05$) were considered not statistically significant.

4.3. Results and discussions

4.3.1. HPLC methodology results

4.3.1.1. HPLC method specificity results

The specificity of the method was evaluated by comparing the chromatogram of the sample solution containing both analytes (INH and PDX) to the chromatogram of a blank sample, as shown in Figure (4.2). From the chromatograms, it can be observed that the retention times of the analytes were 2.55 and 3.44 min for INH and PDX, respectively. The absence of any interference between the peaks of the analytes indicates that the method is specific for each individual analyte.

4.3.1.2. HPLC method linearity

The linearity of the method demonstrated the ability of the method to provide a direct proportion between the analytes concentrations and their corresponding area under the curve (AUC) within the identified calibration plot. The linearity results in Figure (4.3) and Figure (4.4), demonstrate a linear relationship for both INH and PDX, respectively, over the concentration range from 25-175 µg/mL. The linear equations were Y=12.846X and Y=12.416X for INH and PDX, respectively. The corelation co-efficient for both drugs was found to be 1.00, indicating that the developed method is linear.

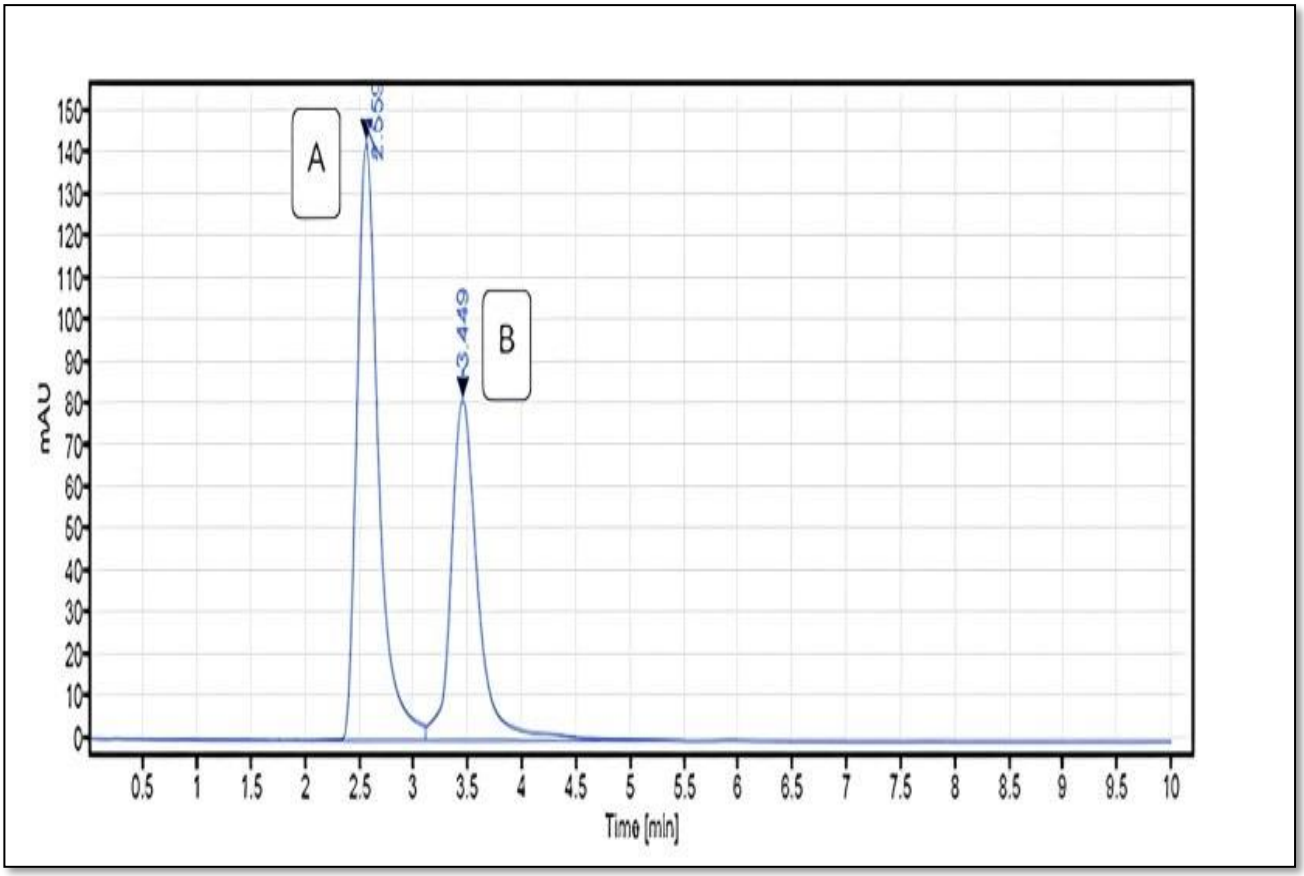

Figure 4.2: *HPLC chromatogram of INH (A) and PDX (B).*

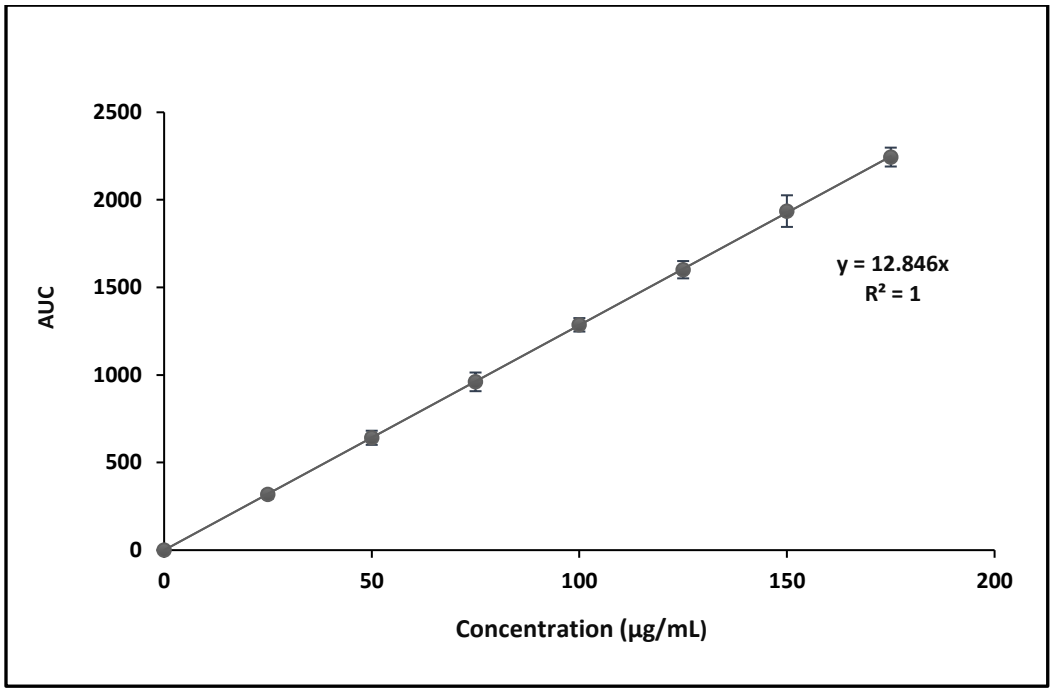

Figure 4.3: *Linearity Curve for INH. Results are presented as mean (n=6) ±SD.*

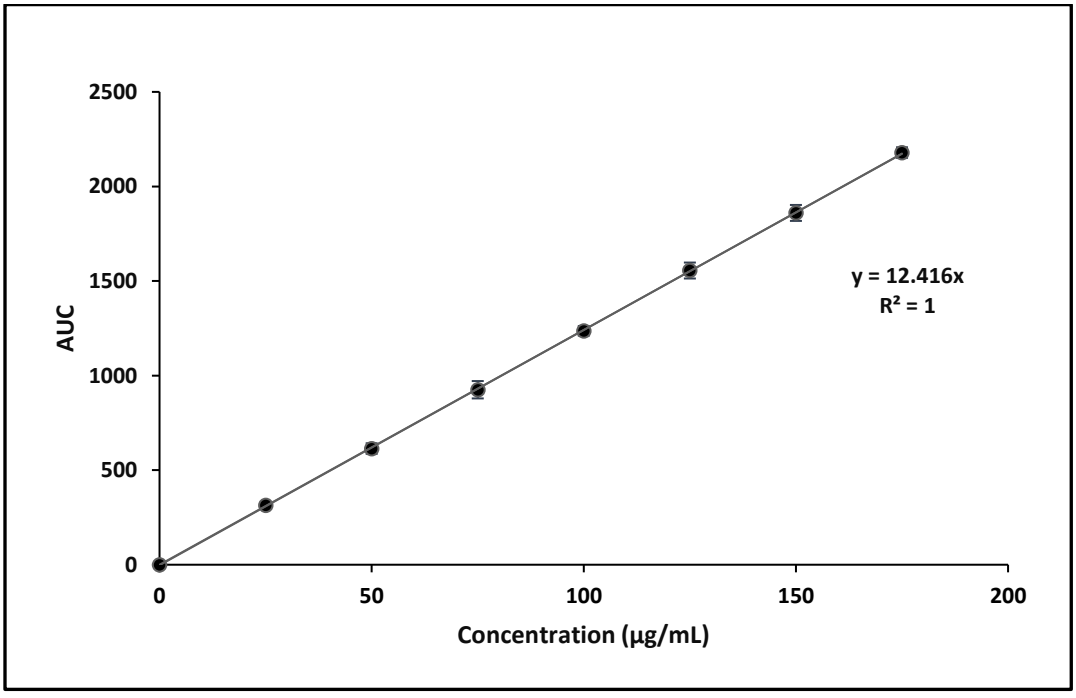

Figure 4.4: *Linearity curve for PDX. Results are presented as mean (n=6) ±SD.*

4.3.1.3. HPLC method accuracy

The accuracy of this method was assessed for both analytes separately. Tables (4.3) and (4.4), represent the accuracy results for INH and PDX, respectively. The results showed that the recovery rate ranged from 99.1% to 101.1% for all the three levels for both drugs, while the RSD values ranged from 0.035% to 0.74%. This confirms that the method was accurate as the accuracy values were within the accepted limits for both recovery ratio (98% to 102%) and % RSD values (≤ 2%).

4.3.1.4. HPLC method precision

Determination of method precision can be evaluated by the closeness of agreements between different measurements of the same homogenous samples, which are tested at different times under the same laboratory conditions. The precision results are summarised in the Tables (4.5) and (4.6). The obtained results demonstrate that the percentage relative standard deviation (% RSD) values for both analytes were less than 2%. This indicates that the developed method is precise.

4.3.1.5. HPLC method sensitivity

Method sensitivity was assessed by determining the limit of detection (LOD) and limit of quantification (LOQ) values, as outlined in Table (4.7). The LOD for INH was determined to be 2.48 µg, indicating the lowest concentration of the analyte that can be reliably detected. The LOQ for INH was calculated as 8.609 µg, representing the lowest concentration at which accurate

quantification can be achieved. For PDX, the LOD and LOQ values were found to be 3.19 µg and 9.68 µg, respectively. These values signify the minimum detectable concentration and the lowest concentration at which reliable quantification can be obtained for PDX using the developed method.

Table 4.3: Accuracy results of INH

Expected Conc. (µg/ml)	Replicate number	Peak Area (AUC)	Found conc. (µg/ml)	Recovery %	Main Recovery (%)	RSD (%)
25	1	315.1	25.4	101.5	101.1	0.3
	2	313.5	25.2	101		
	3	313.4	25.2	101		
100	1	1235.2	99.5	99.5	99.6	0.2
	2	1235.2	99.5	99.5		
	3	1239.6	99.8	99.8		
175	1	2175.9	175.3	100.1	100.3	0.1
	2	2180.5	175.6	100.4		
	3	2181.1	175.7	100.4		

Table 4.4: Accuracy results of PDX

Expected Conc. (µg/ml)	Replicate number	Peak Area (AUC)	Found conc. (µg/ml)	Recovery %	Main Recovery (%)	RSD (%)
25	1	318.9	24.8	99.3	99.1	0.74
	2	320.3	24.9	99.7		
	3	315.7	24.6	98.3		
100	1	1286.9	100.2	100.2	100.2	0.04
	2	1287.6	100.2	100.2		
	3	1286.5	100.2	100.2		
175	1	2242.9	174.6	99.8	99.8	0.04
	2	2243.1	174.6	99.8		
	3	2244.3	174.7	99.8		

Table 4.5: Precision results of INH

No of injection	Isoniazid (INH)					
	Day 1 (AUC)			Day 2 (AUC)		
	25	**100**	**175**	**25**	**100**	**175**
1	321.8	1285.6	2243.2	316.2	1277.4	2231.5
2	317.3	1287.3	2240.2	319.2	1279.5	2236.5
3	319.4	1286.8	2246.8	317.4	1281.3	2234.3
4	323.9	1285.1	2249.1	318.5	1280.7	2239.9
5	316.8	1283.6	2242.7	320.4	1283.3	2230.2
6	318.1	1286.6	2247.3	318.6	1279.9	2235.8
Average	319.6	1285.8	2244.9	318.4	1280.4	2234.7
SD	2.8	1.3	3.4	1.5	1.9	3.5
Found	24.9	100.1	174.8	24.8	99.7	174
Recovery %	99.51	100.1	99.9	99.1	99.7	99.4
RSD %	0.9	0.1	0.2	0.5	0.2	0.2

Table 4.6: Precision results of PDX

No of injections	Pyridoxine (PDX)					
	Day 1 (AUC)			Day 2 (AUC)		
	25	**100**	**175**	**25**	**100**	**175**
1	313.1	1238.5	2176.4	312.1	1237.5	2173.4
2	314.1	1236.1	2182.8	313.6	1236.6	2170.6
3	313.7	1234.1	2178.4	311.4	1235.2	2180.1
4	315.6	1235.7	2179.6	312.6	1234.7	2179.5
5	314.9	1235.5	2175.1	315.9	1238.9	2175.1
6	315.7	1237.7	2174.3	313.6	1235.8	2174.6
Average	314.5	1236.3	2177.8	313.2	1236.5	2175.6
SD	1.1	1.1	3.2	1.6	1.6	3.7
Found	25.3	99.6	175.4	25.2	99.6	175.2
Recovery %	101.3	99.6	100.2	100.9	99.6	100.1
RSD %	0.3	0.1	0.2	0.5	0.11	0.2

Table 4.7: Sensitivity results of INH and PDX.

Measurements	Isoniazid (INH)	Pyridoxine (PDX)
Standard deviation of intercept	11.06	12.02
Slope	12.85	12.42
Limit of detection (LOD)	2.48 µg	3.19 µg
Limit of quantification (LOQ)	8.61 µg	9.68 µg

4.3.2. Drug content

The results of the drug content analysis and HME loading efficiency are summarised in Table (4.8). The findings demonstrate that the loading efficiency of the HME process ranged from 94.4% to 98.4% for all three formulations. In formulation (L1), the drug contents were determined as 15.3 ± 1.12% (w/w) for INH and 5.31 ± 0.98% (w/w) for PDX. For formulation (L2), the loaded content of INH was found to be 24.6 ± 1.87% (w/w), while in formulation (L3), the loaded content of PDX was measured as 14.31 ± 1.24% (w/w). These values represent the percentages of the respective drugs present in the formulations after the HME process.

Although there are numerous reports of thermally induced chemical breakdown occurring during the HME process (Martin 2008, Huang, O'Donnell et al. 2016), and different drugs and excipients might be susceptible to different degradation pathways including oxidation, hydrolysis, isomerisation, photodegradation and dehydration which are triggered mainly by the elevated temperature and other conditions involved in HME process (Blessy, Patel et al. 2014). However, the drug content analysis results showed that both drugs were stable at the HME processing conditions due to the fact that both drugs were HME at temperatures far below the degradation temperatures.

4.3.3. Thermal stability analysis

The results of heat stress study are presented in Figure (4.5). Results demonstrated that both drugs are stable at the process temperatures. After 90 minutes at 130°C, 140°C, and 150°C, the drug remaining percentages for INH were measured as 99.43 ± 0.45%, 99.14 ± 0.33%, and 98.60 ± 0.41%, respectively. For PDX, the drug remaining percentages were found to be 99.61 ± 0.44%, 99.42 ± 0.56%, and 99.04 ± 0.65% at 130°C, 140°C, and 150°C, respectively. The results indicated that both drugs retained more than 99% of their quantity after stressed at 140°C for 90 minutes. These results suggest that the HME processing temperature was suitable for the drug's thermal stability.

Table 4.8: Drug content and loading efficiency in HME formulations

Formulation name	Theoretical drug content % (w/w)		Actual drug content % (w/w) mean ± SD		HME loading efficiency %
	INH	PDX	INH	PDX	
L1	16	5.5	15.3 ± 1.1	5.31 ± 1	95.6, 96.5
L2	25	-	24.6 ± 1.9	-	98.4
L3	-	15	-	14.31 ± 1.2	95.4

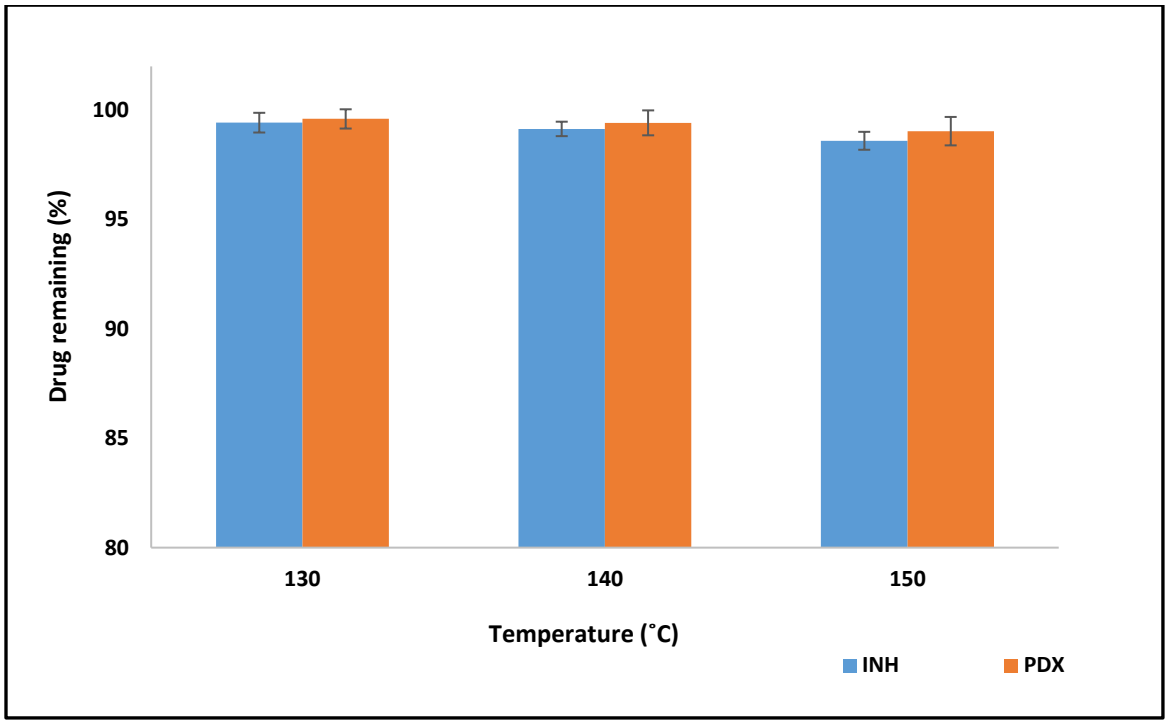

Figure 4.5: *The drug stability under stressed temperatures. Results shown as mean (n=5) ± SD.*

4.3.4. Raman mapping.

Based on the results obtained from Raman mapping for the extrudate form formulation (L1) demonstrated in Figure (3.6). INH and PDX are homogenously distributed within the extrudate as shown in Figures (3.6 A) and (3.6 B), respectively. However, it can be observed that the intensity of INH is higher than the PDX which was expected due to the fact that the INH concentration in this formulation (L1) is approximately three times higher than the PDX. Figure (3.6 C) showed Raman mapping for the Soluplus only while in Figure (3.6 D) demonstrates the Raman mapping with the reference spectra of Soluplus, INH and PDX which highlighted in the red, green, and yellow colours, respectively.

The obtained drug homogeneity might be attributed to the drugs being in amorphous and molecularly dispersed within the polymer matrix. It is well documented that the utilisation of twin-screw hot melt extrusion has ensured that the drugs are homogenously dispersed in their amorphous form within the polymer extrudate (Feng & Zhang, 2018; Keen et al., 2014).

4.3.5. XRD analysis

According to the results obtained from the XRD diffractogram Figure (3.5), the unprocessed drug powders (INH and PDX) showed characteristic crystalline peaks at 2θ between 10˚ and 50˚. However, no crystalline peaks were observed in the patterns of the drug-polymers extrudate. Therefore, within the drug-polymer extrudate, it is confirmed that both drugs (INH and PDX) were either in amorphous form or dispersed in a molecular state within the polymer matrix. These results confirm the Raman mapping data which showed that both drugs where homogenously dispersed within the polymer matrix at a molecular level.

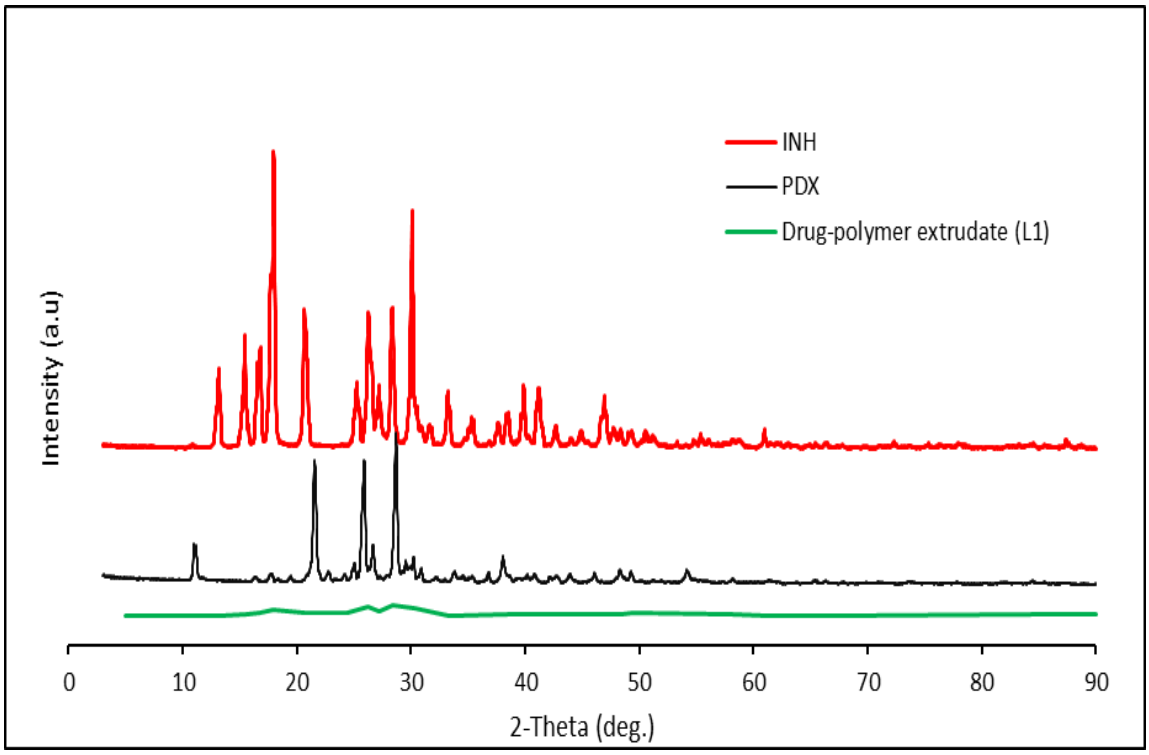

Figure 4.6: *X-ray diffractograms of INH, PDX and drug polymer extrudate in formulation (L1).*

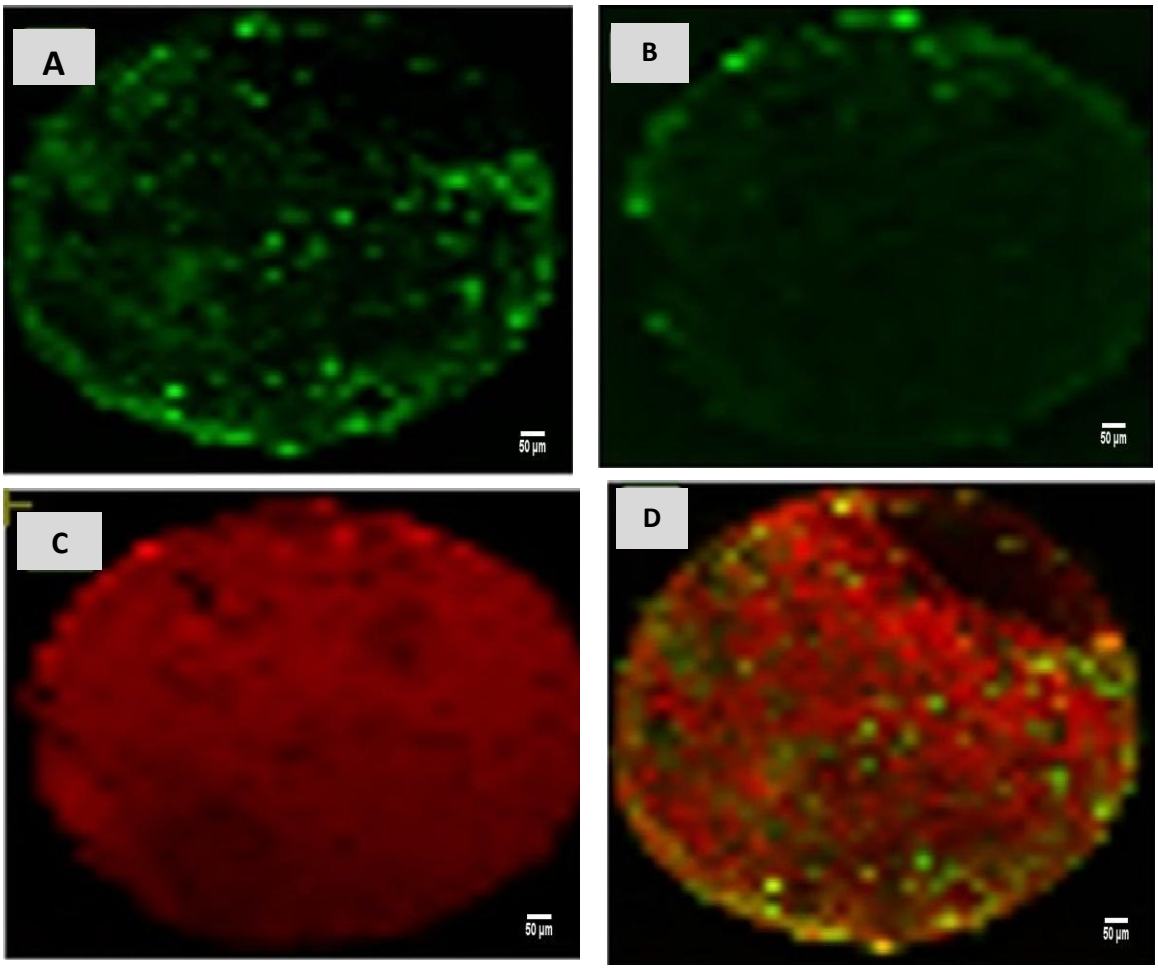

Figure 4.7: *Raman mapping of (L1) formulation where (A): INH, (B): PDX, (C): Soluplus and (D) is the drug-polymer mixture.*

4.3.6. DSC analysis

The DSC thermograms of INH powder, PDX powder, and Soluplus placebo are presented in Figure (4.8). The thermogram of INH, shown in Figure (4.8 A), exhibited a distinct and sharp endothermic peak at 171°C, corresponding to its melting temperature (*Tm*). Additionally, a broader endothermic event observed at 225°C, which could be attributed to thermal degradation of the

compound. (Freire et al., 2009; Sibum et al., 2019). The DSC thermogram of PDX, as shown in Figure (3.7 B), exhibited a distinct, sharp endothermic peak at 212°C, which corresponds to its *Tm*. The DSC thermogram of Soluplus is presented in Figure (3.7 C). A broad peak observed at 71°C. This peak signifies the polymer's transition from a glassy state to a rubbery state, indicating its thermal behaviour. The presence of enthalpy relaxation during this transition was previously reported in the literature (Lee et al., 2015).

4.3.7. Rheology

The influence of temperature on the complex viscosity (η*) was investigated for both the placebo Soluplus polymer and the drug-polymer mixture in formulation (L1). The results are presented in Figures (4.9) and (4.10), respectively. In Figure (4.9), the complex viscosity of the placebo Soluplus polymer exhibited the suitable melt viscosity (ranging from 1000 to 10000) at approximately 169°C. This temperature range indicates the point at which the polymer reaches a viscosity suitable for the HME process.

However, in the case of the drug-polymer formulation (L1), Figure (4.10) clearly shows that the required temperature to achieve a suitable HME viscosity was dramatically reduced, falling within the range of 130°C to 160°C. This reduction in temperature can be attributed to the plasticising influence of PEG, a component present in the drug-polymer mixture.

The findings indicate that the drug-polymer mixture in formulation (L1) exhibits favourable characteristics for HME at a moderate processing temperature, thereby ensuring drug stability. Furthermore, the polymer's appropriate viscosity lowers the likelihood of encountering high torque values that could potentially cause screw breakage during the extrusion process.

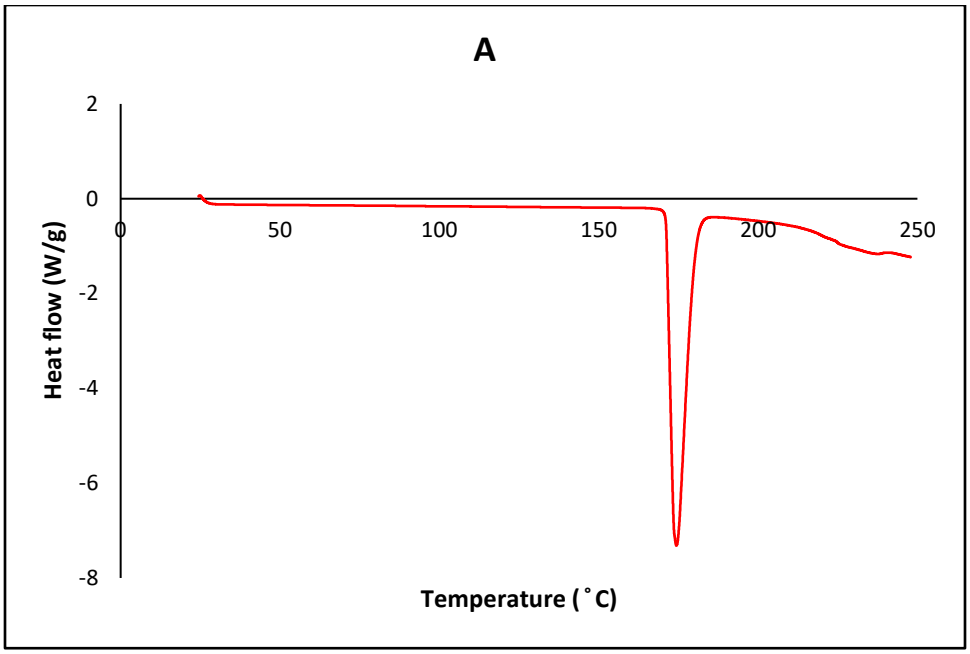

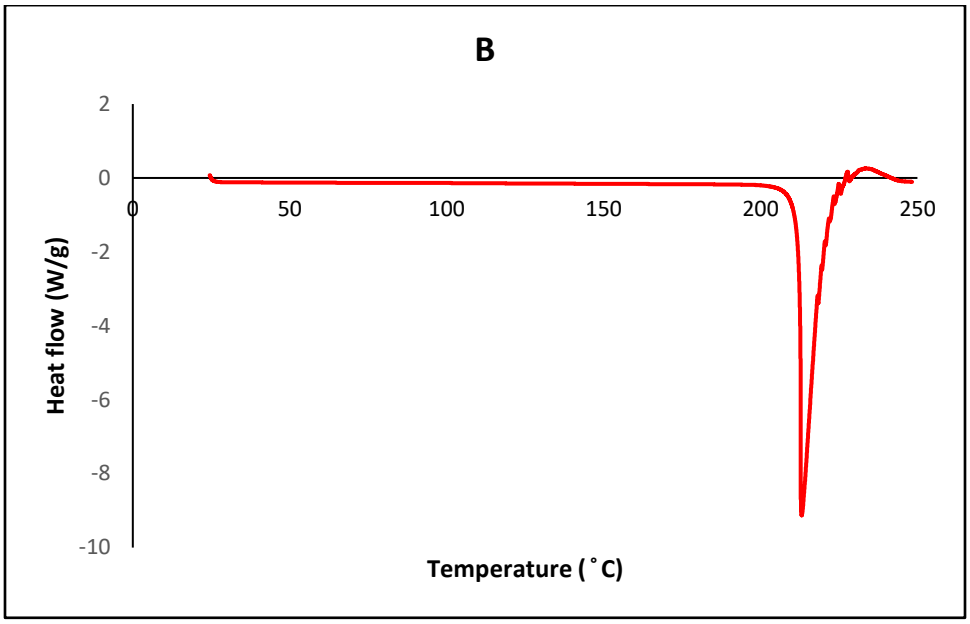

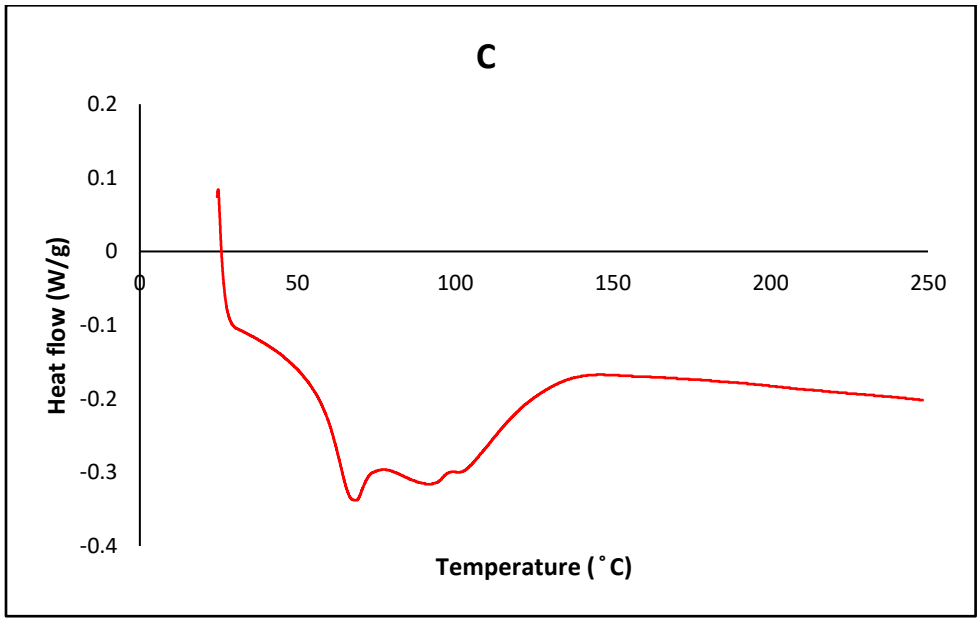

Figure 4.8: *DSC thermogram of INH (A), PDX (B) and Soluplus (C).*

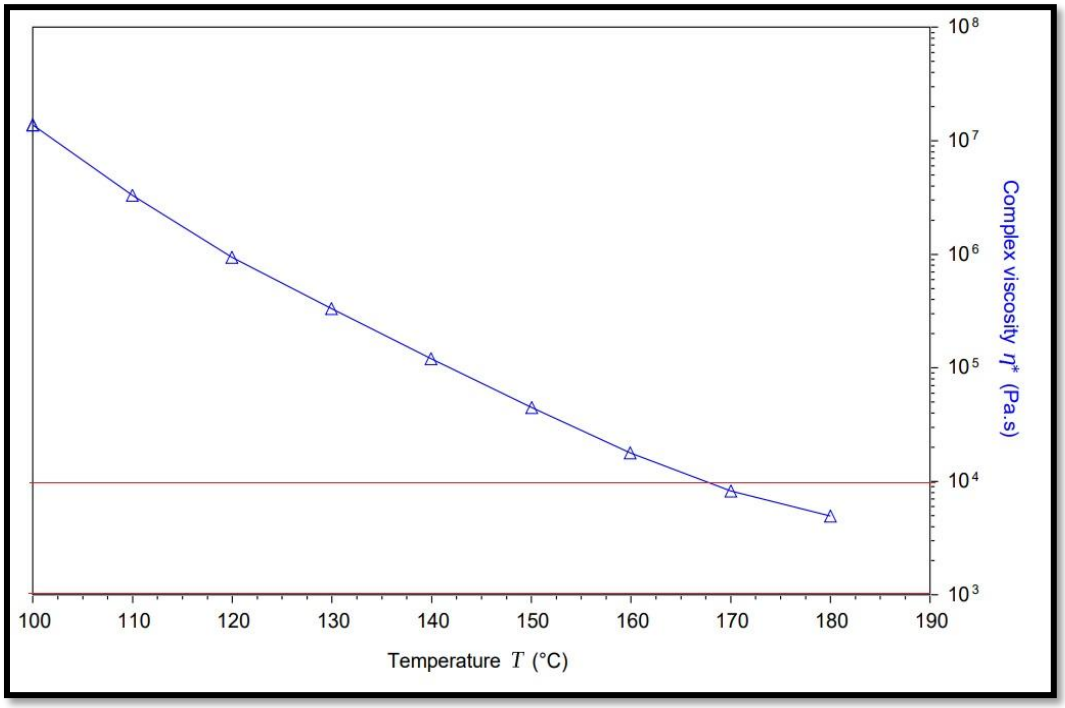

Figure 4.9: *Complex viscosity (η*) of Soluplus vs Temperature (°C). Test was performed at a 5 rad/sec angular frequency and 10°C/5 minutes cooling rate.*

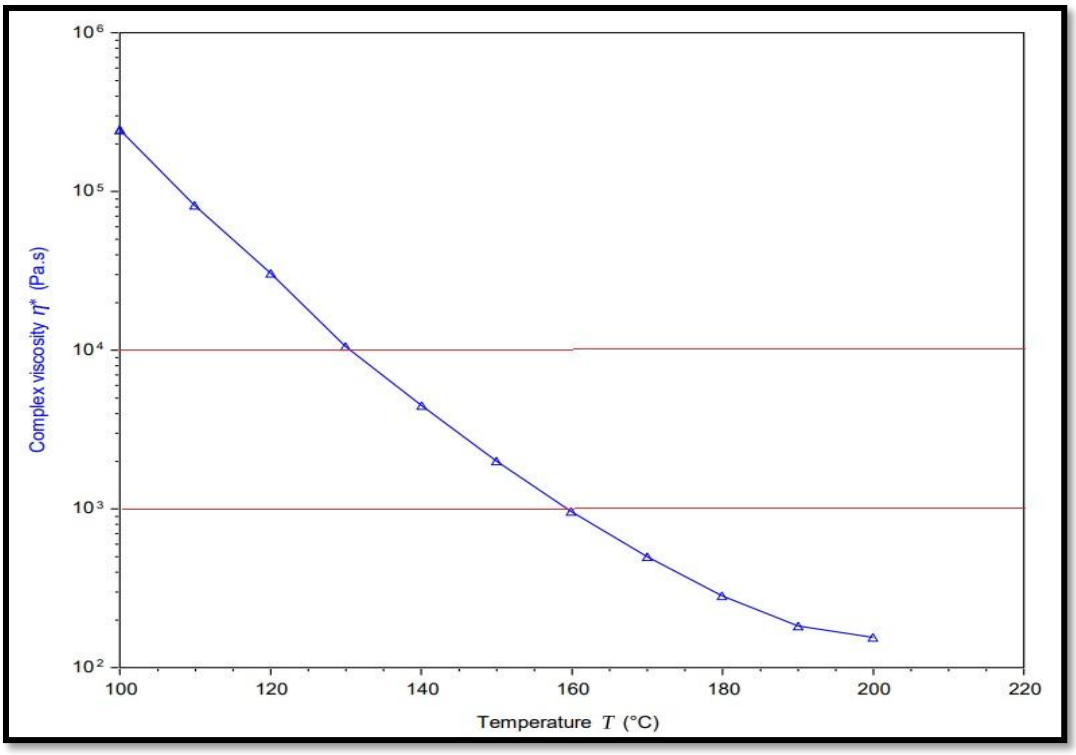

Figure 4.10: *Complex viscosity η* (Pa.s) vs temperature (°C) of (L1) formulation physical mixture. Test was performed at a 5 rad/sec angular frequency and 10°C/5 minutes cooling rate.*

4.3.8. Drug stability in different release medias

The stability of INH was assessed in two different release media: dH_2O and PBS, at various temperatures. The corresponding results are presented in Figures (4.11 A) and (4.11 B), respectively. The findings revealed that INH retained 97% of its stability in both release media over a 72-hour period, with a negligible influence of different temperatures. The findings indicated that PDX demonstrated acceptable stability in dH_2O, with a stability loss of less than 2.5% as depicted in Figure (4.12 A). Conversely, when exposed to PBS, PDX experienced a significant stability decline of over 15%, with the rate of degradation being temperature dependent as demonstrated in Figure (4.12 B). These results indicate that both drugs exhibited greater stability over time in dH2O compared to PBS. Therefore, based on these findings, the decision was made to proceed with dH_2O as the chosen release medium for this study.

4.3.9. Drug solubility

After selecting dH_2O as the release medium, it became crucial to assess the solubility of each drug in order to determine the appropriate volume of release medium required to maintain sink conditions. The results, presented in Figure (4.13), revealed that the water solubility of INH and PDX was measured to be 116.4 ± 4.15 mg/mL and 205.4 ± 6.38 mg/mL, respectively. The solubility study was conducted at a temperature of 37˚C, which was determined as the optimal temperature for the subsequent release study. Determining the solubility of the drugs at the intended release

temperature ensures that the selected release medium will be able to effectively dissolve and maintain the drugs in a soluble form throughout the experiment.

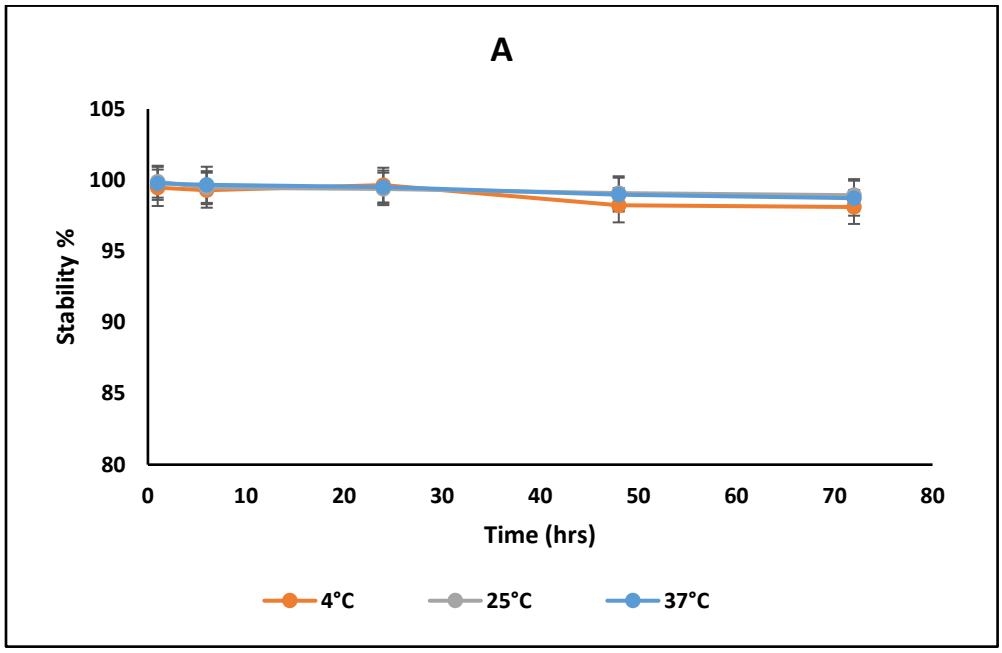

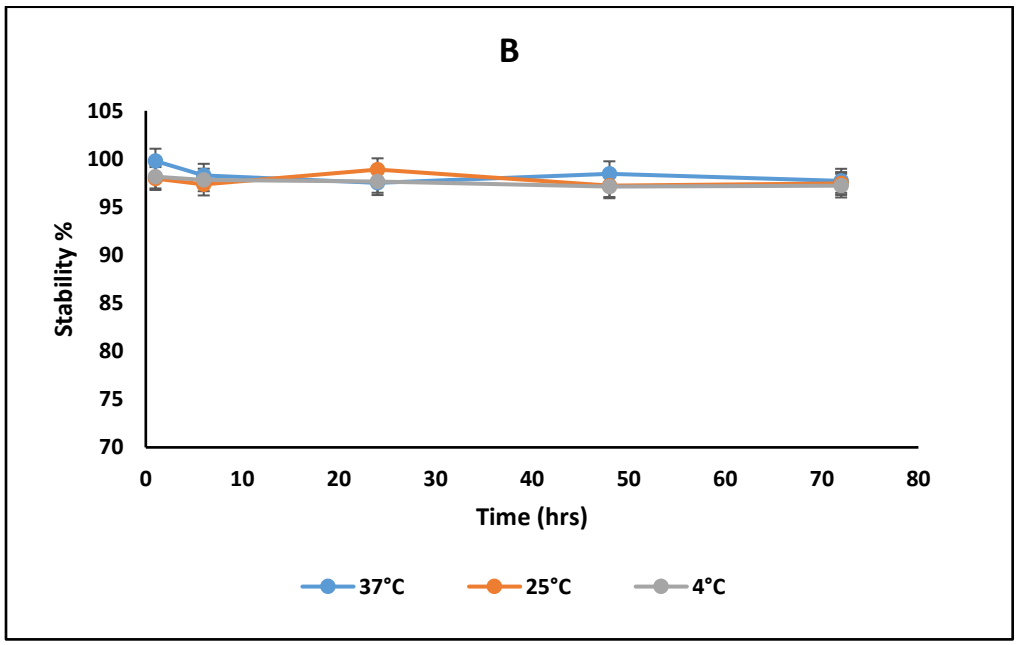

Figure 4.11: *INH stability in dH_2O (A) and in PBS (B) at different temperatures. Results shown as mean (n=3) ± SD.*

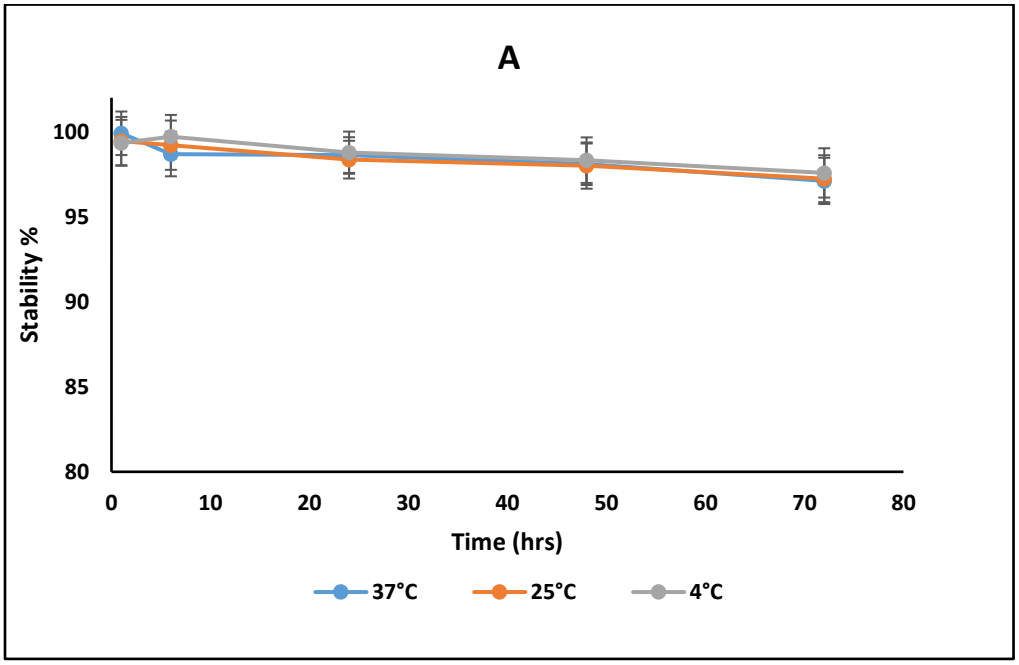

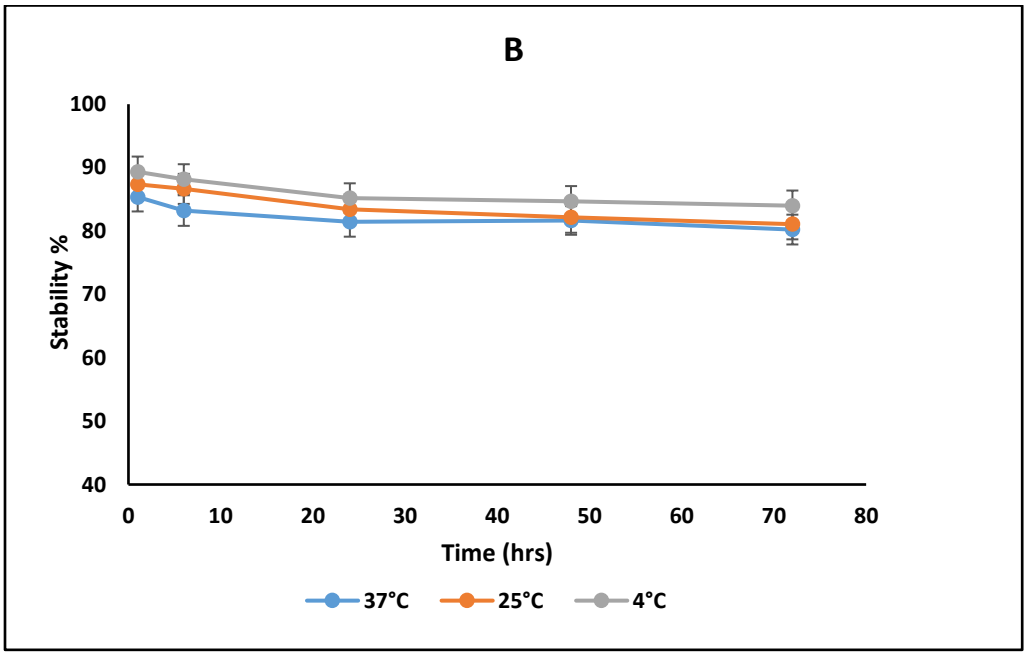

Figure 4.12: *PDX stability in dH_2O (A) and in PBS (B) at different temperatures. Results presented as mean (n=3) ± SD.*

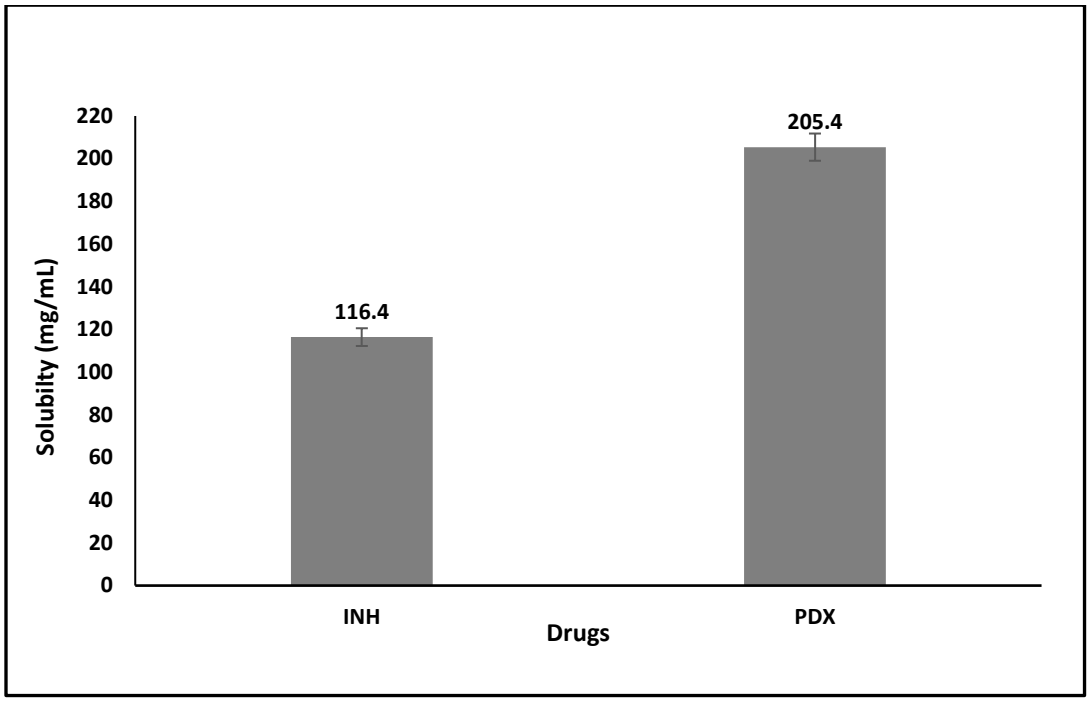

Figure 4.13: *INH and PDX solubility in dH_2O. Results presented as mean (n=3) ± SD.*

4.3.10. Characterisation of the 3D printed tablets

Based on the characterisation of the extruded filaments, they were deemed to be acceptable for 3D printing of the tablets. The filaments were considered acceptable as they exhibited a drug content above 95%, ensuring an efficient drug loading process. Additionally, the characterisation techniques, such as Raman spectroscopy and X-ray diffraction (XRD), demonstrated that the drug was uniformly dispersed within the filaments, indicating a homogenous distribution. The utilisation of FDM based 3D printing demonstrated its capacity to fabricate two distinct tablet designs, including single layer and bilayer configurations.

Figure (4.14) depicts representative images of the CAD tablet designs (A and B) alongside the corresponding 3D printed tablets (C and D). The physical properties of the 3D printed tablets regarding the weight, height and diameter are presented in Table (3.8). There are some variations were observed in the diameters and thickness (cylinder height) of the 3D printed tablets compared to their intended dimensions as specified in the digital designs. Notably, the printing accuracy of the single layer tablet was found to be higher when compared to the bilayer tablets. The single layer tablet exhibited a percentage difference of 2.3% in diameter and 1.6% in thickness compared to the intended dimensions. In contrast, the bilayer tablets showed larger percentage differences, with 11.3% in diameter and 6% in thickness. The variations observed in the dimensions of the bilayer tablets compared to the single layer tablet could be attributed to the use of two different printing nozzles simultaneously during the manufacturing process. When using multiple nozzles, there is an increased potential for slight misalignments or differences in extrusion rates, which can affect the accuracy and consistency of the printed layers. In contrast, the use of a single nozzle for printing the single layer tablet eliminates the potential issues related to extrusion and alignment.

Despite the possibility of decreased resolution, employing a multi-nozzle system in 3D printing allows for the concurrent feeding and printing of diverse materials. This feature reduces manufacturing time by eliminating the need for additional pauses to switch between materials. (Abilgaziyev et al., 2015).

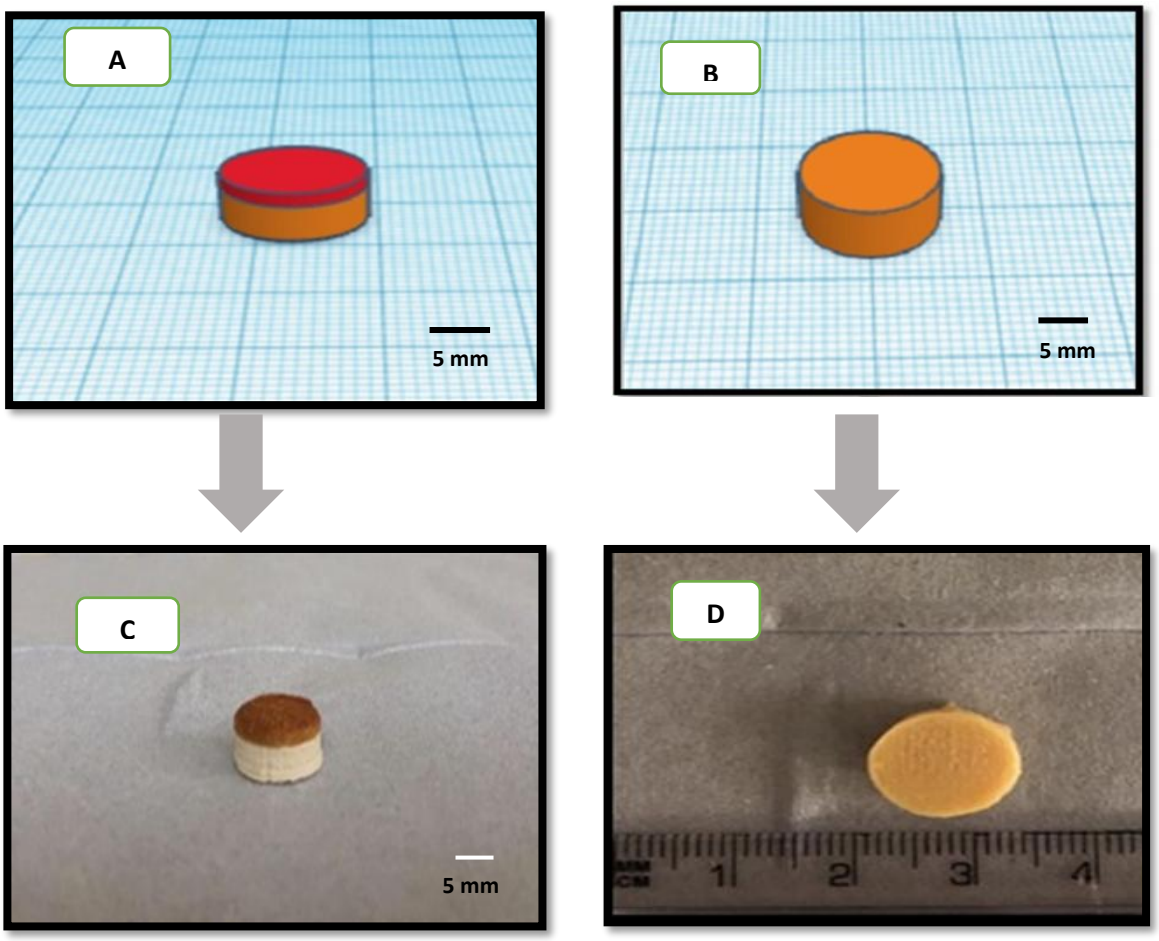

Figure 4.14: *The CAD design of two-layer tablet (A), single-layer (B), 3D printed two-layer tablet (C) and 3D printed single-layer tablet (D).*

Table 4.9: Measured dimensions of 3D printed drug loaded tablets.

Tablet type	Intended diameter (mm)	Actual diameter (mm) Mean (n=3) ± SD	Percentage difference (%) of diameter	Intended tablet height (mm)	Actual height (mm) Mean (n=3) ± SD	Percentage difference (%) of height
Single-layer tablet	10	10.2 ± 0.3	2.3	6	5.9 ± 0.2	-1.7
Two-layer tablet	10	11.1 ± 0.2	11.3	6	6.37 ± 0.1	6

4.3.11. Results of *in vitro* drug release from 3D printed dosage forms

The *in vitro* drug released (%) for both INH and PDX from the single layer and bilayer 3D printed tablets is presented in Figures (4.15 A) and (4.15 B), respectively. Approximately 70% of both drugs were released within the initial 6 hours from both single layer and bilayer tablets. However, the drug release from the bilayer tablets exhibited a slightly faster rate compared to the single layer tablets. Within the first 12 hours, approximately 90% of INH was released from both tablet types. On the other hand, the release of PDX from the bilayer tablet showed a consistent, steady state release pattern after the initial 6 hours, in contrast to the single layer tablet. This difference may be attributed to the faster dissolution of the first layer of the bilayer tablet, which solely contained PDX.

The first order calculated coefficient (R^2) values, specifically 0.9907 for the single layer tablets and 0.9902 for the bilayer tablets, indicate a high level of correlation between the observed drug release data and the first-order release kinetics model. This suggests that the drug release profiles of both tablet types were primarily governed by the relative contributions of two mechanisms: drug diffusion and polymer dissolution.

The statistical analysis conducted on the *in vitro* drug release data demonstrated that there was no statistically significant difference ($P > 0.05$) in the drug release of INH and PDX between the two different tablet designs. This implies that the release profiles of both drugs from the single layer and bilayer tablets were comparable in terms of their *in vitro* release behaviour.

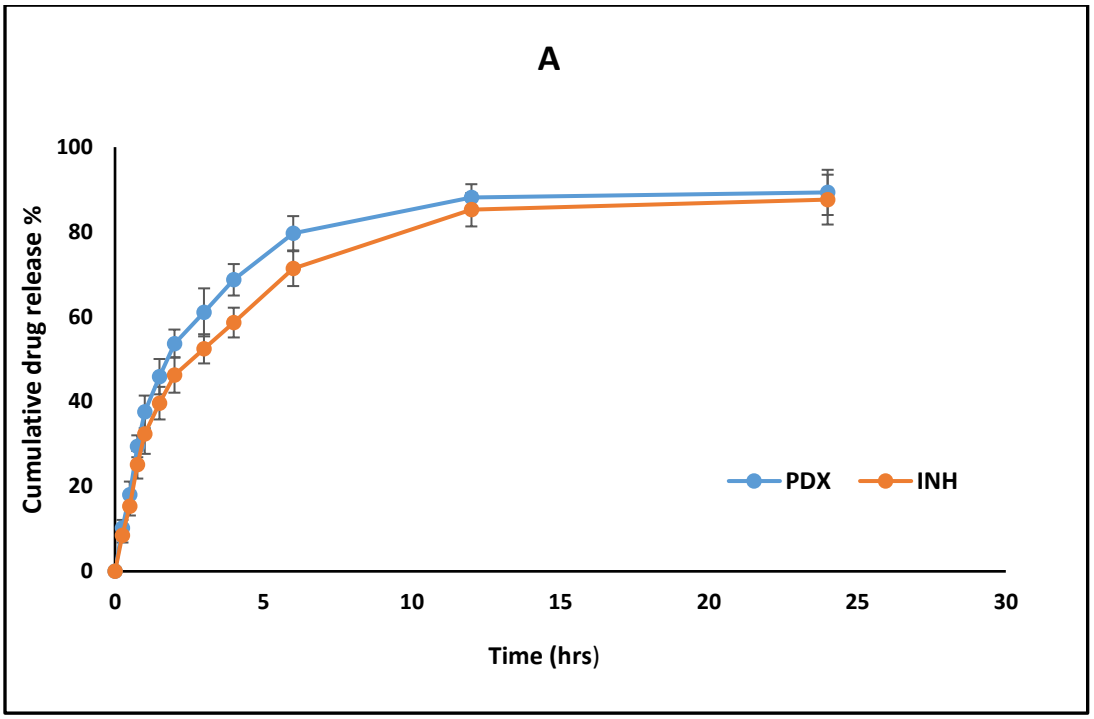

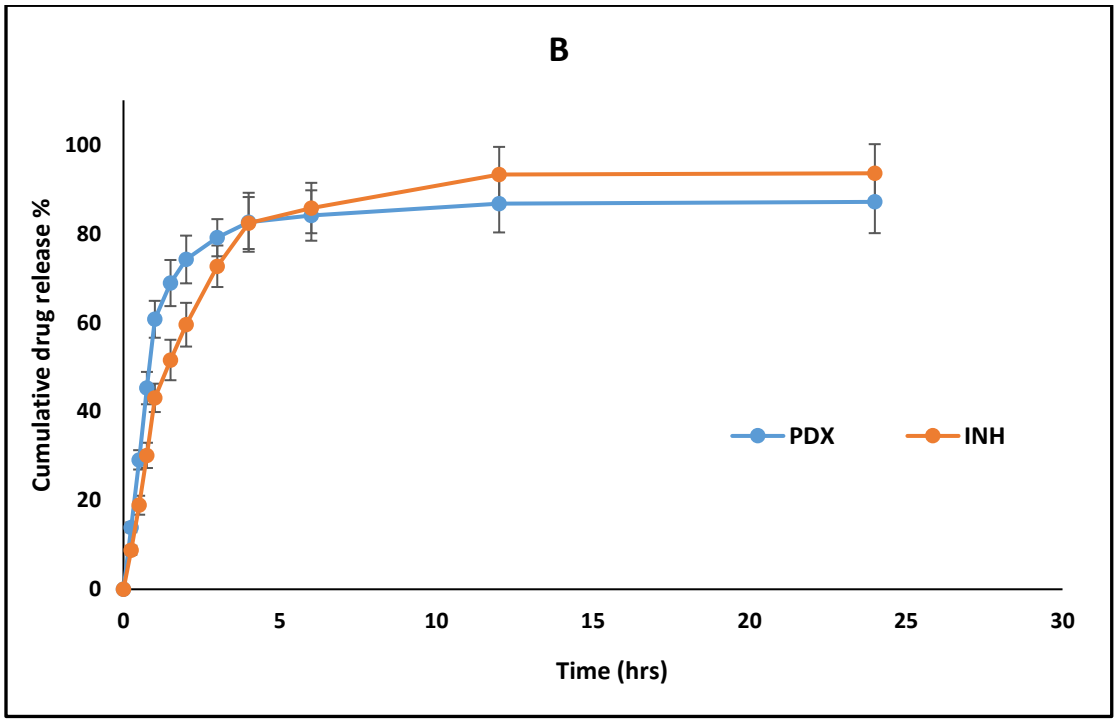

Figure 4.15: *In vitro drug release of single-layer tablet (A) and two-layer tablet (B). Results shown as mean (n=3) ± SD.*

4.4. Discussions

In this chapter, the feasibility of utilising a combination of HME and FDM based 3D printing technology to manufacture an oral dosage form (tablet) containing two different drugs was investigated. The first step involved preparing suitable drug loaded polymer formulations using twin screw HME. In this process, the drugs INH and PDX were incorporated into a pharmaceutically approved polymer called Soluplus, along with other additives such as HPC and PEG. The resulting drug loaded polymer, was subjected to various characterisation tests to evaluate its drug content, drug homogeneity, and crystallographic changes. These tests aimed to assess the quality and performance of the drug loaded polymer formulations for subsequent 3D printing processes.

The extrudate characterisation, specifically regarding the drug content and loading efficiency of the HME process, revealed promising results. In all three formulations (L1, L2, and L3), the drug content loaded exceeded 94% of the targeted theoretical drug content. These findings indicate that the twin screw HME process is highly efficient for achieving the desired drug loading. Furthermore, the results from XRD and Raman mapping demonstrated a good mixing efficiency, as both drugs were uniformly dispersed within the polymer matrix in an amorphous state. This homogeneous dispersion and amorphous state contribute to improved drug stability, as previously reported in the literature (Yang et al., 2010).

The thermal properties were analysed, and it was found that the HME process was carried out at temperatures below the thermal degradation points of both drugs. These thermal degradation temperatures were determined through DSC analysis. The DSC thermograms displayed no peaks indicating thermal degradation within the temperature range used for HME processing (112 to 135°C) or the 3D printing process (60 to 145°C).

The rheological analysis revealed that the temperature needed to achieve the desired melt viscosity range (1000 to 10000 Pa.s) was lower for the drug polymer mixture compared to using Soluplus alone. This can be attributed to the plasticising effect of PEG. It was previously reported in the literature that the inclusion of PEG in the formulation contributes to achieving the desired melt viscosity for HME, thereby facilitating the manufacturing process of the drug loaded polymer system (Dinagaran et al., 2022; Oladeji et al., 2022).

The characterisation of 3D fabricated tablets showed that the physical properties of the single layer tablet displayed slight differences in the diameter and thickness (cylinder height). Specifically, the diameter exhibited a difference of 2.3% and the thickness showed a difference of 1.6% when compared to the theoretical dimensions of the tablet. However, in the case of the fabricated bilayer tablet, there was a higher difference observed. The tablet diameter had a difference of 11.3% compared to the intended theoretical dimensions, while the thickness showed a difference of 6%.

These results indicated that the single layer tablet had relatively smaller variations in size compared to the theoretical dimensions, whereas the bilayer tablet exhibited larger discrepancies. Results suggested that the accuracy of 3D printing of single layer tablet with a single nozzle is higher than dual nozzle. However, it should be borne in mind that the using single nozzle for 3D printing of multilayer dosage forms will be time and effort consuming due to the extra time needed for changing of materials compared to dual extruder 3D printers (Ali et al., 2016).

In general, throughout the 3D printing process, there are several factors affecting the quality of the tablets including but not limiting the selection of suitable materials, adjusting the corresponding printing speed, determining the optimum temperatures (printer tip temperature) and selecting the suitable size of the nozzle. Material selection is crucial for achieving accurate deposition of layers, and the extrusion temperature needs to be controlled to ensure proper material flow and adhesion. Balancing the printing speed and nozzle size is important to maintain precision, resolution, and desired tablet characteristics. Moreover, the geometry and design of the CAD dosage requires accurate dimensions as well as proper alignments during the early stage of the digital design to avoid any printing failure or adding avoidable 3D printing support (Ansari & Kamil, 2021; Shirmohammadi et al., 2021; Zagidullin et al., 2021).

The *in vitro* drug release results of the 3D fabricated drug loaded tablets released significant amount of drug (70%) after the initial 6 hours regardless of the type of design (single or bilayer). However, bilayer tablet exhibited faster drug release compared to the single layer tablets. The amount of drug released from the bilayer tablet were 85.76 ± 5.64 and 84.07 ± 5.67% for INH and

PDX, respectively after 6 hours, while the single layer tablet exhibited INH and PDX release of 71.35 ± 4.11 and 79.69 ± 4.04%, respectively. Although both tablet types were 3D printed at constant 3D parameters such as infill %, layer height and printing temperature, they displayed different release behaviours. This difference in the release profile might be resulted from larger size of the bilayer tablet which consequently provide larger surface area in contact with the release medium. It is also observed that the PDX release was slightly faster than the INH in both types of tablets during early phase of the release, which might be contributed to the hydrogens in the INH hydrazine group establishing hydrogen bonds with the carbonyl groups in either the acetate or caprolactam groups of Soluplus, delaying the INH early release (Keating et al., 2018).

In FDM based 3D printing of pharmaceutical dosage forms, numerous studies in the literature have utilised commercially available thermoplastic filaments, including PLA, PCL, and acrylonitrile butadiene styrene (ABS). These filaments are commonly loaded with the desired drug through a process called impregnation. In this method, the filament is immersed in a drug saturated solution to absorb the drug into its matrix. (Holländer et al., 2016; Sandler et al., 2014; Water et al., 2015). The sustained drug release that these kinds of polymers often exhibit makes them better suited for implants than oral dose forms. However, considering the restricted drug loading capability of the impregnation method and the ongoing preference of patients for oral medication administration (Alhnan et al., 2016), a logical trend is to change impregnation method previously used to incorporate the drug into the commercially available filaments and towards studying polymers that would be suitable for 3D printing of oral dosage forms and FDA approved for oral drug delivery as well as utilising techniques that allow for sufficient drug loading such as the HME.

This approach not only aligns with patients' preferences for oral drug delivery but also provides opportunities for personalised medicine with optimised drug content and release profiles. It represents an exciting direction in the development of advanced pharmaceutical manufacturing techniques and personalised drug delivery systems.

4.5. Conclusion

In this chapter, a novel, rapid and accurate HPLC method for simultaneous determination of INH and PDX was successfully developed. This method was applicable for the analysis of 3D printed dosage tablets containing the two drugs in a single dosage form. Overall, it can be utilised for the assessment of pharmaceutical preparations that typically involve the combination of INH and PDX as tuberculosis therapeutic agents. Two different types of 3D printed tablets were manufactured by employing a combination of FDM based 3D printing and HME. Both types of tablets demonstrated a substantial drug release, with approximately 70% of the drug being released within the initial 6-hour timeframe. Although, this significant drug release was observed irrespective of the specific design characteristics of the tablets, the bilayer tablet exhibited faster drug release compared to the single layer tablet which may be attributed to the higher surface area. FDM based 3D printing showed a potential capacity to manufacture complex pharmaceutical dosage forms. The production of pharmaceutical dosage forms that incorporate multiple drugs offers several advantages in pharmaceutical manufacturing. These formulations prove particularly beneficial in the treatment of chronic conditions such as hypertension, diabetes, and tuberculosis.

Chapter 5 : INVESTIGATING THE FEASIBILITY OF 3D PRINTING OF AN IMPLANTABLE DRUG DELIVERY DEVICE FOR THE TREATMENT OF BRAIN TUMOUR

5.1. Introduction

Despite considerable progress in cancer treatment modalities such as chemotherapy, radiation, and surgeries, cancer continues to be the second most common cause of mortality. However, certain studies have indicated a shift in the landscape, with cancer potentially surpassing cardiovascular disease (CVD) as the leading cause of mortality in high-income countries (Mahase, 2019). Brain tumours, specifically high-grade gliomas (HGG), represent a subset of tumours that are associated with elevated rates of mortality and morbidity. This is primarily attributed to the current standard treatments' inability to achieve long-term disease control (Gandhi et al., 2019).

The standard approach to treating HGG typically involves surgical intervention followed by adjuvant therapies like chemotherapy and/or radiotherapy. However, the effectiveness of these treatments for HGG can be hindered by various factors, one of which is the presence of the blood-brain barrier (BBB). The BBB acts as a protective barrier, limiting the penetration of chemotherapeutic agents into the brain and hindering their ability to reach the tumour at the desired therapeutic concentration (Parrish et al., 2015). In addition, systemic drug delivery methods are often accompanied by dose limiting side effects (Wolinsky et al., 2012), and any residual glioma cells left behind after surgery have a significant likelihood of proliferating and giving rise to new cancerous cells (Binello & Germano, 2011).

To address the limitations of systemic drug delivery, there is a need for innovative and targeted local drug delivery systems. The primary goals of these systems, which can be in the form of implants or injectable systems, are to enhance drug delivery specifically at the tumour site, minimise the adverse effects associated with systemic administration, and improve the overall quality of life for patients. These local drug delivery systems offer advantages such as prolonged release kinetics and spatiotemporal controllability, leading to promising outcomes in the management of certain cancer types (Ramachandran et al., 2017; Yi et al., 2016).

For example, Carmustine wafer (CW) which marketed as Gliadel, is an implantable local drug delivery system specifically approved for the treatment of newly diagnosed and recurrent of HGG (Iuchi et al., 2022). Gliadel contains carmustine (as a chemotherapeutic agent) that is uniformly integrated within a biodegradable polymer composed of 1,3-Bis(p-carboxyphenoxy) propane and sebacic acid in a ratio of 20:80 (Attenello et al., 2012). Previous studies have provided evidence that Gliadel wafers effectively maintain elevated concentrations of the chemotherapeutic agent within the localised tumour bed for a duration of approximately three weeks following implantation. Subsequently, the residual polymer undergoes biodegradation within a timeframe of 6 to 8 weeks (Fleming & Saltzman, 2002; Grossman et al., 1992).

In two clinical trials encompassing 32 and 240 patients, Gliadel exhibited a noteworthy enhancement in the overall survival rate (OSR) among individuals newly diagnosed with glioblastoma multiforme (GBM). The utilisation of Gliadel implanted wafers resulted in a

substantial increase in OSR by 2.9 and 2.3 months, respectively, in comparison to the use of placebo implanted wafers (Valtonen et al., 1997; Westphal et al., 2003).

However, one limitation of Gliadel treatment is its suitability for specific patients. The implantation of Gliadel wafers is dependent on factors such as the size, shape, and location of the resection cavity. Due to the dimensions of each wafer, measuring 1.45 cm in diameter and 1 mm thick, a relatively large resection cavity is required to accommodate the placement of eight wafers (the recommended dose). Therefore, not all patients may meet the criteria for Gliadel treatment, and alternative therapeutic approaches may need to be considered in such cases (De Bonis et al., 2012; Gibaldi et al., 2007).

The use of 3D printing technology within the pharmaceutical and medical research has exponentially expanded (Cornejo et al., 2022). The employment of 3D printing technology in the manufacturing of chemotherapy loaded implants for cancer treatment offers two notable advantages Firstly, it enables the production of targeted local drug therapies that can be administered directly at the specific tumour site, facilitating prolonged drug release over extended periods through the use of extended release implants. Secondly, the ability of 3D printing to customise implant shapes and sizes according to the specific needs of individual patients not only enhances treatment efficacy but also addresses challenges associated with a “one-size-fits-all” approach. This personalised approach to implant design ensures optimal fit and functionality, promoting better treatment outcomes and patient satisfaction. By overcoming the limitations of standardised implants, 3D printing would offers a promising solution to improve patient care and

address the unique anatomical variations found among individuals (Hao et al., 2021; J. Wang et al., 2021).

The primary objective of this experimental chapter is to assess the feasibility of employing FDM based 3D printing as a manufacturing method for a novel implantable drug delivery device. The device is specifically designed for localised treatment of brain tumours. It consists of a biodegradable polymer, Poly(lactic-co-glycolic) acid (PLGA, 5010), cones incorporated with the chemotherapeutic agent, Irinotecan (IRN). These cones are designed to be attached to a flexible base layer composed of Ethylene-vinyl acetate (EVA) with a vinyl acetate content of 18%. In addition to its biocompatibility, chemical stability, and mechanical strength, EVA was chosen as the material of interest in this study because of its favourable flexibility and elasticity. These properties make it an excellent candidate for implants that require conformation to anatomical contours, thereby reducing mechanical stress on both the wound and the surrounding tissues. The study aims to investigate the technical viability of utilising FDM 3D printing technology in fabricating this distinctive device. The manufactured device will be subjected to characterisation in terms of *in vitro* drug release properties.

5.2. Materials and Method

5.2.1. Materials

Ethylene Vinyl acetate (EVA, 18.2) pellets were supplied by Celanese Corp (Texas, USA). D, L-Lactid/ glycolide copolymer (PLGA, 5010) with polymer ratio of (50/50) acquired from (Corbion, the Netherland). Irinotecan hydrochloride trihydrate (IRN) was purchased from LGM Pharma (Erlanger, KY, USA). Acetonitrile and dichloromethane (DCM) were obtained from Thermo-Fisher Scientific (Loughborough, UK). HPLC grade deionised water (dH_2O), type (I) where obtained by laboratory Triple Red water system (Buckinghamshire, UK) and was used throughout the analysis.

5.2.2. Preparation of IRN loaded polymer by hot melt extrusion (HME)

The appropriate amounts of IRN and PLGA were weighed using VWR® T electrical balance (Leicestershire, UK) and blended together in a ratio of 15:85 w/w%. The mixture was then fed into a corotating twin screw extruder (Kapex, USA) operating at a screw speed of 70 RPM. The processing temperature was carefully regulated across three different heating zones, ranging from 126 to 180°C. The extruder is equipped with a 3 mm die and a gravimetric feeder. Following extrusion, the resulting extrudate was pelletised into pellets with diameters ranging from 4 to 6 mm using a GP20 Plastic Shredder Hybrid (3devo, The Netherlands). These pellets were subsequently stored under refrigeration conditions until they were ready to be employed for 3D printing purposes.

5.2.3. Characterisation of IRN loaded polymer

5.2.3.1. IRN content and loading efficiency analysis of prepared extrudate

The drug content of the HME extrudate was analysed by calculating the drug loading efficiency of the prepared extrudate. Three samples of extrudate, weighing 25 mg each, were collected from three different sections (the beginning, middle, and end). These samples were dissolved in 20 mL of DCM. The solution was then covered and heated to 40˚C with magnetic stirring at 250 RPM until complete dissolution. Subsequently, the solution was stored in a fume hood for 3 hours to allow for complete evaporation of the DCM. The drug was extracted by adding 20 mL of mobile phase and subjecting the samples to sonication in a water bath at temperature of 37°C for 10 minutes using a VWR ultrasonic bath (Leicestershire, UK). Following sonication, the samples were centrifuged at 13,000 RPM for 5 minutes utilising Labnet Prism R centrifuge (Edison NJ, USA). The supernatants were collected and analysed using HPLC. The drug loading efficiency was calculated using Equation (5.1). The results were presented as the mean (n=3) ± SD.

HME drug loading efficiency (LE) % = (Mass of the drug in extrudate) / (Mass of the drug in feed) ×100

5.1

5.2.3.2. Differential scanning calorimetry (DSC) analysis

DSC measurements were conducted using the Discovery DSC 250 instrument (TA Instruments, USA). The samples, weighing approximately 6-8 mg, were carefully placed in Tzero aluminium pans. An empty sealed aluminium pan served as the reference. DSC thermograms were obtained by subjecting the samples to cooling-heating ramps, ranging from 25°C to 250°C, with a heating rate of 10°C/min, all under a nitrogen atmosphere.

5.2.3.3. X-Ray Diffractometer (XRD) analysis

The crystallinity of PLGA 5010 placebo, IRN powder, and PLGA/IRN extrudate was determined using the Rigaku MiniFlex 600 instrument (Rigaku, USA), which utilises Cu-Kα radiation of 1.542 Å. The instrument was operated at an applied voltage of 40 kV and a current of 15 mA. Scanning was conducted up to a 2θ angle of 90°. The obtained figures and peaks were analysed using SmartLab Studio-II software.

5.2.3.4. Rheology

The rheological properties of PLGA 5010 polymer and the PLGA/IRN physical mixtures were examined using the Discovery HR-1 instrument (TA Instruments, USA). Dynamic oscillatory measurements were conducted employing a parallel plate geometry with a 20 mm diameter and a gap distance of 500 µm. The temperature range for the analysis spanned from 200°C to 100°C,

with a cooling rate of 10°C/5 minutes. The tests were performed under a constant frequency of 5 rad/s to ensure consistent and reliable data acquisition.

5.2.4. IRN solubility in different media

Over-saturated solutions of IRN were prepared by dissolving an excess amount of IRN in 5 mL of various solvents: dH_2O with pH 5.9, dH_2O with pH 3.5, PBS with pH 7.4, and 70% Dimethyl Sulfoxide (DMSO). The solutions were thoroughly mixed and then covered before being stored in an orbital shaking incubator, Unitron INFORS HT (Surrey, UK), operating at temperature of 37˚C and a speed of 100 RPM for a duration of 48 hours. After the incubation period, the solutions were subjected to centrifugation at 13000 RPM for 5 minutes using Labnet Prism R centrifuge (Edison NJ, USA) to separate the supernatant from any undissolved particles. The drug content of the supernatant was subsequently determined using HPLC. The experimental procedure was performed in triplicate (n=3) to ensure accuracy and consistency. The mean value and standard deviation (SD) were calculated from the obtained data to represent the results.

5.2.5. IRN stability

10 mg of pure IRN powder was separately dissolved in three different solutions containing 10 ml of dH2O (pH 5.9), phosphate buffer solution PBS (pH 7.4) and DMSO 70%. To ensure complete dissolution, all solutions were subjected to sonication in a water bath at for 10 minutes using VWR ultrasonic bath (Leicestershire, UK). Samples were filtered and stored at different temperatures

37˚C, 25˚C and 4˚C. At specific time intervals 1, 3, 7, 14, and 20 days, 0.5 mL samples were collected from each solution analysed via HPLC. Results were presented as mean (n=3) ± SD.

5.2.6. CAD design and 3D printing of IRN loaded implant

The brain implant design was created using 3D CAD software TinkerCAD (Autodesk Inc, USA). The design was then exported in the Stereolithography (STL) format, which was subsequently converted into the G-code format using slicing software (Ultimaker cura, USA) version 3.6.0. The implant consists of two distinct parts, each designed as separate STL files. The first part is a drug-free base layer made of placebo EVA (18.2%), with dimensions of 15 x 15 mm and a thickness of 2 mm. The second part, which contains the drug (PLGA/IRN), is designed with four cone-shaped protrusions. Each protrusion has a height of 6 mm and a base diameter of 5 mm, as depicted in Figure (5.1).

The shape of the implant was designed assuming that the drug loaded protrusions can provide the following advantages:

1- The cone-shaped protrusions can provide increased stability and anchoring within the brain tissue. The tapered shape allows for better fixation and minimises the risk of implant movement or displacement.
2- The gradual tapering of the protrusions allows for a smoother transition between the implant and the tissue, which might help to reduce the risk of inflammation or tissue damage.

3- The cone-shaped protrusions provide a larger surface area for potential interactions with the surrounding tissue.
4- It is a customisable design where the number, size, and arrangement of the cone-shaped protrusions can be tailored to specific requirements and applications. This flexibility allows for customisation based on the target area within the brain.

The designed implant was 3D printed using FDM based 3D printer (Pollen PAM, France). The 3D printer equipped with four separate extruders. Each extruder has three different heating zones: extruder cold, extruder body and extruder head. Two different extruders were used to print the implant. Each extruder's cartridge was filled with the corresponding polymer Figure (5.2). The 3D printing conditions were summarised in Table (5.1).

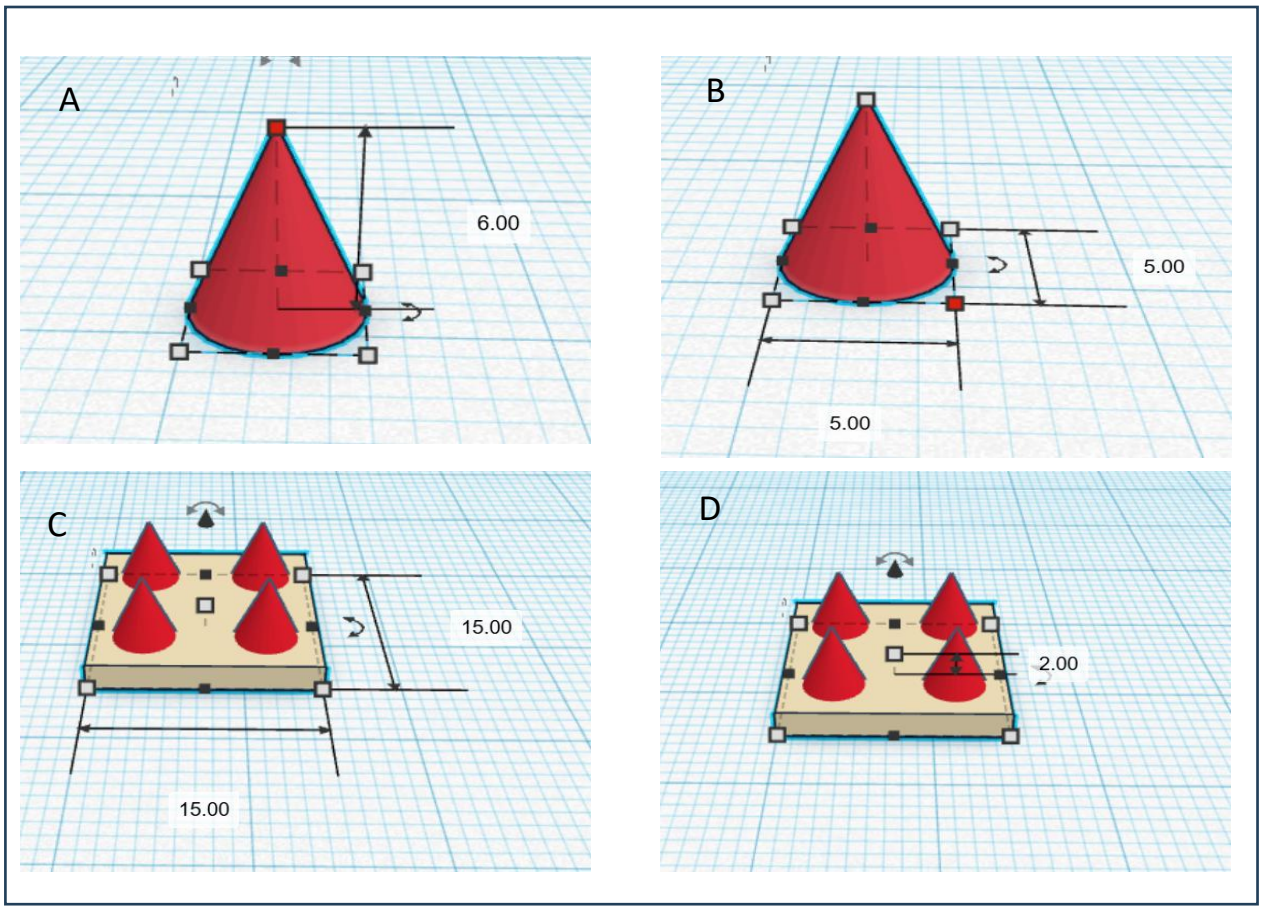

Figure 5.1: *Demonstrates the digital designs of brain implant, height of drug loaded protrusions (A), diameter of drug loaded protrusions (B), dimensions of EVA drug free base (C), thickness of drug free base (D).*

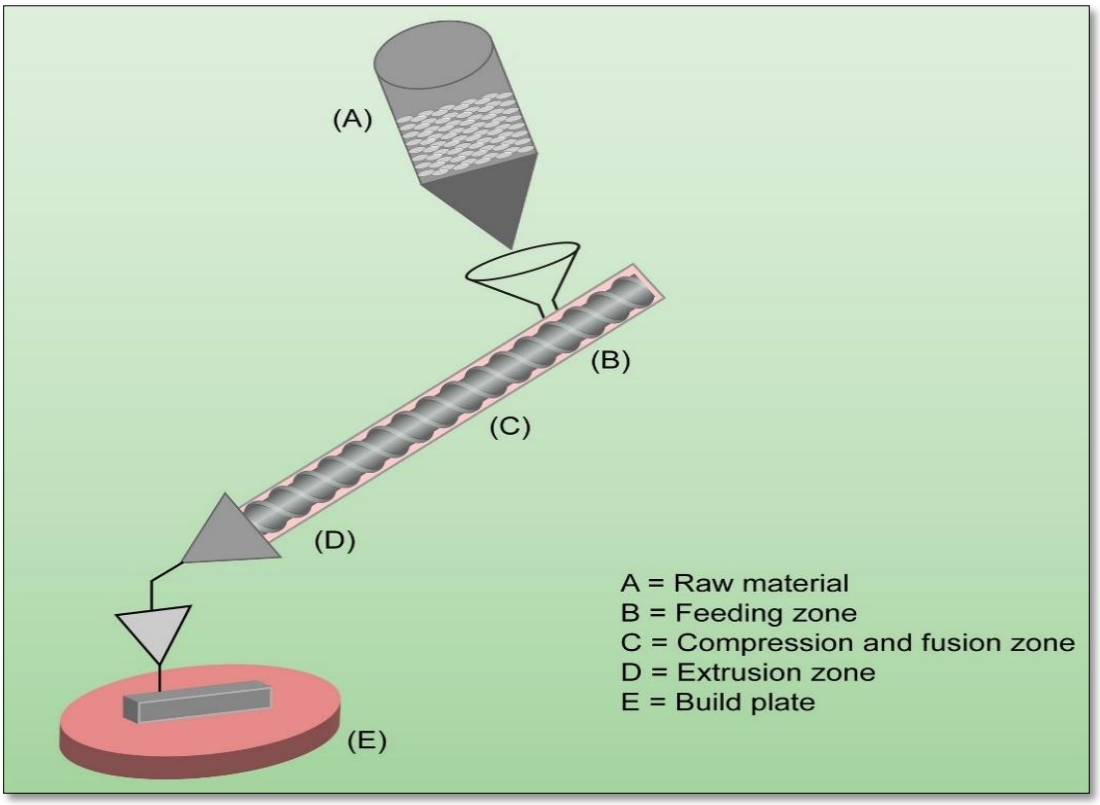

Figure 5.2: *Schematic diagram of the PAM 3D printer*

Table 5.1: FDM based 3D printing conditions.

Dosage form	Type of printer	Implant part	Feeding materials	Temperature (°C)		Printing Speed (mm/s)	Layer Heights (mm)	Infill (%)	Flow rate (%)
				Printing	Bed				
Brain implant	Pellets based FDM 3D printer	Drug loaded (protrusions)	PLGA/IRN 85/15 w/w % pellets	165	65	35	0.15	100	45
		Implant base (placebo)	EVA (18.2) placebo Pellets	145	50	45	0.15	100	35

5.2.7. *In vitro* release of the IRN from 3D printed implant

The 3D printed implants were immersed in 30 mL of dH_2O release media and placed in an orbital shaking incubator, Unitron INFORS HT (Surrey, UK), set at a speed of 100 RPM and a temperature of 37˚C. At specific time intervals, 0.5, 1, 2, 3, 7, 8, 9, 10, 12, 15, 17, and 20 days, 1 mL samples were withdrawn from the release media and replaced with fresh media. The withdrawn samples were subjected to centrifugation at 13000 RPM for 5 min using Labnet Prism R centrifuge (Edison NJ, USA) to separate any solid particles, and the supernatant was then analysed using HPLC. The drug release was calculated using Equation (5.2). The results obtained from the analysis were presented as the mean value based on three replicates (n=3) ± SD.

Drug release (%) = (Released drug)/ (Total drug) × 100 *5.1*

5.2.8. IRN HPLC methodology

5.2.8.1. HPLC chromatographic condition

IRN was analysed using an Agilent HPLC 1260 infinity II. The mobile phase composed of a mixture of 0.02 M potassium di-hydrogen orthophosphate, pH 2.5, adjusted with ortho-phosphoric acid, methanol, and acetonitrile in a ratio of (75/25 v/v). The separation was performed by a Thermo - Scientific C18, 5µm, (150 × 4.6 mm) column at room temperature. The UV wavelength detector

was set at 225 nm with a run time of 10 min. The injection volume was 10 µL with a flow rate of 0.8 mL/min. The retention time for IRN was around 5.82 minutes.

5.2.8.2. Preparation of stock solution and calibration standards.

20 mg of IRN was dissolved in 100 mL of deionised water (dH_2O) to prepare a stock solution with a final concentration 0.2 mg/mL. From this stock solution, 50 mL was transferred into a 100 mL volumetric flask and diluted with the mobile phase to the desired volume, resulting in a standard solution with a final concentration of 100 µg/mL. Different calibration standards ranging from 10, 20, 40, 60, 80, and 100 µg/mL were obtained by appropriately diluting the standard solution with the mobile phase.

5.3. Results and discussions

5.3.1. Characterisation of IRN drug loaded extrudate

In the following sections, the analysis of the extrudate, which was loaded with the drug using HME, encompassed assessments of drug content, thermal stability, rheological properties, and polymorphic profile, with the results detailed.

5.3.1.1. Drug content

The results of the drug content analysis and HME loading efficiency are summarised in Table (5.2). The findings indicate that the initial amount of IRN found in the extrudate was 3.61 ± 0.12%, slightly lower than the theoretical drug content of 3.75 mg. However, in the middle and end sections of the extrudate, the amounts of IRN found were 3.69 ± 0.1% and 3.71 ± 0.12%, respectively.

The HME loading efficiency ranged from 96.2% to 98.9%. These results demonstrate an improvement in the drug content loading in the examined sections of the extrudate, despite the slightly lower drug content observed at the beginning.

Table 5.2: drug content of IRN/PLGA extrudate and HME loading efficiency

Extrudate part	Expected amount (mg)	Average actual amount (mg) (n=3) ± SD	HME loading efficiency (LE) %
Beginning	3.75	3.61 ± 0.12	96.2
Middle	3.75	3.69 ± 0.1	98.4
End	3.75	3.71 ± 0.12	98.9

5.3.1.2. DSC analysis

The DSC thermograms of IRN and PLGA 5010 are depicted in Figure (5.3). The thermogram of IRN displayed an endothermic peak at 100°C, which can be attributed to its glass transition temperature (*Tg*). Additionally, a broad endothermic peak around 223°C was observed, corresponding to the melting point (Tm) of IRN. On the other hand, the thermogram of the PLGA 5010 placebo polymer exhibited an endothermic peak at 50°C, which corresponds to its *Tg*. These findings suggest that both IRN and PLGA 5010 are not prone to thermal degradation at the HME processing temperature range of 126-180°C. The absence of significant thermal degradation suggests that the materials can withstand the processing conditions without undergoing undesirable chemical changes.

5.3.1.3. Rheometer

The influence of temperature on the complex viscosity of the IRN pure and PLGA 5010: IRN physical blend is presented in Figure (5.4). Results demonstrated that the IRN showed a complex viscosity bellow 10000 Pa.s at 155°C , while the PLGA:IRN physical mixture reached a complex viscosity of

10000 Pa.s at 164°C. These findings were beneficial during the HME method adjustment of the processing temperature to ensure sufficient drug polymer mixing while maintaining the torque at reasonable level to avoid the screw damage of the HME or the 3D printer.

5.3.1.4. X-ray diffraction (XRD) analysis results

The XRD results are presented in Figure (5.6). The results indicate that the raw IRN presented in Figure (5.5 A) is entirely crystalline, while the PLGA polymer, depicted in Figure (5.5 B), exhibits a combination of amorphous and crystalline phases. The crystallinity peaks of both materials were reduced after the HME process, as seen in Figure (5.5 C) and completely disappeared after the 3D printing process as shown in Figure (5.5 D). Based on the XRD results, it can be inferred that the IRN loaded into the implant exists in an amorphous form. The transformation from a crystalline to an amorphous state might be attributed to the rearrangement of molecular structures caused by the combined effects of heat and shear strain during both the HME and 3D printing processes. This phenomenon was previously reported in the literature (Jamróz et al., 2018).

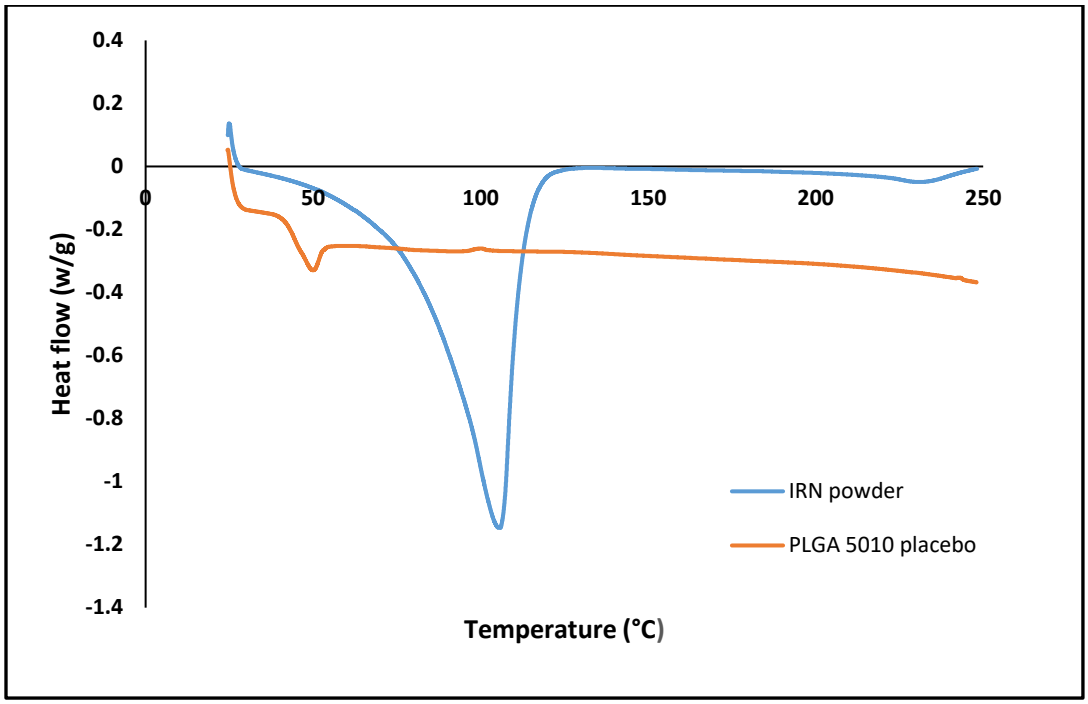

Figure 5.3: *DSC thermogram for IRN powder and PLGA.*

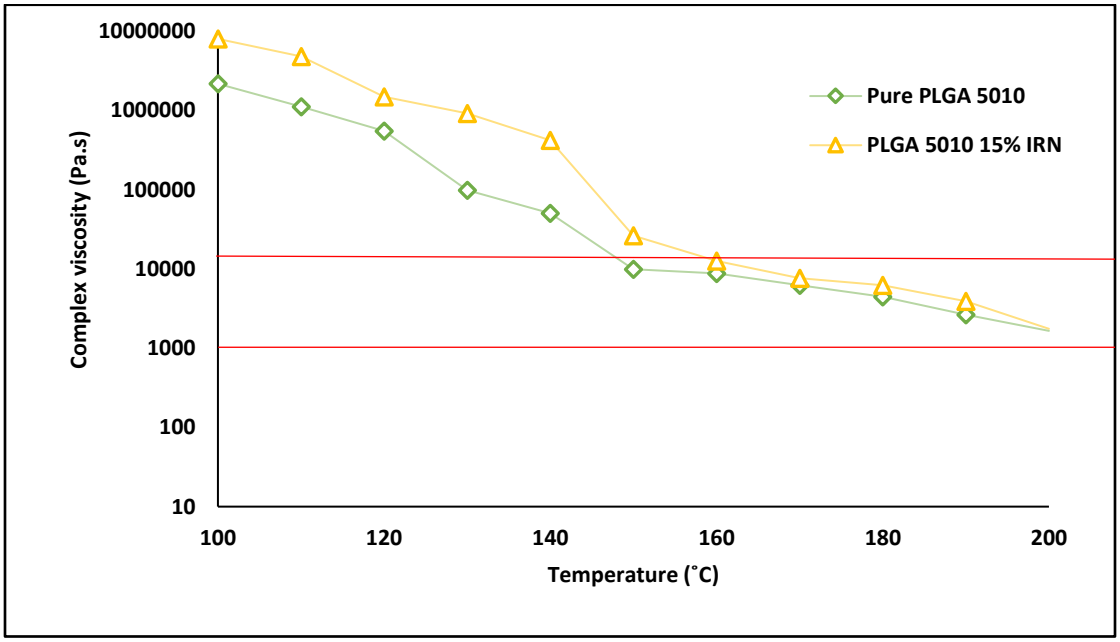

Figure 5.4: *Complex viscosity vs temperature (˚C) for pure PLGA and PLGA 15% IRN physical mixture. Test was performed at a 5 rad/sec angular frequency and 10°C/5 minutes cooling rate.*

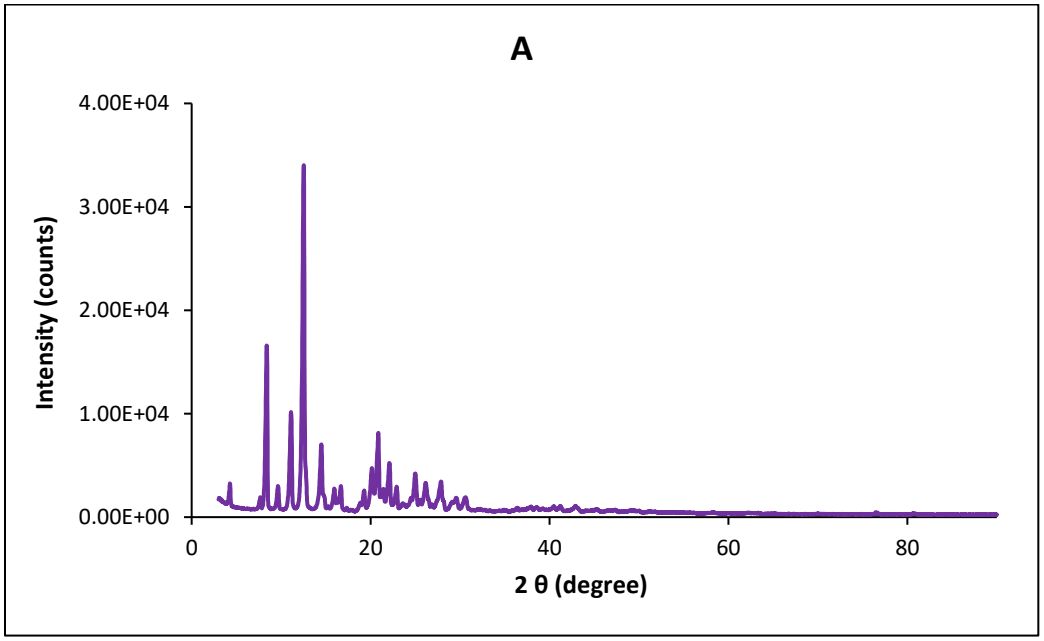
A
4.00E+04
3.00E+04
2.00E+04
1.00E+04
0.00E+00
Intensity (counts)
0
20
40
60
80
2 θ (degree)

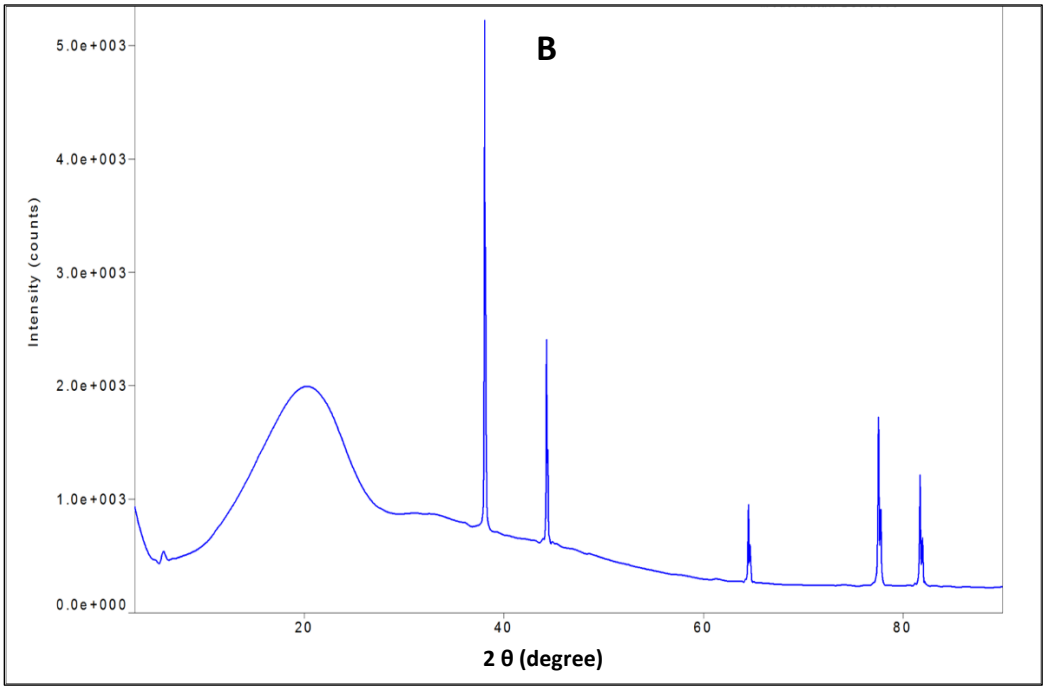
B
5.0e+003
4.0e+003
3.0e+003
2.0e+003
1.0e+003
0.0e+000
Intensity (counts)
20
40
60
80
2 θ (degree)

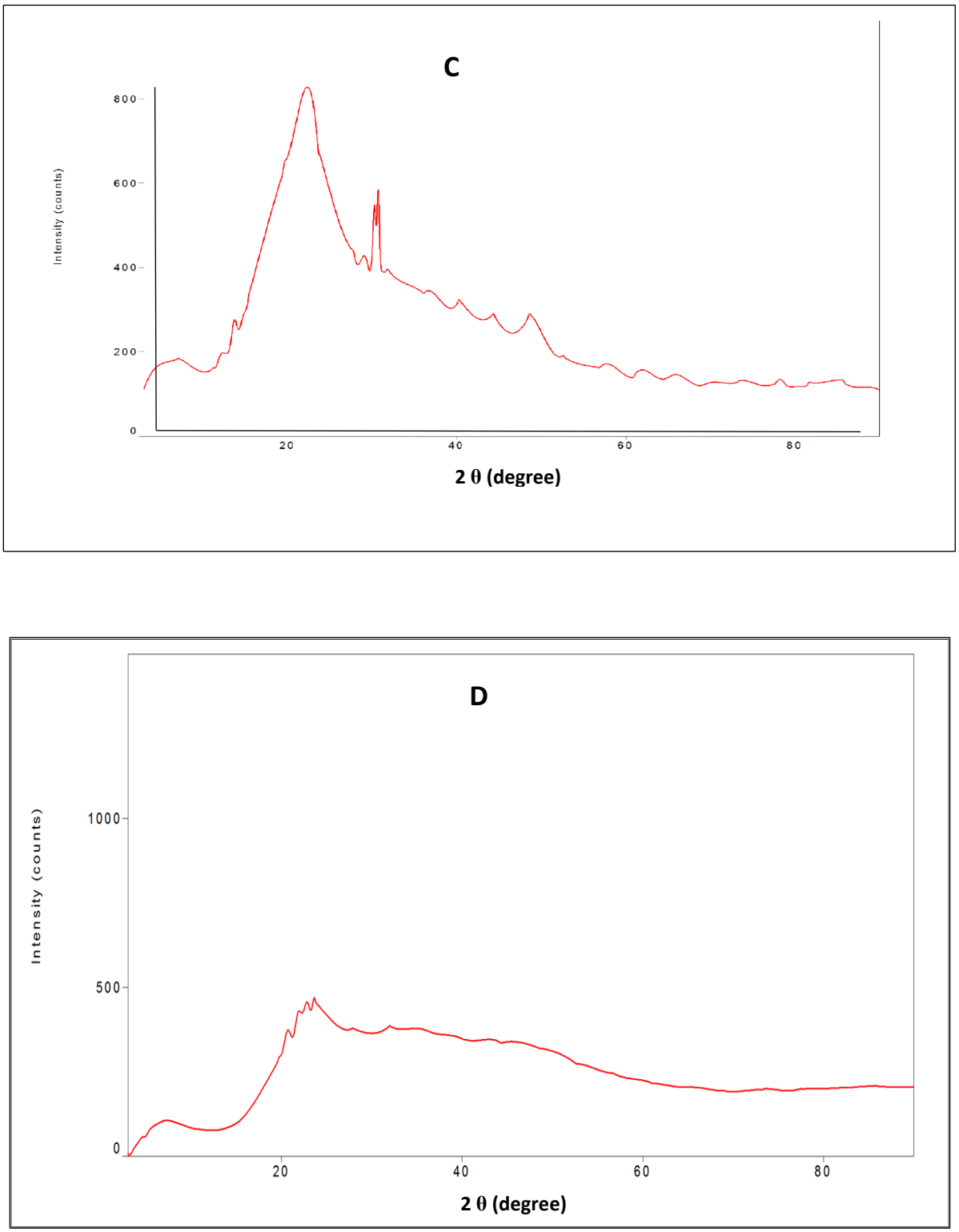

Figure 5.5: *The X-ray diffractometry for IRN powder (A), PLGA 5010 (B), HME prepared extrudate (C) and 3D printed implant (D).*

5.3.2. 3D printed implant

FDM based 3D printing has successfully fabricated IRN loaded implant. Figures (5.6 A) and (5.6 B) showcase images of the HME prepared extrudate contains PLGA loaded with 15% (w/w) of IRN before and after the palletisation process, respectively. The images presented in Figures (5.6 C) and (5.6 D) demonstrate the digital CAD design and the corresponding actual geometry of the manufactured implant, respectively. It should be borne in mind that the thin film surrounding the implant is a removable layer was deliberately printed to increase the implant adhesion to the build plate during the 3D printing process.

There are different types of adhesions supports used in FDM 3D printing such as Raft, Brim, and Skirt as shown in Figure (5.7). Their main function is to prevent warping of the 3D printed object (Lv et al., 2022). A Raft support is a solid, flat base that is printed underneath the object being printed. It serves multiple purposes, including improving bed adhesion, reducing warping, and providing stability during the printing process. By increasing the contact area between the object and the build plate, the Raft helps distribute the printing stresses more evenly, minimising the chances of the object detaching or warping (Durão et al., 2019; Horvath & Cameron, 2014). While A Brim support is a thin, flat extension that is printed around the base of the object. It is particularly useful for objects with a small contact area or materials that have poor bed adhesion properties. The Brim increases the surface area in contact with the build plate, providing better stability and reducing the likelihood of the object detaching or warping during the printing process. Once the printing process is finished, the Brim can be detached, leaving the desired object with a clean and

smooth base. On the other hand, Skirt support involves printing one or more lines around the perimeter of the object, but not directly attached to it. However, it serves to improve the adhesion by helps prime the extruder by purging any leftover filament or air bubbles in the nozzle, ensuring a smooth flow of filament before the actual print begins. Additionally, the Skirt assists with bed levelling and acts as a visual indicator of the initial layer adhesion. It allows for adjustments, if necessary, before the main print starts (Hsiang Loh et al., 2020; Morales et al., 2021).

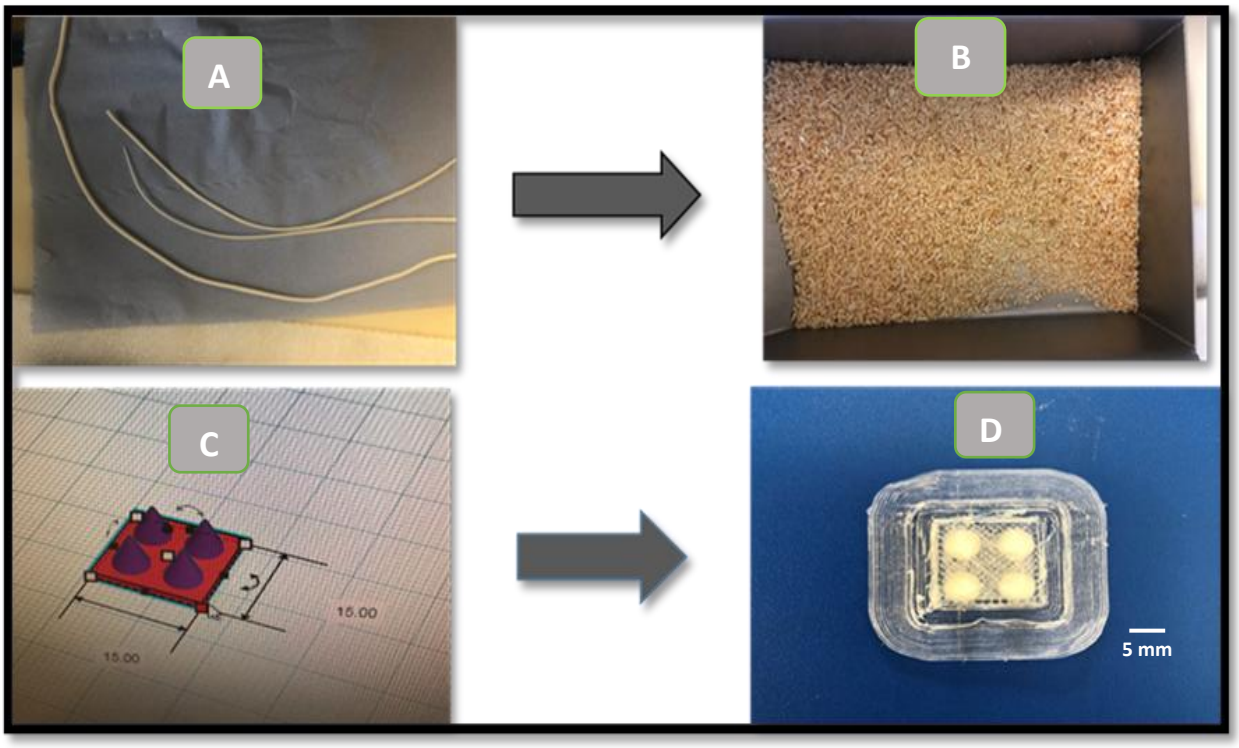

Figure 5.6: *Represents the (A) drug polymer extrudate image, (B): pelletised extrudate, (C) CAD design of implant (D) 3D printed implant image.*

Figure 5.7: *Different types of adhesion support used in FDM 3D printing.*

5.3.3. IRN HPLC analysis

Figure (5.8) demonstrates the IRN standard calibration curve at six different concentrations ranging from 10 to 100 µg/mL. The correlation between the IRN concentrations and their corresponding area under the curve (AUC) indicates an excellent linear relationship, with a correlation coefficient (R^2) value of 0.9999. A linear regression analysis was performed on the IRN graph, resulting in the regression line equation y = 33.712X + 13.214. The data were analysed using regression analysis at a 0.05% confidence level, revealing that the difference between the estimated and found drug concentration was not statistically significant (P > 0.05). The sensitivity of the method was sufficient to detect and quantify drug concentrations of 0.1 µg/mL and 0.311 µg/mL as the limit of detection and limit of quantification, respectively. The method accuracy was

determined by the recovery experiment and found to be 100.56 ± 1.42%. The results of the IRN HPLC analysis are summarised in Table (5.3).

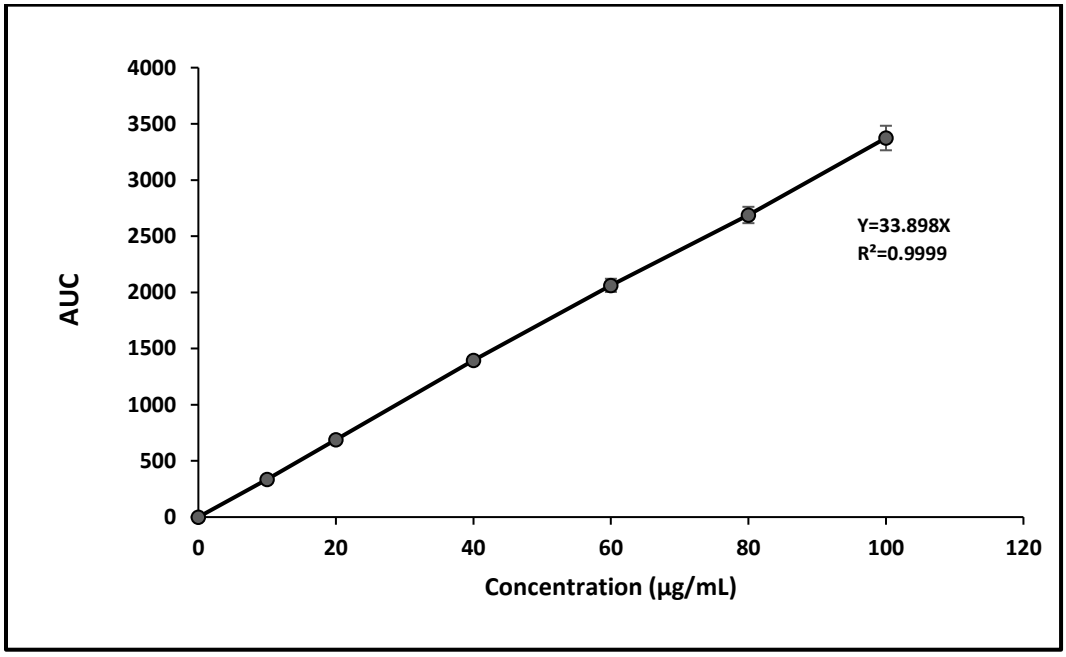

Figure 5.8: *Standard calibration curve of IRN. Results presented as mean (n=9) ± SD.*

Table 5.3: HPLC method validation results.

No.	Assay validation	Results
1	Accuracy (%)	100.56 ± 1.42%
2	Slope	33.898
3	Intercept	0
4	Linearity range	10-100 µg/mL
5	Correlation coefficient (R^2)	0.9999
6	SE of intercept	0.43081
7	SD of intercept	1.055
8	Limit of detection (LOD)	0.1 µg/mL
9	Limit of quantification (LOQ)	0.311 µg/mL

5.3.4. IRN Solubility and stability

Figure (5.9) presents the solubility findings of IRN in various media. The results indicate that IRN exhibits higher solubility in DMSO70% and dH_2O with a pH of (5.9), with solubility values of 13.91 ± 0.21 mg/mL and 12.16 ± 1.26 mg/mL, respectively. In comparison, the solubility of IRN in PBS with a pH of (7.4) and acidic dH_2O with a pH of (3.7) is lower, with solubility values of 6.29 ± 0.12 and 8.91 ± 0.54, respectively. These findings suggest that DMSO70% and slightly acidic dH_2O are more effective solvents for dissolving IRN compared to PBS and acidic dH_2O.

The stability of IRN in different media is presented in Figure (5.10). The results indicate that IRN maintains more than 82% of its stability over a 20-day period in dH_2O with a pH of (5.9), with a negligible impact of different temperatures as shown in Figure (5.10 A). However, within the initial 24 hours, IRN tends to experience a stability loss of approximately 80% in PBS and 65% in DMSO 70%, as demonstrated in Figure (5.10 B) and Figure (5.10 C), respectively. Based on these findings, dH_2O with a pH of (5.9) was selected as the suitable medium for conducting release studies of IRN loaded 3D printed brain implant.

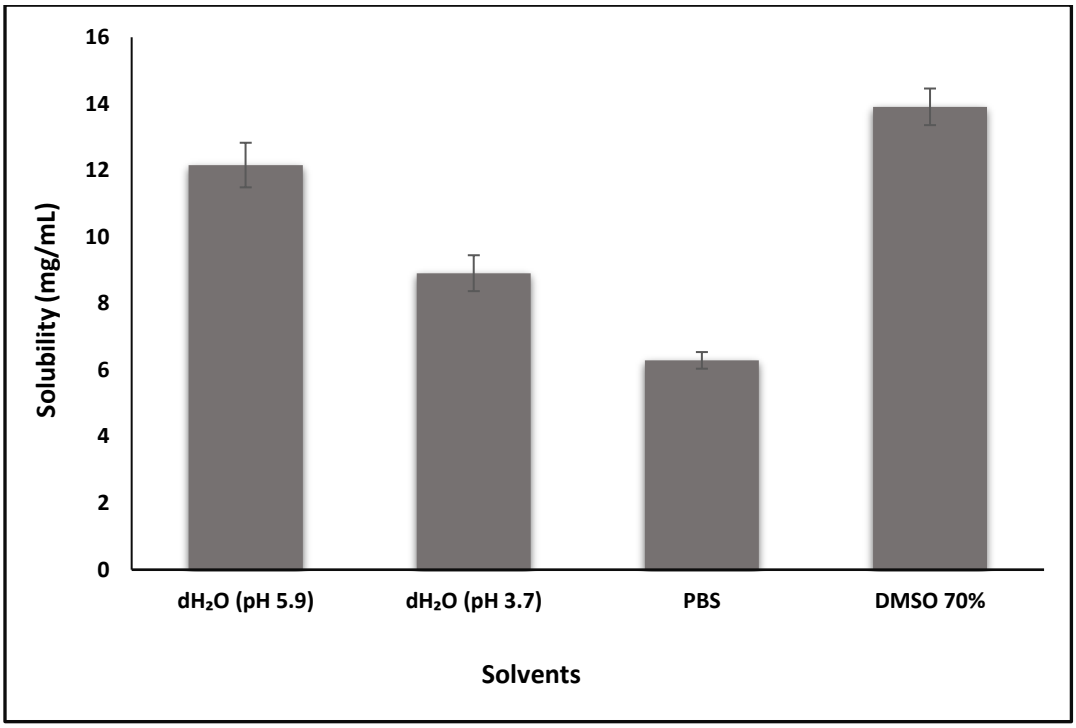

Figure 5.9: *IRN solubility in different solvents. Results shown as mean (n=3) ± SD.*

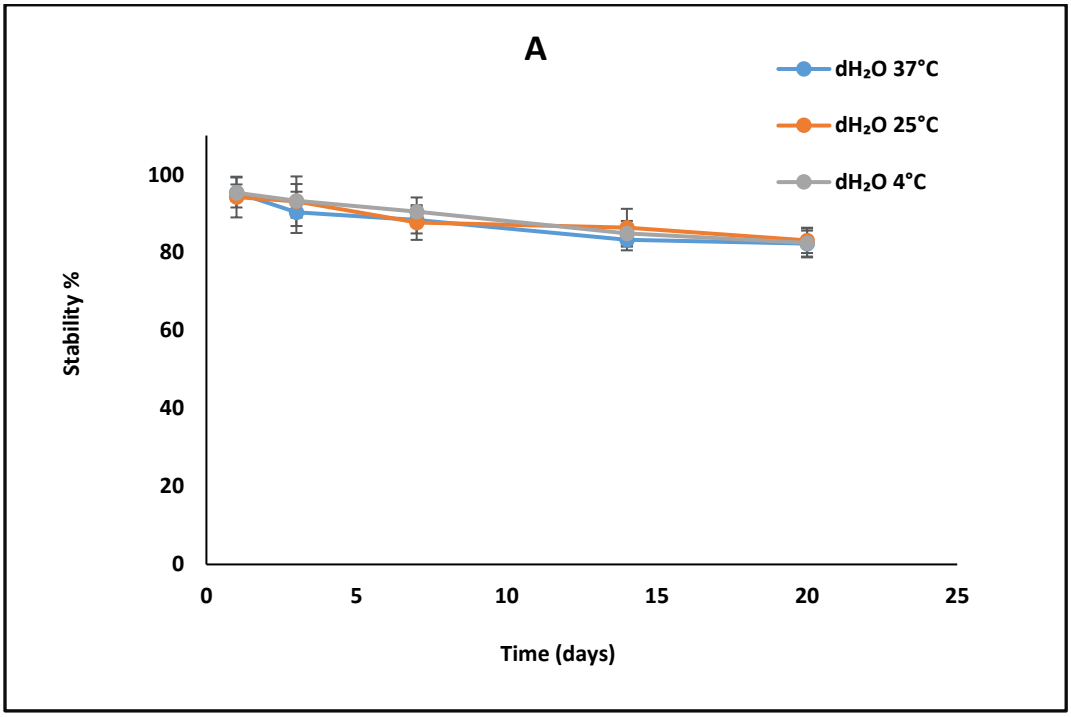

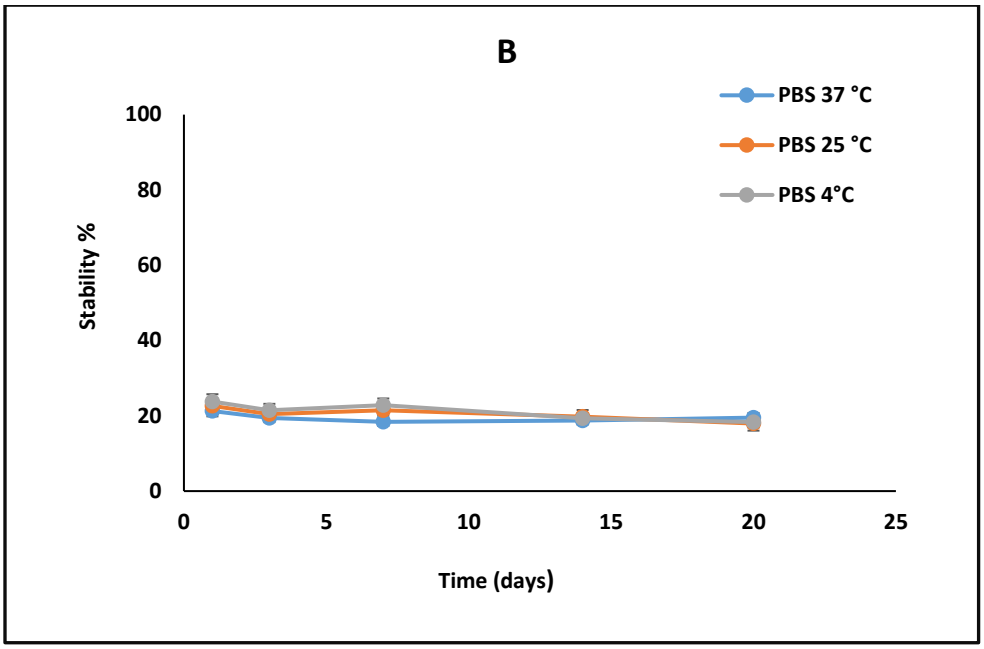

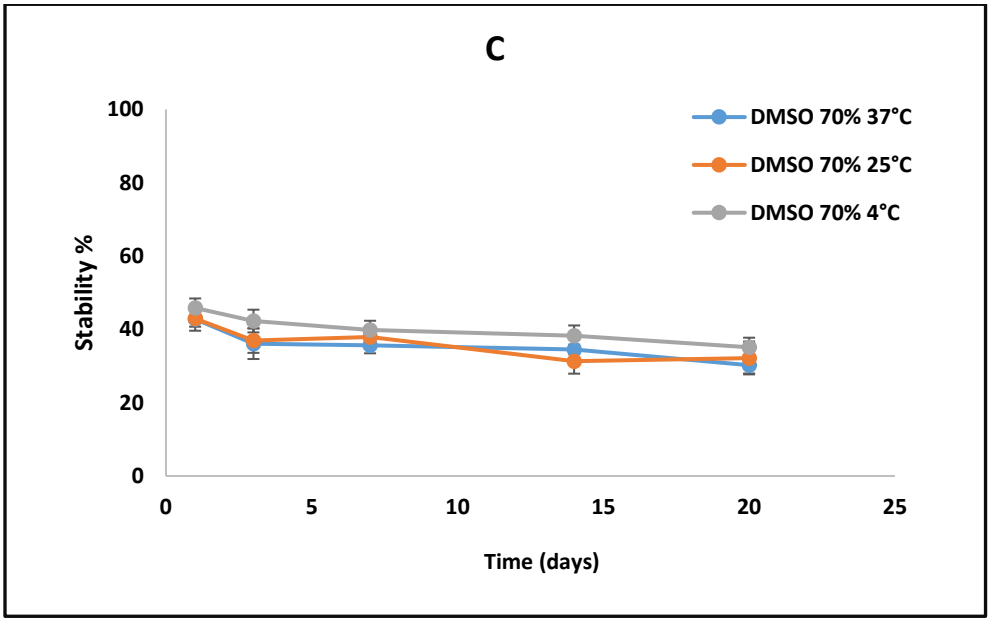

***Figure 5.10**: IRH stability in dH_2O (A), PBS (B), and DMSO 70% (D) at three different temperatures 4, 25 and 37°C. Results shown as mean (n=3) ± SD.*

5.3.5. *In vitro* drug release studies

Figures (5.11) and (5.12) present the *in vitro* cumulative drug release percentage and the mass of drug released from the 3D printed implant, respectively. Over a 20-day period, the release profile exhibits two distinct phases. The first phase, spanning from day 0 to day 9, demonstrates a rapid release of approximately 50% (approximately 9.66 mg/mL) of the IRN content. This initial burst release is likely attributed to the drug's quick dissolution and diffusion the fast dissolution and diffusion of the drug on and just below the surface. Following the initial phase, the second phase shows a slower and sustained release, with an additional 4% (1.71 mg/mL) of the IRN content released over an extended period of 11 days. This sustained release occurs as the drug must diffuse through the PLGA material constituting the implant before being released. This release pattern aligns with previously reported findings in the literature, confirming the consistency of the observed release behaviour. (Gomaa et al., 2023; Solano et al., 2013).

The *in vitro* release data was examined to identify the model that best describes the drug release pattern as presented in Table (5.4). Different release models including zero order, first order, Higuchi, and Korsmeyer-Peppas models, were fitted to the release curves. Results indicated that the IRN release from the implant has followed mostly the Korsmeyer-Peppas and zero-order with a coefficient values (R^2) of 0.9551 and 0.9287, respectively. The release kinetic constants and the Korsmeyer-Peppas model's diffusional exponent (n) value of 0.47 manifested non-Fickian, anomalous diffusion mechanism with IRN released through a combination of diffusion and swelling of PLGA.

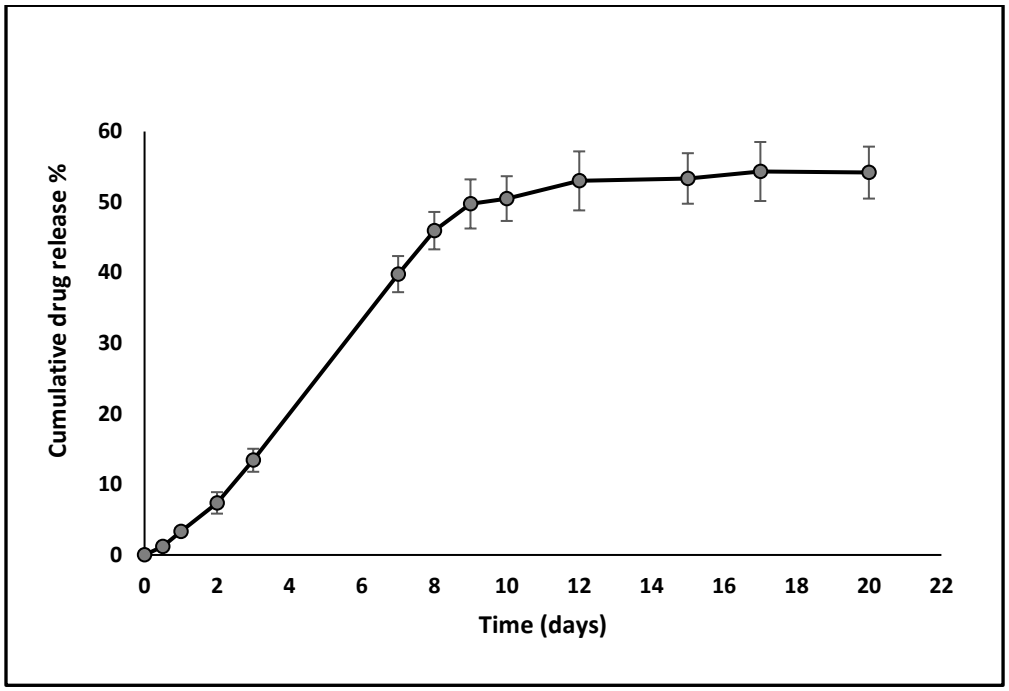

Figure 5.11: *The In vitro cumulative drug release % of IRN loaded implant. Results shown as mean (n=3) ± SD.*

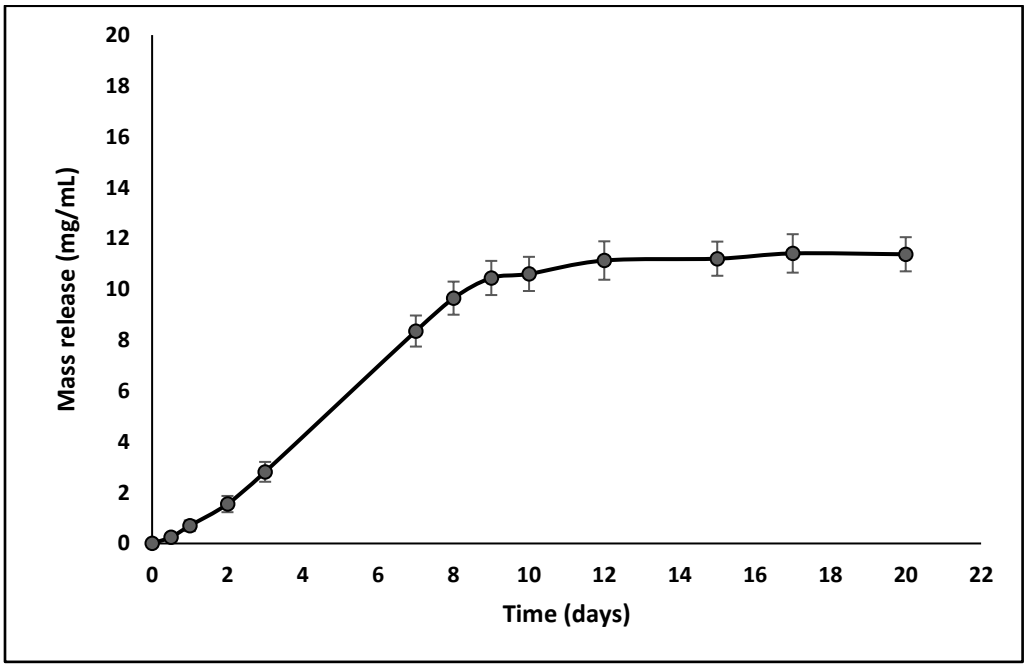

Figure 5.12: *In vitro mass release (mg/mL) from the brain implant. Results presented as mean (n=3) ± SD.*

Table 5.4: Release constants (k) and correlation coefficient (R^2) of release models

Zero-Order		First-Order		Higuchi		Korsmeyer–Peppas		
R^2	k (% h^{-1})	R^2	K (h^{-1})	R^2	k (% $h^{-0.5}$)	R^2	k (%h^{-n})	n
0.9287	3.73	0.8458	0.05	0.9132	13.76	0.9551	1.084	0.47

5.4. Discussions

This chapter investigated the viability of FDM 3D printing to manufacture IRN drug-loaded implants to provide localised drug delivery for the treatment of brain tumour. Polymeric implants have been intensively studied for chemotherapeutic drug delivery in cancer because they may enhance the therapeutic regimen by boosting local concentration and reducing side effects (Weinberg et al., 2008).

Initially, twin screw HME was utilised for loading the IRN into the PLGA 5010 polymer. The twin screw HME is favoured by its high loading efficiency, solvent free process and the production of stable amorphous solid dispersions (Genina et al., 2018). The obtained drug loaded extrudate was characterised in terms of drug content, thermal stability, melt viscosity and nature of crystallinity. The results of drug content analysis revealed that the amount of IRN loaded into prepared extrudate was in a range of 96.2 to 98.9 % of the theoretical drug content, verifying the effective preparation procedure used.

The DSC thermal analysis of IRN showed Tm around 223°C and *Tg* peak at 100°C while the PLGA 5010 exhibited an endothermic peak at 50°C which might be attributed to its *Tg*. The results of DSC thermal analysis indicate that both IRN and PLGA did not undergo thermal degradation during the HME and 3D printing processing window. DSC thermal analysis is a key feature to understand the thermal behaviour of materials during the HME method optimisation to avoid the possibility of drug degradation especially in thermolabile pharmaceutical agents. Moreover, the melt viscosity analysis is considered a crucial step for determining the optimum viscosity range with the corresponding temperature to avoid the possibility of HME process failure due to the high torque. The results suggested that the minimum temperature to provide optimum viscosity range of (1000–10000 Pa.s) was 165°C and 155°C for IRN:PLGA physical blend and PLGA placebo, respectively. The viscosity of the drug polymer appears to increase with lower temperatures reaching more than 10^6 Pa.s at 130°C compared to 10^5 Pa.s exhibited by the PLGA alone at same temperature. The higher temperature exhibited by the drug polymer physical blends might be attributed to the content IRN. However, rapid rise in complex viscosity upon cooling of the PLGA: IRN physical mixture suggests the suitable extrudability while maintain the shape of the die (Arnfast et al., 2017).

According to the XRD spectra, IRN and PLGA possessed crystalline structures. IRN exhibited high intensity peaks at 10.95 and 12.29 while the PLGA multiple peaks with high intensity peaks at 38.9, 43.3 and 78.7. However, the XRD spectra showed that the crystallinity peaks where significantly reduced after the HME process and completely disappeared after the FDM 3D printing. Results suggest that the two steps of heating and shear strain both hot melt extrusion and 3D printing

showed great viability to transform the molecular arrangements of drug polymer from crystalline to amorphous form (Ferrari et al., 2020; Yang et al., 2016).

The *In vitro* release of IRN from the fabricated implant showed that the release pattern possesses two different phases; fast drug release during the first 9 days followed by slow and sustain release pattern over a period of 11 days. This type of release might be attributed to the fast dissolution and diffusion of IRN which loaded on and below the surface of implant protrusions while the IRN within the implant must diffuse through the PLGA matrix before release resulting in slower and sustain release pattern (Solano et al., 2013). Among different release models that were evaluated, the results indicated that the *in vitro* release follows mostly the Korsmeyer-Peppas and zero-order. Moreover, the release kinetic constant and diffusional exponents suggested non-Fickian, anomalous diffusion mechanism with IRN release via a combination of diffusion and swelling of PLGA (Gomaa et al., 2023). The identifying the of drug release mechanism assists to determine the drug release limiting step. Zero order release kinetics is considered the ideal release type. In this scenario, the drug is released at a constant rate over time regardless of how much of it is dissolved in the release medium (Hines & Kaplan, 2013).

The 3D printed brain implant showed the capability of FDM to manufacture such a complicated structure two layer structure. Developing dosage forms from two different polymers is considered challenging process due to the difference in processing parameters as well as the physical properties of each polymer. The brain implant was designed to be consisted of flexible EVA 18.4%

base layer with dimensions 15 X 15 mm and thickness of 2 mm attached to cone shaped protrusions synthesised from PLGA 5010 loaded with IRN. However, multiple extruder FDM based 3D printer provide the opportunity to adjust each extruder's parameters (e.g., temperature, flow rate, printing speed, etc.) based on the physical properties of its feeding materials. Moreover, it provides simultaneous 3D printing process which reduces the chance of solidification while printing from two different layer which consequently improved the adhesion between the two different layers. FDM 3D printer beneficial regarding the simplicity the manufacturing process, rapid prototyping, and versatility to produce limitless drug delivery devices with customised geometries (Wang et al., 2023)

The findings of this study indicate that FDM-based 3D printing holds promise for the manufacturing of brain implants loaded with IRN, enabling sustained release of the drug over a period of 20 days. Additionally, the findings demonstrate that the twine screw HME technique is an effective method for loading drugs, as it enhances the stability of the drug-polymer system through the formation of solid dispersions with an amorphous nature. These findings highlight the promising applications of 3D printing and HME in the development of controlled-release drug delivery systems.

5.5. Conclusion

This chapter has showcased the potential of combining FDM 3D printing technology with HME in the production of implant dosage forms for long-acting delivery of chemotherapeutic agents. Specifically, the chemotherapeutic agent IRN was loaded into PLGA 5010 at a ratio of 15:85 (w/w) using twin-screw HME technology. The HME process showcased a drug loading efficiency surpassing 96% and provided the added benefit of achieving an amorphous solid dispersion. To fabricate the implant, a multi-extruder FDM 3D printing technology was employed, allowing for the precise manufacturing of the implant based on a created CAD model. The 3D printed implant was designed to consist of two distinct layers. The first layer, serving as a drug-free base layer, was fabricated using a flexible polymer EVA 18.2%. The second layer was constructed using PLGA polymer loaded with IRN, as a chemotherapeutic agent. The 3D fabricated implant was hypothesised to provide localised IRN delivery for the treatment of brain cancer. The release investigations of the implant demonstrated long-acting *in vitro* release over 20 days. The release pattern showed two different phases; rapid release during the first 9 days followed by slow and sustained release over the remaining 11 days. Release kinetic results showed that the release followed non-Fickian anomalous diffusion mechanism with rate limiting governed by diffusion and swelling of PLGA matrix. This study has furthermore proved the FDM 3D printer viability to produce complicated drug delivery dosage forms aimed for localised drug delivery.

Chapter 6 : DESIGNING AND 3D PRINTING A NOVEL DRUG DELIVERY DEVICE FOR LOCALISED PANCREATIC CANCER TREATMENT

6.1. Introduction

Pancreatic cancer (PC) ranks eleventh in incidence and seventh among all cancer-related deaths globally with an estimated 466,003 fatalities per year (Kim et al., 2022). Between 1990 and 2019, the incidence and mortality of pancreatic cancer dramatically increased in 27 EU nations and the UK, with annual increases of 0.65% and 0.55%, respectively (Yu et al., 2021). PC is one of the most dangerous tumours with poor prognosis with only 5% of patients survive for five years after their diagnosis (Cepeda-Franco et al., 2023).

The standard treatment for PC generally consists of surgery with an adjuvant therapy such as chemotherapy and/or radiotherapy to prevent the recurrence and metastasis of any hidden malignant cells (Yi et al., 2016). However, one of the challenges in the treatment of PC is the poor outcomes associated with the conventional treatment due to the fact that most of the chemotherapeutic agents, such as 5-floururacil, cisplatin and paclitaxel have poor water solubility and cannot reach the site of the tumour with a sufficient concentration (Loos et al., 2008). Beside the poor water solubility of chemotherapeutic agents, one of the main feature of PC is the dense desmoplasia stroma which accounts more than 70% of tumour cells (Yang et al., 2012), leading to tissue perfusion reduction, vascular compression and a hypoxic microenvironment covered with thick layer of pericytes.

The high mortality rate among cancer patients is often attributed to the severe side effects caused by the systemic administration of chemotherapy. This is primarily due to the accumulation of non-selective anticancer drugs in vital organs and healthy tissues throughout the body. The required high doses of these drugs contribute to the accumulation, resulting in detrimental effects on the body (Senapati et al., 2018; Wolinsky et al., 2012). Therefore, there is a critical need for more targeted and selective delivery systems to minimise the systemic toxicity of chemotherapy and improve patient outcomes.

To overcome the limitations associated with conventional chemotherapy, several local drug delivery methods have been developed, including implantable and injectable systems. These approaches aim to achieve targeted drug delivery directly to the tumour site, thereby reducing systemic side effects by minimising drug circulation throughout the body. One of the primary objectives of local drug delivery systems is to enhance the activity and stability of chemotherapeutic agents by ensuring their localised presence. Furthermore, local drug delivery systems offer the advantage of providing prolonged and controlled release of the drugs. This controlled release mechanism allows for a sustained therapeutic effect over an extended period, reducing the frequency of drug administration. Additionally, it facilitates drug uptake by tumour cells during their division cycles, increasing the effectiveness of the treatment. (Keskar et al., 2006; Matthes et al., 2007; Qi et al., 2018).

In the literature, 3D printing technology was previously utilised to manufacture a biodegradable local drug delivery patch for the treatment of PC. The patch composed of a blend of PLGA and

polycaprolactone (PCL) loaded with 5-flurouracil (5FU) in different concentrations; 10, 50, 100 and 150 mg per gram of the total weight of the patch. The patch exhibited a drug release over a course of 4 weeks and succeeded to suppress the growth of PC xenografts in mice (Yi et al., 2016). In another study, 3D printing was utilised to fabricate an implantable scaffold composed of PLGA, 5-FU, NVP-BEZ235 (PFN) blend to inhibit growth and metastasis of orthotopic breast cancer. The implant scaffold succeeded to provide a prolonged drug release near tumour sites with minimised exposure of normal tissues. Moreover, it exhibited a suppression in the growth of breast tumour in mice as well as a reduction in pulmonary metastasis (Yang et al., 2020).

The aim of this chapter is to employ FDM based 3D printing technology to produce an innovative drug delivery system envisioned to deliver localised chemotherapy for pancreatic cancer treatment. The design and development phase of the device will involve consultation with two clinicians (a pancreatic surgeon and an oncologist) to evaluate the device's dimensions and configuration for suitability in attaching to the cancer margin prior to testing on a pig model.

6.2. Materials and methods

6.2.1. Materials

Ethylene vinyl acetate (EVA) with vinyl acetate (VA) content of (18.2) in pellets form were supplied by Celanese Corp (Texas, USA). Irinotecan hydrochloride trihydrate (IRN) was purchased from LGM Pharma (Erlanger, KY, USA). Two wall clear Silicone tubing with different external : internal diameters (3*5 mm) and (1*2 mm), were purchased from AFS (Essex, UK). Gelfoam® sponge purchased from AEGIS LIFESCIENCES PVT. LTD (Gujarat, India). Type (I) deionised water (dH_2O) supplied by laboratory Triple Red water system (Buckinghamshire, UK).

6.2.2. CAD design of pancreatic device

The pancreatic device was designed using CAD software TinkerCAD (Autodisk, USA) and exported as STL format, which was subsequently converted into G.code format by the slicer Cura3.0 software (Ultimaker, USA). The device was designed to be drug free, where the drug can be loaded after the 3D manufacturing process. It was designed and printed from two separate STL files the first one contains the STL file format of the upper part of the device (the cover) represented in Figure (6.1 A), while the second STL format contains the design of the bottom part of the device Figure (6.1 B). After 3D manufacturing and assembling of the device, it is supposed to produce an internal cavity where the medical sponge will be enclosed with a hole in the upper part will be created as shown in Figure (6.1 C). The purpose of creating this aperture is to establish a

connection point for Silicone tubing, enabling external drug infusion access. Several dimensions and shapes were developed during the design optimisation process. However, the dimensions of the final optimised device were 35, 12 and 10 mm for length, width, and height, respectively.

The bottom layer of the device which is designed to be attached to the tumour site and assumed to be the release controlling membrane. Therefore, it was designed and printed with different 3D parameters to investigate their influence on the *in vitro* drug release. Table (6.1) presents the various formulations designed.

The assembly process of the device after 3D manufacturing involves the following steps:

1- After 3D printing the two parts of the device, the medical sponge will be manually inserted into the bottom layer, as shown in Figure (6.1 A).
2- Pressing the top layer (cover), illustrated in Figure (6.1 B), to effectively enclose the bottom layer simulating, to a certain degree, the method of joining the two parts of the traditional pharmaceutical capsule.
3- Firmly inserting the silicone tube through the aperture indicated in Figure (6.1 C).
4- The resulting fully assembled configuration of the device is depicted in Figure (6.1 D).

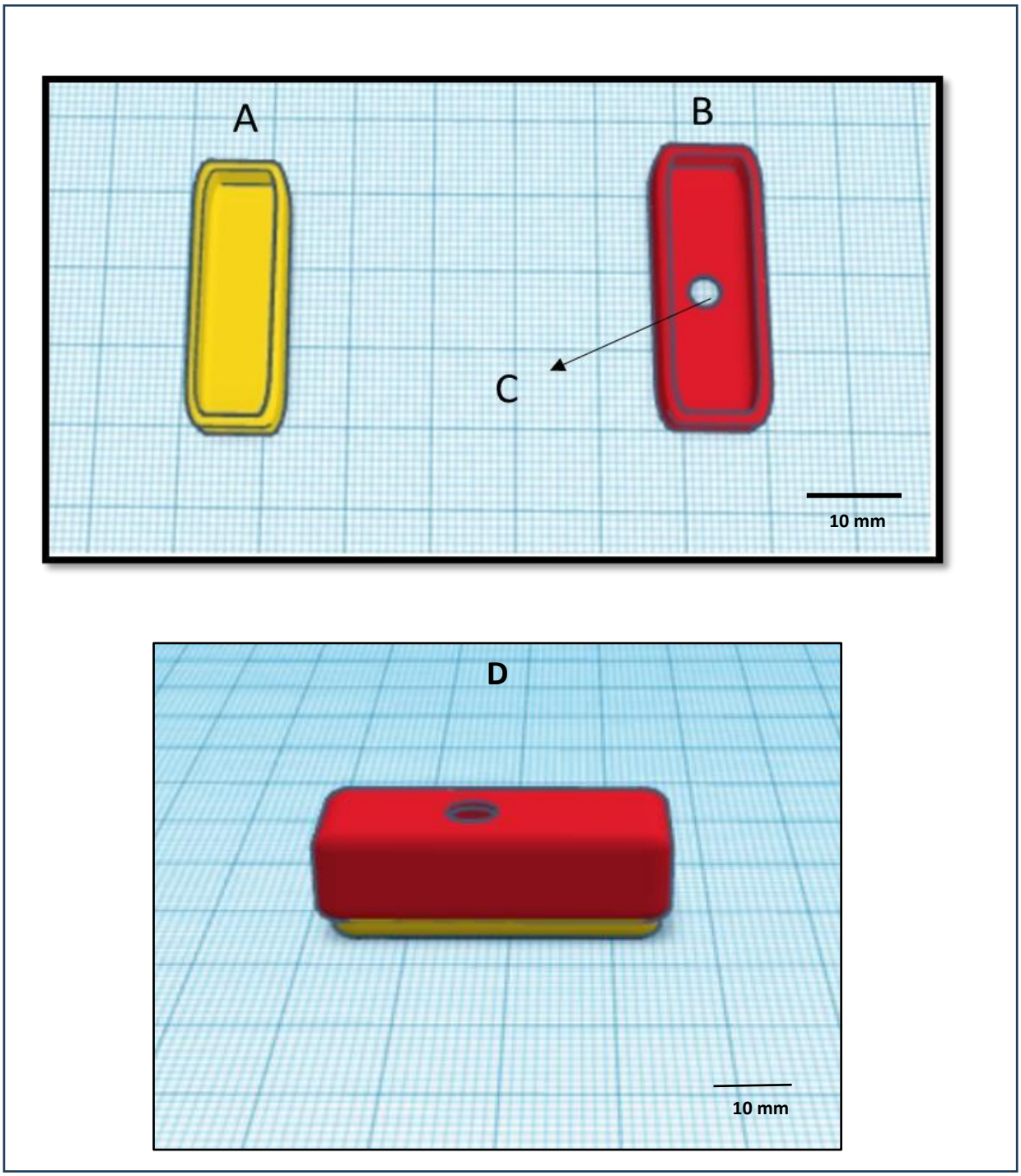

Figure 6.1: *The CAD software design of pancreatic device, (A) the bottom part, (B) the upper part (cover), (C) the external tube opening, (D) the device after assembly.*

Table 6.1: Different 3D printed formulations of the designed device

formulation	Bottom layer (membrane)			
	Membrane thickness (mm)	Infill %	Pore number	Pore size (mm)
F1	1	100	0	-
F2	1	75	0	-
F3	1	50	0	-
F4	1	75	0	-
F5	1.5	75	0	-
F6	2	75	0	-
F7	1	75	1	3
F8	1	75	2	3
F9	1	75	4	3
F10	1	75	2	2
F11	1	75	2	4

6.2.3. 3D printing of the optimised pancreatic device with different 3D parameters

The final optimised CAD design of the device was 3D printed utilising a pellet based FDM based 3D printer (Pollen, France). The 3D printer equipped with an extruder with head nozzle of 0.4 mm and a movable circular build plate of 30 cm diameter. The 3D printing processing parameters and printing conditions are presented in Table (6.2). The same extruder and environmental conditions were maintained constantly during the printing of each formulation. Printing time and dimension measurements were conducted to assess the reproducibility of the 3D printer. Verifying its ability to consistently reproduce objects with accurate dimensions within an acceptable timeframe can serve as quantitative indicators of the printer's performance.

Table 6.2: 3D printing process conditions of the pancreatic device.

Dosage form	Printer used	Feeding materials	Printing temperatures (°C)	Bed Temperature (°C)	Printing Speed (mm/s)	Layer Heights (mm)	Flow rate %
Pancreatic device	Pellets based FDM 3D printer	EVA (18.2%) Placebo pellets	145	50	45	0.15	35

6.2.4. Leaking test

During the initial design and 3D printing stages of the device, a leaking test was performed on each device. The test involved using a 10 ml syringe to infuse a volume of dH_2O that was approximately half of the total volume of the internal cavity of the printed device. Subsequently, the device was placed on tissue and observed for a minimum duration of four hours to detect any visible signs of leakage. This testing protocol aimed to assess the device's ability to retain the infused solution and identify any potential leakage issues.

6.2.5. *In vitro* drug release studies

The 3D printed pancreatic device was loaded with 2 mL solution containing IRN with a concentration of 10 mg/mL. Afterward, the device was hung in 50 mL of dH_2O pH (5.9) release media to guarantee that the release was only from one side (the lower membrane) and placed in an orbital shaking incubator, Unitron INFORS HT (Surrey, UK), at speed of 100 RPM and a temperature of 37˚C. 1 mL samples were withdrawn and replaced with fresh release medium at regular sampling intervals of 1, 3, 5, and 7 days. The collected samples were centrifuged and analysed by HPLC with drug release calculated as mean (n=3) ± SD using Equation (6.1).

$$Drug\ release\ (\%) = (Released\ drug)/\ (Total\ drug) \times 100 \qquad 6.1$$

6.2.6. IRN HPLC analysis

6.2.6.1. HPLC chromatographic condition

IRN was analysed using an Agilent HPLC 1260 infinity II. The mobile phase composed of a mixture of 0.02 M potassium di-hydrogen orthophosphate, pH 2.5, adjusted with ortho-phosphoric acid, methanol, and acetonitrile in a ratio of (75/25 v/v). The separation was performed by a Thermo - Scientific C18, 5µm, (150 × 4.6 mm) column at room temperature. The UV wavelength detector was set at 225 nm with a run time of 10 min. The injection volume was 10 µL with a flow rate of 0.8 mL/min. The retention time for IRN was around 5.82 minutes.

6.2.6.2. Preparation of stock solution and calibration standards

20 mg of IRN was dissolved in 100 mL of deionised water (dH_2O) to prepare a stock solution of final concentration 0.2 mg/mL. From this stock solution, 50 mL was transferred into 100 mL volumetric flask and diluted with mobile phase to volume to prepare a standard solution with final concentration of 100 µg/mL. Different calibration standards ranging from 10, 20, 40, 60, 80, and 100 µg/mL were prepared by appropriate dilution with the mobile phase.

6.2.7. Clinical assessment of the prototype 3D printed device

During the design and development process, each 3D printed device undergoes clinical evaluation. Two clinicians (a pancreatic surgeon and an oncologist) will evaluate the drug delivery device's dimensions, flexibility, and configuration to ascertain its compatibility for attachment to the pancreatic cancer margin before it undergoes assessment in the pig model.

6.2.8. Assessment of the final optimised device on the pig model.

Following the acceptance of clinical assessment, the final optimised device is subjected to fitting test on the pig model. The test aimed to investigate several factors, including the device's dimensions, shape, and overall suitability within the pig cadaver's anatomy. By performing a fitting test on a pig cadaver, which exhibits certain similarities to human anatomy, valuable insights can be obtained regarding the device's suitability and its capability to adapt to the specific anatomical requirements.

6.3. Results and discussions

6.3.1. Preliminary designs of the pancreatic device and the clinical requirements

Prior to commencing the digital design and 3D printing phases for the pancreatic device, several clinical prerequisites were established to ensure the device's viability as a medical pancreatic solution:

a. The device must be constructed from an elastic polymer to minimise potential harm or discomfort to surrounding tissues.

b. It is imperative that the device be manufactured from a nontoxic biocompatible polymer.

c. The device's dimensions and geometry are necessary to be compatible with the targeted site.

d. The device is required to be attached with a tube for external drug infusion.

e. An internal cavity within the device is essential for accommodating a medical sponge to facilitate controlled chemotherapy release.

f. Optimisation of the lower membrane, intended for attachment to the designated organ, involves adjustments in thickness, pore size, and infill percentage to achieve the desired drug release profile.

g. The final device design must be printable while maintaining consistent and uniform sizing throughout.

EVA was selected as the material for the pancreatic device based on several advantageous properties. Firstly, EVA exhibits biocompatibility, allowing for its safe interaction with biological systems. Secondly, it is water insoluble, ensuring the device's stability and integrity in the presence

of bodily fluids. Additionally, EVA possesses the capability to produce elastic dosage forms that maintain their softness and flexibility, enabling comfortable and secure implantation. Moreover, EVA has gained FDA approval for drug delivery applications due to its non-toxic nature (Genina et al., 2016; Henderson, 1993).

Table (6.3) showcases three unique pancreatic devices that were fabricated using 3D printing as part of the design optimisation process. Each device underwent a thorough evaluation, considering factors such as size, geometry, potential leaking issues, and overall suitability for surgical implantation in the desired anatomical organ.

The initial design, depicted in image (1) of Table (6.3), involved the 3D fabrication of a rectangular device with dimensions of 50 mm in length, 30 mm in width, and 10 mm in height. However, this design was discontinued due to two primary reasons. Firstly, the device's size was deemed unacceptable for the intended application as being larger than the intended location. Secondly, during the leaking test, fluid leakage was observed from the side walls of the device. The observed leakage from the side walls can be attributed to the presence of increased air pressure that became trapped inside the device prior to the initiation of the fluid infusion during the test. This elevated air pressure caused detachment between specific layers of the device's walls, thereby causing the leakage of the fluid.

The second design involved the manufacturing of a cylindrical-shaped device with dimensions of 30 mm for the diameter and 10 mm for the height, as depicted in image (2) Table (6.3). However, this design was also terminated due to the occurrence of solution leakage. In response, the design

was modified to incorporate two tubes of similar sizes. One tube was dedicated to solution input, while the other served as an outlet for air discharge. The size and shape of the device remained unchanged, as shown in image (3) of Table (6.3). This modification effectively resolved the issue of solution leakage. The device demonstrated its ability to retain the infused solution for approximately 8 hours without any observable leaks. Despite this success, the design was ultimately discontinued due to concerns regarding the device's inadequate suitability in terms of size and geometry. Image (4) of Tablet (6.3) demonstrates the final optimised device.

The final optimised device was achieved through two key modifications. Firstly, the size of the device was reduced to ensure a proper fit within the desired location. This reduction in size addressed concerns regarding the device's suitability and compatibility with the anatomical site following pancreatectomy. Secondly, a single tube with external diameter of 2 mm was incorporated within other tube with internal diameter of 3 mm. The inner tube served as the conduit for solution input, while the outer tube functioned as the outlet for air discharge as shown in Figure (6.2 D). By having the inner tube housed within the outer tube, the design effectively addressed the issue of air pressure buildup. The optimised device will be further discussed in the subsequent sections, which will cover its *in vitro* release characteristics, and the fitting test conducted on cadavers.

Table 6.3: Preliminary and final optimised designs of pancreatic device. Dimensions*(L) length, (W) width, (H) height (D): diameter.

No.	Image	Dimensions* (mm)	acceptance decision	Cause of termination
1	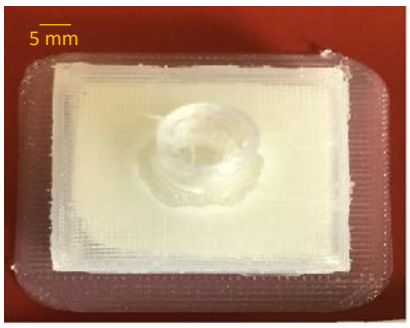	L: 50 W: 30 H: 10	X	Failed clinical assessment (the size and geometry were deemed unsuitable). Failed leaking test due to layer detachment along the side walls.
2	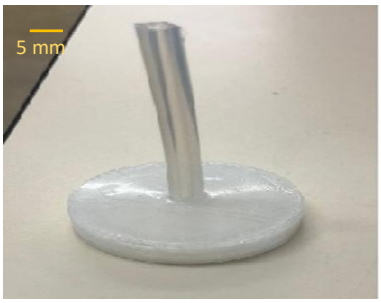	D: 30 H: 10	X	Failed the leaking test due to the air pressure, which resulted in damage to the layers of the device's walls.
3	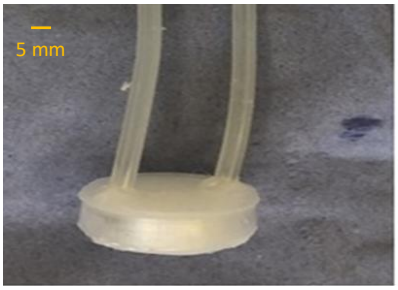	D: 30 H: 10	X	Failed clinical assessment due to (Improper size and the inclusion of two tubes was deemed impractical and not applicable for the device.
4	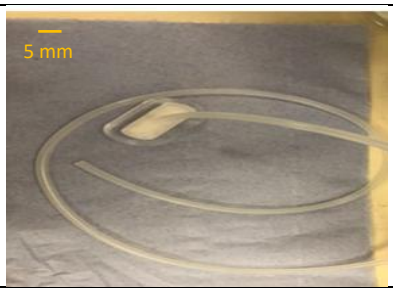	L: 35 W: 12 H: 10	✓	Passed clinical assessment, leaking test and fitting test.

6.3.2. 3D printed of the final optimised pancreatic device

The final optimised pancreatic device, depicted in Figure (6.2), was successfully manufactured using an FDM based 3D printer. The 3D printed device had outer dimensions of 35 mm in length, 12 mm in width, and 10 mm in height. However, due to the design requirement of subtracting the wall thicknesses of both layers and the top and bottom layer thicknesses, the resulting net area of the internal cavity will be reduced. The estimated dimensions of the internal cavity are 31 mm in length, 8 mm in width, and 8 mm in height.

The device underwent thorough investigation to evaluate its fluid leakage performance. The device exhibited excellent capabilities in retaining the infused solution without any detectable leaks for a duration of 8 hours. This achievement was made possible by employing a double tubing design (as described earlier), where a smaller tube was inserted into a larger one. This innovative configuration facilitated the discharge of air while ensuring a seamless infusion of fluid, as illustrated in Figure (6.2 D). A thin layer was intentionally fabricated to surround the device. This layer was designed to be free of drugs or active substances, with its main objective being to optimise adhesion to the build plate during the 3D fabrication process. The incorporation of this layer resulted in improved adhesion during fabrication, additionally it can serve as a means of fixing the device during surgical implantation by suturing it to the desired location.

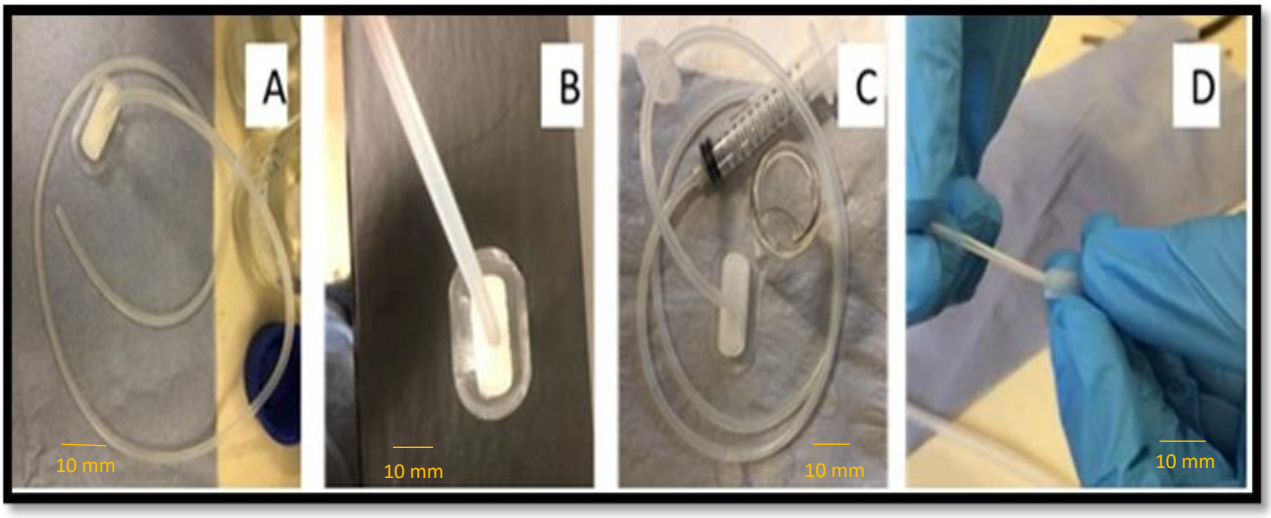

Figure 6.2: *The final optimised device. (A) attached with tube, (B) loaded with sponge, (C) Leaking test, (D) double tubes used for infusion and air discharge.*

6.3.3. IRN HPLC analysis

Figure (6.3) demonstrates the IRN standard calibration curve at six different concentrations ranging from 10 to 100 µg/mL. The correlation between the IRN concentrations and their corresponding area under the curve (AUC) indicates an excellent linear relationship, with a correlation coefficient (R^2) value of 0.9999. A linear regression analysis was performed on the IRN graph, resulting in the regression line equation y = 33.712X + 13.214. The data were analysed using regression analysis at a 0.05% confidence level, revealing that the difference between the estimated and found drug concentration was not statistically significant ($P > 0.05$). The sensitivity of the method was sufficient to detect and quantify drug concentrations of 0.1 µg/mL and 0.311 µg/mL as the limit of detection and limit of quantification, respectively. The method accuracy was determined by the recovery experiment and found to be 100.56 ± 1.42%. The results of the IRN HPLC analysis are summarised in Table (6.5).

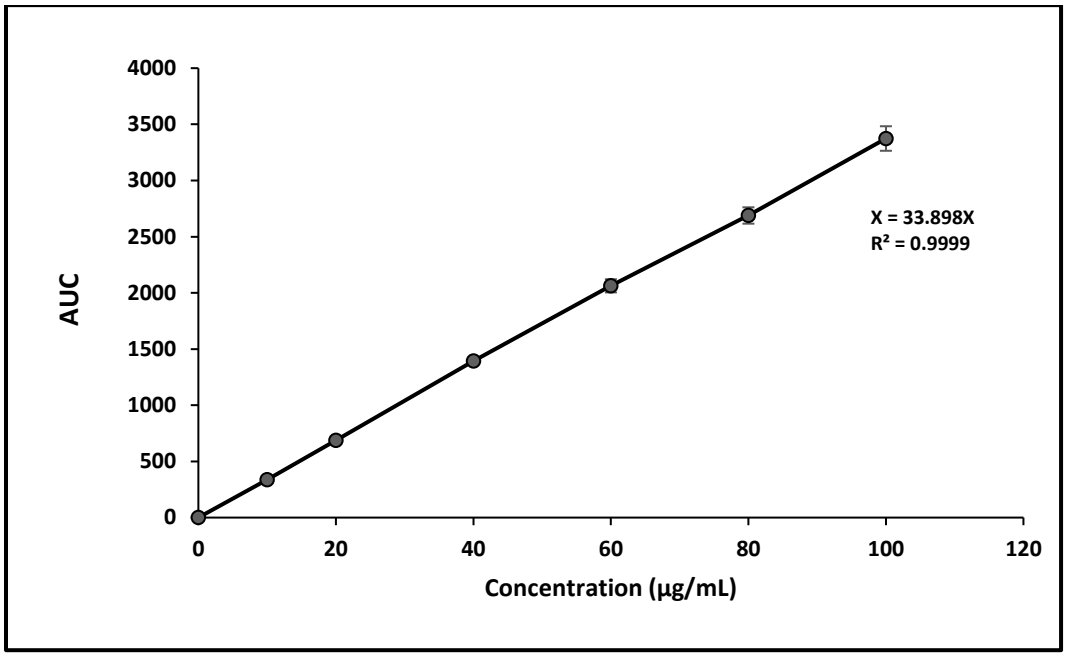

Figure 6.3: *Standard calibration curve of IRN. Results presented as mean (n=9) ± SD.*

Table 6.4: IRN HPLC method assay parameters.

No.	Assay validation	Results
1	Accuracy (%)	100.56 ± 1.42%
2	Slope	33.898
3	Intercept	0
4	Linearity range	10-100 µg/mL
5	Correlation coefficient (R^2)	0.9999
6	SE of intercept	0.43081
7	SD of intercept	1.055
8	Limit of detection (LOD)	0.1 µg/mL
9	Limit of quantification (LOQ)	0.311 µg/mL

6.3.4. Impact of different 3D printing parameters on the *in vitro* release profile of the device

The release of IRN from the 3D fabricated pancreatic device was conducted in dH_2O at a temperature of 37°C. The aim of the analysis was to examine the influence of four different factors on the *in vitro* release pattern. These factors included variations in infill percentage, membrane thickness, pore size, and pore number, which were applied specifically to the lower part (bottom layer) of the pancreatic device. The assumption was made that the lower part of the device plays a vital role in controlling the drug release mechanism due to its direct contact with the anatomical organ following surgical implantation. The evaluation involved analysing the percentage cumulative release and mass release (mg/mL) of IRN over time, are illustrated in Figures (6.4) and (6.5), respectively.

The IRN release patterns obtained from devices with different infill percentages revealed that the amount of drug released from the membrane with 50% infill was higher and faster compared to the 75% and 100% infill as depicted in Figure (6.4 B). This pattern was expected due to the lower infill percentage resulting in higher porosity and subsequently a larger surface area. The membrane with 50% infill displayed a biphasic release pattern. Initially, there was a fast "burst" release, where approximately 20% of the drug was released during the first few days. This was followed by a slow and sustained release over the remaining 5 days, with only an additional 5% of IRN being released. In contrast, the membranes with 75% and 100% infill exhibited slow and sustained release profiles. Over a 7-day period, the maximum release percentages were 18.25% for the 75% infill membrane and 15.22% for the 100% infill membrane.

Regarding the devices with membranes of different membrane thicknesses, the release pattern demonstrated a decrease in drug release as the thickness parameter increased. Specifically, the device with a 1 mm membrane thickness exhibited the highest maximum drug release of 22.31%. In comparison, the device with a 1.5 mm membrane thickness showed a maximum drug release of 18.47%, while the device with a 2 mm membrane thickness had a maximum drug release of 12.45%. These results are depicted in Figure (6.4 A).

The influence of the number of pores and the pore sizes on the device release behaviour are demonstrated in Figures (6.4 C) and (6.4 D), respectively. It was clearly demonstrated that as pore size or pore number rise, the amount of drug released increase due to the reduction in membrane's resistance to water diffusion. The device membrane manufactured with four pores exhibited the highest drug release percentage, reaching 44.56%. In comparison, membranes with one or two pores displayed lower drug release percentages of 25.33% and 33.01%, respectively. Similarly, the membrane with a pore size of 4 mm demonstrated the highest drug release percentage, reaching 48.56%. In contrast, devices with pore sizes of 2 mm and 4 mm exhibited lower drug release percentages of 28.33% and 32.22%, respectively.

The calculated *in vitro* mass release patterns presented in Figure (6.5) provided insights into the release pattern of IRN from the pancreatic device. The figure demonstrated that the various factors applied to the bottom layers of the device had an impact on the amount of IRN released, measured in mg/mL.

In relation to the devices with membranes of varying thicknesses, the release pattern indicated a decline in drug release as the thickness parameter increased. More specifically, the device with a 1 mm membrane thickness demonstrated the highest maximum drug release of 4.03 mg. On the other hand, the device with a 1.5 mm membrane thickness exhibited a maximum drug release of 3.69 mg, while the device with a 2 mm membrane thickness displayed a maximum drug release of 2.49 mg. These outcomes are illustrated in Figure (6.5 A).

In terms of device with membrane of different infill percentages, the membrane with 50% infill demonstrated a biphasic release pattern as displayed in Figure (6.5 B). Initially, there was a rapid "burst" release, where approximately 4.43 mg of the drug was released within the first few days. This was followed by a slow and sustained release over the remaining 5 days, with an additional 0.51 mg of IRN being released. In contrast, the membranes with 75% and 100% infill exhibited gradual and sustained release profiles. Over a 7-day period, the maximum release amounts were 3.65 mg for the 75% infill membrane and 4.87 mg for the 100% infill membrane.

The impact of the number of pores and the pore sizes on the release behaviour of the device is illustrated in Figures (6.5 C) and (6.5 D), respectively. It is evident that as the pore size or the number of pores increases, the amount of drug released also increases due to a reduction in the membrane's resistance to water diffusion. The device membrane with four pores demonstrated the highest amount of drug released, reaching 8.91 mg. In comparison, membranes with one and two pores exhibited lower amounts of drug released, measured at 5.06 mg and 6.61 mg, respectively. Similarly, the membrane with a pore size of 4 mm demonstrated the highest amount

of drug released, reaching 9.71 mg. On the other hand, devices with pore sizes of 2 mm and 3 mm exhibited lower amounts of drug released, measured at 5.66 mg and 6.44 mg, respectively.

The results visually demonstrated how various factors impact the release behaviour of IRN from the pancreatic device, emphasizing the significance of the bottom layers in controlling drug release. The observed variations in release patterns among different factors indicated that the composition and characteristics of the bottom layers influenced the rate and extent of IRN release. This suggests that by altering factors such as pore size, membrane thickness, and pore number in the bottom layers, it may be possible to customize the release behaviour of IRN to achieve specific therapeutic goals.

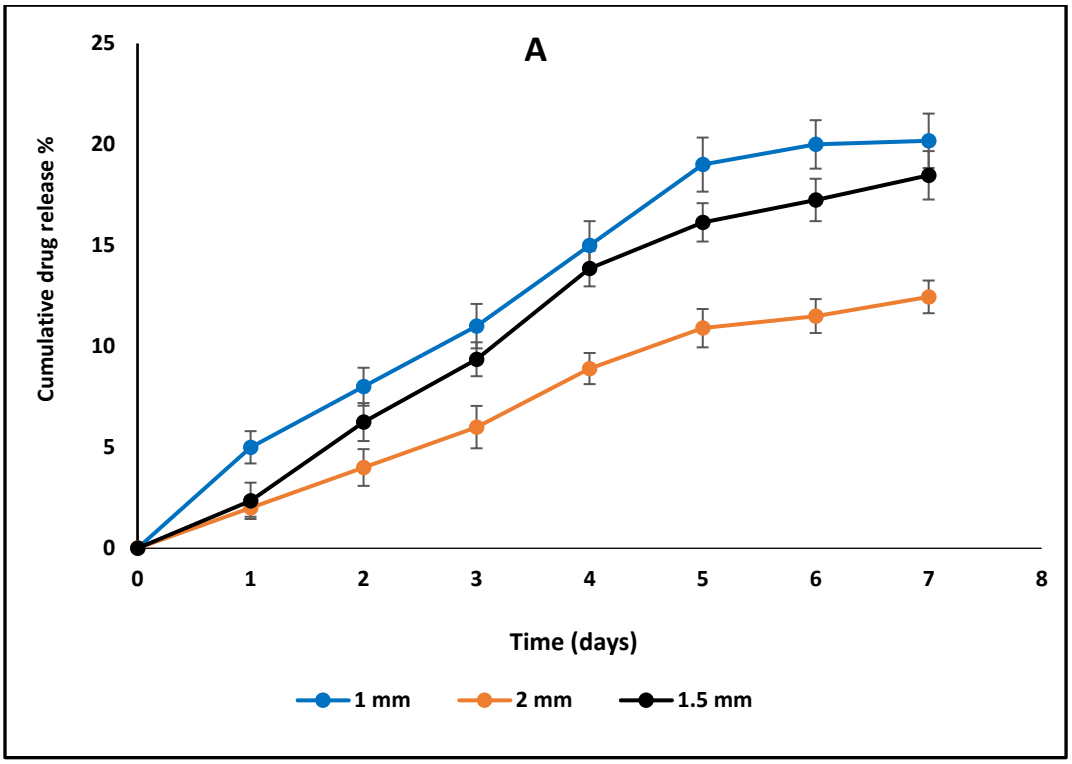
A
Cumulative drug release %
25
20
15
10
5
0
0
1
2
3
4
5
6
7
8
Time (days)
1 mm
2 mm
1.5 mm

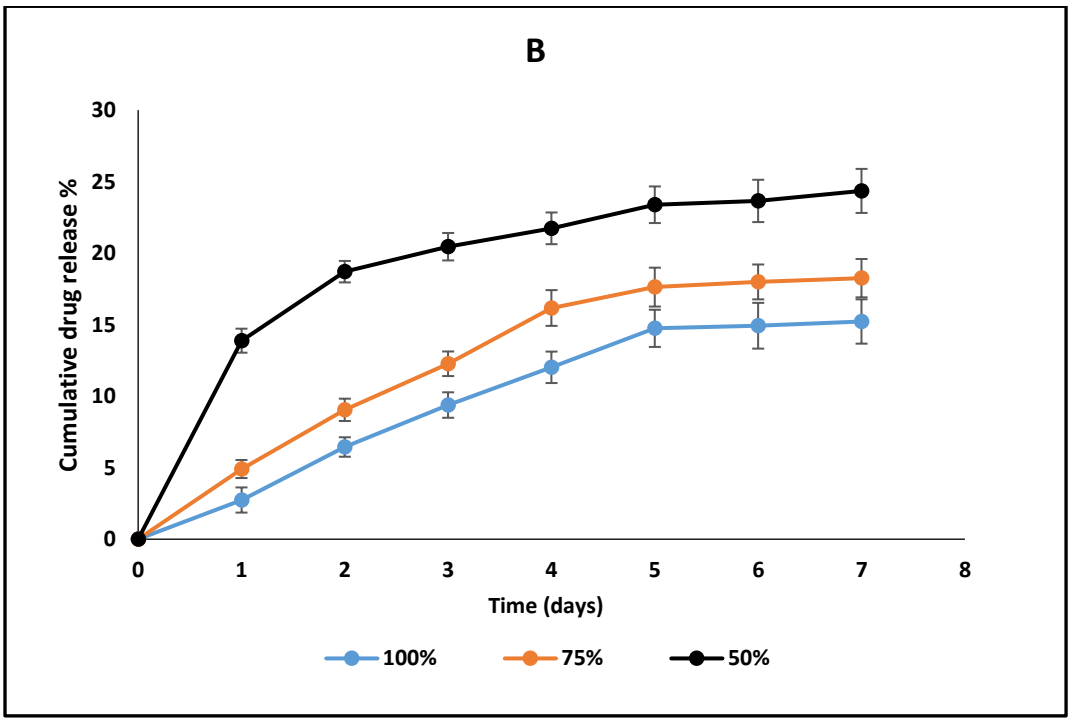
B
Cumulative drug release %
30
25
20
15
10
5
0
0
1
2
3
4
5
6
7
8
Time (days)
100%
75%
50%

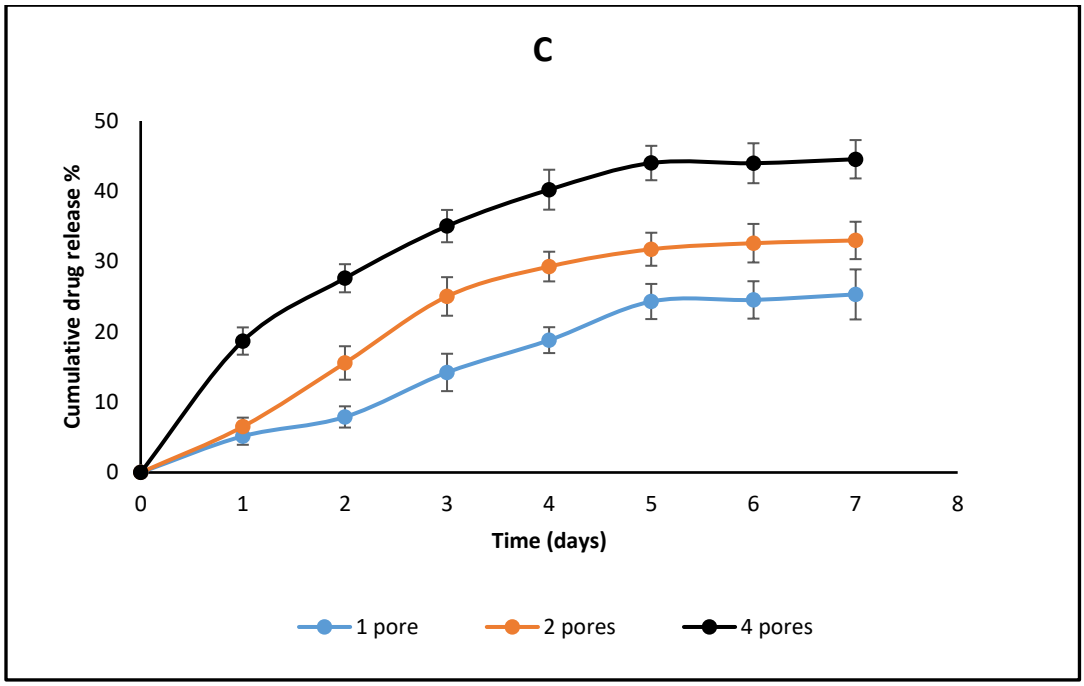

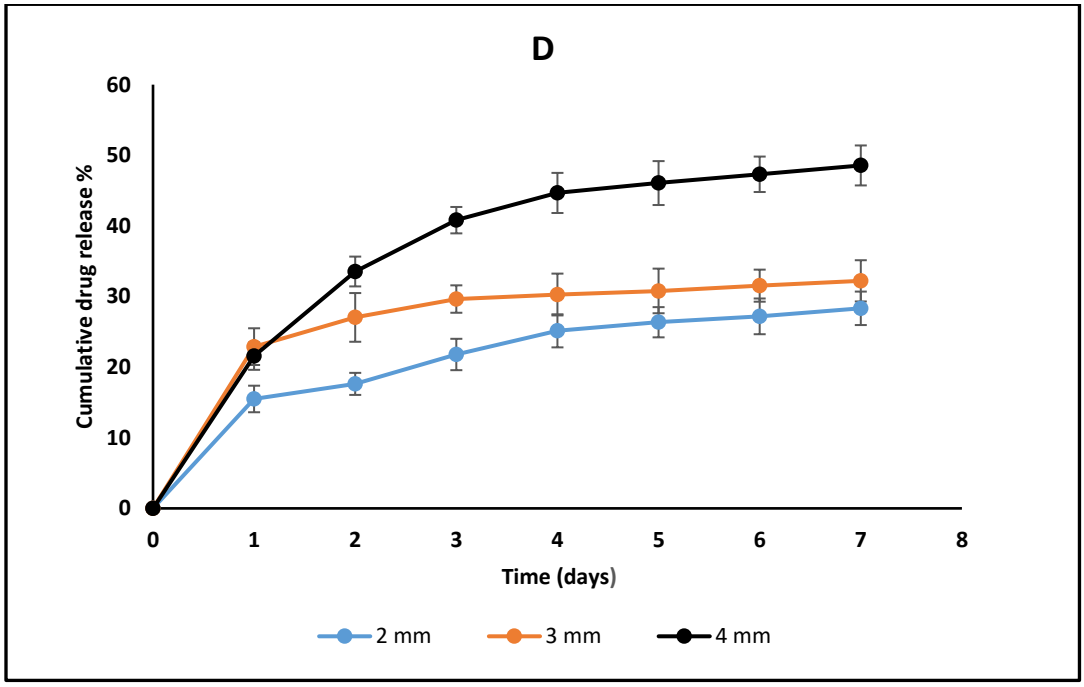

Figure 6.4: *Influence of different 3D printing parameters on the in vitro drug release of pancreatic device (A) different membrane thicknesses, (B) different infill %, (C) different pore number and (D): different pore sizes. Results presented as mean (n=3) ± SD.*

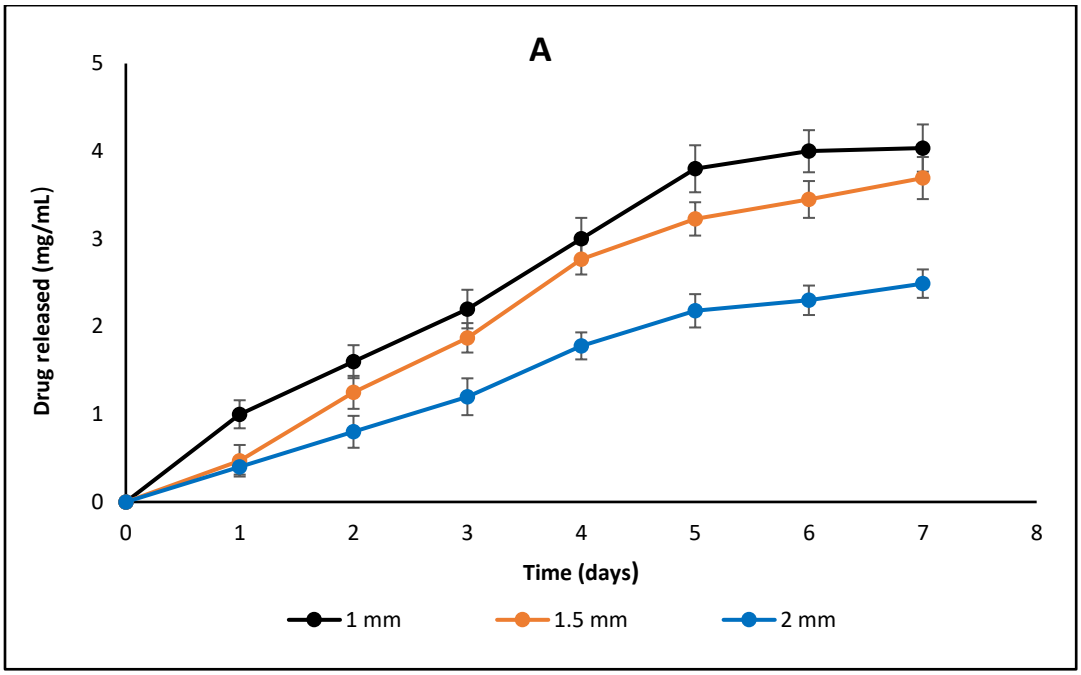
A
Drug released (mg/mL)
0
1
2
3
4
5
0
1
2
3
4
5
6
7
8
Time (days)
1 mm
1.5 mm
2 mm

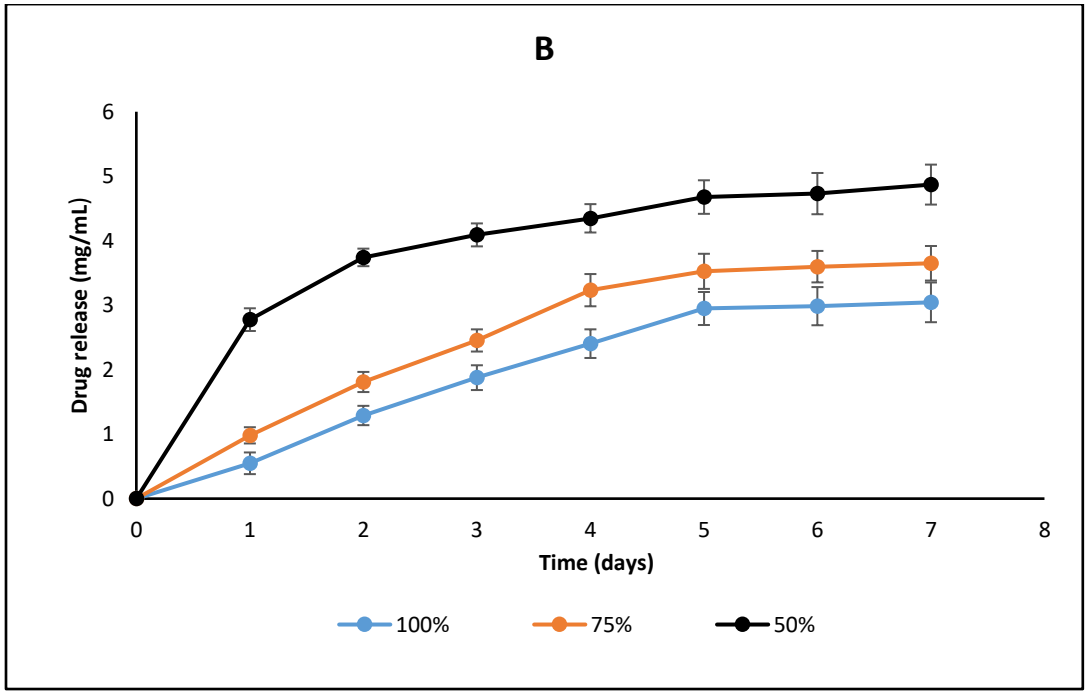
B
Drug release (mg/mL)
0
1
2
3
4
5
6
0
1
2
3
4
5
6
7
8
Time (days)
100%
75%
50%

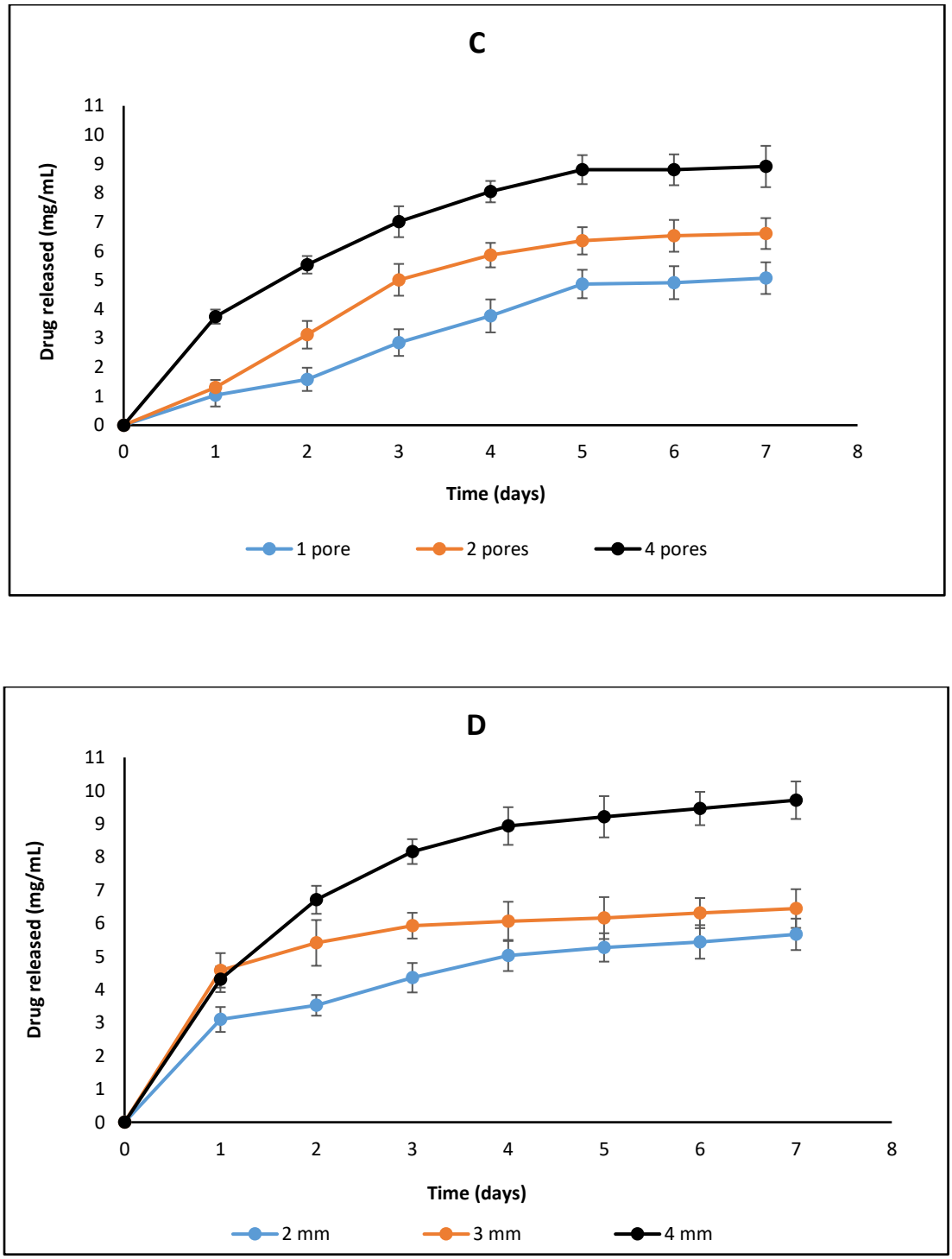

Figure 6.5: *Influence of different 3D printing parameters on the in vitro mass drug released (mg/mL) from pancreatic device; (A) different membrane thicknesses, (B) different infill percentages, (C) different pore number, (D) different pore sizes. Results shown as mean (n=3) ± SD.*

6.3.5. Device fitting to cadaver

Figure (6.6) demonstrates the fitting test of the final optimised pancreatic device on a pig cadaver body involved assessing the device's compatibility in terms of size and geometry for placement within the desired anatomical position. As shown in Figure (6.6 B), the fitting test conducted on the pancreatic device exhibited favourable outcomes, demonstrating that the device achieved a proper fit within the desired anatomical location. The results suggest that the device's dimensions and overall design were well-suited to the anatomical characteristics of the area being targeted. Moreover, it highlights the versatility and adaptability of 3D printing technology, which can be utilised to develop tailored drug delivery devices that accurately fit the specific anatomical needs of patients.

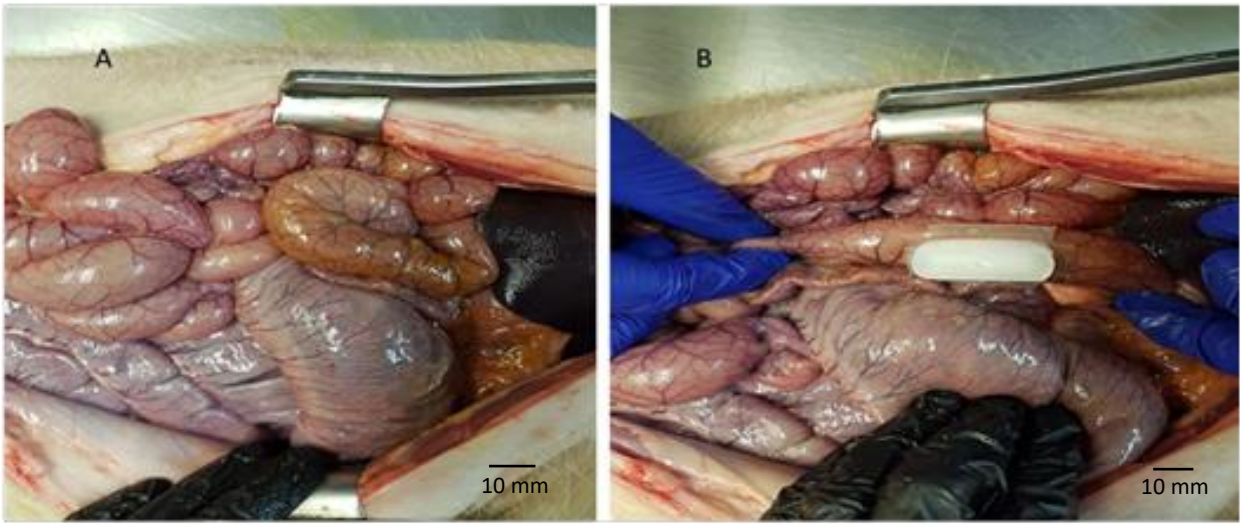

Figure 6.6*: Cadaver fitting test of the optimised pancreatic device. (A) pre-implantation, (B): post-implantation.*

6.4. Discussion

In this chapter, a novel drug delivery device was fabricated using FDM based 3D printing technology, aiming to enable localised chemotherapeutic drug delivery for the treatment of pancreatic cancer. The device was specifically manufactured from EVA, an FDA-approved polymer known for its suitability in drug delivery applications. The selection of EVA was based on its desirable properties, such as biocompatibility, flexibility, and water insolubility. These characteristics make EVA an ideal choice for the development of the drug delivery device, ensuring its compatibility with biological systems while maintaining the integrity and controlled release of the chemotherapeutic agents.(Moroni et al., 2023). During the development and optimisation of the pancreatic device, several challenges were encountered, which will be discussed below:

- *Challenges related to the 3D printing of an over hanged object*

During the 3D printing process, FDM-based 3D printers typically construct physical objects by layering thin layers on top of each other. However, printing objects with internal holes or angles greater than 45˚ can lead to a phenomenon known as "mid-air 3D printing," making the printing process impossible without the addition of support structures. In the case of the desired pancreatic device, which required an internal cavity to be filled with medical sponge and therapeutic solution, the presence of support structures would complicate the removal process and potentially affect the quality of the 3D printed device.

To address this issue, a solution was devised by dividing the device into two separate parts: the upper part, consisting of the device cover and walls, and the lower part (bottom layer), comprising the membrane and its wall. Each part was 3D printed separately, eliminating the need for mid-air printing and the incorporation of support structures. This approach ensured a more efficient printing process and preserved the quality and integrity of the final 3D printed device.

Internal pressure and fluid leak

During the post-printing leaking test, it was observed that the infused solution was leaking from the device, particularly during syringe infusion. This leakage was attributed to air pressure causing damage to the device's walls. To address this issue, a modification was made to the infusion system. Instead of using a single Silicone tube for solution infusion into the device cavity, an additional smaller Silicone tube with an external diameter of 2 mm was inserted into the main tube, which had an internal diameter of 3 mm. This smaller tube was specifically utilised for drug infusion. The slight size difference between the external diameter of the small tube and the internal diameter of the main tube (estimated to be 1 mm) allowed air to be discharged from the device in the opposite direction of the fluid during the infusion process. This technique proved successful in preventing fluid leakage during the infusion process, ensuring a more reliable and efficient drug delivery mechanism for the device.

Ensuring the stability of the device after implantation.

Dislocation of the device after implantation poses a significant concern, as it can impact the safety and effectiveness of the implant. To mitigate the risk of device mobility following surgery, a precautionary measure was taken by incorporating an additional layer around the bottom layer of the device, measuring approximately 5 mm in width. This thin layer enables the surgeon to suture it at the desired location, thereby enhancing device stability without compromising the integrity of the device membrane. Furthermore, to provide supplementary support and minimise movement of the Silicone tubes within the body, two small EVA rings attached to the tubes were 3D printed. These rings are strategically positioned and sutured in suitable locations to offer extra support to the Silicone tubes. This additional support contributes to reducing the potential movement of the tubes inside the body and further enhances the overall stability of the device. By implementing these measures, the risk of device dislocation following implantation can be minimised, ensuring the device remains securely in place throughout its intended use, thereby maximising the safety and efficacy.

The 3D fabricated device underwent optimisation primarily focusing on its size and shape to develop the most suitable device that can effectively fit the targeted organ, particularly after pancreatectomy surgery. The device consists of two main parts: the upper part, referred to as the cover, and the lower part, known as the device membrane. The membrane is the part of the device that is intended to be attached to the tumour site. Therefore, an investigation was conducted to assess the influence of various 3D printing parameters on the *in vitro* drug release from the device.

The device, fabricated with varying membrane thicknesses, demonstrated a decrease in the *in vitro* drug release as the membrane thickness increased. This aligns with the anticipated outcome due to the expected increase in membrane resistance, which impedes drug dissolution. The influence of wall thickness on drug release has been previously documented in the scientific literature (Liu et al., 2000). Regarding the impact of infill percentage on drug release, the study revealed an inverse relationship between the infill percentage of the membrane and the quantity of drug released. Consequently, the device with a 50% infill exhibited higher drug release. These findings are consistent with the results presented in Chapter 2 of this thesis. The higher drug release observed with lower infill percentages can be attributed to the resulting greater porosity, leading to an increased surface area available for drug diffusion. Furthermore, the investigation demonstrated that the amount of drug released was directly proportional to both the size and number of pores in the membrane. This indicates that larger pore sizes and a higher pore count contribute to enhanced drug release.

The results indicated that varying the 3D printing parameters can alter the release pattern of drugs. This finding highlights an additional benefit of utilising 3D printing for the production of complex, customised drug delivery devices.

6.5. Conclusion and future work

A novel drug delivery device, intended for localised treatment of pancreatic cancer, was manufactured utilising FDM based 3D printer technology. The device was fabricated using elastic polymer, EVA with a vinyl acetate content of 18.2%. Throughout the development and optimisation process, a range of shapes and sizes were 3D fabricated and evaluated to determine their suitability for fitting into the targeted tumour location. Additionally, a leakage test was conducted to ensure the integrity of the manufactured device. Among the different pancreatic device designs, a cuboid-shaped device, measuring 35 mm in length, 10 mm in width, and 10 mm in height, was selected for further investigation. Specifically, the influence of various 3D printing parameters on the *in vitro* drug release was examined. These parameters included membrane thicknesses of 1 mm, 1.5 mm, and 2 mm, infill percentages of 50%, 75%, and 100%, pore numbers of 1, 2, and 4, and pore sizes of 2 mm, 3 mm, and 4 mm. Results exhibited that the different parameters showed a remarkable influence on the release behaviour. Specifically, the drug release from the device was increased as the values of infill % membrane thickness increased. On the other hand, the release was directly proportional to the number and size of pores. Therefore, the amount of the drug release could be customised according to these parameters. Based on the results obtained, we propose that this 3D printed device represents a novel and promising drug delivery system for localised post-surgical treatment of pancreatic cancer. Future work requires *in vivo* test to evaluate the device bioavailability, potential toxicity and wound healing assessment.

Chapter 7 : THESIS CONCLUSION AND FUTURE OUTLOOK

7.1. Thesis conclusion

The 3D printing technology is a rapid and promising technique that facilitates the fabrication of 3D objects through the sequential deposition or fusion of multiple layers in a predetermined and controlled manner (Anadioti et al., 2018). In recent times, the prevalence of diverse and challenging diseases has sparked a surge in the pursuit of groundbreaking research in the biomedical and pharmaceutical fields. Among these advancements, 3D Printing technology has emerged as a highly transformative, promising, and progressive technique within the biomedical and pharmaceutical domains (Jiang et al., 2020).

This project highlights the potential of FDM based 3D printing for the production of solid pharmaceutical dosage forms. The primary focus has been on exploring the viability of utilising FDM based 3D printing for manufacturing various types of solid dosage forms, such as tablets, single and multilayer structures, implants, and drug delivery devices. Furthermore, the project has examined the impact of different 3D printing parameters on the characteristics of the produced solid dosage forms, as well as their influence on the *in vitro* release behaviour. In this project, HME technology served as the primary method for incorporating the API into the polymers employed in the fabrication of solid pharmaceutical dosage forms.

In the first experiment of chapter two, the influence of different 3D printing parameters on the physical characteristics of placebo tablets were examined. Commercial PLA polymer and filament

based 3D printer were utilised to manufacture the placebo tablet. The investigated parameters included infill percentage, infill pattern, printing speed, and layer height. The results indicated that among these parameters, infill percentage exerted the most noticeable influence on the weight and density of the fabricated placebo tablets. Specifically, an increase in infill percentage led to higher tablet weight and density. However, the infill percentage had a negligible impact on the tablet dimensions (diameter and cylinder height). The other investigated 3D printing parameters, such as infill patterns, layer height, and printing speed, showed insignificant impact on the weight, density, and dimensions of the fabricated dosage form.

The second experiment conducted in chapter two aimed to investigate the impact of various 3D printing parameters, namely infill percentage, infill pattern, and layer height, on the *in vitro* drug release of 3D printed tablets loaded with a consistent concentration of caffeine. The tablets were fabricated using two different polymers, specifically PVA, as a water soluble polymer and PLA as a water insoluble polymer. The findings indicated that the infill percentage of 25%, a layer height of 0.1 mm, and a Zigzag infill pattern exhibited the highest drug release profile. Conversely, tablets with an infill percentage of 100%, a layer height of 0.3 mm, and a line infill pattern demonstrated the lowest drug release profile.

The third experiment in chapter two aimed to assess the effectiveness of 3D printing in manufacturing two types of coating shells and their impact on drug release. The first type, made of PLA, had 4 pores of varying sizes (1, 1.5 and 2 mm), while the second type, made of PVA, had different wall thicknesses (1, 1.5 and 2 mm) but no pores. The release behaviour of these coated

tablets was compared to uncoated tablets (control). The results indicated that for the PLA coated tablets, the amount of drug released was directly proportional to the pore size, with the 2 mm pore size showing the highest and fastest release. In contrast, for the PVA coated tablets, the amount of drug released decreased with thicker wall thickness, with the 2 mm wall thickness resulting in the lowest release. This experiment demonstrates the potential of 3D-printed coating shells to modify drug release behaviour based on different geometries, highlighting their viability for controlled release applications.

The third chapter of this thesis focused on exploring the use of FDM based 3D printing to create a two-compartment oral dosage form using FDA approved polymers. Specifically, tablets containing Isoniazid and Pyridoxine HCL were manufactured through 3D printing to serve as a combination therapy for latent TB infection. Two different tablet designs were studied: a single-layer tablet and a bilayer tablet. The impact of these designs on the *in vitro* release profile was investigated. The results showed that both types of tablets exhibited significant drug release, with approximately 70% of the drug released within the first 6 hours. Notably, the bilayer tablet demonstrated a faster drug release compared to the single-layer tablet, which can be attributed to its larger surface area. The study demonstrated the potential of FDM based 3D printing for manufacturing multidrug pharmaceutical dosage forms, offering opportunities to enhance the management of chronic diseases like TB by improving treatment compliance and reducing the risk of toxicity.

The fourth chapter of the thesis focused on utilising FDM based 3D printing to create an implant for localised treatment of brain tumours. The implant consisted of two layers: a flexible, drug-free

base layer made of EVA 18.2%, and a second layer made of PLGA loaded with the chemotherapeutic agent Irinotecan. This complex design, made possible by 3D printing, would offers advantages over existing proved implants like Gliadel. For example, the smaller size and adjustable drug strength through varying the number of drug-loaded protrusions. Furthermore, the elasticity of the base polymer reduced stress on surrounding tissues, minimising damage, and aiding in the healing process. The *In vitro* drug release of the 3D fabricated implant demonstrated a sustained release of the drug over 20 days. This FDM based 3D printed implant shows promise for manufacturing localised treatment of brain tumours, offering customisable design features.

The last chapter of this thesis investigated the viability of FDM 3D printing to fabricate a novel drug delivery device aimed to provide a postsurgical localised treatment of pancreatic cancer. The device was 3D fabricated from an elastic biocompatible polymer EVA 18.2%. Among different pancreatic device designs, a cuboid-shaped device, measuring 35 mm in length, 10 mm in width, and 10 mm in height, was selected for further investigation regarding the influence of different 3D printing parameters on the *in vitro* release. Parameters included membrane thickness, infill percentage, pore number, and pore size. The results showed that increasing infill percentage and membrane thickness led to higher drug release. On the other hand, more pores and larger pore sizes resulted in increased drug release. These findings suggest that the device can be customised to control the amount of drug released by adjusting these parameters. Overall, the study proposes that this 3D printed device holds promise as an innovative drug delivery system for localised post-surgical treatment of pancreatic cancer.

Overall, this project showcased the potential of FDM based 3D printing in combination with HME technology for manufacturing solid pharmaceutical dosage forms with complex geometries. Moreover, it provided valuable insights into the influence of various 3D printing parameters on the characteristics of the printed dosage forms, contributing to the advancement of personalised medicine and innovative drug delivery systems.

7.2. Future outlook

In recent years, there has been a notable surge in attention towards the utilisation of 3D printing technology in pharmaceutical and biomedical research. This is evident from the substantial number of global scholarly publications and patents, which exceeded 6,400 research articles and 31 patents in 2020, focusing on the healthcare applications of 3D printing (Huanbutta et al., 2023). However, the widespread implementation of 3D printing in pharmaceutical applications faces several challenges that must be addressed for its successful adoption. The development of 3D printed medications necessitates expertise not only from mechanical engineering and pharmacy researchers but also from professionals in materials science, software engineering, and information engineering. Additionally, the development process must adhere to stringent legal regulations within the pharmaceutical industry, further amplifying the overall complexity involved. Here some examples of the challenges facing the 3D printing industry that need to be addressed:

7.2.1. Overcoming obstacles related to material and machinery processing

FDM-based 3D printing in pharmaceutical applications encounters significant challenges pertaining to both materials and machinery. Material considerations include properties like biocompatibility, thermal stability, and rheological and mechanical properties. The filament feeder, a critical component, can cause damage to stiff filaments, while soft filaments may buckle due to insufficient column strength. Developing filaments with a balance between pliability, hardness, and stiffness is crucial to ensure successful printing without excessive damage (Go et al., 2017). One of the challenges in 3D printing machinery is the optimisation of processing parameters, particularly the printing temperature. Finding the appropriate temperature is difficult as it needs to be high enough to achieve the desired melt viscosity for effective material deposition. However, excessively high temperatures can lead to degradation of drugs and polymers, compromising the quality and integrity of the printed structures. Striking a balance is crucial to ensure both proper material flow and preservation of the desired properties of the printed pharmaceutical products (J. Aho et al., 2019).

As a future outlook, a promising direction is to move away from the time-consuming, costly, and wasteful "trial and error" approach in material selection and printability for 3D printing. Instead, the establishment of predictive models can provide valuable guidance for these processes. By leveraging advanced computational techniques, such as machine learning and data analysis, these models can analyse and predict the behaviour of different materials and their corresponding processing parameters during the printing process. This would enable more efficient and informed decision-making, reducing the need for extensive experimentation and optimising the selection of suitable materials.

For instance, significant advancements have been made in the field of *in silico* computational methods, which allow for the prediction of extrusion and printing temperatures, filament mechanical properties, printability, and drug release of 3D printed tablets and orodispersible films (ODFs). These advancements were achieved by incorporating input data from both in-house measurements and extensive data mining of published literature. The predictive models were established by considering various factors such as filament composition, physical characteristics, equipment specifications, and tablet design, resulting in a high level of accuracy. The open-access software called M3DISEEN offers a valuable tool for preliminary trials, enabling the screening of a wide range of formulations to assess their suitability for 3D printing (Abdalla et al., 2023; Castro et al., 2021; Ong et al., 2022).

7.2.2. Overcoming obstacles related to large scale manufacturing

While 3D printing offers numerous advantages, such as customisation, complex geometries, and rapid prototyping, it is still primarily employed for small-scale production or niche applications. Several factors contribute to the limitations of 3D printing for large-scale production. One of the main challenges is the speed of the printing process. 3D printing is generally slower compared to traditional manufacturing methods, especially when producing a large number of identical parts. The layer by layer nature of 3D printing, where each layer needs to be printed individually, adds to the time required for production (Attaran, 2017; Ngo et al., 2018).

Despite these limitations, researchers and industry professionals are continuously working on advancements in 3D printing technology to address these challenges. For example, Moldenhauer et al. introduced a screen 3D printing technology that utilises a unique process of printing paste onto a substrate through specific openings on a printing screen. This approach differs from traditional 3D printing methods, where a limited number of print heads construct one tablet unit at a time. In contrast, screen 3D printing enables the simultaneous construction of thousands of units using a single screen. This advancement in printing technology allows for increased production efficiency and the ability to fabricate multiple units in parallel, offering new possibilities for large scale manufacturing in the field of 3D printing (Moldenhauer et al., 2021).

In terms of production size, Triastek has reported that using a nozzle array design and MED methodology, has the capability of a daily output of 150 – 200,000 tablets per day (Timothy Tracy et al., 2023). Additionally, Laxxon Medical has reported that the utilisation of Screen Printing Innovative Drug (SPID®) technology has a production capacity of up to 1,500,000 units per day (S., 2023). These advancements highlight the increasing viability of 3D printing in pharmaceutical manufacturing, as it offers competitive production rates and cost efficiencies when compared to conventional tableting methods.

7.2.3. Overcoming obstacles related to policies and regulations

As previously discussed in this thesis, the regulatory landscape for 3D printed pharmaceuticals is still evolving, and clear guidelines and standards are needed to ensure product safety, efficacy, and quality. There is a need for comprehensive regulations that address aspects such as material

selection, printing processes, validation methods, quality assurance, and post-processing considerations. Given the significant importance of digital processing in advanced fabrication, it is imperative that regulations expand their scope to include the CAD process and the interconnected software system chain (Bicudo et al., 2021; Hourd et al., 2015).

Key regulatory concerns for 3D printed drug delivery platforms encompass factors like biodegradability, biocompatibility, drug degradation, and potential toxic reactions. Challenges in formulating regulatory guidelines for 3D printing involve deciding whether the guidelines should cover materials, technology, fabrication processes, and post-printing procedures. Additionally, determining how to regulate 3D printing of biological products, choosing between New Drug Applications and Abbreviated New Drug Applications for approval, and establishing standardised regulatory pathways for personalised or individual-based 3D printed products are also significant considerations (D. Muhindo et al., 2023).

In terms of regulatory of 3D printing of personalised medicine (PM), there is no current policies or guidelines exist that specifically outline the role of and provide a framework for the use of 3D printing techniques in the manufacturing of PM. However, pharmacists can refer to available frameworks that provide guidance on performing on-site extemporaneous production of medicines. These frameworks can serve as references when exploring the application of 3D printing methods for this purpose. In all international compounding frameworks, there were specific criteria established that exempted compounded formulations from needing approval from the relevant pharmaceutical or regulatory agency in that particular country (Englezos et al., 2023).

Additionally, in emergency or exceptional-use situations, an exemption from the standard approval process for personalised implants can be granted as long as specific safety criteria are fulfilled (Food & Administration, 2014).

The FDA released guidelines in 2017 that provide technical considerations for additive manufactured devices. These guidelines concentrate on various aspects such as design, materials, software processing, printing process parameters, postprocessing parameters, and process validation for 3D printed medical products. They also outline important quality concerns for the printed items, including their description, mechanical properties, dimensions, material chemistry, and biocompatibility (Rahman et al., 2018). Although this guidance did not cover the 3D printed pharmaceutical products, it is anticipated that future guidance for 3D printed pharmaceuticals may include more stringent regulations compared to traditional medical devices. Unlike conventional products, where the FDA's focus is primarily on the final drug product during approval, regulations for 3D printed pharmaceuticals are expected to encompass in-process control. This means that the regulations would cover the manufacturing process itself, ensuring quality and control measures are implemented at various stages of production.

Recently the FDA has established the Emerging Technology Team (ETT), a multidisciplinary group comprising representatives from various quality assessment and inspection programs within the agency. The framework and objectives established by the Emerging Technology Team (ETT) can offer significant advantages to sponsors engaged in the development of emerging technologies like 3D printing. These resources can assist sponsors in navigating the complex regulatory

landscape and provide valuable insights to the agency during the evaluation of novel products manufactured through 3D printing. The ETT's guidance and support can facilitate a smoother regulatory process, enabling sponsors to effectively meet the necessary requirements and ensure the safety and efficacy of their 3D printed products. It also allows the agency to stay informed about the latest advancements in technology and make informed decisions regarding the regulatory oversight of these innovative pharmaceutical applications (T. Tracy et al., 2023).

Various standard development organisations, such as ASTM and ISO, are currently working on creating specific standards for additive manufacturing in the medical device industry. With continuous advancements in these standards and the establishment of regulatory frameworks, the full potential of AM can be effectively harnessed.

References

Abdalla, Y., Elbadawi, M., Ji, M. X., Alkahtani, M., Awad, A., Orlu, M., Gaisford, S., & Basit, A. W. (2023). Machine learning using multi-modal data predicts the production of selective laser sintered 3D printed drug products. *International Journal of Pharmaceutics*, *633*, Article 122628. https://doi.org/10.1016/j.ijpharm.2023.122628

Acosta-Vélez, G. F., & Wu, B. (2016). 3D pharming: direct printing of personalized pharmaceutical tablets. *Polym. Sci*, *2*(1), 11.

Acumen Research and Consulting. (2023). *3D Printing in Medical Applications Market Size Growing at 16.6% CAGR Set to Reach USD 11 Billion By 2032*. GlobeNewswire.com. Retrieved 29 March 2023 from https://www.globenewswire.com/news-release/2023/03/27/2634981/0/en/3D-Printing-in-Medical-Applications-Market-Size-Growing-at-16-6-CAGR-Set-to-Reach-USD-11-Billion-By-2032.html

Aho, J., Botker, J. P., Genina, N., Edinger, M., Arnfast, L., & Rantanen, J. (2019). Roadmap to 3D-Printed Oral Pharmaceutical Dosage Forms: Feedstock Filament Properties and Characterization for Fused Deposition Modeling. *Journal of Pharmaceutical Sciences*, *108*(1), 26-35. https://doi.org/10.1016/j.xphs.2018.11.012

Aho, J., Bøtker, J. P., Genina, N., Edinger, M., Arnfast, L., & Rantanen, J. (2019). Roadmap to 3D-printed oral pharmaceutical dosage forms: feedstock filament properties and characterization for fused deposition modeling. *Journal of Pharmaceutical Sciences*, *108*(1), 26-35.

Ai, J.-W., Ruan, Q.-L., Liu, Q.-H., & Zhang, W.-H. (2016). Updates on the risk factors for latent tuberculosis reactivation and their managements. *Emerging microbes & infections*, *5*(1), 1-8.

Al-Hashimi, N., Begg, N., Alany, R. G., Hassanin, H., & Elshaer, A. (2018). Oral modified release multiple-unit particulate systems: compressed pellets, microparticles and nanoparticles. *Pharmaceutics*, *10*(4), 176.

Al Rashid, A., & Koç, M. (2022). Experimental validation of numerical model for thermomechanical performance of material extrusion additive manufacturing process: effect of process parameters. *Polymers*, *14*(17), 3482.

Alexander, A. E., Wake, N., Chepelev, L., Brantner, P., Ryan, J., & Wang, K. C. (2021). A guideline for 3D printing terminology in biomedical research utilizing ISO/ASTM standards. *3D Printing in Medicine*, *7*, 1-6.

Algahtani, M. S., Mohammed, A. A., Ahmad, J., Abdullah, M., & Saleh, E. (2021). 3D printing of dapagliflozin containing self-nanoemulsifying tablets: formulation design and in vitro characterization. *Pharmaceutics*, *13*(7), 993.

Algahtani, M. S., Mohammed, A. A., Ahmad, J., & Saleh, E. (2020). Development of a 3D printed coating shell to control the drug release of encapsulated immediate-release tablets. *Polymers*, *12*(6), 1395.

Algorri, M., Abernathy, M. J., Cauchon, N. S., Christian, T. R., Lamm, C. F., & Moore, C. M. (2022). Re-Envisioning Pharmaceutical Manufacturing: Increasing Agility for Global Patient Access. *Journal of Pharmaceutical Sciences*, *111*(3), 593-607.

Alhijjaj, M., Belton, P., & Qi, S. (2016). An investigation into the use of polymer blends to improve the printability of and regulate drug release from pharmaceutical solid dispersions prepared via fused deposition modeling (FDM) 3D printing. *European Journal of Pharmaceutics and Biopharmaceutics*, *108*, 111-125.

Alhijjaj, M., Nasereddin, J., Belton, P., & Qi, S. (2019). Impact of processing parameters on the quality of pharmaceutical solid dosage forms produced by fused deposition modeling (FDM). *Pharmaceutics*, *11*(12), 633.

Alhnan, M. A., Okwuosa, T. C., Sadia, M., Wan, K.-W., Ahmed, W., & Arafat, B. (2016). Emergence of 3D printed dosage forms: opportunities and challenges. *Pharmaceutical Research*, *33*, 1817-1832.

Ali, M. H., Mir-Nasiri, N., & Ko, W. L. (2016). Multi-nozzle extrusion system for 3D printer and its control mechanism. *The International Journal of Advanced Manufacturing Technology*, *86*, 999-1010.

Alomari, M., Mohamed, F. H., Basit, A. W., & Gaisford, S. (2015). Personalised dosing: Printing a dose of one's own medicine. *International journal of pharmaceutics*, *494*(2), 568-577.

Alshahrani, S. M., Lu, W., Park, J.-B., Morott, J. T., Alsulays, B. B., Majumdar, S., Langley, N., Kolter, K., Gryczke, A., & Repka, M. A. (2015). Stability-enhanced hot-melt extruded amorphous solid dispersions via combinations of Soluplus® and HPMCAS-HF. *Aaps Pharmscitech*, *16*, 824-834.

Alshetaili, A., Alshahrani, S. M., Almutairy, B. K., & Repka, M. A. (2020). Hot melt extrusion processing parameters optimization. *Processes*, *8*(11), 1516.

Altamimi, M. A., & Neau, S. H. (2018). A study to identify the contribution of Soluplus® component homopolymers to the solubilization of nifedipine and sulfamethoxazole using the melting point depression method. *Powder Technology*, *338*, 576-585.

Anadioti, E., Kane, B., & Soulas, E. (2018). Current and emerging applications of 3D printing in restorative dentistry. *Current Oral Health Reports*, *5*, 133-139.

Ansari, A. A., & Kamil, M. (2021). Effect of print speed and extrusion temperature on properties of 3D printed PLA using fused deposition modeling process. *Materials Today: Proceedings*, *45*, 5462-5468.

Arnfast, L., Kamruzzaman, M., Löbmann, K., Aho, J., Baldursdottir, S., Rades, T., & Rantanen, J. (2017). Melt extrusion of high-dose co-amorphous drug-drug combinations: theme: formulation and manufacturing of solid dosage forms guest editors: Tony Zhou and Tonglei Li. *Pharmaceutical research*, *34*, 2689-2697.

Arsac, A., Carrot, C., & Guillet, J. (2000). Determination of primary relaxation temperatures and melting points of ethylene vinyl acetate copolymers. *Journal of thermal analysis and calorimetry*, *61*(3), 681-685.

Arshad, M. S., Zafar, S., Yousef, B., Alyassin, Y., Ali, R., AlAsiri, A., Chang, M.-W., Ahmad, Z., Elkordy, A. A., & Faheem, A. (2021). A review of emerging technologies enabling improved solid oral dosage form manufacturing and processing. *Advanced Drug Delivery Reviews*, *178*, 113840.

Attaran, M. (2017). The rise of 3-D printing: The advantages of additive manufacturing over traditional manufacturing. *Business Horizons*, *60*(5), 677-688.

Attenello, F., Raza, S. M., Dimeco, F., & Olivi, A. (2012). Chemotherapy for brain tumors with polymer drug delivery. *Handbook of Clinical Neurology*, *104*, 339-353.

Auriemma, G., Tommasino, C., Falcone, G., Esposito, T., Sardo, C., & Aquino, R. P. (2022). Additive manufacturing strategies for personalized drug delivery systems and medical devices: fused filament fabrication and semi solid extrusion. *Molecules*, *27*(9), 2784.

Awad, A., Fina, F., Trenfield, S. J., Patel, P., Goyanes, A., Gaisford, S., & Basit, A. W. (2019). 3D printed pellets (miniprintlets): A novel, multi-drug, controlled release platform technology. *Pharmaceutics*, *11*(4), 148.

Awad, A., Trenfield, S. J., Gaisford, S., & Basit, A. W. (2018). 3D printed medicines: A new branch of digital healthcare. *International Journal of Pharmaceutics*, *548*(1), 586-596.

Baghel, S., Cathcart, H., & O'Reilly, N. J. (2016). Polymeric amorphous solid dispersions: a review of amorphization, crystallization, stabilization, solid-state characterization, and aqueous solubilization of biopharmaceutical classification system class II drugs. *Journal of Pharmaceutical Sciences*, *105*(9), 2527-2544.

Bandari, S., Nyavanandi, D., Dumpa, N., & Repka, M. A. (2021). Coupling hot melt extrusion and fused deposition modeling: Critical properties for successful performance. *Advanced Drug Delivery Reviews*, *172*, 52-63.

BARDWELL, T. (2023). *The Best 3D Printing Speed Settings For Every Filament*. 3D SOURCED. Retrieved 02/11/2023 from https://www.3dsourced.com/guides/3d-printing-speed/

Barile, G., Leoni, A., Muttillo, M., Paolucci, R., Fazzini, G., & Pantoli, L. (2020). Fused-deposition-material 3D-printing procedure and algorithm avoiding use of any supports. *Sensors*, *20*(2), 470.

Bartnikowski, M., Dargaville, T. R., Ivanovski, S., & Hutmacher, D. W. (2019). Degradation mechanisms of polycaprolactone in the context of chemistry, geometry and environment. *Progress in polymer science*, *96*, 1-20.

Beer, N., Hegger, I., Kaae, S., De Bruin, M. L., Genina, N., Alves, T. L., Hoebert, J., & Sporrong, S. K. (2021). Scenarios for 3D printing of personalized medicines-A case study. *Exploratory Research in Clinical and Social Pharmacy*, *4*, 100073.

Bicudo, E., Faulkner, A., & Li, P. (2021). Software, risks, and liabilities: ongoing and emergent issues in 3D bioprinting. *Journal of Risk Research*, *24*(10), 1319-1334. https://doi.org/10.1080/13669877.2020.1848904

Bikas, H., Stavropoulos, P., & Chryssolouris, G. (2016). Additive manufacturing methods and modelling approaches: a critical review. *The International Journal of Advanced Manufacturing Technology*, *83*, 389-405.

Binello, E., & Germano, I. M. J. C. s. (2011). Targeting glioma stem cells: a novel framework for brain tumors. *102*(11), 1958-1966.

Blevins, T. L., & Nixon, M. (2011). *Control loop foundation: batch and continuous processes*. ISA.

Brambilla, C. R., Okafor-Muo, O. L., Hassanin, H., & ElShaer, A. (2021). 3DP printing of oral solid formulations: A systematic review. *Pharmaceutics*, *13*(3), 358.

Burke, G., Devine, D. M., & Major, I. (2020). Effect of stereolithography 3D printing on the properties of PEGDMA hydrogels. *Polymers*, *12*(9), 2015.

Cantin, O., Siepmann, F., Willart, J.-F., Danede, F., Siepmann, J., & Karrout, Y. (2021). PEO hot melt extrudates for controlled drug delivery: Importance of the type of drug and loading. *Journal of Drug Delivery Science and Technology*, *61*, 102238.

Carlier, E., Marquette, S., Peerboom, C., Denis, L., Benali, S., Raquez, J., Amighi, K., & Goole, J. (2019). Investigation of the parameters used in fused deposition modeling of poly (lactic

acid) to optimize 3D printing sessions. *International Journal of Pharmaceutics*, *565*, 367-377.
Carneiro, O. S., Silva, A., & Gomes, R. (2015). Fused deposition modeling with polypropylene. *Materials & Design*, *83*, 768-776.
Castro, B. M., Elbadawi, M., Ong, J. J., Pollard, T., Song, Z., Gaisford, S., Pérez, G., Basit, A. W., Cabalar, P., & Goyanes, A. (2021). Machine learning predicts 3D printing performance of over 900 drug delivery systems. *Journal of Controlled Release*, *337*, 530-545. https://doi.org/10.1016/j.jconrel.2021.07.046
Cepeda-Franco, C., Mitxelena-Iribarren, O., Calero-Castro, F. J., Astigarraga, M., Castillo-Tuñon, J. M., Laga, I., Pereira, S., Arana, S., Mujika, M., & Padillo-Ruiz, J. (2023). TARTESSUS: A Customized Electrospun Drug Delivery System Loaded with Irinotecan for Local and Sustained Chemotherapy Release in Pancreatic Cancer. *Bioengineering*, *10*(2), 183.
Chai, X., Chai, H., Wang, X., Yang, J., Li, J., Zhao, Y., Cai, W., Tao, T., & Xiang, X. (2017). Fused deposition modeling (FDM) 3D printed tablets for intragastric floating delivery of domperidone. *Scientific reports*, *7*(1), 2829.
Chapman, H. J., & Lauzardo, M. (2014). Advances in diagnosis and treatment of latent tuberculosis infection. *The Journal of the American Board of Family Medicine*, *27*(5), 704-712.
Charoo, N. A., Barakh Ali, S. F., Mohamed, E. M., Kuttolamadom, M. A., Ozkan, T., Khan, M. A., & Rahman, Z. (2020). Selective laser sintering 3D printing–an overview of the technology and pharmaceutical applications. *Drug Development and Industrial Pharmacy*, *46*(6), 869-877.
Chaudhari, R., Loharkar, P. K., & Ingle, A. (2022). Medical applications of rapid prototyping technology. Recent Advances in Industrial Production: Select Proceedings of ICEM 2020,
ChemBK. (2023). *Hydroxy Propyl Methyl Cellulose*. ChemBK. Retrieved 25/12/2023 from https://www.chembk.com/en/chem/HPMC
Chen, C.-C., Chueh, J.-Y., Tseng, H., Huang, H.-M., & Lee, S.-Y. (2003). Preparation and characterization of biodegradable PLA polymeric blends. *Biomaterials*, *24*(7), 1167-1173.
Chen, D., Xu, X.-Y., Li, R., Zang, G.-A., Zhang, Y., Wang, M.-R., Xiong, M.-F., Xu, J.-R., Wang, T., & Fu, H. (2020). Preparation and in vitro evaluation of FDM 3D-printed ellipsoid-shaped gastric floating tablets with low infill percentages. *AAPS PharmSciTech*, *21*, 1-13.
Chen, Y., Traore, Y. L., Walker, L., Yang, S., & Ho, E. A. (2022). Fused deposition modeling three-dimensional printing of flexible polyurethane intravaginal rings with controlled tunable release profiles for multiple active drugs. *Drug Delivery and Translational Research*, *12*(4), 906-924.
Chiulan, I., Frone, A. N., Brandabur, C., & Panaitescu, D. M. (2017). Recent advances in 3D printing of aliphatic polyesters. *Bioengineering*, *5*(1), 2.
Chou, W.-H., Gamboa, A., & Morales, J. O. (2021). Inkjet printing of small molecules, biologics, and nanoparticles. *International Journal of Pharmaceutics*, *600*, 120462.
Chu, C., Graf, G., & Rosen, D. W. (2008). Design for additive manufacturing of cellular structures. *Computer-Aided Design and Applications*, *5*(5), 686-696.
Chua, C. K., & Leong, K. F. (2014). *3D Printing and additive manufacturing: Principles and applications (with companion media pack)-of rapid prototyping*. World Scientific Publishing Company.

Chua, C. K., Leong, K. F., & An, J. (2020). Introduction to rapid prototyping of biomaterials. In *Rapid prototyping of biomaterials* (pp. 1-15). Elsevier.

Cohn, D. L., O'Brien, R. J., Geiter, L. J., Gordin, F., Hershfield, E., & Horsburgh, C. (2000). Targeted tuberculin testing and treatment of latent tuberculosis infection. *MMWR Morb Mortal Wkly Rep*, *49*(6), 1-54.

Cornejo, J., Cornejo-Aguilar, J. A., Vargas, M., Helguero, C. G., Milanezi de Andrade, R., Torres-Montoya, S., Asensio-Salazar, J., Rivero Calle, A., Martínez Santos, J., & Damon, A. (2022). Anatomical Engineering and 3D printing for surgery and medical devices: International review and future exponential innovations. *BioMed Research International*, *2022*.

Covas, J. A., & Gaspar-Cunha, A. (2011). Polymer extrusion: setting the operating conditions and defining the screw geometry.

Cui, M., Pan, H., Su, Y., Fang, D., Qiao, S., Ding, P., & Pan, W. (2021). Opportunities and challenges of three-dimensional printing technology in pharmaceutical formulation development. *Acta Pharmaceutica Sinica B*, *11*(8), 2488-2504.

D'souza, A. A., & Shegokar, R. (2016). Polyethylene glycol (PEG): a versatile polymer for pharmaceutical applications. *Expert opinion on drug delivery*, *13*(9), 1257-1275.

Daly, R., Harrington, T. S., Martin, G. D., & Hutchings, I. M. (2015). Inkjet printing for pharmaceutics–a review of research and manufacturing. *International Journal of Pharmaceutics*, *494*(2), 554-567.

Danaei, M., Dehghankhold, M., Ataei, S., Hasanzadeh Davarani, F., Javanmard, R., Dokhani, A., Khorasani, S., & Mozafari, M. (2018). Impact of particle size and polydispersity index on the clinical applications of lipidic nanocarrier systems. *Pharmaceutics*, *10*(2), 57.

Dartois, V. A., & Rubin, E. J. (2022). Anti-tuberculosis treatment strategies and drug development: challenges and priorities. *Nature Reviews Microbiology*, *20*(11), 685-701.

De Bonis, P., Anile, C., Pompucci, A., Fiorentino, A., Balducci, M., Chiesa, S., Maira, G., & Mangiola, A. (2012). Safety and efficacy of Gliadel wafers for newly diagnosed and recurrent glioblastoma. *Acta neurochirurgica*, *154*, 1371-1378.

Decuir, F., Phelan, K., & Hollins, B. C. (2016). Mechanical strength of 3-D printed filaments. 2016 32nd Southern Biomedical Engineering Conference (SBEC),

DeStefano, V., Khan, S., & Tabada, A. (2020). Applications of PLA in modern medicine. *Engineered Regeneration*, *1*, 76-87.

Devicharan, R., & Garg, R. (2019). Optimization of the print quality by controlling the process parameters on 3D printing machine. *3D Printing and Additive Manufacturing Technologies*, 187-194.

Dinagaran, S., Gajendiran, J., Raj, S. G., & Gnanam, S. (2022). Study of crystalline growth, structural characteristics, optical behavior, thermo and dielectric properties of isoniazid single crystal. *Optics & Laser Technology*, *156*, 108576.

Douroumis, D. (2012). *Hot-melt extrusion: Pharmaceutical applications*. John Wiley & Sons.

Dumpa, N., Butreddy, A., Wang, H., Komanduri, N., Bandari, S., & Repka, M. A. (2021). 3D printing in personalized drug delivery: An overview of hot-melt extrusion-based fused deposition modeling. *International Journal of Pharmaceutics*, *600*, 120501.

Duran, C., Subbian, V., Giovanetti, M. T., Simkins, J. R., & Beyette Jr, F. R. (2015). Experimental desktop 3D printing using dual extrusion and water-soluble polyvinyl alcohol. *Rapid Prototyping Journal*, *21*(5), 528-534.

Durão, L. F. C., Barkoczy, R., Zancul, E., Lee Ho, L., & Bonnard, R. (2019). Optimizing additive manufacturing parameters for the fused deposition modeling technology using a design of experiments. *Progress in Additive Manufacturing*, *4*, 291-313.

Durgun, I., & Ertan, R. (2014). Experimental investigation of FDM process for improvement of mechanical properties and production cost. *Rapid Prototyping Journal*, *20*(3), 228-235.

Dzogbewu, T. C., Amoah, N., Fianko, S. K., Afrifa, S., & de Beer, D. (2022). Additive manufacturing towards product production: A bibliometric analysis. *Manufacturing Review*, *9*, 1.

Economidou, S. N., & Douroumis, D. (2021). 3D printing as a transformative tool for microneedle systems: Recent advances, manufacturing considerations and market potential. *Advanced drug delivery reviews*, *173*, 60-69.

Ehtezazi, T., Algellay, M., Islam, Y., Roberts, M., Dempster, N. M., & Sarker, S. D. (2018). The application of 3D printing in the formulation of multilayered fast dissolving oral films. *Journal of Pharmaceutical Sciences*, *107*(4), 1076-1085.

Ekren, B. Y., Stylos, N., Zwiegelaar, J., Turhanlar, E. E., & Kumar, V. (2023). Additive manufacturing integration in E-commerce supply chain network to improve resilience and competitiveness. *Simulation Modelling Practice and Theory*, *122*, 102676.

Englezos, K., Wang, L. X., Tan, E. C. K., & Kang, L. F. (2023). 3D printing for personalised medicines: implications for policy and practice. *International Journal of Pharmaceutics*, *635*, Article 122785. https://doi.org/10.1016/j.ijpharm.2023.122785

Evgenii, T., Valerie, L., Michelle, Å., Maria, S., Thomas, K., Julian, Q., & Jonas, L. (2023). Impact of polymer chemistry on critical quality attributes of selective laser sintering 3D printed solid oral dosage forms. *International Journal of Pharmaceutics: X*, *6*, 100203.

Farah, S., Anderson, D. G., & Langer, R. (2016). Physical and mechanical properties of PLA, and their functions in widespread applications—A comprehensive review. *Advanced Drug Delivery Reviews*, *107*, 367-392.

Feng, X., & Zhang, F. (2018). Twin-screw extrusion of sustained-release oral dosage forms and medical implants. *Drug Delivery and Translational Research*, *8*, 1694-1713.

Fernandes, G. J., Rathnanand, M., & Kulkarni, V. (2019). Mechanochemical synthesis of carvedilol cocrystals utilizing hot melt extrusion technology. *Journal of Pharmaceutical Innovation*, *14*, 373-381.

Ferrari, F., Esposito Corcione, C., Montagna, F., & Maffezzoli, A. (2020). 3D printing of polymer waste for improving people's awareness about marine litter. *Polymers*, *12*(8), 1738.

Feuerbach, T., Callau-Mendoza, S., & Thommes, M. (2019). Development of filaments for fused deposition modeling 3D printing with medical grade poly (lactic-co-glycolic acid) copolymers. *Pharmaceutical Development and Technology*, *24*(4), 487-493.

Fina, F., Madla, C. M., Goyanes, A., Zhang, J., Gaisford, S., & Basit, A. W. (2018). Fabricating 3D printed orally disintegrating printlets using selective laser sintering. *International Journal of Pharmaceutics*, *541*(1-2), 101-107.

Fleming, A. B., & Saltzman, W. M. (2002). Pharmacokinetics of the carmustine implant. *Clinical pharmacokinetics*, *41*, 403-419.

Florence, A. T., & Siepmann, J. (2016). Dosage Forms for Personalized Medicine: From the Simple to the Complex. In *Modern Pharmaceutics, Volume 2* (pp. 511-530). CRC Press.

Food, U., & Administration, D. (2014). Custom device exemption guidance for industry and food and drug administration staff. In.

Francis, A., Yang, Y., Virtanen, S., & Boccaccini, A. (2015). Iron and iron-based alloys for temporary cardiovascular applications. *Journal of Materials Science: Materials in Medicine*, *26*, 1-16.

Freire, F., Aragão, C., de Lima e Moura, T., & Raffin, F. (2009). Thermal studies of isoniazid and mixtures with rifampicin. *Journal of thermal analysis and calorimetry*, *97*(1), 333-336.

Funk, N. L., Fantaus, S., & Beck, R. C. R. (2022). Immediate release 3D printed oral dosage forms: how different polymers have been explored to reach suitable drug release behaviour. *International Journal of Pharmaceutics*, 122066.

Gajra*, B., Pandya, S. S., Vidyasagar, G., Rabari, H., Dedania, R. R., & Rao, S. (2012). Poly vinyl alcohol hydrogel and its pharmaceutical and biomedical applications: A review. *Int. J. Pharm. Res*, *4*, 2026.

Gandhi, S., Tayebi Meybodi, A., Belykh, E., Cavallo, C., Zhao, X., Syed, M. P., Borba Moreira, L., Lawton, M. T., Nakaji, P., & Preul, M. C. (2019). Survival outcomes among patients with high-grade glioma treated with 5-aminolevulinic acid–guided surgery: A systematic review and meta-analysis. *Frontiers in oncology*, *9*, 620.

Gasparotti, E., Vignali, E., Losi, P., Scatto, M., Fanni, B. M., Soldani, G., Landini, L., Positano, V., & Celi, S. (2019). A 3D printed melt-compounded antibiotic loaded thermoplastic polyurethane heart valve ring design: an integrated framework of experimental material tests and numerical simulations. *International Journal of Polymeric Materials and Polymeric Biomaterials*, *68*(1-3), 1-10.

Genina, N., Hadi, B., & Löbmann, K. (2018). Hot melt extrusion as solvent-free technique for a continuous manufacturing of drug-loaded mesoporous silica. *Journal of pharmaceutical sciences*, *107*(1), 149-155.

Genina, N., Holländer, J., Jukarainen, H., Mäkilä, E., Salonen, J., & Sandler, N. (2016). Ethylene vinyl acetate (EVA) as a new drug carrier for 3D printed medical drug delivery devices. *European Journal of Pharmaceutical Sciences*, *90*, 53-63.

Gibaldi, M., Lee, M., & Desai, A. (2007). Gibaldi's Drug Delivery Systems in Pharmaceutical Care: American Society of Health-System Pharmacists. In.

Gioumouxouzis, C. I., Karavasili, C., & Fatouros, D. G. (2019). Recent advances in pharmaceutical dosage forms and devices using additive manufacturing technologies. *Drug discovery today*, *24*(2), 636-643.

Giri, B. R., Song, E. S., Kwon, J., Lee, J.-H., Park, J.-B., & Kim, D. W. (2020). Fabrication of intragastric floating, controlled release 3D printed theophylline tablets using hot-melt extrusion and fused deposition modeling. *Pharmaceutics*, *12*(1), 77.

Go, J., Schiffres, S. N., Stevens, A. G., & Hart, A. J. (2017). Rate limits of additive manufacturing by fused filament fabrication and guidelines for high-throughput system design. *Additive Manufacturing*, *16*, 1-11. https://doi.org/10.1016/j.addma.2017.03.007

Gomaa, E., Eissa, N. G., Ibrahim, T. M., El-Bassossy, H. M., El-Nahas, H. M., & Ayoub, M. M. (2023). Development of depot PLGA-based in-situ implant of Linagliptin: Sustained release and glycemic control. *Saudi Pharmaceutical Journal*, *31*(4), 499-509.

Gonzalez-Gutierrez, J., Duretek, I., Arbeiter, F., Kukla, C., & Holzer, C. (2017). Filler content and properties of highly filled filaments for fused filament fabrication of magnets. SPE ANTEC 2017,

Goole, J., & Amighi, K. (2016). 3D printing in pharmaceutics: A new tool for designing customized drug delivery systems. *International Journal of Pharmaceutics*, *499*(1-2), 376-394.
Goudswaard, M., Nassehi, A., & Hicks, B. (2023). A generative-based design methodology to enable the democratisation of 3D printing. *Design Science*, *9*, e21.
Goyanes, A., Buanz, A. B., Hatton, G. B., Gaisford, S., & Basit, A. W. (2015). 3D printing of modified-release aminosalicylate (4-ASA and 5-ASA) tablets. *European Journal of Pharmaceutics and Biopharmaceutics*, *89*, 157-162.
Goyanes, A., Det-Amornrat, U., Wang, J., Basit, A. W., & Gaisford, S. (2016). 3D scanning and 3D printing as innovative technologies for fabricating personalized topical drug delivery systems. *Journal of Controlled Release*, *234*, 41-48.
Goyanes, A., Madla, C. M., Umerji, A., Piñeiro, G. D., Montero, J. M. G., Diaz, M. J. L., Barcia, M. G., Taherali, F., Sánchez-Pintos, P., & Couce, M.-L. (2019). Automated therapy preparation of isoleucine formulations using 3D printing for the treatment of MSUD: First single-centre, prospective, crossover study in patients. *International journal of pharmaceutics*, *567*, 118497.
Goyanes, A., Martinez, P. R., Buanz, A., Basit, A. W., & Gaisford, S. (2015). Effect of geometry on drug release from 3D printed tablets. *International Journal of Pharmaceutics*, *494*(2), 657-663.
Gromat, T., Gardan, J., Saifouni, O., Makke, A., & Recho, N. (2023). Generative design for additive manufacturing of polymeric auxetic materials produced by fused filament fabrication. *International Journal on Interactive Design and Manufacturing (IJIDeM)*, *17*(6), 2943-2955.
Gross, B. C., Erkal, J. L., Lockwood, S. Y., Chen, C., & Spence, D. M. (2014). Evaluation of 3D printing and its potential impact on biotechnology and the chemical sciences. In: ACS Publications.
Grossman, S. A., Reinhard, C., Colvin, O. M., Chasin, M., Brundrett, R., Tamargo, R. J., & Brem, H. (1992). The intracerebral distribution of BCNU delivered by surgically implanted biodegradable polymers. *Journal of neurosurgery*, *76*(4), 640-647.
Gueche, Y. A., Sanchez-Ballester, N. M., Bataille, B., Aubert, A., Leclercq, L., Rossi, J.-C., & Soulairol, I. (2021). Selective laser sintering of solid oral dosage forms with copovidone and paracetamol using a CO2 laser. *Pharmaceutics*, *13*(2), 160.
Gupta, S. S., Meena, A., Parikh, T., & Serajuddin, A. T. (2016). Investigation of thermal and viscoelastic properties of polymers relevant to hot melt extrusion-I: Polyvinylpyrrolidone and related polymers. *Journal of Excipients and Food Chemicals*, *5*(1).
Hao, W., Zheng, Z., Zhu, L., Pang, L., Ma, J., Zhu, S., Du, L., & Jin, Y. (2021). 3D printing-based drug-loaded implanted prosthesis to prevent breast cancer recurrence post-conserving surgery. *Asian journal of pharmaceutical sciences*, *16*(1), 86-96.
Hardung, H., Djuric, D., & Ali, S. (2010). Combining HME & solubilization: Soluplus®—the solid solution. *Drug Deliv Technol*, *10*(3), 20-27.
Hartzke, D., Pössl, A., Schlupp, P., & Runkel, F. E. (2022). Evaluation of Hydroxyethyl Cellulose Grades as the Main Matrix Former to Produce 3D-Printed Controlled-Release Dosage Forms. *Pharmaceutics*, *14*(10), 2103.
Hassan, C., Ward, J., & Peppas, N. (2000). Modeling of crystal dissolution of poly (vinyl alcohol) gels produced by freezing/thawing processes. *Polymer*, *41*(18), 6729-6739.

Hawker, C. J., & Wooley, K. L. (2005). The convergence of synthetic organic and polymer chemistries. *Science*, *309*(5738), 1200-1205.
Healy, A. V., Fuenmayor, E., Doran, P., Geever, L. M., Higginbotham, C. L., & Lyons, J. G. (2019). Additive manufacturing of personalized pharmaceutical dosage forms via stereolithography. *Pharmaceutics*, *11*(12), 645.
Henderson, A. M. (1993). Ethylene-vinyl acetate (EVA) copolymers: a general review. *IEEE Electrical Insulation Magazine*, *9*(1), 30-38.
Hines, D. J., & Kaplan, D. L. (2013). Poly (lactic-co-glycolic) acid− controlled-release systems: experimental and modeling insights. *Critical Reviews™ in Therapeutic Drug Carrier Systems*, *30*(3).
Holländer, J., Genina, N., Jukarainen, H., Khajeheian, M., Rosling, A., Mäkilä, E., & Sandler, N. (2016). Three-dimensional printed PCL-based implantable prototypes of medical devices for controlled drug delivery. *Journal of Pharmaceutical Sciences*, *105*(9), 2665-2676.
Horvath, J., & Cameron, R. (2014). *Mastering 3D printing*. Springer.
Hospodiuk, M., Dey, M., Sosnoski, D., & Ozbolat, I. T. (2017). The bioink: A comprehensive review on bioprintable materials. *Biotechnology advances*, *35*(2), 217-239.
Hourd, P., Medcalf, N., Segal, J., & Williams, D. J. (2015). A 3D bioprinting exemplar of the consequences of the regulatory requirements on customized processes. *Regenerative Medicine*, *10*(7), 863-883. https://doi.org/10.2217/rme.15.52
Hsiang Loh, G., Pei, E., Gonzalez-Gutierrez, J., & Monzón, M. (2020). An overview of material extrusion troubleshooting. *Applied Sciences*, *10*(14), 4776.
Huanbutta, K., Burapapadh, K., Sriamornsak, P., & Sangnim, T. (2023). Practical Application of 3D Printing for Pharmaceuticals in Hospitals and Pharmacies. *Pharmaceutics*, *15*(7), Article 1877. https://doi.org/10.3390/pharmaceutics15071877
Hunde, B. R., & Woldeyohannes, A. D. (2022). Future prospects of computer-aided design (CAD)–A review from the perspective of artificial intelligence (AI), extended reality, and 3D printing. *Results in Engineering*, 100478.
Ibrahim, I. R., Ibrahim, M. I. M., & Al-Haddad, M. S. d. (2012). The influence of consumers' preferences and perceptions of oral solid dosage forms on their treatment. *International journal of clinical pharmacy*, *34*, 728-732.
Ilyés, K., Kovács, N. K., Balogh, A., Borbás, E., Farkas, B., Casian, T., Marosi, G., Tomuță, I., & Nagy, Z. K. (2019). The applicability of pharmaceutical polymeric blends for the fused deposition modelling (FDM) 3D technique: Material considerations–printability–process modulation, with consecutive effects on in vitro release, stability and degradation. *European Journal of Pharmaceutical Sciences*, *129*, 110-123.
Infanger, S., Haemmerli, A., Iliev, S., Baier, A., Stoyanov, E., & Quodbach, J. (2019). Powder bed 3D-printing of highly loaded drug delivery devices with hydroxypropyl cellulose as solid binder. *International Journal of Pharmaceutics*, *555*, 198-206.
Iuchi, T., Inoue, A., Hirose, Y., Morioka, M., Horiguchi, K., Natsume, A., Arakawa, Y., Iwasaki, K., Fujiki, M., & Kumabe, T. (2022). Long-term effectiveness of Gliadel implant for malignant glioma and prognostic factors for survival: 3-year results of a postmarketing surveillance in Japan. *Neuro-Oncology Advances*, *4*(1), vdab189.
Jacob, S., Nair, A. B., Patel, V., & Shah, J. (2020). 3D printing technologies: recent development and emerging applications in various drug delivery systems. *AAPS PharmSciTech*, *21*, 1-16.

Jadhav, A., & Jadhav, V. S. (2022). A review on 3D printing: An additive manufacturing technology. *Materials Today: Proceedings*, *62*, 2094-2099.

Jakubowicz, J. (2020). Ti-based biomaterials: synthesis, properties and applications. In (Vol. 13, pp. 1696): MDPI.

Jamróz, W., Szafraniec, J., Kurek, M., & Jachowicz, R. (2018). 3D printing in pharmaceutical and medical applications–recent achievements and challenges. *Pharmaceutical research*, *35*, 1-22.

Janczura, M., Sip, S., & Cielecka-Piontek, J. (2022). The development of innovative dosage forms of the fixed-dose combination of active pharmaceutical ingredients. *Pharmaceutics*, *14*(4), 834.

Januskaite, P., Xu, X., Ranmal, S. R., Gaisford, S., Basit, A. W., Tuleu, C., & Goyanes, A. (2020). I spy with my little eye: a paediatric visual preferences survey of 3D printed tablets. *Pharmaceutics*, *12*(11), 1100.

Jiang, Z., Diggle, B., Tan, M. L., Viktorova, J., Bennett, C. W., & Connal, L. A. (2020). Extrusion 3D printing of polymeric materials with advanced properties. *Advanced Science*, *7*(17), 2001379.

Johannesson, J., Khan, J., Hubert, M., Teleki, A., & Bergström, C. A. (2021). 3D-printing of solid lipid tablets from emulsion gels. *International journal of pharmaceutics*, *597*, 120304.

Junk, S., & Kuen, C. (2016). Review of open source and freeware CAD systems for use with 3D-printing. *Procedia CIRP*, *50*, 430-435.

Kadry, H., Al-Hilal, T. A., Keshavarz, A., Alam, F., Xu, C., Joy, A., & Ahsan, F. (2018). Multi-purposable filaments of HPMC for 3D printing of medications with tailored drug release and timed-absorption. *International Journal of Pharmaceutics*, *544*(1), 285-296.

Kapoor, D. N., Bhatia, A., Kaur, R., Sharma, R., Kaur, G., & Dhawan, S. (2015). PLGA: a unique polymer for drug delivery. *Therapeutic delivery*, *6*(1), 41-58.

Karakurt, I., Aydoğdu, A., Çıkrıkcı, S., Orozco, J., & Lin, L. (2020). Stereolithography (SLA) 3D printing of ascorbic acid loaded hydrogels: A controlled release study. *International Journal of Pharmaceutics*, *584*, 119428.

Karalia, D., Siamidi, A., Karalis, V., & Vlachou, M. (2021). 3D-Printed oral dosage forms: Mechanical properties, computational approaches and applications. *Pharmaceutics*, *13*(9), 1401.

Karavasili, C., Gkaragkounis, A., Moschakis, T., Ritzoulis, C., & Fatouros, D. G. (2020). Pediatric-friendly chocolate-based dosage forms for the oral administration of both hydrophilic and lipophilic drugs fabricated with extrusion-based 3D printing. *European Journal of Pharmaceutical Sciences*, *147*, 105291.

Keating, A. V., Soto, J., Tuleu, C., Forbes, C., Zhao, M., & Craig, D. Q. (2018). Solid state characterisation and taste masking efficiency evaluation of polymer based extrudates of isoniazid for paediatric administration. *International Journal of Pharmaceutics*, *536*(2), 536-546.

Keen, J. M., Martin, C., Machado, A., Sandhu, H., McGinity, J. W., & DiNunzio, J. C. (2014). Investigation of process temperature and screw speed on properties of a pharmaceutical solid dispersion using corotating and counter-rotating twin-screw extruders. *Journal of pharmacy and pharmacology*, *66*(2), 204-217.

Kempin, W., Domsta, V., Grathoff, G., Brecht, I., Semmling, B., Tillmann, S., Weitschies, W., & Seidlitz, A. (2018). Immediate release 3D-printed tablets produced via fused deposition modeling of a thermo-sensitive drug. *Pharmaceutical research*, *35*, 1-12.

Kempin, W., Franz, C., Koster, L.-C., Schneider, F., Bogdahn, M., Weitschies, W., & Seidlitz, A. (2017). Assessment of different polymers and drug loads for fused deposition modeling of drug loaded implants. *European Journal of Pharmaceutics and Biopharmaceutics*, *115*, 84-93.

Keskar, V., Mohanty, P. S., Gemeinhart, E. J., & Gemeinhart, R. A. (2006). Cervical cancer treatment with a locally insertable controlled release delivery system. *Journal of Controlled Release*, *115*(3), 280-288.

Khaled, S. A., Alexander, M. R., Wildman, R. D., Wallace, M. J., Sharpe, S., Yoo, J., & Roberts, C. J. (2018). 3D extrusion printing of high drug loading immediate release paracetamol tablets. *International Journal of Pharmaceutics*, *538*(1-2), 223-230.

Khaled, S. A., Burley, J. C., Alexander, M. R., Yang, J., & Roberts, C. J. (2015). 3D printing of five-in-one dose combination polypill with defined immediate and sustained release profiles. *Journal of controlled release*, *217*, 308-314.

Khosraviboroujeni, A., Mirdamadian, S. Z., Minaiyan, M., & Taheri, A. (2022). Preparation and characterization of 3D printed PLA microneedle arrays for prolonged transdermal drug delivery of estradiol valerate. *Drug Delivery and Translational Research*, *12*(5), 1195-1208.

Kim, C., Espalin, D., Cuaron, A., Perez, M. A., MacDonald, E., & Wicker, R. B. (2015). A study to detect a material deposition status in fused deposition modeling technology. 2015 IEEE International Conference on Advanced Intelligent Mechatronics (AIM),

Kim, D.-W., & Weon, K. Y. (2021). Pharmaceutical application and development of fixed-dose combination: Dosage form review. *Journal of Pharmaceutical Investigation*, *51*, 555-570.

Kim, H. Y., Lee, Y. J., Chang, W., Cho, J., Park, J. H., Lee, J.-c., Kim, J., Hwang, J.-H., & Kim, Y. H. (2022). Tumor resectability and response on CT following neoadjuvant therapy for pancreatic cancer: inter-observer agreement study. *European Radiology*, *32*(6), 3799-3807.

Kjar, A., & Huang, Y. (2019). Application of micro-scale 3D printing in pharmaceutics. *Pharmaceutics*, *11*(8), 390.

Knop, K., Hoogenboom, R., Fischer, D., & Schubert, U. S. (2010). Poly (ethylene glycol) in drug delivery: pros and cons as well as potential alternatives. *Angewandte chemie international edition*, *49*(36), 6288-6308.

Kolakovic, R., Viitala, T., Ihalainen, P., Genina, N., Peltonen, J., & Sandler, N. (2013). Printing technologies in fabrication of drug delivery systems. *Expert opinion on drug delivery*, *10*(12), 1711-1723.

Konta, A. A., García-Piña, M., & Serrano, D. R. (2017). Personalised 3D printed medicines: which techniques and polymers are more successful? *Bioengineering*, *4*(4), 79.

Kou, Y., Wang, S., Luo, J., Sun, K., Zhang, J., Tan, Z., & Shi, Q. (2019). Thermal analysis and heat capacity study of polyethylene glycol (PEG) phase change materials for thermal energy storage applications. *The Journal of Chemical Thermodynamics*, *128*, 259-274.

Krieger, K. J., Bertollo, N., Dangol, M., Sheridan, J. T., Lowery, M. M., & O'Cearbhaill, E. D. (2019). Simple and customizable method for fabrication of high-aspect ratio microneedle molds using low-cost 3D printing. *Microsystems & nanoengineering*, *5*(1), 42.

Kristiawan, R. B., Imaduddin, F., Ariawan, D., Ubaidillah, & Arifin, Z. (2021). A review on the fused deposition modeling (FDM) 3D printing: Filament processing, materials, and printing parameters. *Open Engineering*, *11*(1), 639-649.

Kukkonen, J., Ervasti, T., & Laitinen, R. (2022). Production and characterization of glibenclamide incorporated PLA filaments for 3D printing by fused deposition modeling. *Journal of Drug Delivery Science and Technology*, *77*, 103843.

Kulinowski, P., Malczewski, P., Łaszcz, M., Baran, E., Milanowski, B., Kuprianowicz, M., & Dorożyński, P. (2022). Development of composite, reinforced, highly drug-loaded pharmaceutical printlets manufactured by selective laser sintering—in search of relevant excipients for pharmaceutical 3D printing. *Materials*, *15*(6), 2142.

Kumar, S. A., & Prasad, R. (2021). Basic principles of additive manufacturing: Different additive manufacturing technologies. In *Additive Manufacturing* (pp. 17-35). Elsevier.

Lakkala, P., Munnangi, S. R., Bandari, S., & Repka, M. (2023). Additive manufacturing technologies with emphasis on stereolithography 3D printing in pharmaceutical and medical applications: A review. *International Journal of Pharmaceutics: X*, 100159.

Lamichhane, S., Bashyal, S., Keum, T., Noh, G., Seo, J. E., Bastola, R., Choi, J., Sohn, D. H., & Lee, S. (2019). Complex formulations, simple techniques: Can 3D printing technology be the Midas touch in pharmaceutical industry? *Asian journal of pharmaceutical sciences*, *14*(5), 465-479.

Lanao, R. P. F., Jonker, A. M., Wolke, J. G., Jansen, J. A., van Hest, J. C., & Leeuwenburgh, S. C. (2013). Physicochemical properties and applications of poly (lactic-co-glycolic acid) for use in bone regeneration. *Tissue Engineering Part B: Reviews*, *19*(4), 380-390.

Lau, G.-K., & Shrestha, M. (2017). Ink-jet printing of micro-electro-mechanical systems (MEMS). *Micromachines*, *8*(6), 194.

Lawrence, X. Y., & Kopcha, M. (2017). The future of pharmaceutical quality and the path to get there. *International Journal of Pharmaceutics*, *528*(1-2), 354-359.

Le, N. (2018). Product Design with Cloud Based and Desktop CAD software: A comparison between SolidWorks and Onshape.

Lee, J.-Y., An, J., & Chua, C. K. (2017). Fundamentals and applications of 3D printing for novel materials. *Applied materials today*, *7*, 120-133.

Lee, J.-Y., Kang, W.-S., Piao, J., Yoon, I.-S., Kim, D.-D., & Cho, H.-J. (2015). Soluplus®/TPGS-based solid dispersions prepared by hot-melt extrusion equipped with twin-screw systems for enhancing oral bioavailability of valsartan. *Drug design, development and therapy*, *9*, 2745.

Li, P., Feng, D., Feng, Y., Zhang, J., Yan, Y., & Zhang, X. (2021). Thermal properties of PEG/MOF-5 regularized nanoporous composite phase change materials: A molecular dynamics simulation. *Case Studies in Thermal Engineering*, *26*, 101027.

Li, X. G., Huang, M. R., & Bai, H. (1999). Thermal decomposition of cellulose ethers. *Journal of Applied Polymer Science*, *73*(14), 2927-2936.

Liang, K., Brambilla, D., & Leroux, J. C. (2019). Is 3D printing of pharmaceuticals a disruptor or enabler? *Advanced Materials*, *31*(5), 1805680.

Linares, V., Galdón, E., Casas, M., & Caraballo, I. (2021). Critical points for predicting 3D printable filaments behaviour. *Journal of Drug Delivery Science and Technology*, *66*, 102933.

Litman, T. (2019). Personalized medicine—concepts, technologies, and applications in inflammatory skin diseases. *Apmis*, *127*(5), 386-424.
Liu, H., Wang, P., Zhang, X., Shen, F., & Gogos, C. G. (2010). Effects of extrusion process parameters on the dissolution behavior of indomethacin in Eudragit® E PO solid dispersions. *International Journal of Pharmaceutics*, *383*(1-2), 161-169.
Liu, L., Ku, J., Khang, G., Lee, B., Rhee, J. M., & Lee, H. B. (2000). Nifedipine controlled delivery by sandwiched osmotic tablet system. *Journal of Controlled Release*, *68*(2), 145-156.
Liu, S., Zhao, P., Wu, S., Zhang, C., Fu, J., & Chen, Z. (2019). A pellet 3D printer: device design and process parameters optimization. *Advances in Polymer Technology*, *2019*, 1-8.
Liu, Y., Du, T., Qiao, A., Mu, Y., & Yang, H. (2022). Zinc-Based Biodegradable Materials for Orthopaedic Internal Fixation. *Journal of Functional Biomaterials*, *13*(4), 164.
Loos, M., Kleeff, J., Friess, H., & Büchler, M. W. J. A. o. t. N. Y. A. o. S. (2008). Surgical treatment of pancreatic cancer. *1138*(1), 169-180.
Lü, J.-M., Wang, X., Marin-Muller, C., Wang, H., Lin, P. H., Yao, Q., & Chen, C. (2009). Current advances in research and clinical applications of PLGA-based nanotechnology. *Expert review of molecular diagnostics*, *9*(4), 325-341.
Lu, M., Guo, Z., Li, Y., Pang, H., Lin, L., Liu, X., Pan, X., & Wu, C. (2014). Application of hot melt extrusion for poorly water-soluble drugs: limitations, advances and future prospects. *Current pharmaceutical design*, *20*(3), 369-387.
Lupuleasa, D., Drăgănescu, D., Hincu, L., Tudosă, C., & Cioacă, D. (2018). Biocompatible polymers for 3D printing. *Farmacia*, *66*(5), 737-746.
Lv, N., Li, Y., & Qiao, Y. (2022). Generation Algorithm of a Novel Platform Attached Support Structure for FDM-Fused Deposition Modeling. *Advances in Materials Science and Engineering*, *2022*.
Ma, R. R., Belter, J. T., & Dollar, A. M. (2015). Hybrid deposition manufacturing: design strategies for multimaterial mechanisms via three-dimensional printing and material deposition. *Journal of Mechanisms and Robotics*, *7*(2), 021002.
Mahase, E. J. B. B. M. J. (2019). Cancer overtakes CVD to become leading cause of death in high income countries. *366*.
Mahmood, A., Akram, T., Shenggui, C., & Chen, H. (2023). Revolutionizing manufacturing: a review of 4D printing materials, stimuli, and cutting-edge applications. *Composites Part B: Engineering*, 110952.
Mancilla-De-La-Cruz, J., Rodriguez-Salvador, M., & Ruiz-Cantu, L. (2020). The next pharmaceutical path: determining technology evolution in drug delivery products fabricated with additive manufacturing. *Форсайт*, *14*(3 (eng)), 55-70.
Maniruzzaman, M., Boateng, J. S., Snowden, M. J., & Douroumis, D. (2012). A review of hot-melt extrusion: process technology to pharmaceutical products. *International Scholarly Research Notices*, *2012*.
Marín, M., Jiménez, A., López, J., & Vilaplana, J. (1996). Thermal degradation of ethylene (vinyl acetate) Kinetic analysis of thermogravimetric data. *Journal of thermal analysis and calorimetry*, *47*(1), 247-258.
Martin, C. (2016). Twin screw extruders as continuous mixers for thermal processing: a technical and historical perspective. *AAPS PharmSciTech*, *17*(1), 3-19.

Mathur, S., & Sutton, J. (2017). Personalized medicine could transform healthcare. *Biomedical reports*, *7*(1), 3-5.

Matthes, K., Mino-Kenudson, M., Sahani, D. V., Holalkere, N., Fowers, K. D., Rathi, R., & Brugge, W. R. (2007). EUS-guided injection of paclitaxel (OncoGel) provides therapeutic drug concentrations in the porcine pancreas (with video). *Gastrointestinal endoscopy*, *65*(3), 448-453.

Mazzoli, A. (2013). Selective laser sintering in biomedical engineering. *Medical & biological engineering & computing*, *51*, 245-256.

Meena, A., Parikh, T., Gupta, S. S., & Serajuddin, A. T. (2016). Investigation of thermal and viscoelastic properties of polymers relevant to hot melt extrusion-II: Cellulosic polymers. *Journal of Excipients and Food Chemicals*, *5*(1).

Melchels, F. P., Feijen, J., & Grijpma, D. W. (2010). A review on stereolithography and its applications in biomedical engineering. *Biomaterials*, *31*(24), 6121-6130.

Melocchi, A., Parietti, F., Maroni, A., Foppoli, A., Gazzaniga, A., & Zema, L. (2016). Hot-melt extruded filaments based on pharmaceutical grade polymers for 3D printing by fused deposition modeling. *International Journal of Pharmaceutics*, *509*(1-2), 255-263.

Min, J. K., Mosadegh, B., Dunham, S., & Al'Aref, S. J. (2018). *3D Printing applications in cardiovascular medicine*. Academic Press.

Mishra, P. K., Senthil, P., Adarsh, S., & Anoop, M. (2021). An investigation to study the combined effect of different infill pattern and infill density on the impact strength of 3D printed polylactic acid parts. *Composites Communications*, *24*, 100605.

Mohamed, O. A., Masood, S. H., & Bhowmik, J. L. (2016). Mathematical modeling and FDM process parameters optimization using response surface methodology based on Q-optimal design. *Applied Mathematical Modelling*, *40*(23-24), 10052-10073.

Mohammed, A. A., Algahtani, M. S., Ahmad, M. Z., & Ahmad, J. (2021). Optimization of semisolid extrusion (pressure-assisted microsyringe)-based 3D printing process for advanced drug delivery application. *Annals of 3D Printed Medicine*, *2*, 100008.

Mohammed, M. I., Badwal, P. S., & Gibson, I. (2017). Design and fabrication considerations for three dimensional scaffold structures. *KnE Engineering*, 120-126.

Moldenhauer, D., Nguyen, D. C. Y., Jescheck, L., Hack, F., Fischer, D., & Schneeberger, A. (2021). 3D screen printing–An innovative technology for large-scale manufacturing of pharmaceutical dosage forms. *International Journal of Pharmaceutics*, *592*, 120096.

Mora-Castaño, G., Millán-Jiménez, M., Linares, V., & Caraballo, I. (2022). Assessment of the extrusion process and printability of suspension-type drug-loaded AffinisolTM filaments for 3D printing. *Pharmaceutics*, *14*(4), 871.

Moradi, M., Aminzadeh, A., Rahmatabadi, D., & Hakimi, A. (2021). Experimental investigation on mechanical characterization of 3D printed PLA produced by fused deposition modeling (FDM). *Materials Research Express*, *8*(3), 035304.

Moradi, M., Meiabadi, S., & Kaplan, A. (2019). 3D printed parts with honeycomb internal pattern by fused deposition modelling; experimental characterization and production optimization. *Metals and Materials International*, *25*, 1312-1325.

Morales, M. A., Atencio Martinez, C. L., Maranon, A., Hernandez, C., Michaud, V., & Porras, A. (2021). Development and characterization of rice husk and recycled polypropylene composite filaments for 3D printing. *Polymers*, *13*(7), 1067.

MorCh, N. (2023). *Analysis of the Effects of Basic Printer Settings on PLA 3D Prints* Massachusetts Institute of Technology].

Moroni, S., Bischi, F., Aluigi, A., Campana, R., Tiboni, M., & Casettari, L. (2023). 3D printing fabrication of Ethylene-Vinyl Acetate (EVA) based intravaginal rings for antifungal therapy. *Journal of Drug Delivery Science and Technology*, 104469.

Muhindo, D., Elkanayati, R., Srinivasan, P., Repka, M. A., & Ashour, E. A. (2023). Recent Advances in the Applications of Additive Manufacturing (3D Printing) in Drug Delivery: A Comprehensive Review [Review]. *AAPS PharmSciTech*, *24*(2), Article 57. https://doi.org/10.1208/s12249-023-02524-9

Muhindo, D., Elkanayati, R., Srinivasan, P., Repka, M. A., & Ashour, E. A. (2023). Recent Advances in the Applications of Additive Manufacturing (3D Printing) in Drug Delivery: a Comprehensive Review (vol 24, 57, 2023). *AAPS PharmSciTech*, *24*(3), Article 75. https://doi.org/10.1208/s12249-023-02542-7

Muppalaneni, S., & Omidian, H. (2013). Polyvinyl alcohol in medicine and pharmacy: a perspective. *J. Dev. Drugs*, *2*(3), 1-5.

Murugan, R., Mitilesh, R., & Singamneni, S. (2019). Influence of process parameters on the mechanical behaviour and processing time of 3D printing. *Int. J. Mod. Manuf. Technol*, *1*, 21-27.

Mwema, F. M., Akinlabi, E. T., Mwema, F. M., & Akinlabi, E. T. (2020). Basics of fused deposition modelling (FDM). *Fused deposition modeling: strategies for quality enhancement*, 1-15.

Nagy, Z. K., Sauceau, M., Nyúl, K., Rodier, E., Vajna, B., Marosi, G., & Fages, J. (2012). Use of supercritical CO2-aided and conventional melt extrusion for enhancing the dissolution rate of an active pharmaceutical ingredient. *Polymers for Advanced Technologies*, *23*(5), 909-918.

Narala, S., Nyavanandi, D., Srinivasan, P., Mandati, P., Bandari, S., & Repka, M. A. (2021). Pharmaceutical co-crystals, salts, and co-amorphous systems: A novel opportunity of hot-melt extrusion. *Journal of Drug Delivery Science and Technology*, *61*, 102209.

Nasereddin, J. M., Wellner, N., Alhijjaj, M., Belton, P., & Qi, S. (2018). Development of a simple mechanical screening method for predicting the feedability of a pharmaceutical FDM 3D printing filament. *Pharmaceutical Research*, *35*, 1-13.

Nee, A. Y. C. (2014). *Handbook of manufacturing engineering and technology*. Springer Publishing Company, Incorporated.

Ngo, T. D., Kashani, A., Imbalzano, G., Nguyen, K. T., & Hui, D. (2018). Additive manufacturing (3D printing): A review of materials, methods, applications and challenges. *Composites Part B: Engineering*, *143*, 172-196.

Nidagundi, V. B., Keshavamurthy, R., & Prakash, C. (2015). Studies on parametric optimization for fused deposition modelling process. *Materials Today: Proceedings*, *2*(4-5), 1691-1699.

Norman, J., Madurawe, R. D., Moore, C. M., Khan, M. A., & Khairuzzaman, A. (2017). A new chapter in pharmaceutical manufacturing: 3D-printed drug products. *Advanced Drug Delivery Reviews*, *108*, 39-50.

Nuchitprasitchai, S., Roggemann, M., & Pearce, J. M. (2017). Factors effecting real-time optical monitoring of fused filament 3D printing. *Progress in Additive Manufacturing*, *2*, 133-149.

Nugroho, A., Ardiansyah, R., Rusita, L., & Larasati, I. L. (2018). Effect of layer thickness on flexural properties of PLA (PolyLactid Acid) by 3D printing. Journal of Physics: Conference Series,

Obeid, S., Madžarević, M., & Ibrić, S. (2021a). Tailoring amlodipine release from 3D printed tablets: Influence of infill patterns and wall thickness. *International Journal of Pharmaceutics*, *610*, 121261.
Obeid, S., Madžarević, M., & Ibrić, S. J. I. J. o. P. (2021b). Tailoring amlodipine release from 3D printed tablets: Influence of infill patterns and wall thickness. *610*, 121261.
Obeid, S., Madžarević, M., Krkobabić, M., & Ibrić, S. (2021). Predicting drug release from diazepam FDM printed tablets using deep learning approach: Influence of process parameters and tablet surface/volume ratio. *International Journal of Pharmaceutics*, *601*, 120507.
Öblom, H., Sjöholm, E., Rautamo, M., & Sandler, N. (2019). Towards printed pediatric medicines in hospital pharmacies: Comparison of 2D and 3D-printed orodispersible warfarin films with conventional oral powders in unit dose sachets. *Pharmaceutics*, *11*(7), 334.
Okafor-Muo, O. L., Hassanin, H., Kayyali, R., & ElShaer, A. (2020). 3D printing of solid oral dosage forms: numerous challenges with unique opportunities. *Journal of Pharmaceutical Sciences*, *109*(12), 3535-3550.
Okwuosa, T. C., Soares, C., Gollwitzer, V., Habashy, R., Timmins, P., & Alhnan, M. A. (2018). On demand manufacturing of patient-specific liquid capsules via co-ordinated 3D printing and liquid dispensing. *European Journal of Pharmaceutical Sciences*, *118*, 134-143.
Okwuosa, T. C., Stefaniak, D., Arafat, B., Isreb, A., Wan, K.-W., & Alhnan, M. A. (2016). A lower temperature FDM 3D printing for the manufacture of patient-specific immediate release tablets. *Pharmaceutical research*, *33*, 2704-2712.
Oladeji, S., Mohylyuk, V., Jones, D. S., & Andrews, G. P. (2022). 3D printing of pharmaceutical oral solid dosage forms by fused deposition: the enhancement of printability using plasticised HPMCAS. *International Journal of Pharmaceutics*, *616*, 121553.
Ong, J. J., Castro, B. M., Gaisford, S., Cabalar, P., Basit, A. W., Perez, G., & Goyanes, A. (2022). Accelerating 3D printing of pharmaceutical products using machine learning. *International Journal of Pharmaceutics-X*, *4*, Article 100120. https://doi.org/10.1016/j.ijpx.2022.100120
Pal, K., Verma, S., Datta, P., Barui, A., Hashmi, S., & Srivastava, A. K. (2022). *Advances in Biomedical Polymers and Composites: Materials and Applications*. Elsevier.
Palaganas, J., de Leon, A. C., Mangadlao, J., Palaganas, N., Mael, A., Lee, Y. J., Lai, H. Y., & Advincula, R. (2017). Facile preparation of photocurable siloxane composite for 3D printing. *Macromolecular Materials and Engineering*, *302*(5), 1600477.
Palekar, S., Nukala, P. K., Mishra, S. M., Kipping, T., & Patel, K. (2019). Application of 3D printing technology and quality by design approach for development of age-appropriate pediatric formulation of baclofen. *International Journal of Pharmaceutics*, *556*, 106-116.
Paraskevoudis, K., Karayannis, P., & Koumoulos, E. P. (2020). Real-Time 3D Printing Remote Defect Detection (Stringing) with Computer Vision and Artificial Intelligence. *Processes*, *8*(11), Article 1464. https://doi.org/10.3390/pr8111464
Park, B. J., Choi, H. J., Moon, S. J., Kim, S. J., Bajracharya, R., Min, J. Y., & Han, H.-K. (2019). Pharmaceutical applications of 3D printing technology: current understanding and future perspectives. *Journal of Pharmaceutical Investigation*, *49*, 575-585.
Park, J., Tari, M. J., & Hahn, H. T. (2000). Characterization of the laminated object manufacturing (LOM) process. *Rapid Prototyping Journal*.

Park, T. G. (1995). Degradation of poly (lactic-co-glycolic acid) microspheres: effect of copolymer composition. *Biomaterials*, *16*(15), 1123-1130.

Parrish, K. E., Cen, L., Murray, J., Calligaris, D., Kizilbash, S., Mittapalli, R. K., Carlson, B. L., Schroeder, M. A., Sludden, J., & Boddy, A. V. J. M. c. t. (2015). Efficacy of PARP inhibitor rucaparib in orthotopic glioblastoma xenografts is limited by ineffective drug penetration into the central nervous system. *14*(12), 2735-2743.

Parulski, C., Jennotte, O., Lechanteur, A., & Evrard, B. (2021). Challenges of fused deposition modeling 3D printing in pharmaceutical applications: Where are we now? *Advanced Drug Delivery Reviews*, *175*, 113810.

Patel, K., Shah, S., & Patel, J. (2022). Solid dispersion technology as a formulation strategy for the fabrication of modified release dosage forms: A comprehensive review. *DARU Journal of Pharmaceutical Sciences*, *30*(1), 165-189.

Patil, H., Tiwari, R. V., & Repka, M. A. (2016). Hot-melt extrusion: from theory to application in pharmaceutical formulation. *AAPS PharmSciTech*, *17*, 20-42.

Patlolla, A., Collins, G., & Arinzeh, T. L. (2010). Solvent-dependent properties of electrospun fibrous composites for bone tissue regeneration. *Acta biomaterialia*, *6*(1), 90-101.

Pereira, B. C., Isreb, A., Isreb, M., Forbes, R. T., Oga, E. F., & Alhnan, M. A. (2020). Additive manufacturing of a Point-of-Care "Polypill:" Fabrication of concept capsules of complex geometry with bespoke release against cardiovascular disease. *Advanced healthcare materials*, *9*(13), 2000236.

Pereira, G. G., Figueiredo, S., Fernandes, A. I., & Pinto, J. F. (2020). Polymer selection for hot-melt extrusion coupled to fused deposition modelling in pharmaceutics. *Pharmaceutics*, *12*(9), 795.

Pereira, R. F., & Bártolo, P. J. (2015). 3D photo-fabrication for tissue engineering and drug delivery. *Engineering*, *1*(1), 090-112.

Pimparade, M. B., Morott, J. T., Park, J.-B., Kulkarni, V. I., Majumdar, S., Murthy, S., Lian, Z., Pinto, E., Bi, V., & Durig, T. (2015). Development of taste masked caffeine citrate formulations utilizing hot melt extrusion technology and in vitro–in vivo evaluations. *International journal of pharmaceutics*, *487*(1-2), 167-176.

Ploch, C. C., Mansi, C. S., Jayamohan, J., & Kuhl, E. (2016). Using 3D printing to create personalized brain models for neurosurgical training and preoperative planning. *World neurosurgery*, *90*, 668-674.

Prasad, L. K., & Smyth, H. (2016). 3D Printing technologies for drug delivery: a review. *Drug Development and Industrial Pharmacy*, *42*(7), 1019-1031.

PresedenceResearch. (2023). *Additive Manufacturing Market*. PR. Retrieved 10/12/2023 from https://www.precedenceresearch.com/additive-manufacturing-market

Prodan Žitnik, I., Černe, D., Mancini, I., Simi, L., Pazzagli, M., Di Resta, C., Podgornik, H., Repič Lampret, B., Trebušak Podkrajšek, K., & Sipeky, C. (2018). Personalized laboratory medicine: a patient-centered future approach. *Clinical Chemistry and Laboratory Medicine (CCLM)*, *56*(12), 1981-1991.

Qi, Y., Min, H., Mujeeb, A., Zhang, Y., Han, X., Zhao, X., Anderson, G. J., Zhao, Y., & Nie, G. (2018). Injectable hexapeptide hydrogel for localized chemotherapy prevents breast cancer recurrence. *ACS applied materials & interfaces*, *10*(8), 6972-6981.

Quanjin, M., Rejab, M., Idris, M., Kumar, N. M., Abdullah, M., & Reddy, G. R. (2020). Recent 3D and 4D intelligent printing technologies: A comparative review and future perspective. *Procedia Computer Science*, *167*, 1210-1219.

Rahman, Z., Barakh Ali, S. F., Ozkan, T., Charoo, N. A., Reddy, I. K., & Khan, M. A. (2018). Additive manufacturing with 3D printing: progress from bench to bedside. *The AAPS journal*, *20*, 1-14.

Ramachandran, R., Junnuthula, V. R., Gowd, G. S., Ashokan, A., Thomas, J., Peethambaran, R., Thomas, A., Unni, A. K. K., Panikar, D., & Nair, S. V. (2017). Theranostic 3-Dimensional nano brain-implant for prolonged and localized treatment of recurrent glioma. *Scientific reports*, *7*(1), 43271.

Reddy Dumpa, N., Bandari, S., & A. Repka, M. (2020). Novel gastroretentive floating pulsatile drug delivery system produced via hot-melt extrusion and fused deposition modeling 3D printing. *Pharmaceutics*, *12*(1), 52.

Reguieg, F., Ricci, L., Bouyacoub, N., Belbachir, M., & Bertoldo, M. (2020). Thermal characterization by DSC and TGA analyses of PVA hydrogels with organic and sodium MMT. *Polymer Bulletin*, *77*(2), 929-948.

Reklaitis, G., Khinast, J., & Muzzio, F. (2010). Pharmaceutical engineering science—New approaches to pharmaceutical development and manufacturing. *Chemical Engineering Science*, *65*(21), iv-vii.

Repka, M. A., Majumdar, S., Kumar Battu, S., Srirangam, R., & Upadhye, S. B. (2008). Applications of hot-melt extrusion for drug delivery. *Expert opinion on drug delivery*, *5*(12), 1357-1376.

Research, C. f. D. E. a. (2022). *Size, Shape, and Other Physical Attributes of Generic Tablets and Capsules*. U.S. FOOD AND DRUG ADMINISTRATION. Retrieved 26/08/2023 from https://www.fda.gov/regulatory-information/search-fda-guidance-documents/size-shape-and-other-physical-attributes-generic-tablets-and-capsules

Riveiro, A., del Val, J., Comesaña, R., Lusquiños, F., Quintero, F., Boutinguiza, M., & Pou, J. (2019). Laser additive manufacturing processes for near net shape components. *Near net shape manufacturing processes*, 105-141.

Robles-Martinez, P., Xu, X., Trenfield, S. J., Awad, A., Goyanes, A., Telford, R., Basit, A. W., & Gaisford, S. (2019). 3D printing of a multi-layered polypill containing six drugs using a novel stereolithographic method. *Pharmaceutics*, *11*(6), 274.

Rodríguez-Pombo, L., Xu, X., Seijo-Rabina, A., Ong, J. J., Alvarez-Lorenzo, C., Rial, C., Nieto, D., Gaisford, S., Basit, A. W., & Goyanes, A. (2022). Volumetric 3D printing for rapid production of medicines. *Additive Manufacturing*, *52*, 102673.

S., K. (2023). *Understanding SPID®, Laxxon's Screen Printed Innovative Drug Technology and its business model*. 3D ADEPT MEDIA. Retrieved 25/12/2023 from https://3dadept.com/understanding-spid-laxxons-screen-printed-innovative-drug-technology-and-its-business-model/

Sachs, E., Cima, M., Williams, P., Brancazio, D., & Cornie, J. (1992). Three dimensional printing: rapid tooling and prototypes directly from a CAD model.

Sadia, M., Arafat, B., Ahmed, W., Forbes, R. T., & Alhnan, M. A. (2018). Channelled tablets: An innovative approach to accelerating drug release from 3D printed tablets. *Journal of Controlled Release*, *269*, 355-363.

Sadia, M., Sośnicka, A., Arafat, B., Isreb, A., Ahmed, W., Kelarakis, A., & Alhnan, M. A. (2016). Adaptation of pharmaceutical excipients to FDM 3D printing for the fabrication of patient-tailored immediate release tablets. *International Journal of Pharmaceutics*, *513*(1-2), 659-668.

Sakellariou, P., Rowe, R., & White, E. (1985). The thermomechanical properties and glass transition temperatures of some cellulose derivatives used in film coating. *International Journal of Pharmaceutics*, *27*(2-3), 267-277.

Sandler, N., & Preis, M. (2016). Printed drug-delivery systems for improved patient treatment. *Trends in pharmacological sciences*, *37*(12), 1070-1080.

Sandler, N., Salmela, I., Fallarero, A., Rosling, A., Khajeheian, M., Kolakovic, R., Genina, N., Nyman, J., & Vuorela, P. (2014). Towards fabrication of 3D printed medical devices to prevent biofilm formation. *International Journal of Pharmaceutics*, *459*(1-2), 62-64.

Savjani, K. T., Gajjar, A. K., & Savjani, J. K. (2012). Drug solubility: importance and enhancement techniques. *International Scholarly Research Notices*, *2012*.

Sen, K., Mehta, T., Sansare, S., Sharifi, L., Ma, A. W., & Chaudhuri, B. (2021). Pharmaceutical applications of powder-based binder jet 3D printing process–a review. *Advanced Drug Delivery Reviews*, *177*, 113943.

Senapati, S., Mahanta, A. K., Kumar, S., & Maiti, P. (2018). Controlled drug delivery vehicles for cancer treatment and their performance. *Signal transduction and targeted therapy*, *3*(1), 7.

Seo, H., Heo, S., Lee, H., & Yoon, H. (2017). Preparation of PEG materials for constructing complex structures by stereolithographic 3D printing. RSC Adv. 7, 28684–28688. In.

Serrano, D. R., Kara, A., Yuste, I., Luciano, F. C., Ongoren, B., Anaya, B. J., Molina, G., Diez, L., Ramirez, B. I., & Ramirez, I. O. (2023). 3D printing technologies in personalized medicine, nanomedicines, and biopharmaceuticals. *Pharmaceutics*, *15*(2), 313.

Shahbazova, G. M., & Masimov, E. A. (2022). Effect of a Various Additivies to the Formation of Aqueous Biphasic System Polyetylenglycole (Peg)/Sodium Citrate/Water. *Open Access Library Journal*, *9*(1), 1-9.

Shakya, N., Agrawal, B., & Kumar, R. (2012). Chemotherapeutic strategies and targets against resistant TB. *Understanding tuberculosis-new approaches to fighting against drug resistance. Rijeka: InTech Publisher*, 33-92.

Sharma, A., & Jain, C. (2011). Solid dispersion: A promising technique to enhance solubility of poorly water soluble drug. *International Journal of Drug Delivery*, *3*(2), 149.

Shirmohammadi, M., Goushchi, S. J., & Keshtiban, P. M. (2021). Optimization of 3D printing process parameters to minimize surface roughness with hybrid artificial neural network model and particle swarm algorithm. *Progress in Additive Manufacturing*, *6*, 199-215.

Sibum, I., Hagedoorn, P., Frijlink, H. W., & Grasmeijer, F. (2019). Characterization and formulation of isoniazid for high-dose dry powder inhalation. *Pharmaceutics*, *11*(5), 233.

SIMPLIFY3D. (2023). *Stringing or Oozing*. SIMPLIFY3D. Retrieved 13/10/2023 from https://www.simplify3d.com/resources/print-quality-troubleshooting/stringing-or-oozing/

Singhal, S., Lohar, V. K., & Arora, V. (2011). Hot melt extrusion technique.

Solanki, N. G., Tahsin, M., Shah, A. V., & Serajuddin, A. T. M. (2018). Formulation of 3D Printed Tablet for Rapid Drug Release by Fused Deposition Modeling: Screening Polymers for Drug Release, Drug-Polymer Miscibility and Printability. (1520-6017 (Electronic)).

Solano, A. G. R., de Fátima Pereira, A., Pinto, F. C. H., Ferreira, L. G. R., de Oliveira Barbosa, L. A., Fialho, S. L., de Oliveira Patricio, P. S., da Silva Cunha, A., da Silva, G. R., & Pianetti, G. A. (2013). Development and evaluation of sustained-release etoposide-loaded poly (ε-caprolactone) implants. *AAPS PharmSciTech*, *14*, 890-900.

Spoerk, M., Gonzalez-Gutierrez, J., Sapkota, J., Schuschnigg, S., & Holzer, C. (2018). Effect of the printing bed temperature on the adhesion of parts produced by fused filament fabrication. *Plastics, Rubber and Composites*, *47*(1), 17-24.

Sterling, T. R., Njie, G., Zenner, D., Cohn, D. L., Reves, R., Ahmed, A., Menzies, D., Horsburgh Jr, C. R., Crane, C. M., & Burgos, M. J. A. J. o. T. (2020). Guidelines for the treatment of latent tuberculosis infection: recommendations from the National Tuberculosis Controllers Association and CDC, 2020. In (Vol. 20, pp. 1196-1206): Wiley Online Library.

Tabriz, A. G., Kuofie, H., Scoble, J., Boulton, S., & Douroumis, D. (2023). Selective Laser Sintering for printing pharmaceutical dosage forms. *Journal of Drug Delivery Science and Technology*, 104699.

Tan, D. K., Maniruzzaman, M., & Nokhodchi, A. (2018). Advanced pharmaceutical applications of hot-melt extrusion coupled with fused deposition modelling (FDM) 3D printing for personalised drug delivery. *Pharmaceutics*, *10*(4), 203.

Tan, L. J., Zhu, W., & Zhou, K. (2020). Recent progress on polymer materials for additive manufacturing. *Advanced Functional Materials*, *30*(43), 2003062.

Taormina, G., Sciancalepore, C., Messori, M., & Bondioli, F. (2018). 3D printing processes for photocurable polymeric materials: technologies, materials, and future trends. *Journal of applied biomaterials & functional materials*, *16*(3), 151-160.

Teo, K., & Yusuf, S. (2018). Polypill variants (quarter pill trials). *American Journal of Hypertension*, *31*(7), 758-761.

Theil, F., Anantharaman, S., Kyerematen, S. O., van Lishaut, H., Dreis-Kühne, S. H., Rosenberg, J. r., Magerlein, M., & Woehrle, G. H. (2017). Frozen in time: kinetically stabilized amorphous solid dispersions of nifedipine stable after a quarter century of storage. *Molecular pharmaceutics*, *14*(1), 183-192.

Tlegenov, Y., Hong, G. S., & Lu, W. F. (2018). Nozzle condition monitoring in 3D printing. *Robotics and Computer-Integrated Manufacturing*, *54*, 45-55.

Tracy, T., Wu, L., Liu, X., Cheng, S., & Li, X. (2023). 3D printing: Innovative solutions for patients and pharmaceutical industry. *International Journal of Pharmaceutics*, *631*, 122480.

Tracy, T., Wu, L., Liu, X., Cheng, S. P., & Li, X. L. (2023). 3D printing: Innovative solutions for patients and pharmaceutical industry. *International Journal of Pharmaceutics*, *631*, Article 122480. https://doi.org/10.1016/j.ijpharm.2022.122480

Trenfield, S. J., Tan, H. X., Awad, A., Buanz, A., Gaisford, S., Basit, A. W., & Goyanes, A. (2019). Track-and-trace: Novel anti-counterfeit measures for 3D printed personalized drug products using smart material inks. *International journal of pharmaceutics*, *567*, 118443.

Triastek. (2023). *Triastek shares positive results from T21 study showcasing the 3D printing technology's ability to effectively target and release medication in the colon*. Triastek. Retrieved 20/09/2023 from https://www.triastek.com/new-d-1.html

Tümer, E. H., & Erbil, H. Y. (2021). Extrusion-based 3d printing applications of pla composites: A review. *Coatings*, *11*(4), 390.

Valtonen, S., Timonen, U., Toivanen, P., Kalimo, H., Kivipelto, L., Heiskanen, O., Unsgaard, G., & Kuurne, T. (1997). Interstitial chemotherapy with carmustine-loaded polymers for high-grade gliomas: a randomized double-blind study. *Neurosurgery*, *41*(1), 44-49.

Varghese, R., Sood, P., Salvi, S., Karsiya, J., & Kumar, D. (2022). 3D printing in the pharmaceutical sector: advances and evidences. *Sensors International*, 100177.

Vaz, V. M., & Kumar, L. (2021). 3D printing as a promising tool in personalized medicine. *AAPS PharmSciTech*, *22*, 1-20.

Venkataramani, S., Sun, X., Wang, N., Chen, C.-Y., Choi, J., Kang, M., Agarwal, A., Oh, J., Jain, S., & Babinsky, T. (2020). Efficient AI system design with cross-layer approximate computing. *Proceedings of the IEEE*, *108*(12), 2232-2250.

Vlachopoulos, J., & Strutt, D. (2003). The role of rheology in polymer extrusion. New Technology for Extrusion Conference,

Wang, B., Hina, K., Zou, H., Zuo, D., & Yi, C. (2018). Thermal, crystallization, mechanical and decomposition properties of poly (lactic acid) plasticized with poly (ethylene glycol). *Journal of Vinyl and Additive Technology*, *24*, E154-E163.

Wang, J., Zhang, Y., Aghda, N. H., Pillai, A. R., Thakkar, R., Nokhodchi, A., & Maniruzzaman, M. (2021). Emerging 3D printing technologies for drug delivery devices: Current status and future perspective. *Advanced Drug Delivery Reviews*, *174*, 294-316.

Wang, S., Chen, X., Han, X., Hong, X., Li, X., Zhang, H., Li, M., Wang, Z., & Zheng, A. (2023). A Review of 3D Printing Technology in Pharmaceutics: Technology and Applications, Now and Future. *Pharmaceutics*, *15*(2), 416.

Wang, Y., Ahmed, A., Azam, A., Bing, D., Shan, Z., Zhang, Z., Tariq, M. K., Sultana, J., Mushtaq, R. T., & Mehboob, A. (2021). Applications of additive manufacturing (AM) in sustainable energy generation and battle against COVID-19 pandemic: The knowledge evolution of 3D printing. *Journal of Manufacturing Systems*, *60*, 709-733.

Water, J. J., Bohr, A., Boetker, J., Aho, J., Sandler, N., Nielsen, H. M., & Rantanen, J. (2015). Three-dimensional printing of drug-eluting implants: preparation of an antimicrobial polylactide feedstock material. *Journal of Pharmaceutical Sciences*, *104*(3), 1099-1107.

Wei, X., Qiu, S., Zhu, L., Feng, R., Tian, Y., Xi, J., & Zheng, Y. (2017). Toward support-free 3D printing: A skeletal approach for partitioning models. *Ieee Transactions on visualization and computer graphics*, *24*(10), 2799-2812.

Weinberg, B. D., Blanco, E., & Gao, J. (2008). Polymer implants for intratumoral drug delivery and cancer therapy. *Journal of pharmaceutical sciences*, *97*(5), 1681-1702.

Westphal, M., Hilt, D. C., Bortey, E., Delavault, P., Olivares, R., Warnke, P. C., Whittle, I. R., Jääskeläinen, J., & Ram, Z. (2003). A phase 3 trial of local chemotherapy with biodegradable carmustine (BCNU) wafers (Gliadel wafers) in patients with primary malignant glioma. *Neuro-oncology*, *5*(2), 79-88.

Wolinsky, J. B., Colson, Y. L., & Grinstaff, M. W. (2012). Local drug delivery strategies for cancer treatment: gels, nanoparticles, polymeric films, rods, and wafers. *Journal of Controlled Release*, *159*(1), 14-26.

Woodruff, M. A., & Hutmacher, D. W. (2010). The return of a forgotten polymer—Polycaprolactone in the 21st century. *Progress in polymer science*, *35*(10), 1217-1256.

Wouters, O. J., McKee, M., & Luyten, J. (2020). Estimated research and development investment needed to bring a new medicine to market, 2009-2018. *Jama*, *323*(9), 844-853.

Wu, B. M., Borland, S. W., Giordano, R. A., Cima, L. G., Sachs, E. M., & Cima, M. J. (1996). Solid free-form fabrication of drug delivery devices. *Journal of Controlled Release*, *40*(1-2), 77-87.

Wu, H., Wang, Y., & Yu, Z. (2016). In situ monitoring of FDM machine condition via acoustic emission. *The International Journal of Advanced Manufacturing Technology*, *84*, 1483-1495.

Xing, J.-F., Zheng, M.-L., & Duan, X.-M. (2015). Two-photon polymerization microfabrication of hydrogels: an advanced 3D printing technology for tissue engineering and drug delivery. *Chemical Society Reviews*, *44*(15), 5031-5039.

Xu, W., Jambhulkar, S., Zhu, Y., Ravichandran, D., Kakarla, M., Vernon, B., Lott, D. G., Cornella, J. L., Shefi, O., & Miquelard-Garnier, G. (2021). 3D printing for polymer/particle-based processing: A review. *Composites Part B: Engineering*, *223*, 109102.

Xu, Y., Liu, X., Cao, X., Huang, C., Liu, E., Qian, S., Liu, X., Wu, Y., Dong, F., & Qiu, C.-W. (2021). Artificial intelligence: A powerful paradigm for scientific research. *The Innovation*, *2*(4), 100179.

Yang, F., Jin, C., Subedi, S., Lee, C. L., Wang, Q., Jiang, Y., Li, J., Di, Y., & Fu, D. (2012). Emerging inorganic nanomaterials for pancreatic cancer diagnosis and treatment. *Cancer treatment reviews*, *38*(6), 566-579.

Yang, F., Su, Y., Zhang, J., DiNunzio, J., Leone, A., Huang, C., & Brown, C. D. (2016). Rheology guided rational selection of processing temperature to prepare copovidone–nifedipine amorphous solid dispersions via hot melt extrusion (HME). *Molecular pharmaceutics*, *13*(10), 3494-3505.

Yang, J., Grey, K., & Doney, J. (2010). An improved kinetics approach to describe the physical stability of amorphous solid dispersions. *International Journal of Pharmaceutics*, *384*(1-2), 24-31.

Yang, K., & Ren, Y. (2010). Nickel-free austenitic stainless steels for medical applications. *Science and technology of advanced materials*.

Yang, Y., Qiao, X., Huang, R., Chen, H., Shi, X., Wang, J., Tan, W., & Tan, Z. (2020). E-jet 3D printed drug delivery implants to inhibit growth and metastasis of orthotopic breast cancer. *Biomaterials*, *230*, 119618.

Yeong, W., Sudarmadji, N., Yu, H., Chua, C., Leong, K., Venkatraman, S., Boey, Y., & Tan, L. (2010). Porous polycaprolactone scaffold for cardiac tissue engineering fabricated by selective laser sintering. *Acta biomaterialia*, *6*(6), 2028-2034.

Yi, H.-G., Choi, Y.-J., Kang, K. S., Hong, J. M., Pati, R. G., Park, M. N., Shim, I. K., Lee, C. M., Kim, S. C., & Cho, D.-W. (2016). A 3D-printed local drug delivery patch for pancreatic cancer growth suppression. *Journal of Controlled Release*, *238*, 231-241.

Yi, S., Wang, J., Lu, Y., Ma, R., Gao, Q., Liu, S., & Xiong, S. (2019). Novel hot melt extruded matrices of hydroxypropyl cellulose and amorphous felodipine–plasticized hydroxypropyl methylcellulose as controlled release systems. *Aaps Pharmscitech*, *20*, 1-14.

Yu, J., Yang, X., He, W., & Ye, W. (2021). Burden of pancreatic cancer along with attributable risk factors in Europe between 1990 and 2019, and projections until 2039. *International journal of cancer*, *149*(5), 993-1001.

Zagidullin, R., Antipov, D., Dmitriev, A., & Zezin, N. (2021). Development of a methodology for eliminating failures of an FDM 3D printer using a “failure tree” and FMEA analysis. Journal of Physics: Conference Series,

Zakeri, S., Vippola, M., & Levänen, E. (2020). A comprehensive review of the photopolymerization of ceramic resins used in stereolithography. *Additive Manufacturing*, *35*, 101177.

Zein, I., Hutmacher, D. W., Tan, K. C., & Teoh, S. H. (2002). Fused deposition modeling of novel scaffold architectures for tissue engineering applications. *Biomaterials*, *23*(4), 1169-1185.

Zenner, D., Beer, N., Harris, R. J., Lipman, M. C., Stagg, H. R., & Van Der Werf, M. J. (2017). Treatment of latent tuberculosis infection: an updated network meta-analysis. *Annals of internal medicine*, *167*(4), 248-255.

Zhang, J., Feng, X., Patil, H., Tiwari, R. V., & Repka, M. A. (2017). Coupling 3D printing with hot-melt extrusion to produce controlled-release tablets. *International Journal of Pharmaceutics*, *519*(1-2), 186-197.

Zhang, J., Thakkar, R., Zhang, Y., & Maniruzzaman, M. (2020). Structure-function correlation and personalized 3D printed tablets using a quality by design (QbD) approach. *International Journal of Pharmaceutics*, *590*, 119945.

Zhang, J., Xu, P., Vo, A. Q., Bandari, S., Yang, F., Durig, T., & Repka, M. A. (2019). Development and evaluation of pharmaceutical 3D printability for hot melt extruded cellulose-based filaments. *Journal of Drug Delivery Science and Technology*, *52*, 292.

Zhang, J., Yang, W., Vo, A. Q., Feng, X., Ye, X., Kim, D. W., & Repka, M. A. (2017). Hydroxypropyl methylcellulose-based controlled release dosage by melt extrusion and 3D printing: Structure and drug release correlation. *Carbohydrate polymers*, *177*, 49-57.

Zhang, P., Li, J., Ashour, E. A., Chung, S., Wang, H., Vemula, S. K., & Repka, M. A. (2024). Development of multiple structured extended release tablets via hot melt extrusion and dual-nozzle fused deposition modeling 3D printing. *International Journal of Pharmaceutics*, *653*, 123905.

Zheng, Y., Deng, F., Wang, B., Wu, Y., Luo, Q., Zuo, X., Liu, X., Cao, L., Li, M., & Lu, H. (2021). Melt extrusion deposition (MED™) 3D printing technology–A paradigm shift in design and development of modified release drug products. *International Journal of Pharmaceutics*, *602*, 120639.